

WENHUA LIU

MODELLING COLOR CHANGES IN WOOD DURING CONVENTIONAL DRYING

Thèse présentée
à la Faculté des études supérieures de l'Université Laval
dans le cadre du programme de doctorat en sciences du bois
pour l'obtention du grade de Philosophiae Doctor (Ph. D.)

DÉPARTEMENT DES SCIENCES DU BOIS ET DE LA FORÊT
FACULTÉ DE FORESTERIE, DE GÉOGRAPHIE ET DE GÉOMATIQUE
UNIVERSITÉ LAVAL
QUÉBEC

2011

Résumé

La coloration du bois pendant le séchage diminue la qualité et la valeur du produit fini, augmente les coûts de production et diminue le rendement matière. C'est un processus complexe qui est difficile à prédire. Le développement d'un modèle de changement de couleur du bois en cours de séchage peut donc favoriser l'économie de temps et de matière première. Deux séries de six essais ont été effectuées dans cette étude sur l'aubier du bouleau à papier et de l'érable à sucre afin de mesurer le changement de couleur du bois pendant un séchage conventionnel à trois niveaux différents de température sèche (40, 60 et 80°C) et deux niveaux de dépression au thermomètre humide (4 et 15°C). Les données de ces essais ont conduit au développement de modèles statistiques du changement de l'indice de clarté L^* pour chaque espèce, séparément pour la surface et l'intérieur du bois, en utilisant des modèles de régression mixte avec la planche considérée comme effet aléatoire. Deux types de modèles ont été développés, soit en considérant les trois températures sèches (40, 60 et 80°C) d'une part, et les deux températures les plus élevées seulement (60 et 80°C) d'autre part. Finalement, les modèles statistiques furent combinés à un modèle existant de transfert de masse et de chaleur (DRYTEK) afin de simuler les changements de couleur pour tout autre programme spécifique de séchage à moyenne température. Les paramètres du modèle numérique de transfert de masse et de chaleur ont été mesurés préalablement pour les deux espèces. Les modèles statistiques et les modèles intégrés de changement de couleur furent enfin validés en réalisant pour chaque espèce un essai indépendant de séchage à une température sèche de 70°C et à une dépression au thermomètre humide de 10°C.

Les résultats des essais de mesure de couleur aux températures de 60 et 80°C montrent que les valeurs de L^* des deux espèces à l'intérieur de la planche diminuent rapidement avec une diminution de la teneur en humidité (M) jusqu'au point de saturation des fibres. Par la suite, les valeurs de L^* diminuent lentement jusqu'à 15 - 25% M où celles-ci peuvent même commencer à augmenter. Le changement de couleur du bois à 40°C est très faible ou inexistant. Les valeurs de L^* à la surface de la planche diminuent également de façon substantielle avec la diminution de la teneur en humidité, exception faite à 40°C. Pour l'ensemble de l'épaisseur du bois, plus élevée est la température de séchage, plus grande est

la diminution des valeurs de L^* . Réciproquement, plus forte est la dépression au thermomètre humide, plus faible est le changement de couleur à une température sèche donnée. Les composantes a^* et b^* montrent un comportement similaire à L^* par rapport aux variations de la température de séchage et de la dépression au thermomètre humide. Par contre, les valeurs de a^* et b^* augmentent avec la teneur en humidité au lieu de diminuer.

La comparaison des valeurs de L^* obtenues des modèles statistiques de prévision avec les valeurs de L^* mesurées expérimentalement à partir des essais de validation montre une très forte similarité des deux types de résultats dans le cas de l'érable de sucre. Pour le bouleau à papier, un écart important est observé entre les valeurs prédites et mesurées au-dessus du point de saturation des fibres.

La relation teneur en humidité-potential hydrique mesurée expérimentalement montre que le potentiel hydrique augmente avec la température à une teneur en humidité donnée. Pour les deux espèces, un plateau caractéristique est observé dans la gamme de potentiels hydriques entre -2000 et -6000 J kg^{-1} . Tel que prévu, la conductivité hydrique effective augmente avec le contenu d'humidité et la température, et elle est plus élevée en direction radiale qu'en direction tangentielle. Le coefficient de transfert convectif de masse augmente avec la température de séchage à une dépression au thermomètre humide donnée, alors qu'il diminue avec la dépression au thermomètre humide à une température de séchage donnée.

Finalement, la comparaison des mesures de changement de couleur au cours des essais de validation avec les valeurs simulées à partir des modèles statistiques combinés au modèle de transfert de masse et de chaleur montre une évolution des valeurs de L^* très similaire dans le cas de l'érable à sucre. À l'instar des modèles statistiques, un écart important existe entre les deux types de résultats pour le bouleau à papier dans la première partie du séchage.

Abstract

Wood discoloration during drying is diminishing quality and value of end product, increasing production costs and decreasing yield. Wood discoloration during drying is a complex process which is difficult to predict. The development of a wood color model can save material and time by simulating color changes for any specific drying conditions. A set of six experiments were performed in this study on paper birch and sugar maple sapwood to measure wood color changes during conventional drying at three different levels of dry-bulb temperature (40, 60 and 80°C) and two levels of wet-bulb depression (4 and 15°C). Statistical wood color models for lightness L^* were proposed for each species, both for the wood surface and through the board thickness, to predict the wood color changes during conventional drying using mixed regression models with the board sample taken as the random effect. Three temperature (3T) (40, 60 and 80°C) and two temperature (2T) (60 and 80°C) models were developed. Finally, the statistical wood color models were integrated into an existing heat and mass transfer numerical model (DRYTEK) in order to simulate, for any conventional dynamic wood drying schedule, wood color changes on the surface and through the board thickness. The numerical model parameters (moisture content-water potential relationship, effective water conductivity, convective mass transfer coefficient) were experimentally determined for paper birch and sugar maple at the three drying temperatures. Both types of wood color predictive models were then validated by means of an independent drying run conducted at the dry-bulb temperature of 70°C and the wet-bulb depression of 10°C.

The results of the wood color measurement tests show that at the dry-bulb temperatures of 60 and 80°C, the L^* values of both species below the surface decrease rapidly with a decrease of the moisture content (M) from the green state to the fiber saturation point. Then, the L^* values decrease slowly until about 15 - 25% M where they may even start to increase. Wood color changes at 40°C were found very small, either positive or negative. The L^* values at the surface also decrease as the moisture content decreases and, except for the temperature of 40°C, the changes in color increase with the drying temperature. In general, the higher is the dry-bulb temperature, the greater is the decrease of the L^* values through the board thickness. Conversely, the higher is the wet-bulb depression at a given

dry-bulb temperature, the smaller are the color changes. The color components a^* and b^* follow a similar behavior as L^* with respect to drying temperature and wet bulb depression. However, contrarily to the L^* values, the a^* and b^* values increase with a decrease of M .

The comparison of the predicted L^* values obtained from the statistical models with the experimental L^* values obtained from the validation tests shows a very good agreement between both types of results in the case of sugar maple. For paper birch, a fairly large discrepancy is observed during the first part of drying between predicted and experimental results but a better agreement is found at the end of drying.

The results of the moisture content-water potential relationship determination show that the water potential increases with temperature at a given moisture content. A characteristic plateau was found in the water potential range of -2,000 and -6,000 J kg⁻¹. As expected, the effective water conductivity increases with moisture content and temperature and it is higher in the radial direction than in the tangential direction. The convective mass transfer coefficient increases with dry-bulb temperature at a given wet-bulb depression, whereas it decreases with an increase of web-bulb depression at a given dry-bulb temperature.

Finally, the comparison of the wood color measurements during the validation tests on paper birch and sugar maple with the wood color values simulated with the integrated statistical/numerical models shows a very good agreement between both types of results in the case of sugar maple. As it was observed for the statistical models, the fit was poorer in the case of paper birch, especially above the fiber saturation point where the initial moisture content seems to be an important factor in the color changes behavior of wood during drying.

Foreword

This work was conducted at the “Centre de recherche sur le bois” de l’Université Laval in collaboration with FPInnovations, Québec. Financial support was provided by special research programs of Développement Économique Canada, Ressources naturelles Canada (programme Valeur au bois) and other internal fundings.

This thesis is presented in the classical format containing an introduction, three chapters and a conclusion. The first chapter describes the literature review on the thesis subject. The second chapter describes the materials and methods used to conduct different kinds of experiments and data analysis. The third chapter describes the results and discussion, presenting the measurement results obtained from experiments and further data analysis to develop color change predictive models. A general conclusion, a bibliography and appendixes complete the main document. So as not to overload the main body of the text, complementary information about experimental results and the data analysis such as figures, tables and SAS[®] programs can be found in several appendixes.

Acknowledgements

I always think that the pursuit of knowledge is one of the most important things in my life. I would like to take this occasion to express my appreciation and thanks to any person and organization that helped me in the course of my Ph. D. study.

I am very thankful to my supervisor, Prof. Yves Fortin, of Département des sciences du bois et de la forêt de l'Université Laval. Without him, the study would have not been possible. During the study, he helped me solving many problems and directed me on the right track with his extended knowledge in wood science and statistics. His continuous trust, understanding, support, encouragement and guidance were an essential source of the achievement. He spent a lot of time and energy to make many important corrections in this thesis. I learned a lot from him. Furthermore, I wish to show my thanks to Prof. Tatjana Stevanovic of Département des sciences du bois et de la forêt de l'Université Laval, and Dr. Carl Tremblay from FPInnovations for their constructive suggestions, consideration and encouragement.

I deeply thank Mr. Gaétan DAIGLE of Département de mathématiques et de statistiques de l'Université Laval who analyzed the experimental data and wrote several SAS® programs. The statistical analysis made the models practical.

I also thank all members at the Centre de recherche sur le bois (CRB) for their help and cooperation. I'm deeply grateful to Mr. Aziz Laghdir for his help with experimental setup and data analysis, Mr. Nicolas Renald, Sylvain Auger, David Lagueux, Daniel Bourgault, Luc Germain, Yves Bédard, and Éric Rousseau for their material preparation and important technical support to my experiments. Thanks go to all professors (Alain Cloutier, Bernard Riedl, Robert Beauregard and Roger Hernández) for their teaching and administration and all administration staff (Mrs. Colette Bourcier and Guylaine Bélanger, Mr. Benoît St-Pierre) because their efforts make the Wood Research Center into a pleasurable workplace.

I appreciate a lot the help and encouragement that I received from my friends: Benoît Harbour, Daniel Fuentealba, Javier Chung, Julie Cool, Marcia Quaquarelli, Messaoud Nabhani, Papa Niokhor Diouf, Suying Xing, Xiaodong Wang, Zaira Silva Latorre, etc.

“If we knew what it was we were doing, it would not be called research, would it?”

by Albert Einstein (1879-1955)

Table of contents

Résumé.....	i
Abstract.....	iii
Foreword.....	v
Acknowledgements.....	vi
Table of contents.....	viii
List of tables.....	xi
List of figures.....	xiii
Introduction.....	1
Chapter 1. Background and literature review	3
1.1 Color of wood	3
1.1.1 Mechanism of color recognition	3
1.1.2 Representation and determination of color	5
1.1.3 Characteristics of wood color	9
1.1.3.1 Coloring substances of wood.....	9
1.1.3.2 Physical factors affecting wood color	9
1.2 Chemistry of wood discoloration	11
1.2.1 Types of wood discoloration.....	11
1.2.2 Chemical analysis of wood discoloration during drying	12
1.3 Effect of harvest season, storage and growing site on wood color	14
1.3.1 Fresh wood.....	14
1.3.2 Dried wood	15
1.4 Effect of moisture content on wood discoloration during drying	17
1.5 Modelling of wood color with drying parameters.....	19
1.5.1 The effect of drying temperature	19
1.5.2 The effect of drying time, wood thickness and relative humidity	25
1.6 The drying model based on water potential concept.....	29
1.6.1 The concept of water potential.....	30
1.6.2 Heat and mass transfer equations.....	31
1.7 Physical material properties used for the heat and mass transfer model.....	35
1.7.1 The moisture content-water potential relationship (M- ψ) of wood	35
1.7.2 The effective water conductivity of wood	38
1.7.3 The convective mass transfer coefficient.....	40
1.7.4 The ratio of vapour diffusion to the total water movement in wood	44
1.8 Purpose of the study	45
Chapter 2. Materials and methods.....	47
2.1 Wood color measurements during drying	47
2.1.1 Material	47
2.1.2 Methods	48
2.2 DRYTEK code	55

2.3	Measurement of the wood drying model parameters.....	57
2.3.1	Moisture content-water potential relationship	57
2.3.1.1	Material.....	57
2.3.1.2	Methods	58
2.3.2	Effective water conductivity.....	59
2.3.2.1	Material.....	59
2.3.2.2	Methods	60
2.3.3	Convective mass transfer coefficient.....	62
2.3.3.1	Material.....	62
2.3.3.2	Methods	62
2.4	Validation of color model	63
2.4.1	Material.....	63
2.4.2	Methods	64
Chapter 3.	Results and discussion.....	65
3.1	Wood color change measurements.....	65
3.1.1	Drying curves.....	65
3.1.2	Wood temperature profiles	69
3.1.3	Moisture content profiles	70
3.1.4	Wood color profiles	73
3.2	Development of statistical models of wood color change during drying.....	77
3.2.1	Determination of separate equations for the six drying conditions	77
3.2.2	Global models of wood color change during drying	81
3.2.2.1	Wood color 3T global models	82
3.2.2.2	Wood color 2T global models	86
3.3	Physical material properties of the heat and mass transfer model	89
3.3.1	Determination of the $M-\psi$ relationship of wood	89
3.3.2	Determination of the effective water conductivity	95
3.3.3	Determination of the convective mass transfer coefficient for wood drying.....	100
3.3.3.1	Calculation of the convective mass transfer coefficient in the constant drying rate period	100
3.3.3.2	Fine tuning of the convective mass transfer coefficient below the constant drying rate period	102
3.4	Validation tests for the statistical and the integrated color change models	103
3.4.1	Experimental results	103
3.4.2	Prediction of wood color change from the global statistical models.....	106
3.4.3	Numerical simulations	108
3.4.3.1	Drying curves	108
3.4.3.2	Moisture content and lightness profiles of wood	108
Chapter 4.	Conclusions et recommendations	113
	Bibliography	117
Appendix A:	Drying schedules used for the color measurement tests and the measured wood temperature profiles.....	126
Appendix B:	Color component a^* and b^* profiles obtained during color measurement tests.....	130

Appendix C:	M-L* relationship measured from the color measurement tests	134
Appendix D:	SAS® program for the separate wood color model on the wood surface	140
Appendix E:	SAS® program for the separate wood color model below the wood surface	145
Appendix F:	Graphical technique for the 3T global wood color models	153
Appendix G:	Graphical technique used for the 2T global wood color models	161
Appendix H:	SAS® programs for the global predictive models	167
Appendix I:	Calculation of the convective mass transfer coefficient in the constant drying rate period	173
Appendix J:	Curve fitting of simulated and experimental results from the color measurement tests	175

List of tables

Table 1.1	Color value ranges of bright white or white-colored hard maple desired by the industry measured with spectrophotometer (adapted from Smith and Montoney 2000) and colorimeter (adapted from Smith and Herdman 1998).	8
Table 1.2	Characteristics of wood stain (adapted from Hon and Shiraishi 2001).	11
Table 1.3	Experimental parameters drying Scot pine, Norway spruce and birch (adapted from Sundqvist 2002a).	23
Table 1.4	Drying for birch wood in constant temperature and RH conditions from IMC to below 20% M (adapted from Stenudd 2004).	26
Table 1.5	Kiln schedules for 32-mm- (5/4-in.-) thick samples dried from green to 7% M (adapted from Stenudd 2004).	28
Table 1.6	Drying thick birch wood at different ‘critical’ temperature levels in the capillary phase from green to 55% M (adapted from Stenudd 2004).	29
Table 2.1	One-step drying schedules used for paper birch or sugar maple sapwood specimens from green to final dry condition.	50
Table 2.2	Setpoints of water baths for the drying tunnel for specific drying conditions...	50
Table 3.1	Comparison of target and measured kiln conditions for wood color tests.	66
Table 3.2	Drying rate values obtained during wood color tests.	66
Table 3.3	Regression parameter estimates for the fixed part of the random coefficient model for the wood lightness of paper birch for different drying conditions. ...	79
Table 3.4	Regression parameter estimates for the fixed part of the random coefficient model for the wood lightness of sugar maple at different drying conditions. ...	80
Table 3.5	Coefficient of determination R^2 (%) values for the separate regression equations of wood lightness for the six drying conditions of paper birch and sugar maple.	81
Table 3.6	Regression parameter estimates for the fixed part of the random coefficient model for 3T global equations of paper birch.	84
Table 3.7	Regression parameter estimates for the fixed part of the random coefficient model for 3T global equations of sugar maple.	85
Table 3.8	Regression parameter estimates for the fixed part of the random coefficient model for 2T global equations of paper birch.	88
Table 3.9	Regression parameter estimates for the fixed part of the random coefficient model for 2T global equations of sugar maple.	88
Table 3.10	Summary of the results of the M- ψ determinations for paper birch.	91
Table 3.11	Summary of the results of the M- ψ determinations for sugar maple.	92

Table 3.12	Experimental and calculated temperature coefficients for the $M-\psi$ relationship of sugar maple obtained in the present study in comparison of those reported by Defo et al. (1999a).	95
Table 3.13	Convective mass transfer coefficients of paper birch and sugar maple for wood drying during the constant drying rate period.	101
Table F.1	Separate regression models of wood lightness for the six drying conditions of paper birch and sugar maple.	153
Table F.2	Wood color 3T sub-global equations for the lightness on and below the wood surface of paper birch and sugar maple at two wet-bulb depressions.....	156
Table G.1	Separate regression models of wood lightness for the four drying conditions of paper birch and sugar maple at 60 and 80°C (This table is a part of Table F.1)	161
Table G.2	Wood color 2T sub-global equations for the lightness on and below the wood surface of paper birch and sugar maple at two wet-bulb depressions.....	164

List of figures

Figure 1.1	A portion of the electromagnetic spectrum showing the relationship of the visible region to other types of radiation (adapted from Hon and Shiraishi 2001).	4
Figure 1.2	The transformation of color spaces from CIEL*a*b* to L*C*h. <i>To the left:</i> The color sphere where the cross-section at $L^* = 50$ is shown. ΔE^*_{ab} is the distance between two colors (points). <i>To the right:</i> The cross-section at $L^* = 50$ showing the axes from green to red (a^*) and from blue to yellow (b^*), and the coordinates of C^* and h (adapted from Sundqvist 2002b).	6
Figure 1.3	Scanned transverse plane color images of hard maple dried at 43°C(110°F), 9% EMC (equilibrium moisture content), from 0.5 through 12 days; the increasing black areas with drying time were due to tangential shrinkage (adapted from Yeo and Smith 2004).	8
Figure 1.4	Lightness after kiln-drying plotted against initial moisture content for pre-dried 20- by 100-mm samples dried at 51°C and 75% relative humidity (RH) (adapted from Stenudd 2004).	17
Figure 1.5	Interior transverse surface L*a*b* color values of hard maple during drying at 32°C(90°F), 35°C(95°F), 38°C(100°F), 41°C(105°F), 43°C(110°F), 54°C(130°F), and 66°C(150°F) (adapted from Yeo and Smith 2004).	19
Figure 1.6	Drying schedules. Charge 1: ventilation was set to 100% (about 5 m/s) from heating up to 25 ~ 30% M and under that to 70%. Charge 2: ventilation was set to 40% from heating up to 25 ~ 30% M and under that to 20%. Charge 3: ventilation was the same as that in charge 2. DF = drying force, T = temperature, EMC = equilibrium moisture content (adapted from Luostarinen and Luostarinen 2001).	20
Figure 1.7	Schematic view of position in cross-section when taken from a small-diameter log, 50 by 100 mm board. Two sides of the board are defined as outer side and inner side (adapted from Sundqvist 2002a).	22
Figure 1.8	Schematic plot of the drying design. T = dry-bulb temperature; ΔT = wet-bulb depression; t = times elapsed. Index 1 belongs to the capillary phase (I) and index 2 to the diffusion phase (II) (adapted from Sundqvist 2002a).	22
Figure 1.9	Partial least square model. Color of kiln-dried birch planed 3 mm. 'I' is inner side and 'O' is outer side. Numbers denote run number (adapted from Sundqvist 2002a).	24
Figure 1.10	A relationship between the wood lightness (average value presented by horizontal bar) and the capillary phase temperature after kiln-drying 32 by 100 mm (5/4 by 4 in.) samples (adapted from Stenudd 2004).	29
Figure 1.11	Moisture content-water potential relationship of red pine sapwood along the boundary desorption curve at 18, 56 and 85°C (adapted from Tremblay et al. 1996).	37

Figure 1.12 Moisture content-water potential relationship of sugar maple sapwood at 40 and 60°C from green to dry conditions and boundary drainage curve at 21°C (adapted from Defo et al. 1999a).	37
Figure 1.13 Effective water conductivity of red pine sapwood along the boundary desorption curve in the radial (K_R) and tangential (K_T) directions at 18, 56, and 85 °C (Tremblay et al. 2000a).	40
Figure 1.14 Correction factor for the convective mass transfer coefficient for aspen sapwood at 20(♦), 35(▲) and 50°C(●) (adapted from Cloutier et al. 1992).	42
Figure 1.15 Convective mass transfer coefficient vs. the wood surface M at 56°C and air velocities of 1.0, 2.5 and 5.0 m s ⁻¹ (adapted from Tremblay et al. 2000b).	43
Figure 1.16 Convective mass transfer coefficient vs. the wood surface M at 90°C and air velocities of 1.2, 2.2 and 5.0 m s ⁻¹ (adapted from Nabhani et al. 2003).	43
Figure 1.17 Effect of air velocity and temperature on the convective heat and mass transfer coefficients at the constant drying rate period (adapted from Nabhani et al. 2003).	44
Figure 2.1 Experimental drying tunnel setup including a drying chamber (a), a vapor saturator (b), two thermostatic water baths (c), and temperature data acquisition system (d).	49
Figure 2.2 Schematic drawing of the temperature control board and thermocouples used to measure the temperature profile through thickness.	51
Figure 2.3 a) Setup to cut the 32-mm in diameter plug from the M&C control board; b) one M&C control board with the initial 32-mm in diameter plug removed and the hole fitted with a dummy plug.	52
Figure 2.4 a) Slicing device in action; b) Slices removed from the 32-mm in diameter test plug.	52
Figure 2.5 A stack of boards as seen from the open door of the drying chamber.	53
Figure 2.6 A moisture content and color control board being removed five plugs and filled with varnished dummy plugs.	54
Figure 2.7 Color-guide 45/0 spectrophotometer made by BYK-Gardner and the CIEL*a*b* coordinate system.	55
Figure 2.8 An interface showing model parameters to be filled in the DRYTEK code before a simulation.	56
Figure 2.9 An interface showing drying schedule to be filled in the DRYTEK code.	57
Figure 2.10 Schematic diagram of the pressure membrane apparatus (adapted from Tremblay et al. 1996) with the temperature acquisition system.	59
Figure 3.1 Drying curves measured from three M control boards during the six color tests on paper birch.	67
Figure 3.2 Drying curves measured from three M control boards during the six color tests on sugar maple.	68

Figure 3.3	Moisture content profiles through the board thickness of paper birch at five different drying times during drying at six different drying conditions.	71
Figure 3.4	Moisture content profiles through the board thickness of sugar maple at five different drying times during drying at six different drying conditions.	72
Figure 3.5	Wood lightness profiles through the board thickness of paper birch at five different times during drying at six different drying conditions.	74
Figure 3.6	Wood lightness profiles through the board thickness of sugar maple at five different times during drying at six different drying conditions.	75
Figure 3.7	M- ψ relationship of paper birch sapwood at 40, 60 and 80°C from green to dry conditions. The water potential values near or below the FSP were calculated according to the data obtained by Djolani (1970) and Keylwerth and Noack (1964).	93
Figure 3.8	M- ψ relationship of sugar maple sapwood at 40, 60 and 80°C from green to dry conditions. The water potential values near or below the FSP were calculated according to the data obtained by Djolani (1970), Keylwerth and Noack (1964) and Defo et al. (1999a).	93
Figure 3.9	Effective water conductivity of paper birch at 40, 60 and 80°C from green to dry conditions: (a) radial direction (K_R); (b) tangential direction (K_T).	96
Figure 3.10	Effective water conductivity of sugar maple at 40, 60 and 80°C from green to dry conditions: (a) radial direction (K_R); (b) tangential direction (K_T).	97
Figure 3.11	Comparison of the effective water conductivity of paper birch sapwood in the radial (K_R) and tangential (K_T) directions from green to dry conditions at 40, 60 and 80 C.	98
Figure 3.12	Comparison of the effective water conductivity of sugar maple sapwood in the radial (K_R) and tangential (K_T) directions from green to dry conditions at 40, 60 and 80 C.	98
Figure 3.13	Drying schedules obtained from the validation tests at $T_s = 70^\circ\text{C}$ and $\Delta T = 10^\circ\text{C}$	104
Figure 3.14	The evolution of the M profiles measured during drying at $T = 70^\circ\text{C}$ and $\Delta T = 10^\circ\text{C}$	105
Figure 3.15	Comparison of the experimentally determined wood lightness profiles with the predicted values of the 2T statistical global wood color models for the validation drying test conducted at $T = 70^\circ\text{C}$ and $\Delta T = 10^\circ\text{C}$	107
Figure 3.16	Comparison of the drying curves simulated with with the DRYTEK code and those measured during the validation tests.	109
Figure 3.17	Comparison of the M profiles simulated with the DRYTEK code and those measured during drying at $T = 70^\circ\text{C}$ and $\Delta T = 10^\circ\text{C}$	110
Figure 3.18	Comparison of L^* profiles simulated using the integrated DRYTEK with the 2T global wood color models and those measured during the validation drying test at $T = 70^\circ\text{C}$ and $\Delta T = 10^\circ\text{C}$	112

Figure A.1	Drying schedules measured from the six wood color tests on paper birch.....	126
Figure A.2	Drying schedules measured from the six wood color tests on sugar maple. ...	127
Figure A.3	Wood temperature profiles measured from wood color tests on paper birch. .	128
Figure A.4	Wood temperature profiles measured from wood color tests on sugar maple.	129
Figure B.1	Wood a^* profiles through the board thickness of paper birch at five different times during drying at six different drying conditions.....	130
Figure B.2	Wood a^* profiles through the board thickness of sugar maple at five different times during drying at six different drying conditions.....	131
Figure B.3	Wood b^* profiles through the board thickness of paper birch at five different times during drying at six different drying conditions.....	132
Figure B.4	Wood b^* profiles through the board thickness of sugar maple at five different times during drying at six different drying conditions.....	133
Figure C.1	M-L* relationship on the wood surface of paper birch boards at five different drying times and at six different drying conditions.	134
Figure C.2	M-L* relationship at 6 mm below the wood surface of paper birch boards at five different drying times and at six different drying conditions.	135
Figure C.3	M-L* relationship at 10 mm below the wood surface of paper birch boards at five different drying times and at six different drying conditions.	136
Figure C.4	M-L* relationship on the wood surface of sugar maple boards at five different drying times and at six different drying conditions	137
Figure C.5	M-L* relationship at 6 mm below the wood surface of sugar maple board at five different drying times and at six different drying conditions.	138
Figure C.6	M-L* relationship at 10 mm below the wood surface of sugar maple boards at five different drying times and at six different drying conditions.	139
Figure F.1	Relationships between the regression coefficients in all separate equations for L^* values on the wood surface and the dry-bulb temperatures	154
Figure F.2	Relationships between the regression coefficients in all separate equations for L^* values below the wood surface and the dry-bulb temperatures.....	155
Figure F.3	Relationships between the regression coefficients in the 3T sub-global equations for L^* values on the surface of paper birch sapwood boards and the wet-bulb depression.	157
Figure F.4	Relationships between the regression coefficients in the 3T sub-global equations for L^* values on the surface of sugar maple sapwood boards and the wet-bulb depression.	158
Figure F.5	Relationships between the regression coefficients in the 3T sub-global equations for L^* values below the surface of paper birch sapwood boards and the wet-bulb depression.	159

Figure F.6 Relationships between the regression coefficients in the 3T sub-global equations for L^* values below the surface of sugar maple sapwood boards and the wet-bulb depression.	160
Figure G.1 Relationships between the regression coefficients in the separate equations for L^* values on the wood surface and the dry-bulb temperature from 60°C to 80°C.....	162
Figure G.2 Relationships between the regression coefficients in the separate equations for L^* values below the wood surface and the dry-bulb temperature from 60°C to 80°C.....	163
Figure G.3 Relationships between the regression coefficients in the 2T sub-global equations and the wet-bulb depression for L^* values on the surface of paper birch sapwood boards.	165
Figure G.4 Relationships between the regression coefficients in the 2T sub-global equations and the wet-bulb depression for L^* values on the surface of sugar maple sapwood boards.	165
Figure G.5 Relationships between the regression coefficients in the 2T sub-global equations and the wet-bulb depression for L^* values below the surface of paper birch sapwood boards.	166
Figure G.6 Relationships between the regression coefficients in the 2T sub-global equations and the wet-bulb depression for L^* values below the surface of sugar maple sapwood boards.	166
Figure I.1 Relationships between dry-bulb temperature and convective mass transfer coefficient for drying paper birch and sugar maple sapwood during the constant drying rate period.	173
Figure I.2 Relationships between wet-bulb depression and coefficients in the equations of convective mass transfer coefficients for drying paper birch and sugar maple sapwood during the constant drying rate period.	174
Figure J.1 Comparison of simulated and measured drying curves of paper birch.	175
Figure J.2 Comparison of simulated and measured drying curves of sugar maple.	176

Introduction

La couleur est une propriété importante des produits d'apparence du bois. Malheureusement, des colorations non souhaitables peuvent se produire dans l'arbre et au moment de sa transformation, notamment au cours du stockage des billes et des sciages verts ainsi qu'au cours du séchage. Les colorations peuvent également se développer en cours de service quand la lumière, l'eau ou les produits chimiques réagissent avec les surfaces exposées du bois. Alors que les variations naturelles de la couleur du bois sont parfois appréciées, les changements de couleur induits artificiellement le sont rarement. En général, l'industrie recherche une couleur uniforme, ce qui est dicté par les tendances du marché concernant l'utilisation des produits d'apparence. En effet, l'apparence esthétique de la surface du bois est de grande importance pour les espèces utilisées dans l'ameublement, les menuiseries et le plancher. C'est entre autres le cas pour le bouleau à papier et l'érable à sucre, deux espèces feuillues très répandues au Canada dont le bois d'aulx est beaucoup apprécié pour sa couleur pâle naturelle.

Généralement, la coloration du bois est considérée comme un défaut, que celui-ci se développe dans l'arbre vivant, au cours du stockage du bois vert, du séchage ou autres traitements hygrothermiques. La coloration diminue la qualité et la valeur du bois, augmente les coûts de production et les pertes financières suite à l'augmentation de la fréquence des plaintes des clients sur la qualité du produit fini (Straze et al. 2003). L'aulx

du bouleau à papier peut brunir lorsque séché artificiellement. L'aubier de l'érable à sucre est sujet également au noircissement lorsque séché à des températures trop élevées. La blancheur de l'aubier est souvent une caractéristique recherchée de ces deux espèces, et le brunissement ou noircissement réduit leur valeur commerciale. Puisque la couleur du bois est sensible à la température du séchage artificiel, l'industrie s'est adaptée à ce problème en diminuant les températures de séchage. Une conséquence négative causée par la diminution des températures de séchage est l'augmentation du temps de séchage de 30 à 40%, et de là l'augmentation des coûts de production (Stenudd 2004). Même si plusieurs études ont été réalisées sur le sujet, la coloration du bois au cours du séchage artificiel demeure encore un phénomène complexe plus ou moins bien compris (Dawson-Andoh et al. 2004, Hiltunen et al. 2004).

La coloration du bois est directement reliée à la composition chimique des cellules du bois, en particulier les extractibles de nature phénolique. Certains extractibles sont solubles dans l'eau, d'autres ne le sont pas. Le mouvement de ces produits chimiques peut être relié au mouvement de l'eau dans le bois au cours du séchage. De plus, la température est un facteur clé de la plupart des réactions chimiques. Il y aurait donc des gammes de températures et de teneurs en humidité particulièrement propices au développement des colorations du bois au cours du séchage.

L'objectif ultime de cette étude était de développer un modèle de prédiction des changements de couleur dans l'aubier du bouleau à papier et de l'érable à sucre dans des conditions hygrothermiques représentatives du séchage à moyenne température. Les paramètres du modèle sont la température sèche de l'air, la dépression au thermomètre humide, ou l'humidité relative, la teneur en humidité du bois, et la position dans l'épaisseur de la planche sous la surface. Un modèle statistique de la couleur du bois a été développé et alors combiné à un modèle existant de transfert de masse et de chaleur de façon à prédire les changements de couleur du bois pour tout programme de séchage à moyenne température utilisé dans l'industrie.

Chapter 1. Background and literature review

1.1 Color of wood

1.1.1 Mechanism of color recognition

Wood absorbs and reflects light. This kind of physical interaction makes the color of wood ranging from almost white, as in the sapwood of many species, to almost black, as in the heartwood of black ebony. Light is not colored. Color is recognized only when a ray of light enters the eyes and is absorbed by cones and rods, the light sensitive receptor cells in the retina (Hon and Shiraishi 2001).

Visible light, which produces the visual sense for human eyes, is part of an electromagnetic wave. Its wavelength ranges from 380 to 780 nm, as shown in Figure 1.1. Ultraviolet (UV) light is at the lower end and infrared (IR) light at the upper end. Visible sensitivity varies with wavelength. When visible light strikes an object, if all the light is reflected, we recognize the object color as white. If no scattering occurs it is recognized as a mirror-like surface. In contrast, when all the light is absorbed, we recognize the color as black. Most materials absorb certain wavelengths and reflect the rest. The reflected light is recognized as a color, which is dependent on the composition and amount of the reflected light. For example, the reflection of wavelengths longer than 590 nm produces an orange color (Hon and Shiraishi 2001).

Absorption of light by a material excites its electrons. Generally, electrons are in the lowest energy state or ground state. If adequate energy is absorbed by the electron from outside, the electron will transit to a higher energy state, or excited state. Light is an aggregate of photons that have energy, so depending on its wavelength, it can provide the energy necessary for electron excitation and transition. The electron of an unsaturated bond (e.g. $>C=C<$, $>C=O$, $>C=NH$) can transfer easily to an excited state with a small amount of energy. An atomic group having π electron, such as an unsaturated bond, is called a chromophore. These molecules have base structures with conjugated double bonds and chromophoric groups (e.g. carbonyls). The conjugated double bonds enable the delocalization of electrons, i.e., loosely bound electrons which can be easily excited by photons with the energy in the visible region of light (Hon and Minemura 1991). Another type of chromophore is phenolic compounds that are complex bonded to metal ions and form complexes that strongly absorb light (Falkehag et al. 1966). An atomic group having isolated electron pairs, such as $-OH$, $-COOH$, and $-OR$, is called an auxochrome. Auxochromes assist the action of chromophores by intensifying the coloration or enabling the absorption of light having a longer wavelength (Hon and Shiraishi 2001).

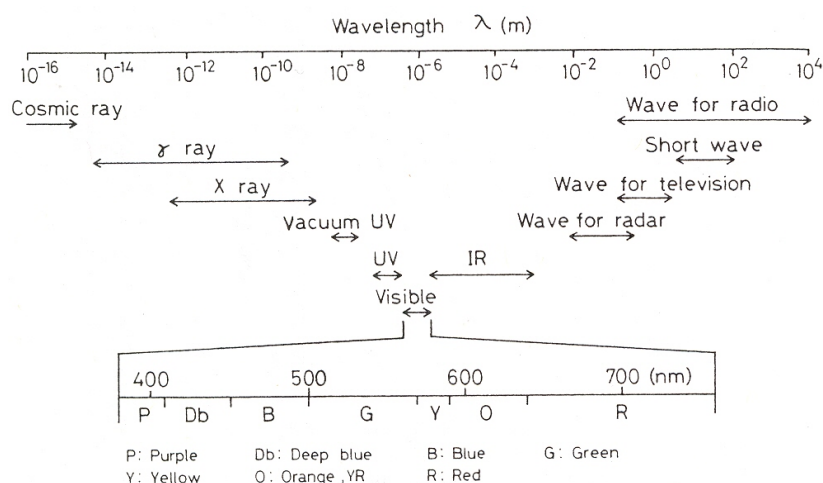


Figure 1.1 A portion of the electromagnetic spectrum showing the relationship of the visible region to other types of radiation (adapted from Hon and Shiraishi 2001).

1.1.2 Representation and determination of color

Color is mainly evaluated visually in the majority of wood using industry. But color is affected by the ambient light source and individual human perception. Therefore, mechanical color analysis is often used by industries which must produce consistent color (Rappold and Smith 2004). The reflection curve in the visible region most accurately represents the color of a material. In addition, the numerical representation of color can be derived by two methods. One is based on a comparison with a color specimen whose various colors are classified and numbered. Another is based on trichromatic quality, which means that any color can be made by mixing three other colors. Color specification systems such as XYZ, RGB, L^*C^*h , $L^*a^*b^*$, and UVL have been used to determine trichromatic quality (Hon and Shiraishi 2001).

The CIE (Commission Internationale d'Eclairage) 1976 $L^*a^*b^*$ color space system is the color space system which most nearly models human color perception (Brunner et al. 1990). It has often been used to measure the color of wood. This system quantifies color based on the opponent theory of color vision, which states that colors cannot be perceived as both green and red at the same time, or blue and yellow at the same time. Colors are perceived as combinations of green and blue, green and yellow, red and blue, and red and yellow. Using the three-dimensional CIE $L^*a^*b^*$ color space, each color can be expressed as a point in the Euclidean space defined by three coordinates correlating with subjective color perception (Figure 1.2). Coordinate L^* for lightness represents the position on the black-white axis ($L = 0$ for black, $L = 100$ for white), while the chroma value a^* defines the position on the red-green axis ($-a^*$ indicating green and $+a^*$ indicating red), and b^* the position on the yellow-blue axis ($-b^*$ indicating blue and $+b^*$ indicating yellow). Loss of lightness is observed as a smaller value of L^* . The larger the value of a^* , the more red chroma is observed, and large b^* values represent a strong presence of yellow chroma. On the negative sections of the chroma scales a^* and b^* , an intense green color is expressed with a great negative value of a^* , and for a bright blue, b^* becomes large with a negative sign. Zero values for a^* or b^* denote absence of redness/greenness or yellowness/blueness (Billmeyer and Saltzman 1981).

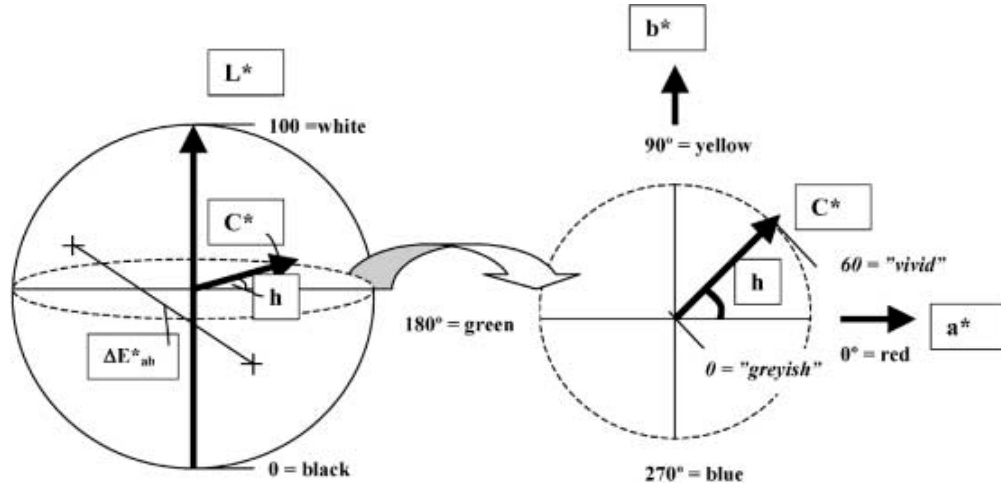


Figure 1.2 The transformation of color spaces from CIEL*a*b* to L*C*h. *To the left:* The color sphere where the cross-section at $L^* = 50$ is shown. ΔE^*_{ab} is the distance between two colors (points). *To the right:* The cross-section at $L^* = 50$ showing the axes from green to red (a^*) and from blue to yellow (b^*), and the coordinates of C^* and h (adapted from Sundqvist 2002b).

In order to relate actual differences in color values to visually perceived differences, one method was developed that the color metric difference ΔE^*_{ab} (Billmeyer and Saltzman 1981) is expressed as the Euclidean distance between two points in the color coordinate system,

$$\Delta E^*_{ab} = \sqrt{(L^*_2 - L^*_1)^2 + (a^*_2 - a^*_1)^2 + (b^*_2 - b^*_1)^2} \quad [1.1]$$

where $L^*_1 a^*_1 b^*_1$ and $L^*_2 a^*_2 b^*_2$ stand for the coordinates of colors.

The smallest color difference still distinguishable to the human eye in agricultural or horticultural applications is for the values of ΔE^*_{ab} ranging between 1.0 and 3.0 (Voss and Hale 1998). Terziev and Boutelje (1998) and Mononen et al. (2002) considered a color metric difference $\Delta E^*_{ab} = 2$ sufficient to convey visually perceivable color differences. Also, they suggest that color metric differences may vary between wood species and can be dependent upon colorimetric variables.

Moreover, the CIEL*a*b* coordinates can be transformed into CIEL*C*h coordinates according to Equations [1.2] and [1.3]:

$$C^* = \sqrt{a^{*2} + b^{*2}} \quad [1.2]$$

$$h = \arctan\left(\frac{b^*}{a^*}\right) \quad [1.3]$$

where C^* stands for the chroma or saturation where 0 represents only greyish colors and 60, for instance, represents very vivid colors. h stands for the hue of a color; described in degrees where 0 or 360 degrees is red, 90 degrees is yellow, 180 degrees is green and 270 degrees is blue (Hunt 1991). The CIEL*C*h system is suitable for industrial purposes (Hunt 1998).

There are two methods of determining color mechanically: by determining the percentage of spectral reflectance and by reading tristimulus values directly. A spectrophotometer and standard white plate of magnesium oxide or magnesium carbonate are used for the former method. The whiteness of the white plate is considered to be 100%. Relative spectral distribution to it is shown by the reflectance curve in the visible region. The proportion of up-and-down areas of the curves relates to lightness. The upper part of the curve means high lightness. A photoelectric colorimeter is used for photoelectric tristimulus colorimetry. A test specimen is irradiated with a xenon light, the reflected light is collected with an integrative globe that leads to the XYZ light receiver, and it is converted to electric current by a photocell to indicate the numerical value (e.g. L*a*b* values) (Hon and Shiraishi 2001). Generally, the spectrophotometer and colorimeter were used with the D65 (daylight, 6500 K-color temperature) light source illumination (Bekhta and Niemz 2003, Yeo and Smith 2004), or wide-area-illumination, illuminant C (Stenudd 2004), and 10° observer (Bekhta and Niemz 2003) and specular included option (Yeo and Smith 2004), 2° (standard observer CIE 1931), or 0° over a Ø50 mm circular area (Stenudd 2004).

Smith and Herdman (1998) and Smith and Montoney (2000) have evaluated the color of hard maple wood with spectrophotometers or colorimeters and presented data using the CIEL*a*b* color coordinates as shown in Table 1.1. Surfaced bright white or white-

colored hard maple desired by the industry can be defined as having the range of color values.

But, with the present-day status of technology even spectrophotometric or colorimetric color description is of limited practical significance. Therefore, Yeo and Smith (2004) obtained color data via imaging with a flat-bed scanner (HP Scanjet 5370C, Hewlett-Packard Co.) as supplement. Figure 1.3 shows a representation of the results obtained.

Table 1.1 Color value ranges of bright white or white-colored hard maple desired by the industry measured with spectrophotometer (adapted from Smith and Montoney 2000) and colorimeter (adapted from Smith and Herdman 1998).

Color measurement instruments	surfaced white-colored hard maple			surfaced bright white hard maple		
	L*	a*	b*	L*	a*	b*
Spectrophotometer	79 ~ 88	3 ~ 7	14 ~ 19	n/a	n/a	n/a
Colorimeter	81 ~ 83	1.5 ~ 3	17 ~ 19	82 ~ 87	0.5 ~ 1.5	15 ~ 17

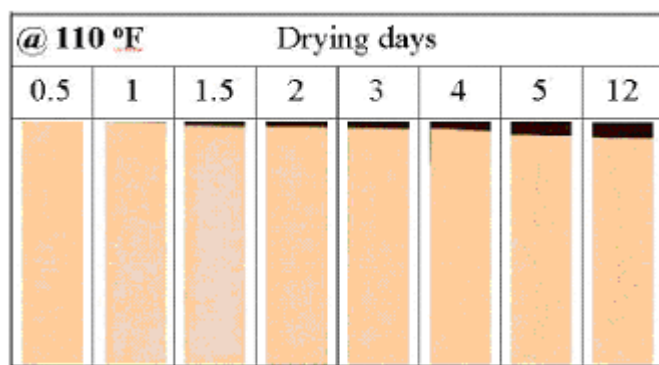


Figure 1.3 Scanned transverse plane color images of hard maple dried at 43°C(110°F), 9% EMC (equilibrium moisture content), from 0.5 through 12 days; the increasing black areas with drying time were due to tangential shrinkage (adapted from Yeo and Smith 2004).

1.1.3 Characteristics of wood color

1.1.3.1 Coloring substances of wood

The color of wood depends on the chemical components in wood that interact with light. The main structural materials in wood are cellulose, hemicelluloses and lignin. Cellulose is the most abundant component in wood as the skeleton, namely 40 ~ 50% of the dry weight in both softwoods and hardwoods. Hemicelluloses are the matrix of wood accounting for about 20 ~ 35% of the dry weight. Hemicelluloses are polysaccharides with much lower molecular weight than cellulose. Lignins are three-dimensional polymers as encrusting substance binding wood cells together. The amount of lignin ranges from 20 to 25% in hardwood and 25 to 35% in softwood. In addition, heartwood contains many low-molecular-weight organic compounds known as extractives or extraneous substances. These are commonly located in the lumens but may also occur in the cell wall as in *Sequoia sempervirens*. The content of extractives in wood may vary from 0 to 25% by weight. Inorganic constituents or ash seldom exceed 0.1 to 0.5% (Siau 1984; Siau 1995; Cloutier 2005).

Cellulose and hemicelluloses only scatter visible light but do not absorb visible light, and they would alone most likely give a greyish appearance. Native lignins isolated with minimum chemical or physical changes are pale yellow. It is assumed that lignin absorbs wavelengths below 500 nm. Moreover, many woods absorb light beyond 500 nm by phenolic extractives, such as tannin, lignan, flavonoids, stilbene and quinone. Generally, sapwood has a lighter color than heartwood. The transition of sapwood into heartwood is accompanied by the formation of various organic substances with darker color. Most colored materials extracted from rosewood and ebony are presumably high-molecular-weight pigments which are insoluble in solvent while some low-molecular-weight pigments also exist (Hon and Shiraishi 2001).

1.1.3.2 Physical factors affecting wood color

Wood is extremely nonhomogeneous. Its structural and chemical variability is reflected in wide ranges in its physical properties such as permeability, capillary behavior, thermal

conductivity, and the diffusion of bound water (Siau 1984). Naturally, the surface of wood is not uniform. It is composed of cells of various sizes, which, along with the difference of components, causes delicate differences of color even on the same wood surface.

When light is irradiated on the surface of wood, one part is reflected directly and the other part enters wood cells containing voids and pigments. The pigments will absorb some wavelengths of the entering light. The light that is not absorbed by the cells is emitted again through scattering, reflection and transmission. Finally, we recognize the unabsorbed light as the wood color.

Wood cells are slender in shape and arranged in layers in one direction. Therefore, the wood color can be slightly different according to the irradiating direction of the light. Lightness is lowest when the progression of an incident light is in the direction of the wood fiber. It is highest when the incident light crosses the wood fiber at a right angle because the quantity of the light that reflects and scatters on the surface without penetration into a wood cell might become larger. The behaviors of a^* and b^* are contrary to that of lightness. Therefore, saturation is lowest when the light meets wood fiber at right angles. The hue does not change (Hon and Shiraishi 2001).

Stokke et al. (1995) investigated the effect of grain angle of white oak on lightness values. Lightness readings were significantly different along the grain versus across the grain. Lightness obtained along the grain had an average of 60.4 (standard deviation 3.81) while the average of lightness taken across the grain was 64.9 (standard deviation 3.82). However, there was some correlation between them. Moisture content in wood also affects wood color. Hon and Shiraishi (2001) report that, when a wood cell cavity is filled with water, incident light can transmit deep into the cell but scatter slightly in the cell wall. This kind of wood color is called wetting color. Lightness may be at times lower in unseasoned wood than in seasoned wood. For instance, it was shown that the lightness of a sample of green Todomatsu sapwood with 175% M (moisture content) was 68.9 while the lightness increased to 80.9 after drying at room temperature. The wetting color is thought to be similar to the color of wood coated with a clear paint.

The roughness of surface affects the color of wood too. If the wood surface is even, the reflectance and scattering of light on the surface become larger, causing the lightness to rise (Hon and Shiraishi 2001).

1.2 Chemistry of wood discoloration

1.2.1 Types of wood discoloration

Wood may discolor when it is decomposed by microorganisms as a biological material, or reacts chemically with substances such as metal ions, acid and alkali. Water-soluble substances or salts are often deposited in the voids of wood during the growing of tree or after logging and then change the color of wood. Table 1.2 summarizes the characteristics of discoloration according to the influencing factors (Hon and Shiraishi 2001). Biological discolorations have been understood and prevented very well (Zink and Fengel 1988).

Table 1.2 Characteristics of wood stain (adapted from Hon and Shiraishi 2001).

Classification			Cause of stain	Example
After logging	Addition of source of stain from the outside	Biological source	Propagation of microorganism	Blue stain
		Chemical source	Bonding of metal ion	Iron stain
			Bonding of acid	Reddish discoloring of zelkova
			Bonding of alkali	Adhesion of cement
		Physical source	Heating	Sticker mark
			Irradiation of light	Discoloration by sunlight
	Immanence of source of stain		Metal ion	Blackish discoloring of sugi
			Enzyme	Red discoloration of alder
			Resin	Exudation of resin
In shade			Imperfect pruning	Brown stripes
			Deposition of substance	Existence of specks

1.2.2 Chemical analysis of wood discoloration during drying

Wood discoloration during drying is a poorly understood complex process (Dawson-Andoh et al. 2004). The chemistry of this type of discoloration is also poorly documented (Luostarinen and Möttönen 2004). Oxidative and hydrolytic reactions are mainly considered to be the cause for production of chromophores during thermal treatment of wood, where hydrolytic reactions generally are the dominant process when moisture is present (Fengel and Wegener 1984).

The phenolic extractives have been widely studied in relation to the natural color of wood (Sundqvist 2002b). The formation of colored substances from a phenolic compound oxidized with air and the formation of dark material from hydrolysis of hemicellulose have been considered the causes of discoloration in artificial seasoning of todomatsu (Millett 1952). In brown stain of oak, colored polyphenolic polymers and complex esters, hexahydroxydiphenolesters are found in larger amounts than in non-stained wood. Discoloration during kiln drying may be the result of hydrolysis and oxidative transformation of ellagitannins (Charrier et al. 1995). Concerning sticker stain in sugar maple, the amount of acetone-water-soluble materials in the stained part was less than in the clear part. This suggests that phenolic extractives accumulated under the sticker stain during drying and then oxidized to insoluble polyphenolic compounds (Miller et al. 1990). In western hemlock, *d*-catechin polymerizes oxidatively to give an insoluble polymer and to cause the brightness loss (Hrutford et al. 1985). The oxidation and condensation of phenolic extractives of wood are known to produce insoluble colored compounds, which are seen in wood as discoloration. Luostarinen and Möttönen (2004) found a correlation between proanthocyanidin (condensed tannins) concentration and color of birch wood in mature birch trees. Fuentealba et al. (2008) came to a similar conclusion for paper birch.

McMillen (1975), Forsyth and Amburgey (1991) and Wengert (1992) stated that changes in natural color of hard maple occurred as a result of chemical reactions that take place between naturally occurring precursors to stain formation (phenolic extractives) and enzymes present in the wood. These enzyme-mediated processes began in viable parenchyma cells where tiny globules of amorphous material accumulated and occluded the

cell lumens. This material subsequently turned dark upon exposure to high temperatures and slow drying conditions. The darkening was similar to oxidative browning of freshly sliced fruits and vegetables (Yeo and Smith 2004). Chemical precursors and enzymes move and concentrate on the lumber surface as a result of the moisture content gradient between the surface and interior regions of the wood (Dawson-Andoh et al. 2004). Because the reactivity of oxygen in liquid water is higher than in air, Yeo and Smith (2004) believed that the increased darkening at elevated temperature when above the fiber saturation point (FSP) was due to this higher oxygen reactivity with high temperature, resulting in an increase in the oxidation of naturally present chemicals in the wood. Accelerated kiln drying without oxygen can prevent discoloration in European oak (Charrier et al. 1992).

Besides phenolic extractives, degradation products from hemicelluloses and lignin resulting from thermal treatment, for example, can also be a reason for coloring processes. Increased extractive content is believed to be a result of hemicellulose degradation during pressure steam drying (McGinnes and Rosen 1984). The presence of arabinose in extraction from kiln dried radiata pine is believed to be a result of hemicellulose degradation (Kreber et al. 1998). In thermally treated beech and Scots pine, the liberation of acetic acid is a result of hemicellulose degradation, and acetic acid catalyses further lignin degradation (Tjeerdsma et al. 1998).

Furthermore, nutritive compounds such as simple sugars and amino acids have been observed to redistribute towards the surface in wood during thermal treatment, accumulating 0.5 ~ 1.5 mm below the surface to produce discoloration (Millett 1952, King et al. 1976, Theander et al. 1993). The redistribution has been investigated in Scots pine (Terziev 1995), radiata pine (Kreber et al. 1998). Kiln brown stain in radiata pine (*Pinus radiata*) sapwood may be caused by an Amadori-Maillard reaction between low-molecular sugars such as fructose, sucrose, or glucose and glutamatic acid (Kreber et al. 1998).

1.3 Effect of harvest season, storage and growing site on wood color

1.3.1 Fresh wood

In temperate zones, trees undergo seasonal changes, which are most obvious in deciduous wood species because of defoliation in fall. Metabolism of trees is reduced during the winter season and this is reflected in a decrease in water uptake and sap flow. These seasonal changes also influence the composition of certain compounds in living trees (Kreber and Byrne 1994). For example, extractives possibly involved in discolorations of hem-fir lumber were also shown to undergo seasonal changes in living western hemlock trees (Barton and Gardner 1966).

Mononen et al. (2002) found that the color of fresh wood of silver birch (*Betula pendula*) depends on the felling season. All fresh samples felled in autumn or in winter displayed high lightness ($L^* > 83.23$), low redness ($a^* < 3.69$) and average yellowness ($b^* = 19.63 \sim 26.90$). Spring- and midsummer-felled samples went into another category having lower lightness ($L^* < 71.93$), higher redness ($a^* > 6.32$) and higher yellowness ($b^* > 26.31$). Luostarinen et al. (2002) also found that felling date affected the color of fresh silver birch wood. But, differences in the color of fresh and unstored wood were limited only to lightness, the wood L^* values of summer-, winter-, autumn- and spring-felled trees were 87.7, 87.6, 87.3 and 86.6 respectively, so that the wood of spring-felled trees was the darkest.

After the logs had been stored for 5 or 10 weeks, a very considerable color change was observed for samples taken from autumn- and winter-felled silver birch trees (Mononen et al. 2002). After five weeks of outside storage in the open air, autumn-felled and winter-felled samples had a significant decrease in lightness ($L^* = 67.51 \sim 72.21$) as well as an increase in redness ($a^* > 7.34$) and yellowness ($b^* > 27.93$); furthermore, the total color difference compared with the corresponding fresh and unstored samples was $\Delta E^*_{ab} > 16.49$. But the color of spring-felled samples was not changed considerably, where $\Delta E^*_{ab} < 2.19$. Samples felled in midsummer showed a decrease in lightness and a small increase towards red and yellow chroma, and $\Delta E^*_{ab} < 2.95$. As an exception, after 10 weeks of

storage, the color of autumn felled samples was changed towards white with diminishing chromaticity, and $\Delta E^*_{ab} = 3.52 \sim 7.65$. Winter-felled samples lost their lightness but they became redder and more yellow, where $\Delta E^*_{ab} > 17.52$. The samples taken from trees felled in spring and midsummer had a slight decrease in lightness, a minor increase in redness and a moderate decrease in yellowness, where $\Delta E^*_{ab} = 6.23 \sim 14.04$. However, Möttönen and Luostarinen (2001), Luostarinen et al. (2002) and Möttönen (2005) did not find that the storage period influenced the color of fresh wood.

Growing site slightly affected the fresh silver birch wood (Luostarinen et al. 2002). The color was slightly lighter and also less red and yellow in the fresh wood of trees from the medium fertility MT-site (Myrtillus-Type) than in trees from the low fertility VT-site (Vaccinium-type) mineral soil. The effect of growing site on wood color may depend on the different proportions of early wood at different sites. The chemical composition of wood also differs between sites (Luostarinen et al. 2002).

1.3.2 Dried wood

Fresh and stored birch wood (moisture content 70 ~ 100%) always had a lighter color than dried wood (Luostarinen et al. 2002). Factors such as felling date, length and season of storage, and climatic conditions before felling were thought to affect discoloration in wood during drying (Kreber and Byrne 1994). But, compared to drying conditions, they have lower effects (Luostarinen et al. 2000).

Felling date slightly affected the color of conventionally and vacuum dried birch wood in the study of Luostarinen et al. (2002) and Möttönen (2005). Regardless of drying methods, birch wood was the darkest in summer-felled trees and lightest in winter- and autumn-felled trees in conventionally dried and in vacuum-dried wood, respectively. With both drying methods, redness and yellowness of the inner wood of boards were greatest in summer-felled trees and lowest in autumn-felled trees. With room drying, all three color coordinates differed significantly between felling dates: the wood was lightest and both least red and least yellow if the trees were felled in winter. In addition, the felling date affected discoloration in vacuum drying differently than in conventional drying.

The storage of logs increased the intensity of discoloration during conventional drying of the wood from summer-felled and winter-felled trees (Möttönen 2005). Luostarinen et al. (2002) stated that the length of the storage period influenced the birch wood discoloration during drying only slightly, mostly by making the color lighter. However, the discoloration caused by storage was covered by the discoloration caused by drying.

Mononen et al. (2002) concluded that the original color of fresh wood and the change in color during storage did not affect the final color of dried boards. Similarly, no significant differences were found among samples taken from trees felled in different seasons. The colors of all dried boards in either a partial vacuum kiln or a conventional kiln were similar regardless of the felling season or duration of storage when taking all color coordinates into account. For discoloration of oak wood (*Quercus robur*, *Q. petraea*), Charrier et al. (1992) also found no difference between felling dates. Tarvainen et al. (2001) found that the felling time and wet storage slightly affected the color of dried timbers of Scots pine and Norway spruce.

In an investigation of Rappold and Smith (2004), hard maple trees were harvested in winter, spring, and summer. For each harvest season 1-inch boards were sawn from freshly cut logs, logs stored for 4 weeks, and logs stored for 8 weeks. They were kiln dried using USDA T8-C3 and T3-C5 drying schedules (Simpson 1991), and air-drying method. There was no visual difference in color between log age treatment groups. There were no visual or measured color changes across each harvest season between all of the measured variables.

No differences in discoloration during drying were found between birch wood felled in two growing sites (Luostarinen et al. 2002, Möttönen 2005). For discoloration of oak wood (*Quercus robur*, *Q. petraea*), Charrier et al. (1992) found that after artificial drying, oaks from different growing sites gave slightly different lightness values. Tarvainen et al. (2001) also found that there were no significant differences in dried wood color of Scots pine and Norway spruce harvested from fertile and poor sites.

1.4 Effect of moisture content on wood discoloration during drying

The initial moisture content (IMC) was found to be a significant factor but to a lesser extent for silver birch discoloration during drying from green to 20% M in the 30 to 60°C span (Stenudd 2001). In the study of Stenudd (2004), the major color-controlling phase of silver birch was during the diffusive drying phase (where free water is not present) in the 30 ~ 60°C span at low M levels, presumably in the 30 ~ 20% M range. When the initial moisture content was around FSP, it was shown to be an influential factor controlling the lightness of the wood. The relation was most apparent in only one of four settings. A reduction in initial moisture content increases the lightness (Figure 1.4). Furthermore, the effect of drying time and temperature on the wood color was related to the moisture content of wood. The time a local layer of wood was kept in the range of moisture content between approximately the FSP and 15 ~ 20% M was decisive for the final wood color. In the critical moisture content zones, increased temperature and prolonged drying time decreased the lightness and made the wood color more saturated and reddish.

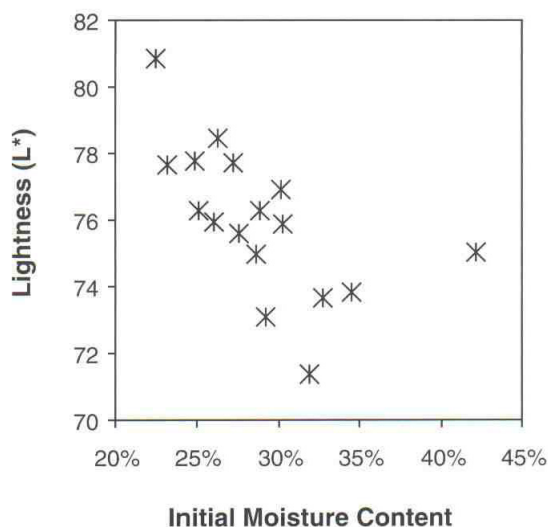


Figure 1.4 Lightness after kiln-drying plotted against initial moisture content for pre-dried 20- by 100-mm samples dried at 51°C and 75% relative humidity (RH) (adapted from Stenudd 2004).

This supports findings of Luostarinen et al. (2000, 2002) and Luostarinen and Luostarinen (2001). The timing of discoloration during conventional drying from green to 20 ~ 25% M at 38 ~ 42 °C and then at 60 ~ 65°C suggested that for silver birch wood there were two critical moisture content values: the first one was about 30% when the discoloration started; and the other was 18 ~ 20%, when the wood was at its darkest, again becoming lighter after that. As for beech (*Fagus sylvatica* L.), another common light colored hardwood species, a brown red discoloration of the core occurred when the central parts of the wood dried down to 35 ~ 25% M during convection drying at about 40°C. Steep moisture gradients also seemed to enhance discoloration processes (Thomassen 1986). This indicates that the majority of the coloring process occurs when the local M dries below the FSP (Stenudd 2004).

However, according to Kreber et al. (1998) and Sundqvist (2002b), compared with the whole drying process, the color induced by drying was considered to be dominant when there was capillary water in the wood. Yeo and Smith (2004) also found that interior darkening develops in hard maple if temperatures were above 43°C (110°F) when the M was at and above the FSP, and that there was minimal color change when drying below the FSP. While drying at 43°C, interior darkening started after about 2 days, when the average M was about 25%, and core M was still above FSP. The darkening continued for 3 days, when average M was about 20% and expected core M was around FSP, and ended after about 5 days drying, when average M was about 15%, and core M was lower than FSP (Figure 1.5). One way ensuring the acceptably bright and light color of final kiln-dried wood was suggested as keeping the wood core temperature below 43°C until the wood core had dried below FSP.

Sundqvist (2002a) showed that capillary phase and diffusion phase were similarly important for the color change of Scots pine, Norway spruce and downy birch. It was assumed that not only hydrolysis but other mechanisms were important, since free water was not necessary for the production of colored compounds. Coloration of the wood occurred throughout the entire drying process. This agreed with the color study of kiln-dried Scots pine and Norway spruce by Wiberg (1996).

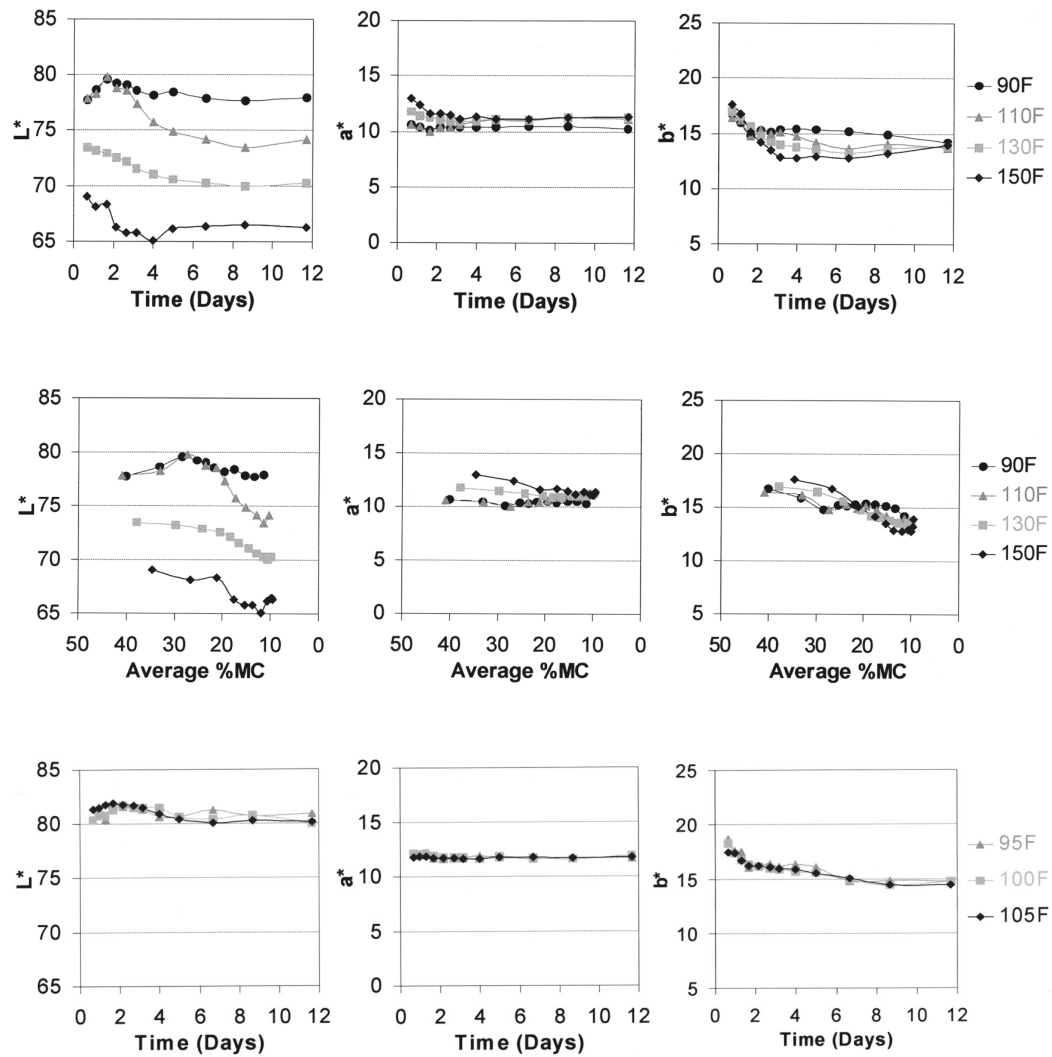


Figure 1.5 Interior transverse surface L*a*b* color values of hard maple during drying at 32°C(90°F), 35°C(95°F), 38°C(100°F), 41°C(105°F), 43°C(110°F), 54°C(130°F), and 66°C(150°F) (adapted from Yeo and Smith 2004).

1.5 Modelling of wood color with drying parameters

1.5.1 The effect of drying temperature

Kiln-drying is a process using heat and steam with air circulation; a kiln schedule is a series of dry- and wet-bulb temperatures that establish the temperature and relative humidity in the kiln and are applied at various stages of the drying process. Drying temperatures have generally increased in recent decades, mainly to speed up the process and lower energy consumption. Unfortunately, color changes often occur when temperatures are raised in industrial kiln drying. To reduce discoloration, it has been recommended that timber be

dried rapidly (low relative air humidity, high air velocity) at low temperature (Taylor 1997).

Luostarinen and Luostarinen (2001) studied the discoloration of birch (*Betula sp.*) parquet boards (30 × 75 × 1000 mm) during conventional drying. The drying schedules included a severe high temperature (charge 1) schedule with high air velocity, moderate temperature (charge 2) and low temperature (charge 3) schedules with low air velocity (Figure 1.6). The target M was set to 5.0%. During the drying processes, the color of the inner wood was measured several times by ripping and planing two boards. It was found that the warmer the conditions were, the darker the wood turned causing the light margins in the ripped boards to become narrower. The decrease in brightness is considerable while the change in saturation or hue is very small. In the study of Luostarinen et al. (2002), drying temperature seemed to be important for the final color of birch wood, which can be seen in the highest lightness of the room-dried boards at the temperature of about 20°C.

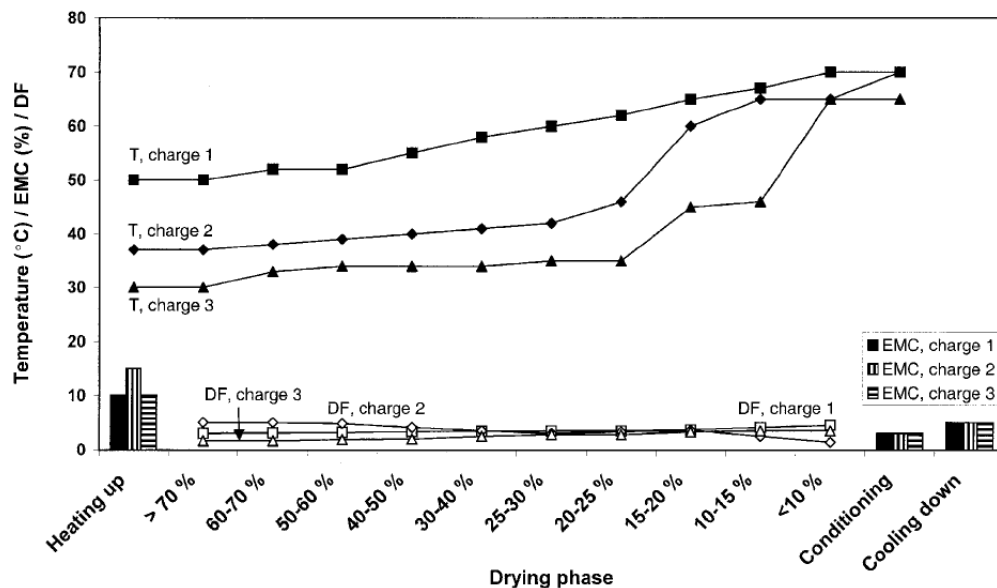


Figure 1.6 Drying schedules. Charge 1: ventilation was set to 100% (about 5 m/s) from heating up to 25 ~ 30% M and under that to 70%. Charge 2: ventilation was set to 40% from heating up to 25 ~ 30% M and under that to 20%. Charge 3: ventilation was the same as that in charge 2. DF = drying force, T = temperature, EMC = equilibrium moisture content (adapted from Luostarinen and Luostarinen 2001).

Temperature has also been observed to play an important role in discoloration of radiata pine (Kreber and Haslett 1997) and sugar maple (McMillen 1968). A drying schedule with an initial dry-bulb temperature of 43°C (110°F) or less and a wet-bulb depression of at least 10°F will produce white-colored hard maple lumber. Initial dry-bulb temperatures greater than 110°F will produce the normal orange-yellow colored hard maple lumber (Simpson 1991).

Further, Yeo and Smith (2004) demonstrated that the critical temperature causing interior darkening in hard maple (*Acer saccharum* Marsh.) lumber seems to be around 43°C. All-clear sapwood specimens (16 in. long) were cut from freshly sawn 4/4 in. × 4 in. × 9 ft boards and dried at 32°C (90°F)/44% RH (relative humidity), 35°C (95°F)/45% RH, 38°C (100°F)/46% RH, 41°C (105°F)/47% RH, 43°C (110°F)/48% RH, 54°C (130°F)/52% RH, and 66°C (150°F)/57% RH (9% EMC conditions), with 1 m/s air velocity in temperature and humidity controlled environmental chambers. The wood color was measured from the interior transverse surface of the 1 in. long samples periodically cut from the end of the specimens during drying. The results are shown in Figure 1.5. Drying below 43°C dry-bulb temperature did not result in any interior darkening. At 43°C, interior darkening started after about 2 days. However, drying above 43°C, resulted in core darkening quickly. Noticeably, L* values changed much more than a* or b* values. When dried at 54°C and 66°C, wood interior darkening occurred immediately.

Sundqvist (2002a) investigated and modelled the wood coloration of Scots pines (*Pinus sylvestris*), Norway spruce (*Picea abies*) and birch (*Betula pubescens* Ehrh.) during kiln-drying using multivariate techniques: principal component analysis (PCA) and partial least square (PLS). The importance of temperature was found on dried wood color. In the investigation, green boards of the three species were taken from small diameter logs (Figure 1.7). For inner side, mainly radial surfaces were measured while mainly tangential surfaces were measured for outer side. It was assumed that outer side represents sapwood and inner side represents heartwood. The drying design and experimental parameters are shown in Figure 1.8 and Table 1.3. After drying, the wood color was measured from each side of each board separately before planed, after 1 mm planed and 3 mm planed. But, only

the measurements for 3 mm planed wood were modelled, since this depth is the most important for manufacturing furniture, joinery, etc.

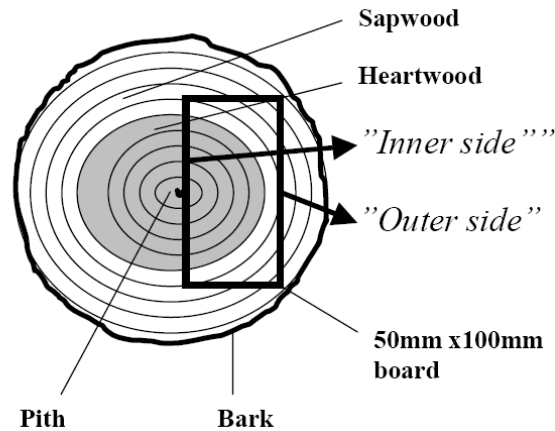


Figure 1.7 Schematic view of position in cross-section when taken from a small-diameter log, 50 by 100 mm board. Two sides of the board are defined as outer side and inner side (adapted from Sundqvist 2002a).

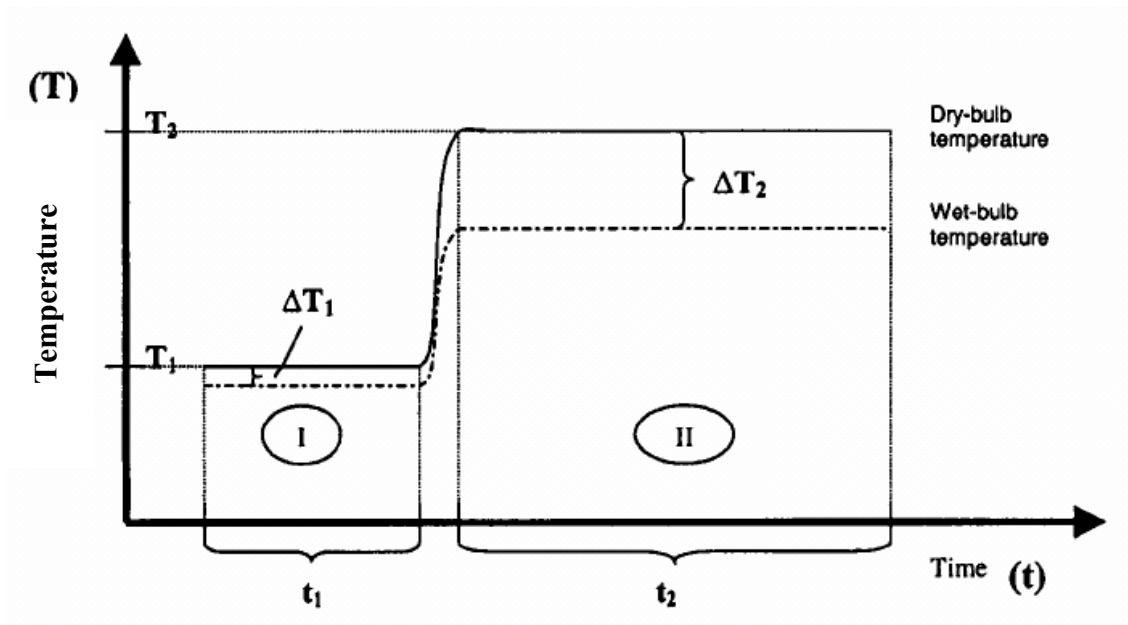


Figure 1.8 Schematic plot of the drying design. T = dry-bulb temperature; ΔT = wet-bulb depression; t = times elapsed. Index 1 belongs to the capillary phase (I) and index 2 to the diffusion phase (II) (adapted from Sundqvist 2002a).

Table 1.3 Experimental parameters drying Scot pine, Norway spruce and birch (adapted from Sundqvist 2002a)

Species	Run no.	t_1	T_1	ΔT_1	t_2	T_2	ΔT_2
		(hr.)	----- (°C) -----		(hr.)	----- (°C) -----	
Pine	1	47	48	4	60	84	18
	2	49	65	4	37	82	17
	3	51	82	6	37	103	16
Spruce	4	20	63	3	38	92	17
	5	25	73	4	35	100	16
	6	21	82	4	33	111	19
Birch	7	37	40	4	58	69	17
	8	37	52	4	57	68	15
	9	40	57	3	54	85	17

t_1 = time elapsed in capillary phase; T_1 = dry-bulb temperature in capillary phase; ΔT_1 = wet-bulb depression in capillary phase; t_2 = time elapsed in diffusion phase; T_2 = dry-bulb temperature in diffusion phase; ΔT_2 = wet-bulb depression in diffusion phase; nine drying runs.

At first, an overall PCA was carried out involving the three species where responses (average color values of each species, run and side) were treated as variables. And then, predictive PLS model was separately built for six observations of each species. These models showed the importance of temperature for the wood color. The model for Scots pine was quite weak. Norway spruce and birch were also modelled in the same way as Scots pine. But strong models were generated. For example, the model for birch was defined by:

$$L^* = 81.511 - 3.654S - 0.045T_1 - 0.105T_2 \quad [1.4]$$

$$C^* = 24.428 - 0.821S - 0.043T_1 - 0.023T_2 \quad [1.5]$$

$$h = 82.548 + 2.658S - 0.074T_1 - 0.113T_2 \quad [1.6]$$

where, L^* = lightness, C^* = chroma (saturation), h = hue, S = inner side (0) or outer side (1) of the board, T_1 = dry-bulb temperature in capillary phase, T_2 = dry-bulb temperature in diffusion phase.

In Figure 1.9, the observations were projected in two dimensions of the principal components in the score plot. The direction where the data has the largest variation is defined as the first principal component $t(1)$, the direction where the data has the second

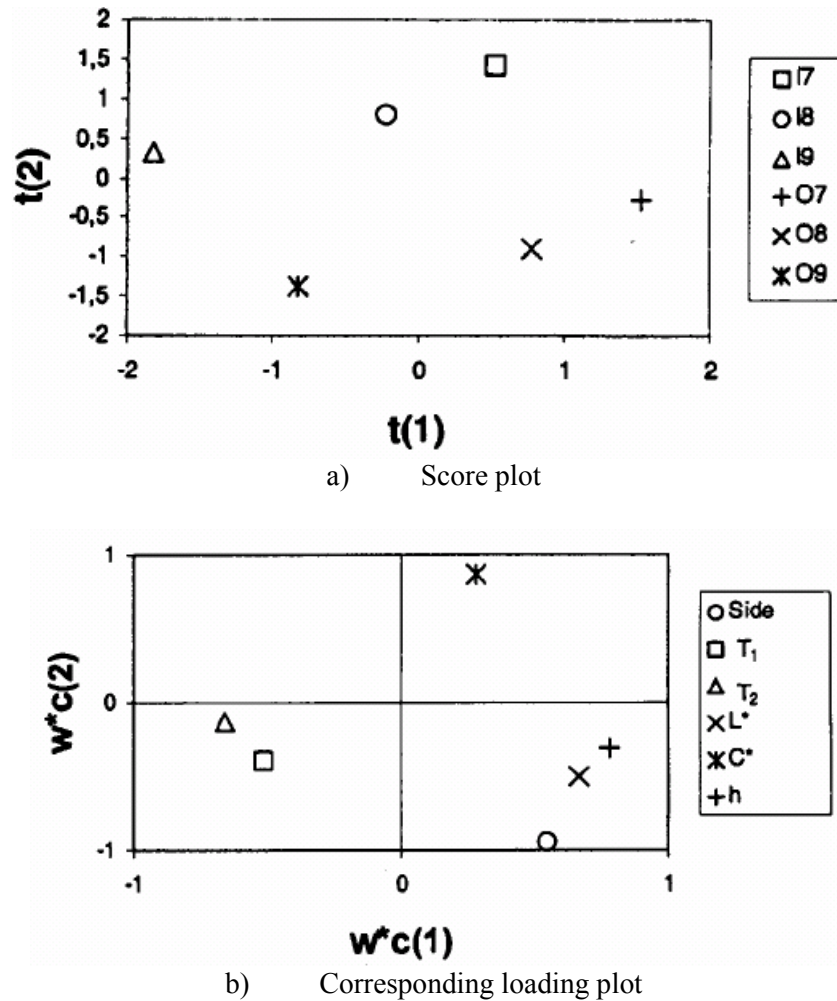


Figure 1.9 Partial least square model. Color of kiln-dried birch planed 3 mm. ‘I’ is inner side and ‘O’ is outer side. Numbers denote run number (adapted from Sundqvist 2002a).

most variation as the second principal component $t(2)$. The relationship between variables and responses was presented in two dimensions in the loading plot where $w*c(1)$ or (2) is the weighted loading in the corresponding direction in the score plot. The score plot (Figure 1.9a) showed well-distributed observations according to variables and responses. The variable S mainly spreaded in the direction of the second principal component while the drying runs (the variable T) spreaded in the direction of the first principal component. The loading plot (Figure 1.9b) revealed that birch wood became darker, less saturated, and redder when dry-bulb temperatures were increased, since T_1 and T_2 oppose L^* , C^* and h , mainly in the first component. The loading plots also revealed that Scots pine and Norway

spruce become darker, redder and more saturated when drying temperatures were raised. Moreover, the loading plots revealed that outer side and inner side were distinctly different in wood color. Birch wood inner side was obviously darker and redder, somewhat more saturated than outer side. Scots pine inner side was lighter, more saturated and more yellow than outer side, but these loadings were weak in the second component. Norway spruce inner side was clearly more yellow, lighter, and less saturated than outer side. No general conclusion could be drawn about the color changes of sapwood and heartwood due to drying or hydrothermal treatment and their internal color differences. These average color differences were small, around 1 ~ 3 units, and were difficult to distinguish by the naked eye (Sundqvist 2004). Finally, Sundqvist (2002a) concluded that multivariate PLS modelling was a powerful tool for batch color control of kiln-dried wood.

In addition, Sundqvist (2002b) observed the accelerated darkening for the green clear wood of Scots pine, Norway spruce and birch when about 80°C was exceeded in the capillary phase heat treatment at 65 to 90°C for 0 to 6 days, followed by drying at 35°C for 2 days.

1.5.2 The effect of drying time, wood thickness and relative humidity

Stenudd (2004) investigated the parametric effects of temperature, RH, IMC, and wood thickness on small samples (10 or 16 mm thick, 80 mm wide and 240 mm long) of silver birch (*Betula pendula* Roth.) wood dried from green or 30% to 20% M in a climate chamber with an average air speed of 2 m/s. Samples were dried in constant climate at 30/60°C (86/140°F) and 62/82% RH, in a total of 16 different combinations (see Table 1.4). Half of the samples were pre-dried to 30% M at room temperature and naturally diminishing RH from 85 to 60% before drying in the climate chamber. After drying and 2 months of storage in room climate, the color measurement was conducted on the surface after 5 mm wood planed from the bark side.

Results were statistically analyzed based on one-way ANOVA and regression analysis using Minitab 10th version software. Regression models for drying green wood to 20% M (kiln drying settings 1 to 8, Table 1.4) were defined as:

Table 1.4 Drying for birch wood in constant temperature and RH conditions from IMC to below 20% M (adapted from Stenudd 2004).

Setting	Dimension (mm)	IMC (%)	No.	Temperature (°C/°F)	RH (%)	Lightness (L*)	Saturation (C*)	Hue (h)	Time (hr)
1	10 by 80	65.7	7	30/86	82	81.4(1.5)	20.0(1.3)	80.0(0.8)	63.0
2	10 by 80	68.2	7	30/86	62	83.6(1.6)	18.8(1.6)	81.2(0.3)	47.4
3	10 by 80	64.6	7	60/140	82	73.6(1.2)	22.0(0.2)	77.0(1.5)	16.3
4	10 by 80	66.0	7	60/140	62	75.0(2.2)	21.9(0.5)	76.7(1.6)	8.7
5	16 by 80	69.1	7	30/86	82	78.0(0.8)	21.8(0.4)	77.1(0.9)	152
6	16 by 80	75.1	7	30/86	62	80.8(1.2)	19.6(0.5)	78.0(1.3)	68.6
7	16 by 80	65.4	7	60/140	62	71.3(1.7)	22.4(0.6)	73.7(1.9)	19.6
8	16 by 80	67.5	7	60/140	82	70.7(1.4)	22.7(0.7)	73.4(2.6)	27.9
9	10 by 80	29.1	7	30/86	62	83.1(1.8)	18.9(1.5)	80.6(1.1)	10.7
10	10 by 80	29.1	7	30/86	82	81.3(1.2)	20.2(0.8)	80.2(1.1)	43.3
11	10 by 80	29.4	7	60/140	62	76.7(1.4)	22.2(0.7)	77.1(1.3)	4.3
12	10 by 80	29.5	7	60/140	82	76.5(2.5)	21.5(0.9)	77.2(2.0)	5.8
13	16 by 80	28.9	6	30/86	62	80.2(1.1)	20.9(1.0)	78.7(0.8)	24.7
14	16 by 80	30.3	7	30/86	82	77.5(1.4)	21.9(0.5)	76.6(1.2)	90.4
15	16 by 80	29.6	7	60/140	82	74.3(1.4)	22.4(0.6)	74.6(1.1)	11.2
16	16 by 80	30.1	7	60/140	62	73.7(1.0)	22.2(0.4)	73.7(1.4)	5.5

Note: Board dimension, IMC and number in each kiln setting, drying condition, average dried wood color values (standard deviation within parentheses) in CIE L*C*h coordinates and average total drying times are presented.

$$L^* = 103 - 0.292T - 0.0909RH - 0.533D, \quad R^2 = 90.1\% \quad [1.7]$$

$$C^* = 4.24 + 0.258T + 0.154RH + 0.156D - 0.00245TRH, \quad R^2 = 68.8\% \quad [1.8]$$

$$h = 89.7 - 0.126T - 0.526D, \quad R^2 = 72.6\% \quad [1.9]$$

where T = the temperature during climate chamber drying (°C), RH = the relative humidity during climate chamber drying (%), D = the sample thickness (mm).

The models for drying from 30 to 20% M (kiln climate settings 9 to 16, Table 1.4) in the climate chamber were defined as:

$$L^* = 93.7 - 0.221T - 0.363D - 0.0431\Delta t, \quad R^2 = 82.0\% \quad [1.10]$$

$$C^* = 15.6 + 0.0769T + 0.126D + 0.0216\Delta t, \quad R^2 = 60.4\% \quad [1.11]$$

$$h = 89.7 - 0.142T - 0.395D - 0.0283\Delta t, \quad R^2 = 77.8\% \quad [1.12]$$

where Δt = the drying time in the climate chamber in hours.

Temperature and sample thickness are the two main factors controlling the color during the drying from green (74% M) to 20% M. An increased temperature level or thickness turns the wood darker, more saturated and reddish. Relative humidity was also important for lightness and chroma. The wood turned darker and more saturated when the relative humidity increased. As the relative humidity is properly lowered, drying is more uniform, and the risk of initiating discoloration (especially chemical discoloration) is reduced (Denig et al. 2000). The interaction of T and RH works in an opposite way by decreasing the chroma. But during drying from 30 to 20% M, the effect of RH on color had not been found.

McCurdy et al. (2003) also reported that there was generally a great decrease in lightness with slower, higher RH schedule drying *Pinus radiata* sapwood boards. To reduce discoloration, it has been recommended that timber be dried rapidly (low relative air humidity, high air velocity) at low temperature (Taylor 1997).

Furthermore, capillary drying of thicker standard dimension boards was also investigated (Stenudd 2004). The schedules are shown in Table 1.5, and results in Table 1.6 and Figure 1.10. A rather weak correlation between capillary phase temperature and lightness ($r = 0.47$) and a stronger correlation with chroma ($r = -0.71$) was found. Process time also showed a strong correlation with chroma ($r = 0.79$). Increased temperature increases the lightness and decreases the saturation. The response for hue did not show significant differences between the samples dried at 35°C (95°F) and 45°C (113°F).

It is also interesting that the reference samples dried at room temperature became darkest in color (Figure 1.10), which differs from some other studies (Luostarinen et al. 2000). But, it agrees with the findings on beech and birch where fast drying at a slightly increased temperature, 30°C compared to 20°C, resulted in lighter color (Stenudd 2001). Accordingly, Stenudd (2004) concluded that during capillary drying ($M > 55\%$), time was more important than the temperature. Swift initial drying even at elevated temperatures increased the lightness and decreased the saturation.

The fact that sample thickness, process time, and IMC values between 20 and 30% were important for color indicates that the time a local layer of wood spent in a moisture content range between approximately the FSP and 15 ~ 20% M was decisive for the final wood color. Prolonged drying time and increased temperature in the critical M zones decreased the lightness and made the wood more saturated and reddish.

The results support earlier findings in the capillary phase heat treatment at 65 to 95°C (Sundqvist 2002b) that time was more important than temperature for the color response for birch (*Betula pubescens*) while time and temperature had similar importance for Scots pine and Norway spruce. Hydrolysis was suggested to be the main process causing these color changes in this phase. Since capillary water was present in the lumen, the degradation of hemicelluloses was assumed to be mainly hydrolytic, which can be involved in the production of colored compounds (Fengel and Wegener 1984).

Straze et al. (2003) reported that, during conventional drying ash wood, lower drying rates, higher temperatures and critical moisture content of ash wood between 36 and 29% were favourable conditions for development of discoloration.

Table 1.5 Kiln schedules for 32-mm- (5/4-in.-) thick samples dried from green to 7% M (adapted from Stenudd 2004).

M (%)		Kiln climate setting 1			Kiln climate setting 2			Setting 1&2
From	To	Temperature		RH (%)	Temperature		RH (%)	EMC (%)
		(°C)	(°F)		(°C)	(°F)		
80	60	45	113	75	35	95	73	13.3
60	55	45	113	70	35	95	68	11.9
55	40	35	95	68	35	95	68	11.9
40	30	35	95	56	35	95	56	9.6
30	25	35	95	44	35	95	44	7.7
25	20	50	122	40	50	122	40	6.5
20	15	70	158	40	70	158	40	5.6
15	10	70	158	36	70	158	36	4.9
10	7	70	158	26	70	158	26	3.7

Note: Both settings are identical except the first two steps from 80 to 55% M.

Table 1.6 Drying thick birch wood at different ‘critical’ temperature levels in the capillary phase from green to 55% M (adapted from Stenudd 2004).

Kiln climate setting No.	Sample dimension (mm)	Number of samples	Critical temperature (°C/°F)	Lightness (L*)	Saturation (C*)	Hue (h)	Drying time to 55% M (hr)
1	32 by 100	18	45/113	76.8(1.4)	19.3(0.7)	73.2(1.7)	62
2	32 by 100	18	35/95	75.2(1.9)	19.6(0.7)	72.8(2.0)	85
3	32 by 100	5	20/68	74.3(2.1)	22.1(0.5)	73.5(2.0)	--

Note: Total drying time to below 10% M was approximately 260 hours for both settings 1 and 2.

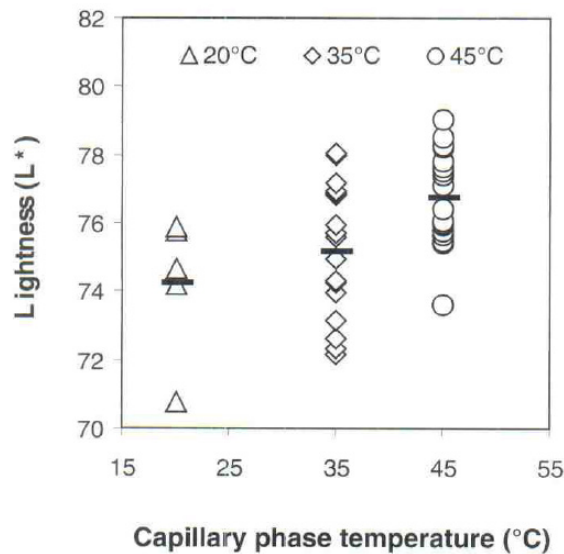


Figure 1.10 A relationship between the wood lightness (average value presented by horizontal bar) and the capillary phase temperature after kiln-drying 32 by 100 mm (5/4 by 4 in.) samples (adapted from Stenudd 2004).

1.6 The drying model based on water potential concept

In order to understand and characterize the moisture retention and moisture movement phenomena taking place in wood during drying, many approaches have been presented. Generally speaking, two main approaches can be identified: (1) models based on a potential energy term; and (2) multi-component models.

Luikov (1966) stated that the moisture transfer in porous medium was the results of temperature, concentration and pressure. Water movement in wood was assumed to be caused by the moisture potential gradient and the temperature gradient where there was no

convective mass transfer. Equations of mass and heat transfer in wood were respectively presented by Thomas et al. (1980), Irudayaraj et al. (1990), Liu and Cheng (1991) and Gui et al. (1994). Furthermore, the gradient in chemical potential (Kawai et al. 1978; Siau 1983; Skaar and Kuroda 1985; Stanish et al. 1986; Siau 1992) or the gradient in water potential (Fortin 1979; Cloutier et al. 1992; Cloutier and Fortin 1994; Siau 1995) was taken as the driving force for moisture movement in wood. The approach of irreversible thermodynamics was also used by Skaar (1988) and Siau (1992), but the driving force was still based on the chemical potential.

In the multi-component model proposed by Whitaker (1977), different driving forces were used depending on the state of the water in wood. The gradient in pressure within the liquid was taken as driving force when considering water in the liquid state in wood. The gradient in total pressure and the gradient in moisture content or in chemical potential were considered as driving forces for gaseous water and bound water. Therefore, in this model, mass and energy conservation relations were respectively written for liquid water, water vapor and for the gaseous mixture (water vapor + air), and bound water. In a set of macroscopic equations, the fluxes of the different components were described using different transport coefficients and driving forces (Plumb et al. 1985; Stanish et al. 1986; Ben Nasrallah and Perré 1988; Perré and Maillet 1989). The multi-component approach provides a comprehensive description of the mechanisms of wood drying but it results in large sets of equations requiring the knowledge of moisture transport coefficients, driving forces and other physical parameters which were not easily obtainable (Tremblay et al. 2000a).

1.6.1 The concept of water potential

The water potential concept was stated by Fortin (1979) to characterize the three different phases of water in wood in terms of free energy. Further, the water potential concept was used by Cloutier and Fortin (1993), Tremblay et al. (1996) and Defo et al. (1999a). The water potential, ψ , is derived from classical thermodynamics. It is defined as:

$$\psi = \overline{G} - \overline{G}_0 \quad [1.13]$$

where \overline{G} is the specific Gibbs free energy of water in the state under consideration and \overline{G}_0 is the specific Gibbs free energy of water in the standard reference state.

The standard reference state generally used is a hypothetical pool of pure free water at atmospheric pressure, at a given elevation and at the same temperature as the water in the porous material. Under these conditions, ψ is equal to zero. The water potential is fundamentally expressed in terms of energy per unit mass, using units of J kg^{-1} .

The water potential may be thought of as the sum of the separate contributions of the various force fields acting on the water in wood (Fortin 1979):

$$\psi = \psi_m + \psi_o + \psi_p + \psi_g + \psi_{e.f.} + \dots \quad [1.14]$$

where ψ_m = matric potential due to the combined effect of the capillary and sorptive forces; ψ_o = osmotic potential due to the presence of solutes in the water; ψ_p = pressure potential describing the effect of a system bulk pressure either greater or less than the reference bulk pressure; ψ_g = gravitational potential accounting for gravity; $\psi_{e.f.}$ = a component potential representing the integrated sum of the effects of all external force fields exclusive of gravity. The dots on the right-hand side of the equation indicate that additional component potentials are theoretically possible.

In the case of wood drying at low temperatures and at atmospheric pressure, the only important component potentials are ψ_m and ψ_o . The matric component, ψ_m , can be derived from an indirect approach. If an air pressure, P_m , is applied on the wood sample side of a porous membrane permeable to water but impermeable to air, the equilibrium is reached when P_m has counterbalanced the effect of the capillary and sorptive forces and raised the energy state of water in the wood sample, \overline{G} , to that of pure free water, \overline{G}_0 , on the other side (Cloutier and Fortin 1991).

1.6.2 Heat and mass transfer equations

In the water potential concept, the effective water conductivity was used by Fortin (1979). A model of isothermal wood drying using the gradient in water potential as the driving

force was further presented by Cloutier et al. (1992) and used by Tremblay (1999) and Defo (1999). Unsaturated moisture movement in wood is given by the following conservation relation:

$$\frac{\partial C}{\partial t} + \vec{\nabla} \cdot \vec{q}_m = 0 \quad [1.15]$$

where C = moisture concentration ($\text{kg}_{\text{water}} \text{ m}^{-3}_{\text{moist wood}}$); t = time (s); \vec{q}_m = moisture flux vector (liquid water + water vapor + bound water) ($\text{kg}_{\text{water}} \text{ m}^{-2}_{\text{moist wood}} \text{ s}^{-1}$). The symbol, $\vec{\nabla}$, denotes the divergence of the mass flux in the three dimensions.

The moisture concentration can be defined as:

$$C = G_m \rho_w \frac{M}{100} \quad [1.16]$$

where G_m = specific gravity of wood ($\text{kg}_{\text{oven-dry wood}} \text{ m}^{-3}_{\text{moist wood}} \text{ kg}^{-1}_{\text{water}} \text{ m}^3_{\text{water}}$); ρ_w = density of water ($\text{kg}_{\text{water}} \text{ m}^{-3}_{\text{water}}$); and M = moisture content expressed in percentage ($\text{kg}_{\text{water}} \text{ kg}^{-1}_{\text{oven-dry wood}} \times 100$).

Under the assumption of negligible temperature gradients, the moisture flux vector is given by:

$$\vec{q}_m = -K(M, T) \cdot \vec{\nabla} \psi \quad [1.17]$$

where $K(M, T)$ = effective water conductivity tensor ($\text{kg}^2_{\text{water}} \text{ m}^{-1}_{\text{moist wood}} \text{ s}^{-1} \text{ J}^{-1}$) (function of moisture content M and temperature T); and $\vec{\nabla} \psi$ = gradient in water potential ($\text{J kg}^{-1}_{\text{water}} \text{ m}^{-1}_{\text{moist wood}}$).

The moisture flux in one dimension was determined from the following equation:

$$q_m = \frac{\partial}{\partial t} \left(\int_{xq=0}^{xi} C dx \right) \quad [1.18]$$

Considering G_m and ρ_w as constant, the conservation equation can be rewritten as:

$$\frac{\partial M}{\partial t} + \frac{100}{G_m \rho_w} \vec{\nabla} [-K(M, T) \cdot \vec{\nabla} \psi] = 0 \quad [1.19]$$

For a one-dimensional problem, the initial condition for Equation [1.19] is given by:

$$\psi(x, t = 0) = \psi_0 \quad [1.20]$$

The convective mass transfer boundary condition on the wood surface is given by:

$$q_{mc} = h_\psi (\psi_s - \psi_\infty) = -K_x(M, T) \frac{\partial \psi}{\partial x} \quad [1.21]$$

where q_{mc} = convective moisture flux normal to the wood surface ($\text{kg water m}^{-2} \text{ drying surface s}^{-1}$); h_ψ = convective mass transfer coefficient ($\text{kg}^2 \text{ water m}^{-2} \text{ drying surface s}^{-1} \text{ J}^{-1}$); ψ_s = the water potential of wood at the board surface ($\text{J kg}^{-1} \text{ water}$); ψ_∞ = the water potential of the surrounding air-water-vapour mixture ($\text{J kg}^{-1} \text{ water}$).

The governing equation for heat transfer includes the change of total enthalpy, the transfer of heat by conduction and the phase change term:

$$\frac{\partial H}{\partial t} + \vec{\nabla} \cdot \vec{q}_h - \varepsilon (\Delta h_o + \beta \Delta h_s) \frac{\partial C}{\partial t} = 0 \quad [1.22]$$

where H = the enthalpy of the wood-air-water system ($\text{J m}^{-3} \text{ moist wood}$); \vec{q}_h = the conductive heat flux vector ($\text{J m}^{-2} \text{ moist wood s}^{-1}$); ε = the ratio of vapor diffusion to the total water movement (dimensionless); Δh_o = the latent heat of vaporization ($\text{J kg}^{-1} \text{ water}$); Δh_s = the differential heat of sorption ($\text{J kg}^{-1} \text{ water}$); $\beta = 0$ for $M > \text{FSP}$; and $\beta = 1$ for $M \leq \text{FSP}$.

The second term on the left side of Equation [1.22] stands for heat transfer by conduction. The third term stands for the heat transfer due to phase change in wood during drying. The heat transfer by advection inside wood is not included, which is generally considered as negligible for wood drying below 100°C (Sutherland et al. 1992).

The transfer of heat by conduction is described by Fourier's law:

$$\vec{q}_h = -\underline{k}(M) \cdot \vec{\nabla}T \quad [1.23]$$

where $\vec{\nabla}T$ = the temperature gradient (K m^{-1}); $\underline{k}(M)$ = the thermal conductivity tensor ($\text{W m}^{-1} \text{moist wood K}^{-1}$) as a function of moisture content.

Substituting Equation [1.23] into Equation [1.22], the following equation can be obtained:

$$\frac{\partial H}{\partial t} + \vec{\nabla} \cdot (-\underline{k}(M) \vec{\nabla}T) - \varepsilon(\Delta h_o + \beta \Delta h_s) \frac{\partial C}{\partial t} = 0 \quad [1.24]$$

For a one-dimensional problem, the initial condition for Equation [1.24] is given by:

$$T(x, t = 0) = T_0 \quad [1.25]$$

The convective heat transfer boundary condition on the wood surface is given by:

$$q_{hm} = h_h(T_s - T_\infty) + (1 - \varepsilon)(\Delta h_o + \beta \Delta h_s)h_\psi(\psi_s - \psi_\infty) = -K_x(M) \frac{\partial T}{\partial x} \quad [1.26]$$

where q_{hm} = net heat flux ($\text{J m}^{-2} \text{drying surface s}^{-1}$); h_h = convective heat transfer coefficient ($\text{W m}^{-2} \text{drying surface K}^{-1}$); T_s = temperature on the wood surface (K); T_∞ = temperature of the ambient air–vapor mixture (K).

The latent heat of vaporization Δh_o required for the vaporization of liquid water can be considered as a constant of $2.5 \times 10^6 \text{ J kg}^{-1} \text{water}$. The differential heat of sorption Δh_s is the energy required to free the bound water from wood. On one hand, when $M > \text{FSP}$, $\beta = 0$ because the hypothesis is made that water is free above FSP. On the other hand, when $M \leq \text{FSP}$, $\beta = 1$ and Δh_s increases with the reduction of M under the FSP (Tremblay et al.1999).

1.7 Physical material properties used for the heat and mass transfer model

In order to develop or apply a model of wood drying using the water potential as driving force of moisture movement in wood, some model parameters must be known.

1.7.1 The moisture content-water potential relationship ($M-\psi$) of wood

The techniques used to determine the relationship between moisture content and water potential in wood were equilibration over saturated salt solutions for low moisture values, the tension plate, the pressure plate, pressure membrane and centrifuge for high moisture values. Fortin (1979) determined the boundary desorption and absorption curves of the $M-\psi$ relationship of western hemlock at high moisture contents by the tension plate and pressure plate methods with specimens 10 mm thick in the longitudinal direction. The relationship presents a strong hysteretic behavior which can be attributed mainly to the “ink-bottle effect” since the wood capillary system consists of large cavities interconnected by narrow channels.

Cloutier and Fortin (1991) evaluated the boundary curves of the $M-\psi$ relationship of aspen sapwood at three different temperatures (20, 35 and 50°C) in the radial and tangential directions. The tension plate, pressure plate and pressure membrane was used at high moisture values while equilibration over saturated salt solutions was used at lower moisture values. The specimen thickness was also 10 mm in the flow direction (radial or tangential). The water potential increases as the moisture content increases. And, at a given value of moisture content, the water potential also increases with temperature. The curves exhibit a sigmoid shape with a plateau occurring at M values between 110 and 120% or between 110 and 130% for tangential desorption.

In a further study, Cloutier et al. (1995) showed that the $M-\psi$ relationship was not a function of the wood structural direction. In the study of Tremblay et al. (1996), only the radial direction of red pine sapwood was considered due to the shorter equilibration time. The specimen thickness was reduced into 5 mm in order to facilitate equilibrating in the specimens while keeping the specimen thick enough to macroscopically represent the wood

(in this case, the thickness represents 125 times the average tracheid diameter). The pressure membrane and pressure plate techniques were used. The M - ψ relationship data obtained at 18, 56 and 85°C are presented graphically in Figure 1.11. Likewise, the water potential increases with temperature at a given moisture content. There is no significant variation of $\partial\psi/\partial T$ with temperature when moisture contents varied from 40% to 110%. In addition, there is no intermediate plateau like the one found for the M - ψ relationship of aspen sapwood. This is due to differences between the capillary structure of aspen and red pine wood.

Defo et al. (1999a) determined the moisture content-water potential relationships of sugar maple sapwood at 40°C and 60°C, as well as that of white spruce heartwood at 60°C from green to dry conditions. The pressure membrane technique was used for high moisture contents and the equilibration over saturated salt solutions for low moisture contents. The results are presented graphically in Figure 1.12 for sugar maple. When water potential values are less than -1000 J kg⁻¹, the M - ψ drainage curves obtained from the green condition are similar in shape to those obtained from the fully saturated state (boundary desorption). At a given ψ value above -1000 J kg⁻¹, the equilibrium moisture contents (EMC) obtained from the green state are lower than those from full saturation. It is recommended that the sorption history should be taken into account when modeling wood drying. The green moisture content-water potential relationship of sugar maple samples exhibits a characteristic plateau at water potentials between -2,000 and -6,000 J kg⁻¹. This can be explained by the effective pore size distribution of sugar maple wood. For sugar maple, a large proportion of the pit membrane openings in fibers and ray parenchyma cells range from 0.018 µm to 0.2 µm with a maximum at 0.02 µm.

The difference in the M - ψ relationship between hardwoods and softwoods can be mainly explained by their differences in anatomical feature (Defo et al 1999a). Hardwoods have a more complex structure than softwoods. According to Panshin and de Zeeuw (1980), sugar maple consists of 21% vessels for water transport that softwoods lack, 61% fibers (including fiber tracheids and libriform fibers) and 17.9% ray parenchyma whereas softwoods contain more than 90% tracheids.

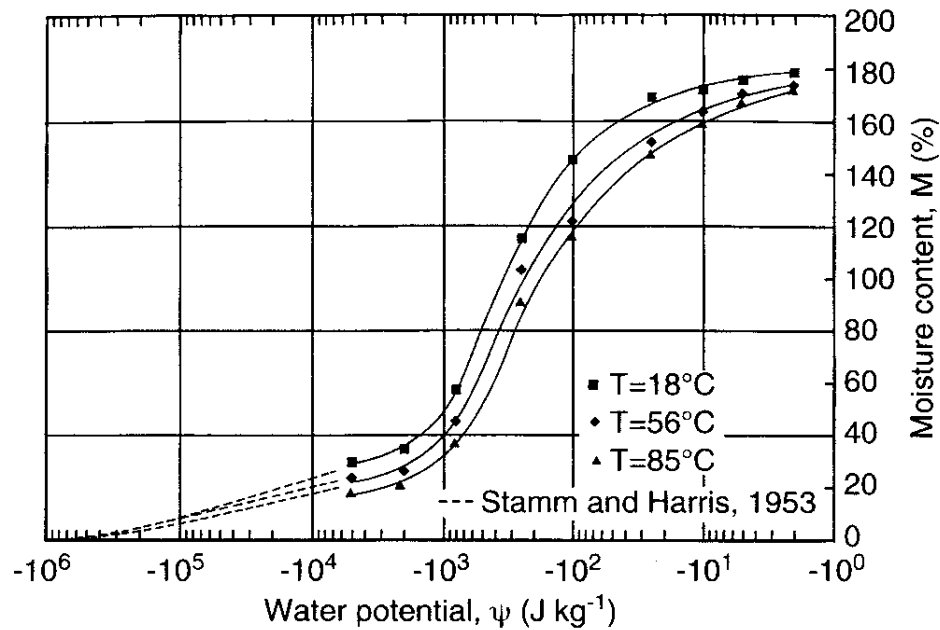


Figure 1.11 Moisture content-water potential relationship of red pine sapwood along the boundary desorption curve at 18, 56 and 85°C (adapted from Tremblay et al. 1996).

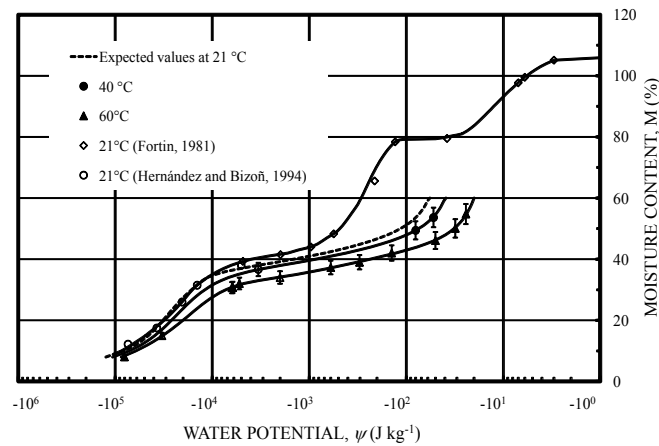


Figure 1.12 Moisture content-water potential relationship of sugar maple sapwood at 40 and 60°C from green to dry conditions and boundary drainage curve at 21°C (adapted from Defo et al. 1999a).

1.7.2 The effective water conductivity of wood

Many different techniques have been used to determine the diffusion coefficient (D) of moisture movement in wood below the FSP. Among them, the vapometer cup method, based on Fick's first law of diffusion, has been used by Comstock (1963), Choong (1965), etc. Above the FSP, numerical solutions of Fick's second law of diffusion have been considered for the determination of the diffusion coefficient. The initial and boundary conditions related to these solutions are the following: (a) M is initially uniformly distributed throughout the specimen; (b) the surface instantaneously reaches the equilibrium moisture content; and (c) the material behaves as an infinitely thick solid, meaning that the solution can be applied to wood up to the point in time when M at the center of the specimen starts to change. Beyond that point the sample ceases to behave as an infinitely thick solid. This last assumption is quite restrictive and implies that the technique can be used only on limited ranges of moisture contents.

Within a large range of moisture contents, the methods determining moisture transport coefficients are divided in two types, namely steady-state and transient methods. The steady-state methods involve the establishment of a one-dimensional flow system where the moisture flux and driving force are known and constant with time. Perré (1987) used a steady-state method based on Darcy's law and found that the specific permeability of green sapwood specimens was higher than that of dry specimens due to pit aspiration. Fortin (1979) also used a steady-state method to determine the saturated effective water conductivity of western hemlock. A water potential gradient was applied on each side of a saturated wood specimen.

The transient methods involve the establishment of a one-dimensional flow system in which the moisture flux and the moisture content vary with both position and time. An interesting transient method is the so-called 'one-step method' (Doering 1965; Gardner 1962). An advantage of the one-step method is that the determination of $D_x(M)$ or $K_x(M)$ can be made simultaneously with the measurement of the M - ψ relationship by the pressure membrane or porous plate methods without involving additional experimental work, except

collecting outflow data. But, the hypothesis of a negligible M gradient in the direction of flow could be difficult to be accepted (Tremblay et al. 2000a).

Kawai et al. (1978) and Fortin (1979) used the instantaneous profile method, also called Egner method, to evaluate moisture transport coefficients in unsteady state conditions. This method has two important advantages. First, the flux-gradient proportionality can be verified directly. Proportionality between flux and gradient at a given moisture content and temperature is a basic condition for the validity of the expression of the moisture flux vector. Second, no specific set of boundary conditions needs to be imposed since the gradient and the resulting flux are measured directly in wood. The flux is required to be known at one position. This latter requirement may be fulfilled by simply closing one end of the flow system. The main disadvantage is that this method is time consuming. Fortin (1979) used this method to evaluate $K_L(M)$ of western hemlock at high moisture contents. The conductivity varies by several orders of magnitude from saturated to unsaturated state. There is a strong hysteretic behaviour caused by the “ink-bottle effect” like that in the M - ψ relationship of western hemlock established by Fortin (1979).

Cloutier and Fortin (1993) used the instantaneous profile method determining the effective water conductivity in the radial (K_R) and tangential (K_T) directions of aspen sapwood from nearly saturated to dry conditions at 20, 35 and 50°C. The results show that K_R is higher than K_T at intermediate and high moisture contents. $K_R(M,T)$ and $K_T(M,T)$ decrease by several orders of magnitude as M decreases. Also, at a given M value, $K_R(M,T)$ and $K_T(M,T)$ increase as the temperature rises.

Tremblay et al. (2000a) established the boundary desorption curve of the effective water conductivity function of red pine (*Pinus resinosa* Ait.) sapwood using the instantaneous profile method. The test results in the radial and tangential directions from nearly saturated to dry conditions at 18, 56 and 85 °C are shown in Figure 1.13. The curves were hand fitted to the data points. The curves have a similar shape as those of aspen sapwood obtained by Cloutier and Fortin (1993). The effective water conductivity decreases by several orders of magnitude (10^4 - 10^5) as moisture content decreases from nearly saturated to dry conditions

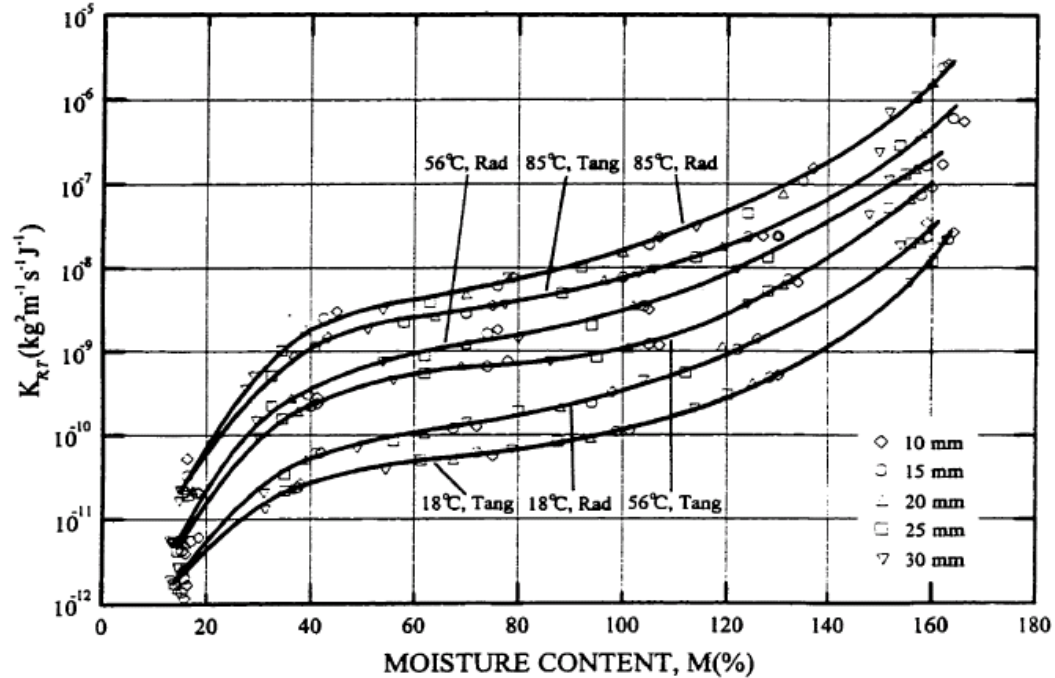


Figure 1.13 Effective water conductivity of red pine sapwood along the boundary desorption curve in the radial (K_R) and tangential (K_T) directions at 18, 56, and 85 °C (Tremblay et al. 2000a).

at a given temperature and a given flow direction. The radial or tangential effective water conductivity also increases by a factor varying between 10 and 50 as temperature rises from 18 to 85°C in the moisture content range considered. The effective water conductivity was generally higher in the radial direction than in the tangential direction in a ratio varying from about 1/1 to 3/1 depending on moisture content and temperature.

1.7.3 The convective mass transfer coefficient

As seen above, the knowledge of the convective heat and mass transfer coefficients is required for the characterization of the boundary conditions of the heat and mass transfer equations of the wood drying model based on water potential (Tremblay et al. 2000b).

The water potential difference between the wood drying surface and the ambient humid air was proposed by Cloutier et al. (1992) as the convective mass transfer driving force. The water potential is assumed to be zero on the wood surface during the constant drying rate.

But, this assumption is not appropriate beyond the constant drying rate period. Therefore, a correction factor (β) is defined as a function of the saturation percentage (S_p) and was determined from measured mass fluxes and corresponding surface water potentials, as shown in Figure 1.14. With the correction factor involved, the moisture content values are no longer overestimated at intermediate drying times in the wood drying model based on water potential. The convective mass transfer equation is expressed below with a correction factor $\beta(S_p)$ considered in order to reduce the convective mass transfer coefficient h_ψ when free water is no longer available at the drying surface of wood:

$$q_{mc} = \beta(S_p) h_\psi (\psi_s - \psi_\infty) \quad [1.27]$$

where $\beta(S_p)$ = correction factor (dimensionless). S_p expresses the volume of water present in a porous medium relative to the total pore volume, and could be defined as below:

$$S_p = \frac{M}{\frac{1}{G_m} - \frac{1}{G_{ws}}} \quad [1.28]$$

where M = moisture content of wood (dry basis) ($\text{kg}_{\text{water}} \text{kg}^{-1}_{\text{oven-dry wood}} \times 100$); S_p = saturation percentage ($\text{m}^3_{\text{water}} \text{m}^{-3}_{\text{pores}} \times 100$); G_m = specific gravity based on the moist wood volume at moisture content M of wood ($\text{kg}_{\text{oven-dry wood}} \text{m}^{-3}_{\text{moist wood}} \text{kg}^{-1}_{\text{water}} \text{m}^3_{\text{water}}$); G_{ws} = specific gravity of the wood substance ($\text{kg}_{\text{oven-dry wood substance}} \text{m}^{-3}_{\text{oven-dry wood substance}} \text{kg}^{-1}_{\text{water}} \text{m}^3_{\text{water}}$).

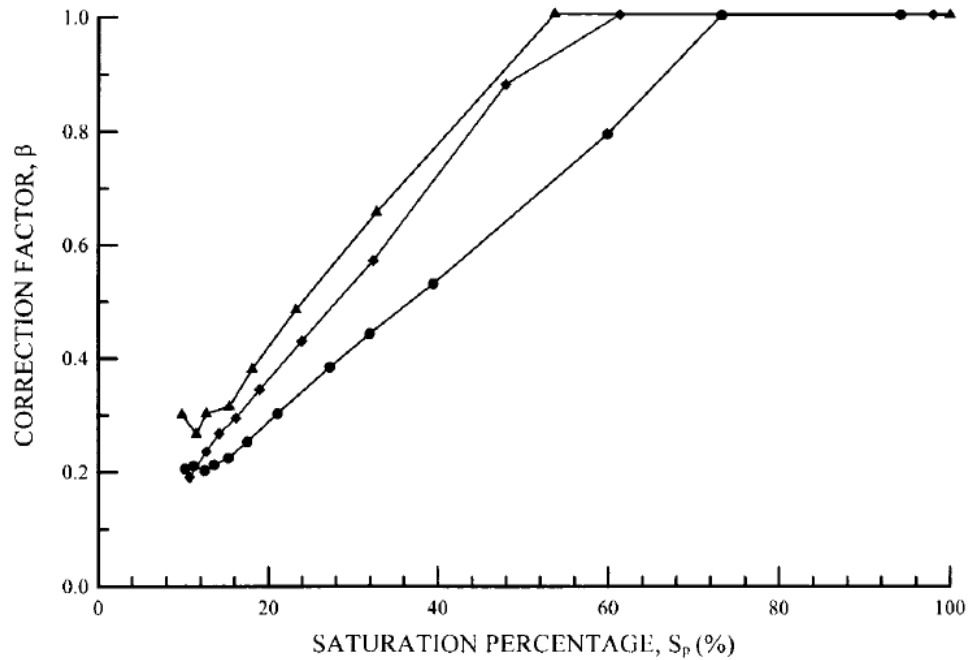


Figure 1.14 Correction factor for the convective mass transfer coefficient for aspen sapwood at 20(♦), 35(▲) and 50°C(●) (adapted from Cloutier et al. 1992).

Tremblay et al. (2000b) experimentally obtained values of h_{ψ} at 56°C and three air velocities ($v_{\text{air}} = 1.0, 2.5$ and 5.0 m s^{-1}), by drying red pine (*Pinus resinosa* Ait.) sapwood from nearly saturated to dry conditions, as shown in Figure 1.15. The results showed that h_{ψ} values were constant at high moisture contents (M), but were moisture content dependent below 80% M. It also increased more or less linearly with air velocity.

Further, Nabhani et al. (2003) improved the version of the measurement technique of Tremblay et al. (2000b) and determined the heat and mass transfer coefficients for the drying of red pine (*Pinus resinosa* Ait.) sapwood from nearly saturated to dry conditions at 30, 60 and 90°C and air velocities of 1.2, 2.2 and 5.0 m s^{-1} . Figure 1.16 presents the experimental results of the mass transfer coefficients at 90°C and air velocities of 1.2, 2.2 and 5.0 m s^{-1} . The results show that convective mass transfer coefficients are constant until the wood surface moisture content reaches about 60%, and then decrease more or less gradually as the moisture content decreases further. At a given temperature, the coefficients at the constant drying rate period increase with air velocity, as shown in Figure 1.17 (a). In

addition, at a given air velocity, the coefficients at the constant drying rate period increase with temperature, as shown in Figure 1.17 (b).

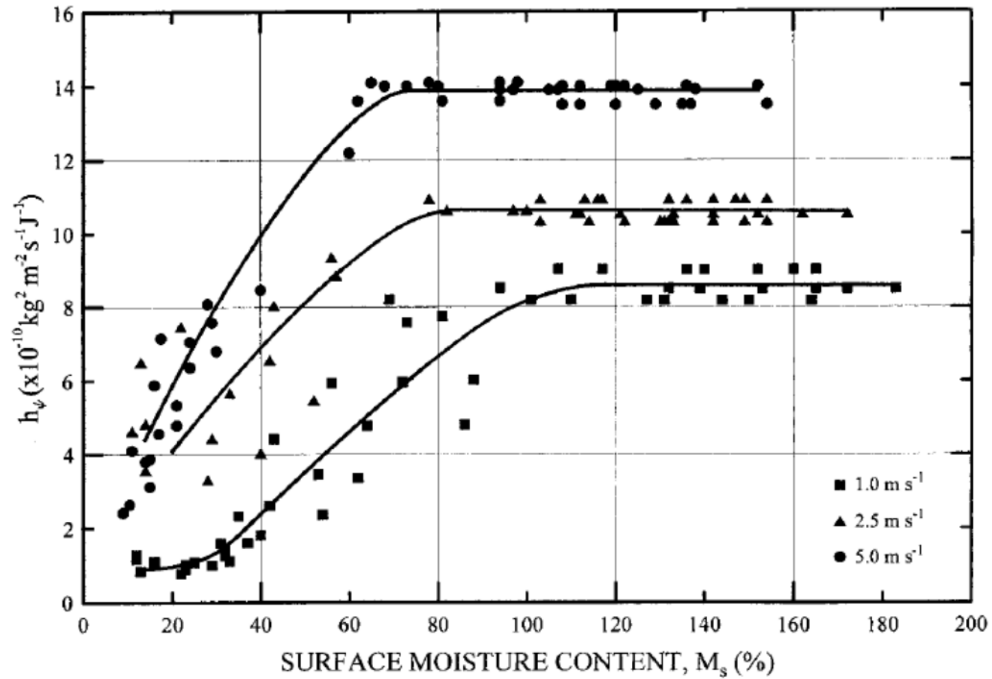


Figure 1.15 Convective mass transfer coefficient vs. the wood surface M at 56°C and air velocities of 1.0 , 2.5 and 5.0 m s^{-1} (adapted from Tremblay et al. 2000b).

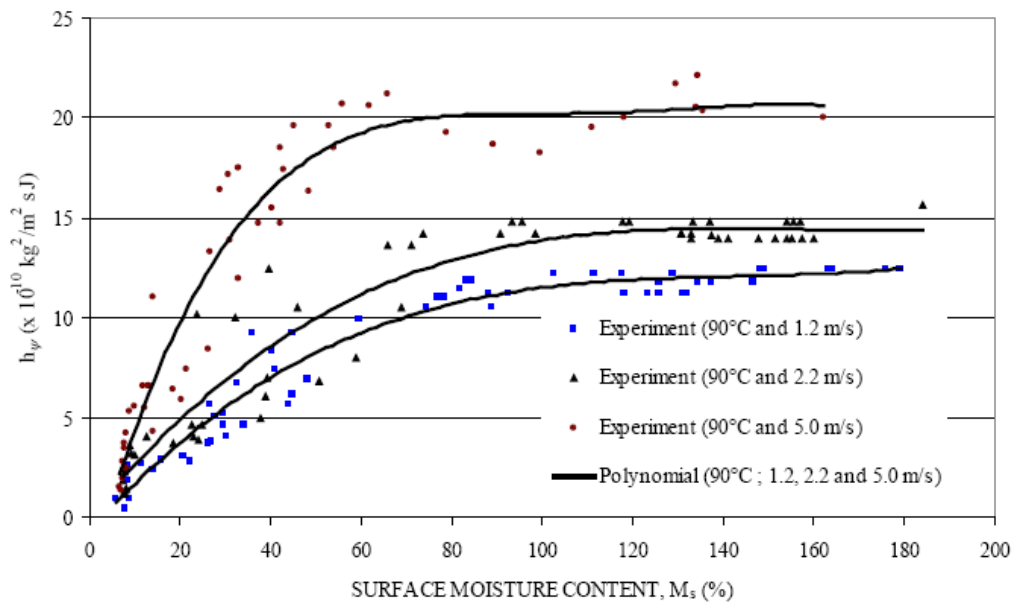
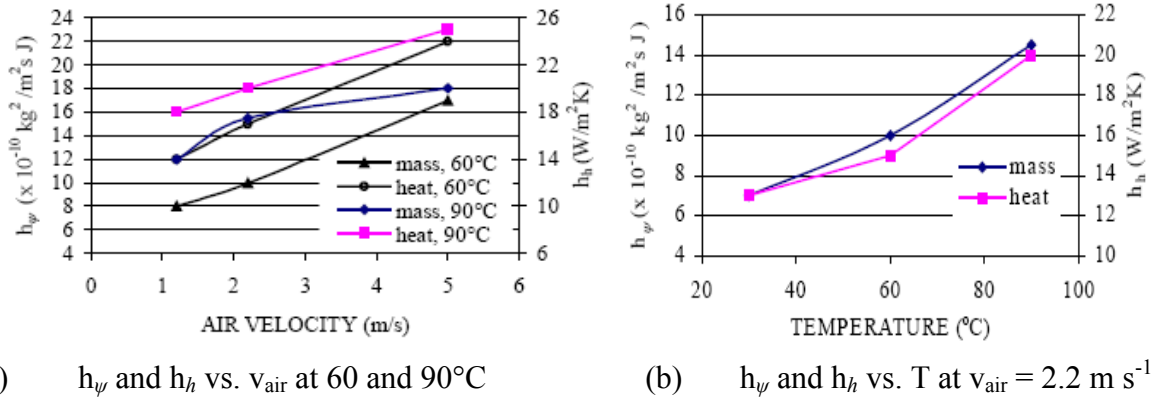


Figure 1.16 Convective mass transfer coefficient vs. the wood surface M at 90°C and air velocities of 1.2 , 2.2 and 5.0 m s^{-1} (adapted from Nabhani et al. 2003).



a) h_ψ and h_h vs. v_{air} at 60 and 90°C (b) h_ψ and h_h vs. T at $v_{\text{air}} = 2.2 \text{ m s}^{-1}$
 Figure 1.17 Effect of air velocity and temperature on the convective heat and mass transfer coefficients at the constant drying rate period (adapted from Nabhani et al. 2003).

1.7.4 The ratio of vapour diffusion to the total water movement in wood

The ratio of vapour diffusion to the total water movement, ε , must be known to consider phase change in the heat and mass transfer model. ε varies between zero to one. It is equal to one if the total water movement occurs in the vapour phase only. On the opposite, ε is zero for water movement occurring in the liquid phase only. There are different values of ε in the literature. Thomas et al. (1980) as well as Liu and Cheng (1989, 1991) used a constant ε value of 0.3. In reality, this property may be function of either moisture content or temperature (Liu and Cheng 1991). Irudayaraj et al. (1990) considered a constant ε value of 0.1 for M higher than 30% and a linear increment from 0.1 to 1.0 for M varying respectively from 30% to 0%. Also, Viktorin (1991) considered ε value varying with the M range as follows: ε was about 0.10; 0.40 and 1.0 for M varying respectively from 100% to 65%; 65% to 30%; and 30% to 0%. It seems that ε is usually determined on the basis of the results obtained with numerical models. Tremblay et al. (1999) determined ε from the original drying experiments of red pine sapwood (*Pinus resinosa* Ait.) in the radial direction at 18, 56 and 85°C. The experimental results show that ε increases from 0.15 to 0.5 as moisture content decreases from values close to saturation (160%) to about 15%. ε reaches a plateau at about 0.33 for intermediate moisture contents (35 to 110%).

1.8 Purpose of the study

The general objective of this study was to develop a color predicting model for paper birch and sugar maple sapwoods under the hygrothermic conditions of conventional kiln drying. A statistical color model was first established and then combined to a heat and mass transfer model in order to predict wood color change during a dynamic drying schedule.

Based on the literature review and the preliminary results, the following hypotheses were proposed:

- Wood color change during drying is continuous. It is related to outside drying parameters, such as dry-bulb temperature and wet-bulb depression.
- Wood color change is also related to intrinsic drying parameters, such as drying rate, wood temperature, moisture content and position from the board surface.

Therefore, the specific objectives of this project can be summarized below:

- To run one-step drying experiments on paper birch and sugar maple sapwood within the temperature range used for conventional drying (40, 60 and 80°C) and 4 or 15°C wet-bulb depressions, and to measure the evolution of color, moisture content and temperature profiles in wood during drying.
- To build wood color predictive models using a statistical method based on the experimental data.
- To experimentally determine the physical parameters used for the heat and mass transfer model DRYTEK at 40, 60 and 80°C, namely, the $M-\psi$ relationships, the $K_{R,T}(M,T)$ functions and the convective mass transfer coefficients for drying.
- To integrate the wood color statistical models into the DRYTEK program.
- To perform independent experiments at 70°C as validation tests. And to make simulations with the enhanced DRYTEK program at the same drying conditions. Then to compare the simulated results to the respective experimental ones obtained from the validation tests.

This study is original in several aspects, namely the fact of using a large range of dry-bulb temperatures and two widespread wet-bulb depressions, the fact of considering both the changes in color at the surface and through the thickness of the board, the fact of considering the continuous change of color during the course of drying, and finally the fact of combining a statistical approach to an existing heat and mass transfer simulation numerical code in order to extend the predicting models to any industrial drying conditions afterwards.

Chapter 2. Materials and methods

Paper birch and sugar maple sapwood were chosen as test material. Experiments were performed to determine the statistical model of color change during drying, the physical parameters of the heat and mass transfer model DRYTEK, and to validate the simulation results obtained from the statistical wood color predictive model and the combined statistical/numerical wood color model.

2.1 Wood color measurements during drying

2.1.1 Material

The test material used to determine the statistical wood color model was made of paper birch (*Betula papyrifera* Marsh.) and sugar maple (*Acer saccharum* Marsh.) 1 by 4 inch (about 28 mm × 104 mm × 2.44 m) commercial sapwood boards obtained from a sawmill located in the Lac-St-Jean region of Quebec province. Immediately after sawing, the boards were transported to Université Laval where they were randomly stacked, covered with a polyethylene sheet and stored in a freezer at -5°C until required.

Before each experiment, five to six boards were randomly taken out of the freezer and 300-mm long pieces were removed from each end in order to eliminate the risk of gathering end-dry material. The 1.80-m-long boards were cut into three to four 380-mm-long specimens, which were further planed to 25 mm in thickness and 100 mm in width in order

to expose fresh surfaces and have uniform thickness. These specimens were marked on the edge in order to identify their original positions in the respective original boards. Twenty test boards were then selected with no visual defects to constitute the test material. All specimens were weighed and seven of these with weight around the mean value were selected as control specimens, which will be called thereafter “control boards”. Three control boards were used to monitor the drying process, three other boards were used to measure moisture content and color profiles through board thickness, and one board was used to measure temperature profile through board thickness. Both ends of the seven control boards were sealed with silicone and aluminium foil. Three control boards chosen for the monitoring of the drying process were weighed again in order to get the weight of sealant for the accurate calculation of moisture content in the course of drying. After selection and classification, the 7 control boards and the 13 other dummy boards were put in sealed polyethylene bags and stored in a freezer at -5°C until required during the experiment. After the drying chamber had reached the drying conditions, the 20 test boards were taken out of the freezer and kept at room temperature for 24 hours before putting them in the drying chamber.

The average green specific gravity (based on oven-dry weight and green volume of wood) of sugar maple sapwood was 0.611 (varying from 0.559 to 0.687) and the average initial moisture content was 51% (varying from 43 to 63%). The average green specific gravity of paper birch sapwood was 0.534 (varying from 0.472 to 0.580) and the average initial moisture content was 60% (varying from 34 to 72%).

2.1.2 Methods

The 20 test specimens were dried in a small laboratory home built drying tunnel made of a vapor saturator (top of Figure 2.1) and a lower chamber of about 1 m long, 460 mm in width and 680 mm in height. Three side doors allow easy access to the drying chamber. The temperature of the water at the bottom of the vapor saturator is maintained constant to $\pm 0.1^{\circ}\text{C}$ with a thermostatic water bath (Model 1156D VWR Refrigerating/Heating Circulator). Another thermostatic water bath (Model 1135-1 VWR Refrigerating/Heating Circulator by PolyScience) controls the temperature of the air to $\pm 0.1^{\circ}\text{C}$ through a radiator

installed at the exit of the vapor saturator. The average air velocity in the drying chamber was maintained at about 1.5 m s^{-1} . Two sets of dry-bulb and wet-bulb thermometers were separately installed in the vapor saturator and in the drying chamber to monitor the temperature and relative humidity of the drying tunnel. Water flow to the wet-bulb thermometer was provided through a constant level floating valve connected to the laboratory demineralised water supply.

Six one-step drying runs were conducted for each species: three different dry-bulb temperatures (40, 60 and 80°C) and two wet-bulb depressions (4 and 15°C). The six combinations of dry-bulb temperatures and wet-bulb depression temperatures and equilibrium moisture contents are presented in Table 2.1. These drying conditions were chosen so as to cover the range of conditions found in industrial drying schedules of paper birch and sugar maple wood (Boone et al. 1998).

The temperature setpoints of both water baths for each combination of drying conditions in the drying chamber are shown in Table 2.2.

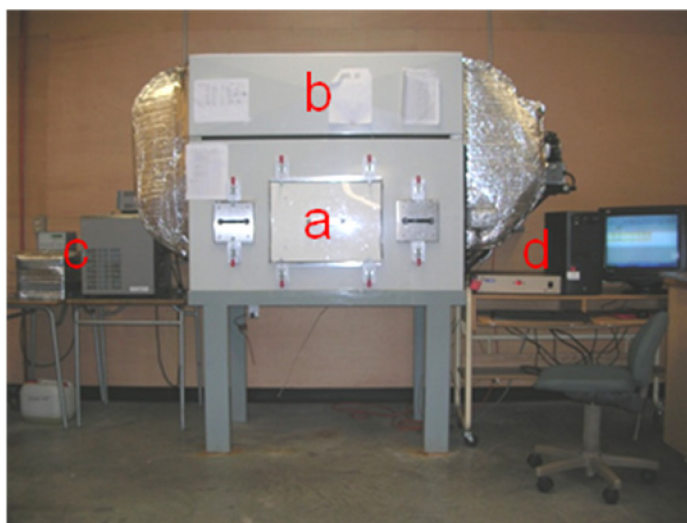


Figure 2.1 Experimental drying tunnel setup including a drying chamber (a), a vapor saturator (b), two thermostatic water baths (c), and temperature data acquisition system (d).

Table 2.1 One-step drying schedules used for paper birch or sugar maple sapwood specimens from green to final dry condition.

Run No.	1	2	3	4	5	6
Dry-bulb temperature, T ($^{\circ}\text{C}$)	40	60	80	40	60	80
Wet-bulb depression, ΔT , ($^{\circ}\text{C}$)	4	4	4	15	15	15
Relative humidity (%)	76	81	85	29	43	51
EMC (%)	14.3	14.2	14.1	5.6	5.9	5.9

Table 2.2 Setpoints of water baths for the drying tunnel for specific drying conditions

Run No.		1	2	3	4	5	6
Desired drying conditions in drying chamber	Dry-bulb temperature T ($^{\circ}\text{C}$)	40	60	80	40	60	80
	Wet-bulb depression, ΔT ($^{\circ}\text{C}$)	4	4	4	15	15	15
Temperature setpoints of water baths	T_{air} ($^{\circ}\text{C}$)	42.5	63.0	84.0	46.0	65.3	85.5
	T_{water} ($^{\circ}\text{C}$)	32.0	55.0	77.5	4.5	35.5	67.0

Note: T_{water} – temperature setpoint of the water bath controlling water temperature in the vapour saturator; T_{air} – temperature setpoint of the water bath controlling air through the radiator

Before drying, three copper-constantan thermocouples were inserted into one control board to measure the evolution of the temperature profile during drying. One thermocouple was fixed at 1 mm below the upward surface, another one at quarter thickness and the third one at mid-thickness (Figure 2.2).

One 32-mm in diameter wood plug was also removed with a drill bit cutter from each of the three moisture content and color test boards (M&C control boards) for the measurement of the initial moisture content and color profiles (Figure 2.3). More than 15 dummy dried wood plugs of 38-mm in diameter and 25-mm in thickness were prepared using a lathe. These plugs were then fully varnished to prevent moisture exchange with the surrounding material. Following the plug removal, a dummy wood plug was immediately fitted tight into the hole left in the board in order to avoid moisture loss during drying. The color (L^* , a^* , b^*) of the plug upward face was first measured with a spectrophotometer (BYK-Gardner CC-6692 color-guide 45/0) with a standard illuminant D65 and 10° observer, and then, one slice of about 0.5 mm thick was cut with an industrial slicing device (Figure 2.4a), followed by 14 more slices of about 0.8 mm thick through half-thickness (Figure

2.4b). After each slice was cut, its exact thickness was taken with a digital caliper of ± 0.01 mm accuracy and the color of the new exposed fresh face on the plug was measured immediately. The weight of the 15 slices was measured at the end of the slicing process with a balance of ± 0.0001 g accuracy. In order to minimize the loss of moisture during the slicing process and weighing measurement, the wood slices were kept in SARSTEDT 50 ml centrifuge tubes, which had been previously labelled and weighed to avoid removing the slice from the tube during the weighing process. The same procedure was applied to determine the oven-dry weight after oven drying at $103 \pm 2^\circ\text{C}$ for 24 hours.

Finally, three other control boards (M control boards) were used to monitor the drying process (plotting of the drying curve). Before starting the drying test, two plugs of 10-mm in diameter were removed from each of the three M control boards to evaluate their initial moisture content. Both holes were filled with silicone in order to avoid moisture loss through these openings. The boards were weighed before and after filling both holes with silicone. The moisture content of the plugs was then measured with the gravimetric method.

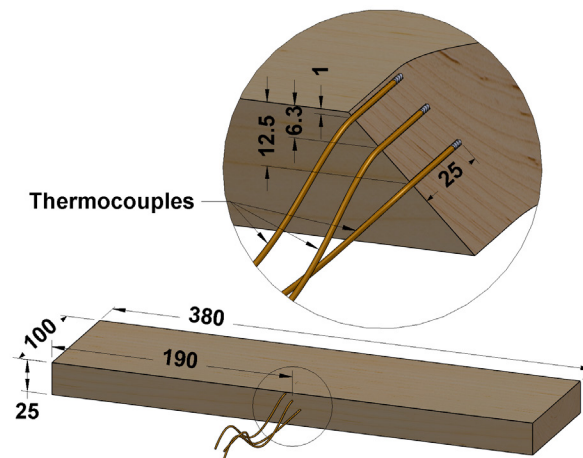
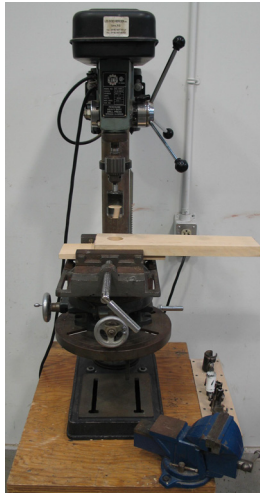
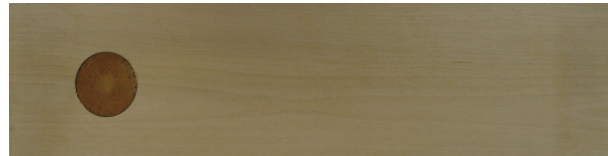


Figure 2.2 Schematic drawing of the temperature control board and thermocouples used to measure the temperature profile through thickness.

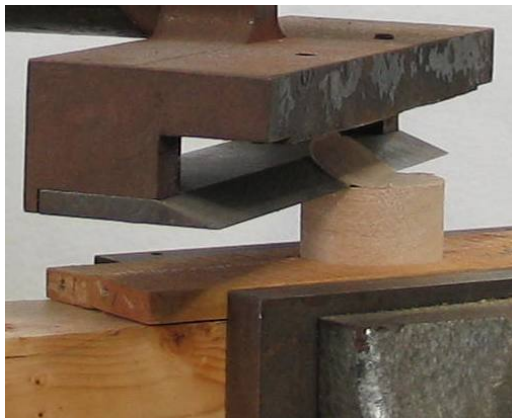


a)



b)

Figure 2.3 a) Setup to cut the 32-mm in diameter plug from the M&C control board; b) one M&C control board with the initial 32-mm in diameter plug removed and the hole fitted with a dummy plug.



a)



b)

Figure 2.4 a) Slicing device in action; b) Slices removed from the 32-mm in diameter test plug.

Once all the initial measurements were completed, the three M control boards, the three M&C control boards and the temperature control board, along with other 13 dummy pieces, were stacked inside the drying chamber (Figure 2.5). The board stack consisted of five rows of four sample boards laid on fixed stickers. The three M control boards were placed from the second to fourth row and in the second column while the three M&C profile boards were placed from the second to fourth row in the third column. The temperature control board was laid on the middle row and the fourth column near the air entrance of the

drying chamber. The distance between each row was about 21 mm, which is close to the conventional sticker thickness in industrial wood kilns in Eastern Canada.

During drying, the three M control boards were periodically taken out of the chamber, their weight taken, and then the drying curves were plotted. When the average moisture content of the M control boards respectively reached about 40, 30 and 20%, the three M&C boards were taken out of the chamber for the measurement of the color and moisture content profiles through the plug removing procedure. The three M&C boards were put back in their original positions in the chamber to pursue the drying. Then, 15 slices were cut from each plug to measure the color and moisture content profiles through thickness. When the average moisture content of M control boards reached the equilibrium moisture content (EMC) (14.3 ~ 5.1%, depending on specific drying condition), the moisture content of the three control boards were measured, with a WAGNER L612 Digital Recording Moisture Meter for quickly confirming the moisture content obtained by the gravimetric method. If the average M of the three boards was near the equilibrium moisture content at the specific drying condition, the three M&C control boards were taken out of the chamber for the last plug removal (Figure 2.6).



Figure 2.5 A stack of boards as seen from the open door of the drying chamber.

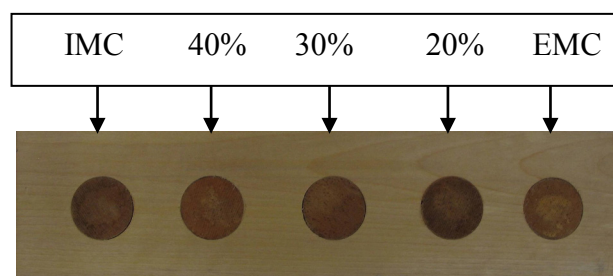


Figure 2.6 A moisture content and color control board being removed five plugs and filled with varnished dummy plugs.

After drying, the actual moisture content values of the three M control boards were measured with a pin-type moisture meter (Delmhorst RDM-1 Wood Moisture Meter) on each wide face at the surface, at $\frac{1}{4}$ thickness and at $\frac{1}{2}$ thickness. The average moisture content was calculated for each board. Then, the actual oven-dry weight of each M control board was recalculated in order to bring a correction on the drying curve based on the oven-dry weight inferred from the initial 10-mm plug sampling.

The BYK-Gardner color-guide 45/0 spectrophotometer used for wood color measurement is shown in Figure 2.7. Its 20-mm aperture, together with the sample area locator, guarantees repeatable results. Although the calibration of this instrument is supposed to be very stable and long-term, a calibration check was conducted each time it was used for color measurement. Preliminary tests were also conducted to evaluate the wood temperature effect on color measurement. No significant temperature effect was detected. Included easy-link software allows easy and direct data transfer from the instrument to Excel[®]. The results were expressed in the CIE $L^*a^*b^*$ coordinate system which has often been used to measure the color of wood in the industry. The three coordinates of CIE $L^*a^*b^*$ space represent the lightness of the color ($L^* = 0$ yields black and $L^* = 100$ indicates white), its position between red and green (a^* , negative values indicate green while positive values indicate red) and its position between yellow and blue (b^* , negative values indicate blue and positive values indicate yellow). The a^* and b^* axes have not specific numerical limits.

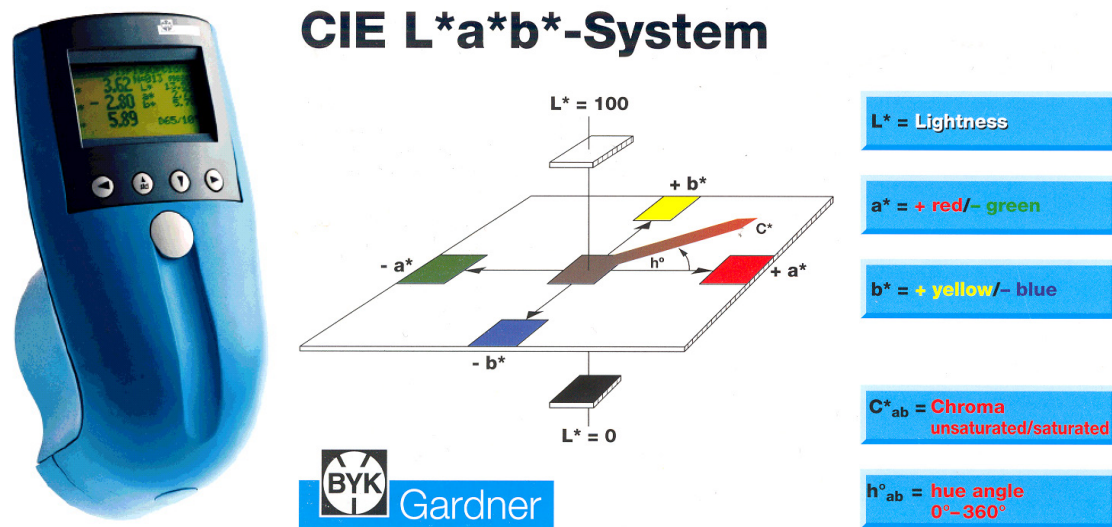


Figure 2.7 Color-guide 45/0 spectrophotometer made by BYK-Gardner and the CIE $L^*a^*b^*$ coordinate system.

2.2 DRYTEK code

The evolution of the moisture content profile with respect to time, which is an independent variable of the statistical predictive wood color mode, has to be known if the model is to be made applicable to any industrial drying conditions. Such information can be provided by the DRYTEK software, a two-dimensional wood drying model based on the water potential concept and developed at Laval University and Forintek Canada Corp. DRYTEK has recently been validated for conventional batch drying of commercial softwood species of Eastern Canada. The model relies on water retention and flow property data measured from green to dry conditions and at temperatures representative of conventional industrial kiln drying. It allows an arbitrary schedule of dry- and wet-bulb temperatures and air velocities, the step changes being made either on the basis of average moisture content or time. A user friendly graphical interface has been developed to facilitate the use of the simulation program by students and kiln managers or operators (Fortin et al. 2004).

The DRYTEK code was developed based on the finite element method, and was written in FORTRAN computer language. The code contains a series of algorithms and data bases which make it possible for reading the intrinsic and extrinsic model parameters and solving the equations of the model, and representing the results. Each time a new species has to be

added to the code library, laboratory work has to be conducted to measure a series of intrinsic model parameters, namely, the moisture content-water potential relationship ($M-\psi$), the moisture content-effective water conductivity relationship ($M-K$), the convective mass and heat transfer coefficients (h_ψ and h_h), and the ratio of vapour diffusion to the total water movement (ϵ). In this study, the $M-\psi$ and $M-K$ relationships and the mass transfer coefficient were determined for both species at three temperatures (40, 60 and 80°C). The other intrinsic parameters were assumed to be independent of wood species and inferred from previous internal studies (Nabhani 2002), or from literature.

Figures 2.8 and 2.9 show the input parameters and the drying schedules to be entered into the graphical interface each time a new simulation is conducted. After a simulation, results can be presented as required, including drying curves, moisture content and temperature profiles through board thickness at different drying times with a selected time step. Since DRYTEK contains a maximum wood stress calculation option, properties of the elasticity tensor has also to be filled in.

The screenshot shows the 'Paramètres de simulation' window with the following details:

- Section: CARACTÉRISTIQUES DU BOIS**
 - Espèce: Épinette noire (dropdown)
 - Densité basale Db(kg/m3): 410 (text input)
 - Type de débitage: sur dosse (dropdown)
 - Dimension des pièces (po): 2 x 4 (dropdown)
 - Teneur en humidité initiale, H(%): 55 (text input)
 - Température initiale, T(°C): 15 (text input)
- Section: CALCUL DES CONTRAINTES**
 - Optionnel: oui (dropdown)
 - Pas de calcul: 2 (dropdown)
 - Module d'élasticité tangentiel, ET (MPa): 493 (text input)
 - Module d'élasticité radial, ER (MPa): 832 (text input)
 - Module de cisaillement, GRT (MPa): 66 (text input)
 - Coefficient de poisson: uTR: 0.31405, uRT: 0.53 (text inputs)
- Section: GÉOMÉTRIE DE LA PILE**
 - Largeur de la pile (m): 1.22 (text input)
 - Épaisseur des baguettes (m): 0.019 (text input)
 - Écartement entre les baguettes (m): 0.6 (text input)
- Section: RÉSOLUTION NUMÉRIQUE**
 - Maillage: Fin (dropdown)
 - Pas de temps (s): 900 (text input)
 - Indice d'impression des résultats: Courbes séchage: 2 (dropdown), Profils: 15 (dropdown)

At the bottom, there are 'VALIDER' and 'ANNULER' buttons.

Figure 2.8 An interface showing model parameters to be filled in the DRYTEK code before a simulation.

Édition d'une étape de la table de séchage

Étape #	Température sèche (°C)	Température humide (°C)	Durée de l'étape (min)	Accroissement de la température	Teneur en H cible (%)	Vitesse de l'air (m/s)
0	25	25	0	instantané	0	2.5

Table de séchage courant

0	25.00	25.00	0.00	0	0.00	2.50
1	60.00	60.00	120.00	1	0.00	2.50
2	60.00	57.20	0.00	0	35.00	2.50
3	60.00	56.10	0.00	0	30.00	2.50
4	65.60	59.40	0.00	0	25.00	2.50
5	71.10	62.80	0.00	0	20.00	2.50
6	76.70	65.60	0.00	0	15.00	2.50
7	82.20	54.40	0.00	0	10.00	2.50
8	82.20	74.40	900.00	0	0.00	2.50
9	82.20	77.70	240.00	0	0.00	2.50

Buttons: Ajouter une étape, Insérer une étape, Supprimer une étape, Sauvegarder, Annuler

Figure 2.9 An interface showing drying schedule to be filled in the DRYTEK code.

2.3 Measurement of the wood drying model parameters

2.3.1 Moisture content-water potential relationship

2.3.1.1 Material

The material used for the measurement of the M - ψ relationship came from live trees felled in the Beauce region of Quebec, during winter in the case of sugar maple and during fall for paper birch. Three trees for each species were then cut into four 1.2-m long bolts, and transported to the laboratory for further processing. More than 84 sapwood blocks of 45 x 10 x 45 mm (L x R x T) in dimension were cut for each tree, the radial direction being the moisture flow direction of the specimen in contact with the pressure membrane described below. Only the blocks free of any visual defects were selected as test specimens, except for some birch specimens that showed some discoloration on part of the cross section. Nine matched groups were prepared. Each group was composed of 12 specimens, namely four specimens from each tree. After selection and classification, the specimens were kept in sealed polyethylene bags and stored in a freezer at -5°C until required during the experiments. Before each experiment, the specimens were taken out of the freezer and kept over demineralized water in a closed desiccator at room temperature for about 24 hours until they thawed.

The average green specific gravity of sugar maple specimens was 0.630 (varying from 0.590 to 0.666) and the average initial moisture content was 50% (varying from 47% to 55%). The average green specific gravity of paper birch specimens was 0.513 (varying from 0.481 to 0.580) and the average initial moisture content was 91% (varying from 74% to 103%).

2.3.1.2 Methods

The pressure membrane technique was used to measure the M- ψ relationship at 40, 60 and 80°C corresponding to the temperature range used for conventional drying of lumber industrial conditions. A schematic diagram of the pressure membrane apparatus is shown in Figure 2.10. A detailed description of the apparatus and procedures is given in Cloutier and Fortin (1991) and Tremblay et al. (1996). An improvement was made in this study concerning the temperature control in the pressure chamber by adding a thermocouple close to the wood specimens. A data acquisition system (QuickLog[®] software) was used to monitor the temperature on a continuous basis. Four pressure membrane extractors with maximum capacity of 1, 10, 20 and 50 bars, were used to conduct the M- ψ relationship determination from the green state to approximately the fiber saturation point. Each pressure membrane apparatus was covered with a heating box connected to a thermostatic water bath for temperature control.

To conduct a specific test, 12 green wood specimens were put in contact with the pressure membrane made of a cellulose acetate sheet permeable to water but impermeable to air, capable of resisting to an air pressure of more than 50 bars once saturated with water. A blotting paper was put in between the pressure membrane and the stainless steel screen placed underneath to help keeping the membrane saturated with water over time. Furthermore, a 2-mm thick saturated clay layer was put on the pressure membrane to ensure permanent hydraulic contact with the specimens. Once the specimens were in place, the pressure vessel was closed, and pressure applied gradually up to the equilibrium pressure, but only after reaching the desired test temperature inside the chamber. The volume of the water outflow was then measured periodically and the test stopped once an

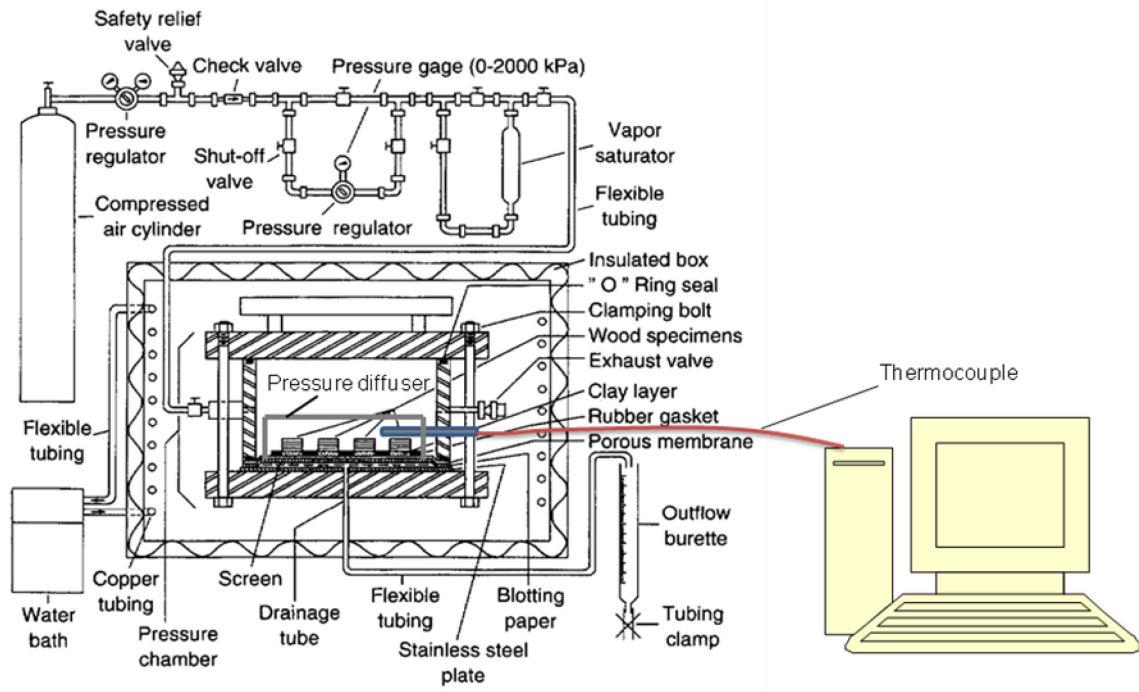


Figure 2.10 Schematic diagram of the pressure membrane apparatus (adapted from Tremblay et al. 1996) with the temperature acquisition system.

apparent equilibrium had been reached for at least 72 hours. And then, the pressure vessel was opened and the equilibrium moisture content (EMC) of each specimen was determined by the gravimetric method. The matric potential can be expressed as follows (Cloutier and Fortin 1991):

$$\psi_m = -\bar{V}_w P_m \quad [2.1]$$

where, \bar{V}_w is specific volume of water ($\text{m}^3 \text{kg}^{-1}$); P_m is also named as equivalent matric pressure (Pa).

2.3.2 Effective water conductivity

2.3.2.1 Material

The material used to determinate the effective water conductivity of wood were of the same origin as the one used to determine the M- ψ relationship. The dimensions of the sapwood test specimens were 45 x 45 x 45 mm (L x R x T). Seven end-matched groups of paper birch specimens and five end-matched groups of sugar maple specimens were separately

formed for each combination of temperature and relative humidity. More groups were needed for birch because of the higher initial moisture content. Each group was made up of three specimens, i.e., one specimen for each tree. After selection and classification, the specimens were kept in sealed polyethylene bags and stored at -5°C until required during the experiments. Before each experiment, the specimens were taken out of the freezer and kept over demineralized water in closed desiccators at room temperature for about 24 hours until they thawed.

2.3.2.2 Methods

In order to ensure unidirectional moisture flow (radial or tangential), the four edges of the green specimens were coated with silicone sealant and aluminium foil, using flash drying to get a better fixation of the sealant. Then, the bottom end of the specimens was covered with a 2-mm thick neoprene gasket and a sheet of aluminium foil with a pinhole at the center so as to allow pressure equalization through the pinhole. The top face was also temporarily covered with an aluminium foil until the beginning of the conductivity experiment.

A conditioning chamber (Envirotronics[®] Model SH27) with workspace dimensions of $0.9 \times 0.9 \times 0.9$ m in which an air flow diffuser was installed was used for the experiment. The specimens were placed in five or seven rows, depending on the species, each row corresponding to a different data point along the M-K relationship, and each column corresponding to a different tree (repetitions). Three control specimens were also used to monitor the drying rate through periodically weighing. The drying face of the specimens was then exposed to a horizontal air stream of about 1.0 m/s. The dry-bulb temperatures were 40, 60 and 80°C and the relative humidity adjusted to give an EMC of 9%. A water pan had to be added at 80°C to help maintain the drying conditions through the whole test, which lasted more than two weeks. Dry-bulb and wet-bulb thermocouples were placed inside the conditioning chamber at the exit of the specimen area in order to have an independent check of the chamber climate.

The instantaneous profile method (Cloutier and Fortin 1993) was used to determine the mass flux q_{mx} . The measurements were done at the following average moisture contents of

the three control specimens: green condition, 60, 50, 40, 30, 20 and 10% for paper birch specimens; and green condition, 40, 30, 20 and 10 for sugar maple specimens. When a target moisture content value was reached, for a given direction of flow, one group of three specimens was taken out of the chamber for determination of the moisture content (M) profiles. The specimens were sawn into 9 slices using a thin kerf band saw. The moisture content of each slice was measured by the gravimetric method at the nearest 0.0001 g and the volume was determined by the water immersion method. The corresponding moisture concentration (C) value was calculated. Each data was shown in a C-x coordinate system to represent the average C at a given position (x) for the three slices of a group. The average C profiles were fitted to the data points by hand.

The specimen bottom side was defined as the position corresponding to the lower limit of

the integral $\int_{x_{q=0}}^{x_i} C dx$, namely $x_{q=0}$, where $x = 0$ mm. From the bottom side, six positions were

considered, namely $x_i = 10, 15, 20, 25, 30$ and 35 mm. The integral $\int_{x_{q=0}}^{x_i} C dx$, at a specific

drying time t_j and a specific position x_i , was then estimated by graphical integration of the area defined by the average C profile at t_j and the planes $x = x_i$ and $x_{q=0}$. All values

of $\int_{x_{q=0}}^{x_i} C dx$ at position x_i were plotted against drying time. By graphically measuring the slope

at time t_j , $\left[\frac{\partial}{\partial t} \left(\int_{x_{q=0}}^{x_i} C dx \right) \right]_{x_i, t_j}$ at the position x_i was determined.

The ψ gradient $[\partial \psi / \partial x]_{x_i, t_j}$ was inferred from the M profiles obtained in this experiment and the M- ψ relationship measured at the same temperature. The ψ profile at t_j was plotted and the ψ gradient at x_i was evaluated by measuring the slope graphically.

The effective water conductivity in the flow direction x at position x_i and time t_j , $[K_x]_{x_i, t_j}$, may be calculated using the following equation (Cloutier and Fortin 1993, Tremblay et al. 2000a):

$$[K_x]_{x_i, t_j} = \frac{\left[\frac{\partial}{\partial t} \left(\int_{x_q=0}^{x_i} C dx \right) \right]_{x_i, t_j}}{\left[\frac{\partial \psi}{\partial x} \right]_{x_i, t_j}} \quad [2.2]$$

2.3.3 Convective mass transfer coefficient

2.3.3.1 Material

Because of time constraint, no specific experiments were conducted to measure the heat and mass transfer coefficients with respect to moisture content and temperature. The heat transfer coefficient was inferred from the values of Nabhani (2002). The mass transfer coefficient at high moisture contents, i.e. in the moisture content range where it is maximum and constant, was determined from the drying curves measured during the wood color tests. According to theory, the constant rate period of the initial phase of the drying curve can be used to obtain a good approximation of the maximum value of the mass transfer coefficient. The decreasing zone of the mass transfer coefficient was then obtained by a curve fitting technique which will be explained later in the text.

2.3.3.2 Methods

Using the drying curves obtained from the color tests, the convective mass transfer coefficient h_ψ was determined from the following equation:

$$h_\psi = \frac{q_{mc}}{\psi_s - \psi_\infty} \quad [2.3]$$

where, q_{mc} is the convective moisture flux normal to the wood surface ($\text{kg}_{\text{water}} \text{m}^{-2} \text{drying surface s}^{-1}$); ψ_s is the water potential at the specimen surface, inferred from the surface moisture

content and the M - ψ relationship, and ψ_∞ is the water potential of the ambient air-vapor mixture. The water potential of the air-vapor mixture was calculated with the following equation (Cloutier et al. 1992):

$$\psi_\infty = \frac{RT}{M_w} \cdot \ln \frac{p_v}{p_{vs}} \quad [2.4]$$

where, R = the universal gas constant ($8.314 \text{ J mol}^{-1} \text{ K}^{-1}$), T = the dry-bub temperature (K); M_w = the molecular weight of water ($18.015 \times 10^{-3} \text{ kg/mol}$), p_v = the partial pressure of vapour in equilibrium with the water in wood (Pa), and p_{vs} = the partial pressure of vapour in equilibrium with pure free water (Pa).

The convective moisture flux q_{mc} was calculated by the following function:

$$q_{mc} = (dM/dt)V_{wood}D_b / A \quad [2.5]$$

where dM/dt = slope of a drying curve during the constant drying rate period ($\text{kg}_{\text{water}} \text{ kg}^{-1}_{\text{oven-dry wood}} \text{ s}^{-1}$), V_{wood} = volume of moist wood ($\text{m}^3_{\text{moist wood}}$), D_b = basic density of wood ($\text{kg}_{\text{dry wood}} \text{ m}^{-3}_{\text{moist wood}}$), and A = area of wood specimen subjected to evaporation (m^2).

2.4 Validation of color model

2.4.1 Material

The test material used for this part of the study was of the same origin as the one used for the color test. Because of the biological variability, the average properties were, however, slightly different. The average green specific gravity of sugar maple sapwood was 0.660 (varying from 0.602 to 0.695) and the average green specific gravity of paper birch was 0.489 (varying from 0.464 to 0.534). The average initial moisture content was 51% (varying from 48 to 56%) and 63% (varying from 56 to 68%), respectively.

2.4.2 Methods

One validation drying test was performed for each species in the same drying tunnel as that used for the color tests. Following identical experimental procedures (section 2.1.2), one-step drying schedule was applied with the dry-bulb temperature at 70°C and wet-bulb depression temperature at 10°C. These drying conditions were chosen in order to conduct an independent set of experiments, midway between the drying conditions at 60 and 80°C. The same procedures were followed during the validation test as the ones used for the tests of color measurements at 40, 60 and 80°C.

Chapter 3. Results and discussion

3.1 Wood color change measurements

3.1.1 Drying curves

The drying curves of three M control boards for the six color tests are shown in Figure 3.1 and Figure 3.2 for paper birch and sugar maple, respectively. The observed drying conditions are shown in Figure A.1 and A.2 (Appendix A) and in Table 3.1 in order to help the analysis of the drying curves. Taking into account the accuracy of the thermocouples ($\pm 0.5^{\circ}\text{C}$), the dry-bulb temperatures were very close to the target values in all cases. However, the wet-bulb temperatures were up to 1.1°C away from the target values, which made the target wet-bulb depression either too high (target value of 4°C) or too low (target value of 15°C). Because of the inertia of the vapor saturator conditioning system, this was difficult to correct during the experiments. As shown in Table 3.1, the average maximum deviation of the wet-bulb depression from the target values was of 0.7°C in the former case and 1.4°C in the latter case. The error caused by these deviations in terms of EMC values remained fairly small with a maximum difference of 1.6% M for a target EMC of about 14% and of 1.3% M for a target EMC varying between 5.6 and 5.9% (Table 3.1).

The first observation on Figures 3.1 and 3.2 is that the drying time, at a given wet-bulb depression, decreases with an increase of dry-bulb temperature, which is in agreement with

the theory. The drying curves of both species become then noticeably steeper as the dry-bulb temperature increases. Likely, at a given dry-bulb temperature, the drying curves of both species become noticeably steeper as the wet-bulb depression increases. Because the relative humidity of air is reduced when the wet-bulb depression increases, the moisture content in the wood surface layers tends to be smaller. Thus, the driving force of moisture in wood becomes higher, and so for the drying rate. This can be seen in Table 3.2 which gives the drying rates calculated at various M values of the drying curves.

Table 3.1 Comparison of target and measured kiln conditions for wood color tests

Target ΔT (°C)	Kiln conditions		Species					
			Paper Birch			Sugar Maple		
			Target dry-bulb T (°C)			Target dry-bulb T (°C)		
			40	60	80	40	60	80
4	Measured	Dry-bulb T (°C)	39.8	60.1	80.1	40.2	60.0	80.4
		Wet-bulb T (°C)	35.8	56.3	75.7	35.7	55.9	75.7
		ΔT (°C)	4.0	3.8	4.4	4.5	4.1	4.7
		RH (%)	76.8	82.4	82.9	74.2	81.1	81.8
		EMC (%)	14.0	14.4	12.9	13.2	13.9	12.5
	Target EMC (%)		14.3	14.2	14.1	14.3	14.2	14.1
15	Measured	Dry-bulb T (°C)	39.9	59.7	79.6	39.7	59.7	80.5
		Wet-bulb T (°C)	26.1	45.7	64.8	26.1	46.0	66.0
		ΔT (°C)	13.8	14.0	14.8	13.6	13.7	14.5
		RH (%)	33.3	45.7	51.1	33.8	46.6	52.1
		EMC (%)	6.2	7.1	6.8	6.3	7.2	6.8
	Target EMC (%)		5.6	5.9	5.9	5.6	5.9	5.9

Table 3.2 Drying rate values obtained during wood color tests

Target ΔT (°C)	Drying ranges (% M)	Drying rate (%/hr)					
		Paper Birch			Sugar Maple		
		Target T (°C)			Target T (°C)		
		40	60	80	40	60	80
4	50	0.71	0.80	0.98	0.60	0.66	0.77
	40	0.60	0.70	0.85	0.50	0.58	0.65
	30	0.33	0.41	0.60	0.30	0.37	0.47
	20	0.13	0.19	0.25	0.07	0.12	0.21
	15	0.04	0.06	0.11	0.02	0.03	0.07
15	50	1.55	1.80	2.15	1.75	1.90	2.05
	40	1.05	1.40	1.90	1.55	1.75	1.88
	30	0.51	0.75	0.95	0.70	1.00	1.19
	20	0.26	0.37	0.47	0.28	0.40	0.50
	10	0.04	0.06	0.12	0.04	0.11	0.15

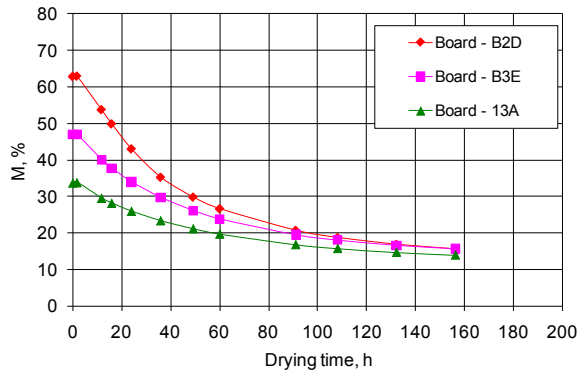
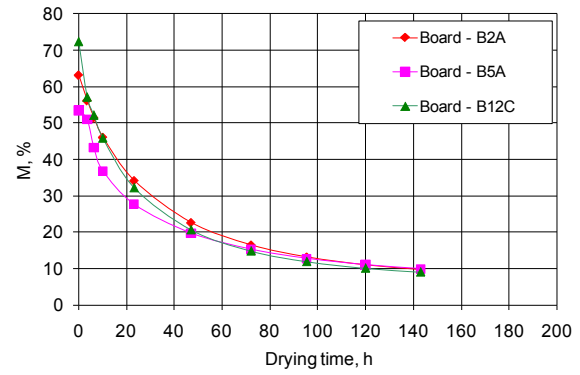
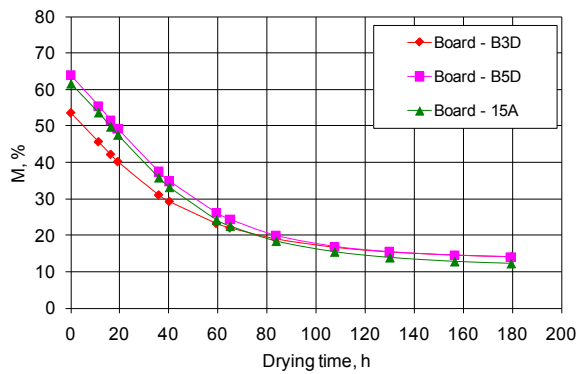
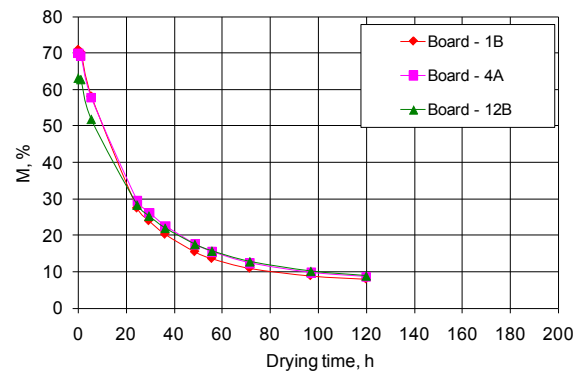
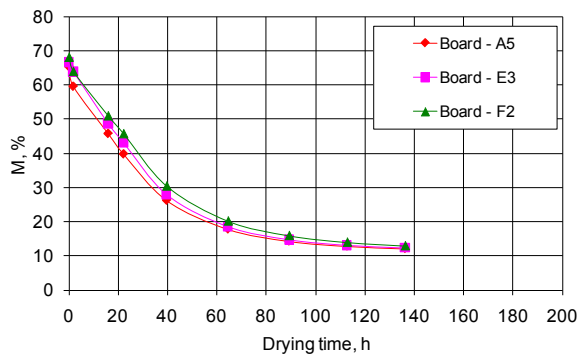
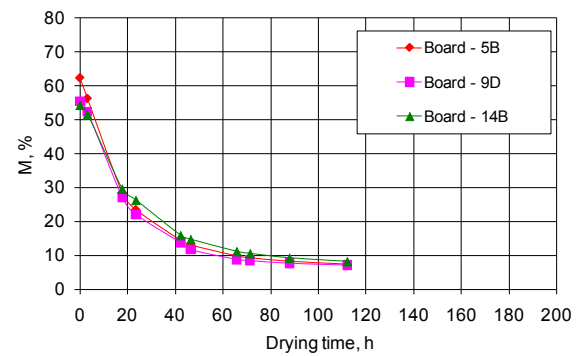
(a) $T = 40^{\circ}\text{C}$ and $\Delta T = 4^{\circ}\text{C}$;(b) $T = 40^{\circ}\text{C}$ and $\Delta T = 15^{\circ}\text{C}$;(c) $T = 60^{\circ}\text{C}$ and $\Delta T = 4^{\circ}\text{C}$;(d) $T = 60^{\circ}\text{C}$ and $\Delta T = 15^{\circ}\text{C}$;(e) $T = 80^{\circ}\text{C}$ and $\Delta T = 4^{\circ}\text{C}$;(f) $T = 80^{\circ}\text{C}$ and $\Delta T = 15^{\circ}\text{C}$;

Figure 3.1 Drying curves measured from three M control boards during the six color tests on paper birch.

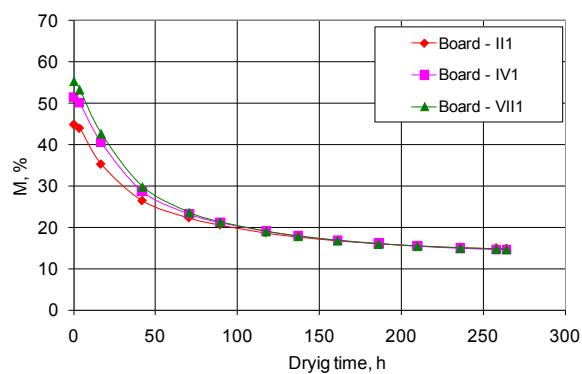
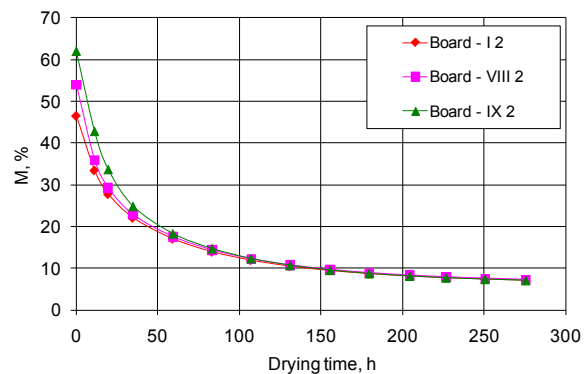
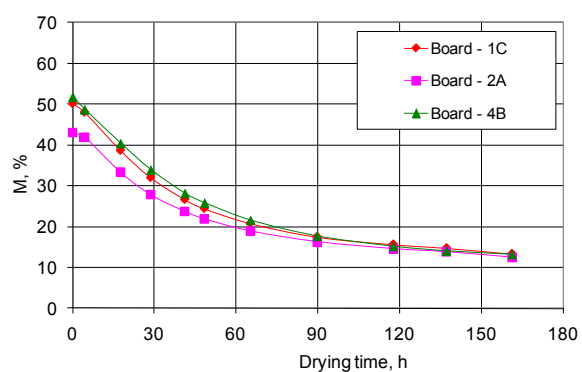
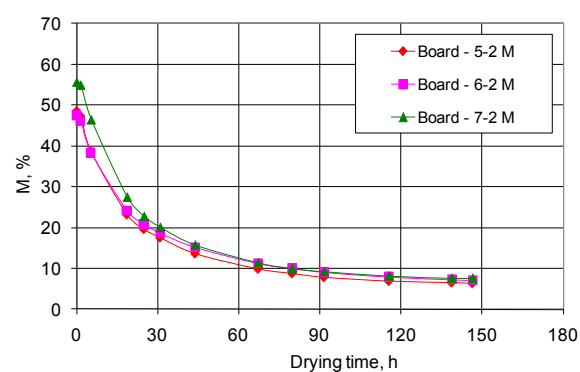
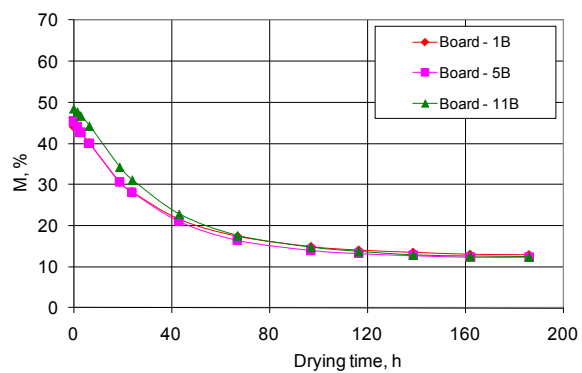
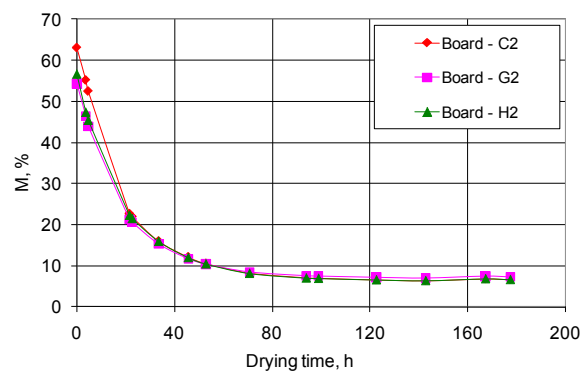
(a) $T = 40^{\circ}\text{C}$ and $\Delta T = 4^{\circ}\text{C}$;(b) $T = 40^{\circ}\text{C}$ and $\Delta T = 15^{\circ}\text{C}$;(c) $T = 60^{\circ}\text{C}$ and $\Delta T = 4^{\circ}\text{C}$;(d) $T = 60^{\circ}\text{C}$ and $\Delta T = 15^{\circ}\text{C}$;(e) $T = 80^{\circ}\text{C}$ and $\Delta T = 4^{\circ}\text{C}$;(f) $T = 80^{\circ}\text{C}$ and $\Delta T = 15^{\circ}\text{C}$;

Figure 3.2 Drying curves measured from three M control boards during the six color tests on sugar maple.

The drying rate values from Table 3.2 show a very clear increase of the drying rate with the increase of dry-bulb temperature and the wet-bulb depression. Also, the drying rate at 50% M is about two or three times as much as that at 30% M. It is interesting to note that the drying rate above FSP at 40°C dry-bulb and 15°C wet-bulb depression is higher than the drying rate at 80°C dry-bulb and 4°C wet-bulb depression. Thus, the effect of wet-bulb depression on the drying rate above FSP is more important than the effect of temperature. The explanation of this difference is found in the respective equilibrium moisture contents of both drying conditions (see Table 2.1). However, below FSP the effect of temperature is more important than the effect of the wet-bulb depression.

As far as the drying time is concerned, it was shorter than the normal drying times found in industrial kilns for paper birch or sugar maple at the corresponding dry-bulb temperature. The fact of using one-step drying schedule inevitably shortens the drying time. The use of multiple step drying schedules would have been preferable but this would have made very complicated the development of a predictive color model because of the possible interactions between the drying parameters from one step to the other within the drying schedule.

3.1.2 Wood temperature profiles

The evolution of wood temperature profiles through board thickness during the six color tests are presented in Figures A.3 and A.4 (Appendix A) for paper birch and sugar maple, respectively. The temperature profiles tend to be flatter for sugar maple than for paper birch, although the temperature gradients in wood remain very small at all times during drying. Furthermore, the wood temperature took longer to get near the dry-bulb temperature when the wet-bulb depression was higher. In theory, the wood temperature should remain close to the wet-bulb temperature as long as there is free water in wood. This did not happen in the present study since the wood moisture content was down to 35 ~ 40% M only a few hours after the start of the drying run.

3.1.3 Moisture content profiles

The M profiles measured on the M control boards are shown in Figures 3.3 and 3.4 for paper birch and sugar maple, respectively. Each profile represents the average of three control boards. In order to have the moisture content data points at the same position as the color data points, the moisture content of a given slice was attributed to the top position of the next slice, i.e. the position where the measurement of the wood color was performed. One exception to this rule was the surface moisture content which was also taken as that of the first slice instead of using an extrapolated value. This is why the first two data points of each profile on Figures 3.3 and 3.4 show the same value. The consequence of this was to move the profile close to the surface slightly to the right. The error caused by this procedure was difficult to assess accurately but a graphical analysis with the data points at the mid slice thickness position revealed that it was kept small in all cases. Concerning the accuracy of the M measurement with the slicing technique, maximum error calculations showed that the maximum error due to the weighing process was near 1%. However, in the wet state, an additional error of about 1 ~ 2% could have been produced by the plug cutting technique and the slicing technique.

A first observation is the fact that the M profiles for sugar maple are flatter than those of paper birch. This is likely due to the lower water conductivity of the latter above FSP, which will be shown later in the text. In the case of maple, the M gradients build in the vicinity of the board surface while in the case of birch, they tend to build gradually from the core to the surface. Furthermore, in both cases the surface moisture content tends more or less gradually toward the equilibrium moisture content of the ambient air, this happening faster as the wet-bulb depression and the dry-bulb temperatures are higher. It is also happening faster in the case of birch, probably due again to its lower water conductivity.

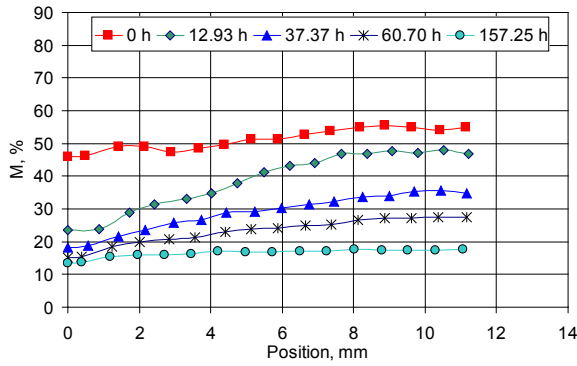
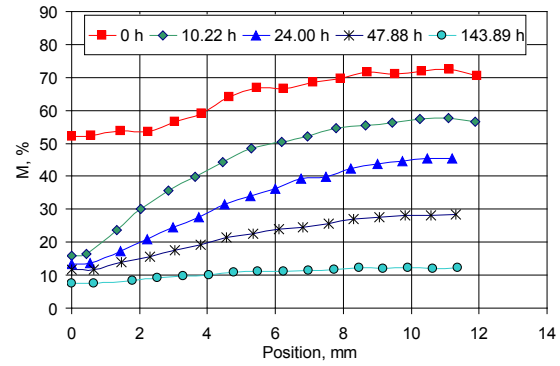
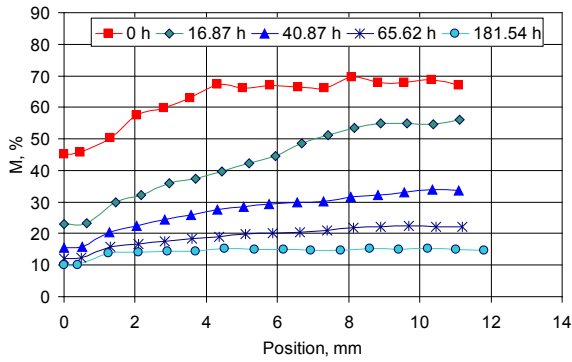
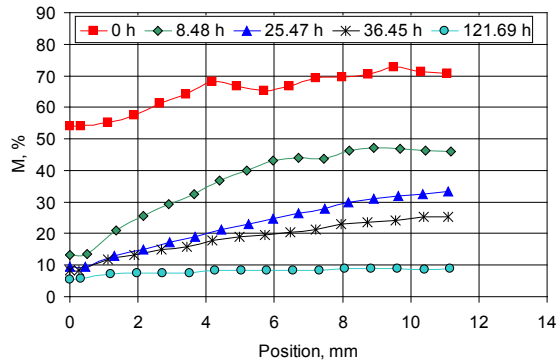
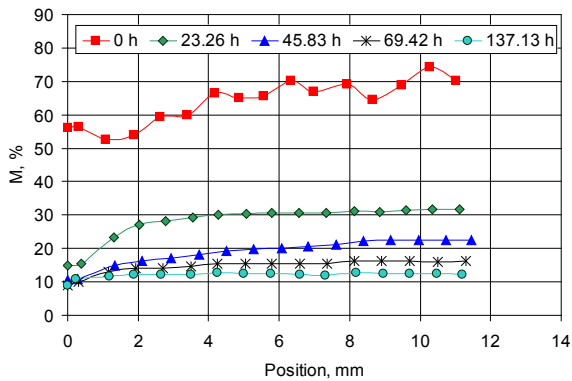
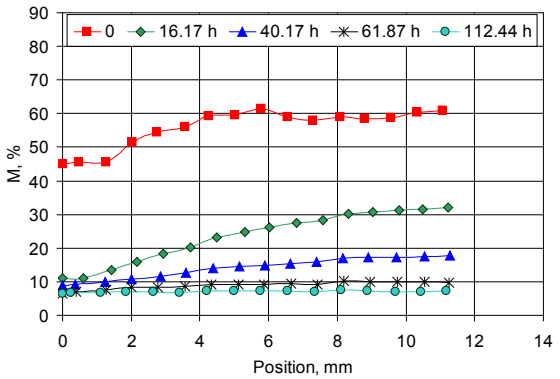
(a) $T = 40^{\circ}\text{C}$ and $\Delta T = 4^{\circ}\text{C}$;(b) $T = 40^{\circ}\text{C}$ and $\Delta T = 15^{\circ}\text{C}$;(c) $T = 60^{\circ}\text{C}$ and $\Delta T = 4^{\circ}\text{C}$;(d) $T = 60^{\circ}\text{C}$ and $\Delta T = 15^{\circ}\text{C}$;(e) $T = 80^{\circ}\text{C}$ and $\Delta T = 4^{\circ}\text{C}$;(f) $T = 80^{\circ}\text{C}$ and $\Delta T = 15^{\circ}\text{C}$;

Figure 3.3 Moisture content profiles through the board thickness of paper birch at five different drying times during drying at six different drying conditions.

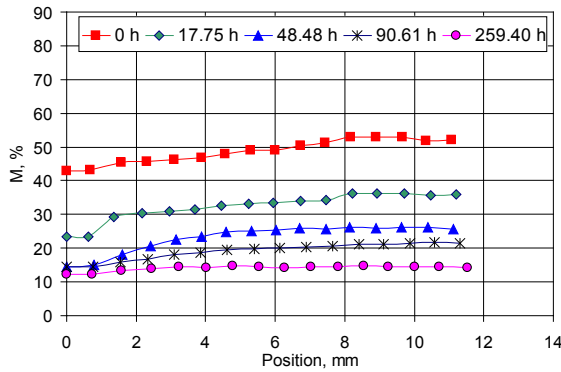
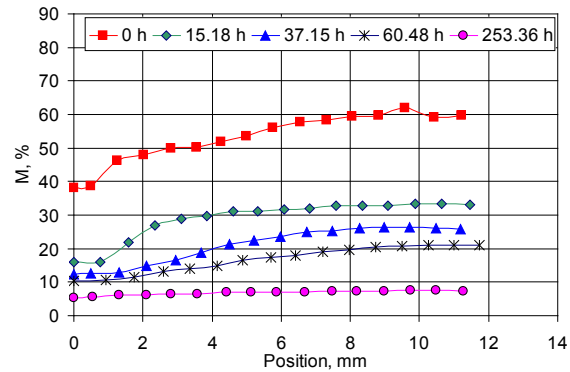
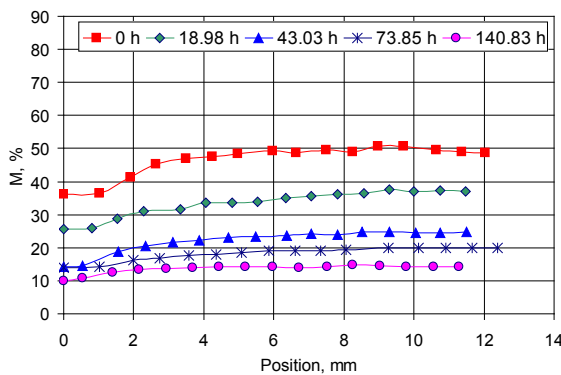
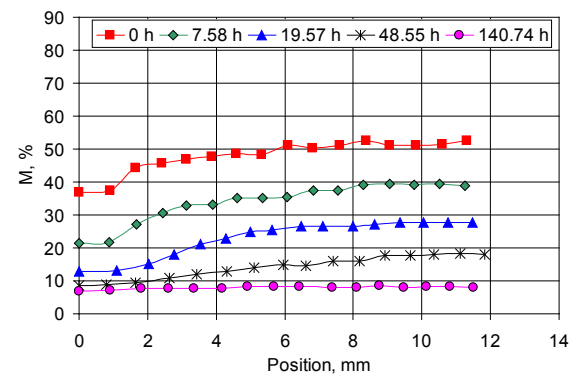
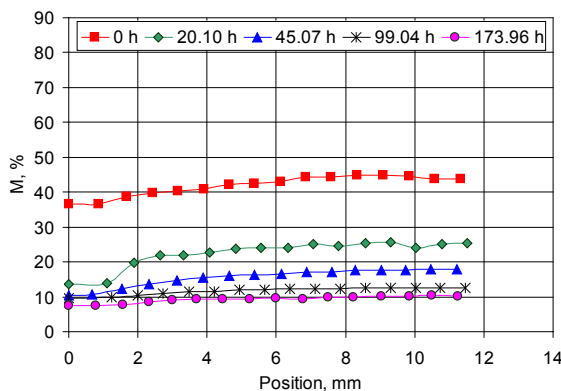
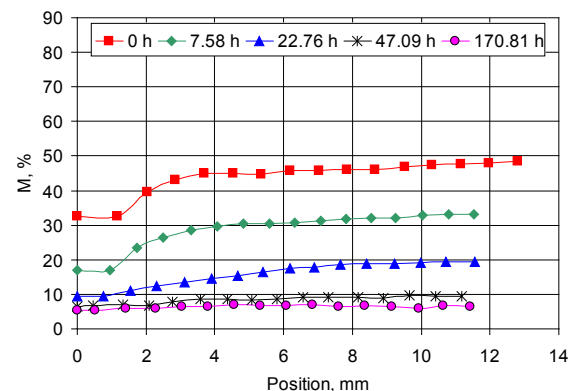
(a) $T = 40^{\circ}\text{C}$ and $\Delta T = 4^{\circ}\text{C}$;(b) $T = 40^{\circ}\text{C}$ and $\Delta T = 15^{\circ}\text{C}$;(c) $T = 60^{\circ}\text{C}$ and $\Delta T = 4^{\circ}\text{C}$;(d) $T = 60^{\circ}\text{C}$ and $\Delta T = 15^{\circ}\text{C}$;(e) $T = 80^{\circ}\text{C}$ and $\Delta T = 4^{\circ}\text{C}$;(f) $T = 80^{\circ}\text{C}$ and $\Delta T = 15^{\circ}\text{C}$;

Figure 3.4 Moisture content profiles through the board thickness of sugar maple at five different drying times during drying at six different drying conditions.

3.1.4 Wood color profiles

The measured L^* profiles on paper birch sapwood boards are shown in Figure 3.5 and those of sugar maple sapwood boards are shown in Figure 3.6. Before drying, for both species, the L^* value obtained on the wood surface (0 h) is always lower than the values measured inside the wood. This is easily explained by the fact that the surface M at 0 h was in all cases lower than the inside M (Figures 3.3 and 3.4). As the drying goes on, the L^* values on the surface and inside the board decrease, although at different rates. The lower the wet-bulb depression, the higher the decrease of the L^* value is during the drying test, and the higher the dry-bulb temperature, the higher the decrease of the L^* value is. This means that a relatively low dry-bulb temperature (in the vicinity of 40°C) and fairly large wet-bulb depression are the critical conditions to minimise discoloration during kiln drying. The L^* profiles between 0.3 mm below the wood surface to the center of the board remain either relatively flat, or tend to form a negative slope at the opposite of the moisture content profile evolution. The latter mainly occurred between one and two days of drying at dry-bulb temperatures of 60°C and 80°C and at 15°C wet-bulb depression (Figures 3.5d, f and Figures 3.6d, f).

The change of the L^* value during drying at 40°C dry-bulb temperature was fairly small, except for paper birch at the 4°C wet-bulb depression (Figure 3.5a). For sugar maple, there was even an increase of the L^* value during drying (Figure 3.6b). The final L^* profile of paper birch at 80°C dry-bulb temperature and 15°C wet-bulb depression is higher than that at 60°C dry-bulb temperature and 4°C wet-bulb depression. One can observe a similar behavior for sugar maple except the part of the profile from the surface to about 2 mm thickness. Stenudd (2004) concluded that during capillary drying phase ($M > 55\%$), drying time was more important than the dry-bulb temperature. The lightness of wood increased if the initial drying was fast even at elevated temperatures.

The times when boards were taken out of the drying chamber and cut for obtaining M and L^* profiles were not the same at different drying tests. The M - L^* relationships on the wood surface and at 6 and 10 mm below the wood surface are separately shown in Figures C.1, C.2 and C.3 (Appendix C) for paper birch and in Figures C.4, C.5 and C.6 for sugar maple.

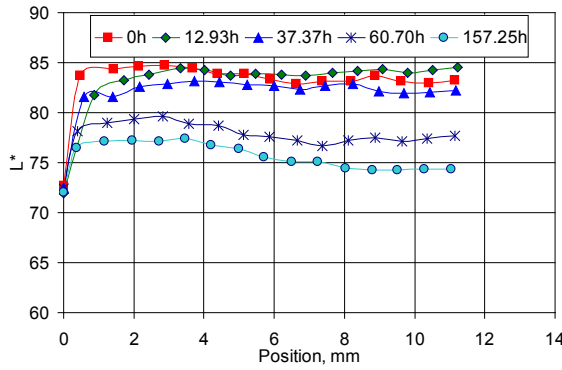
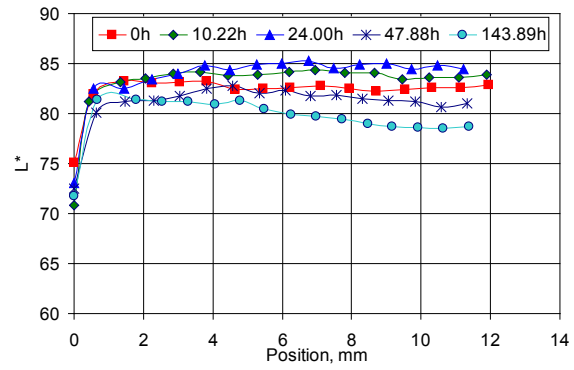
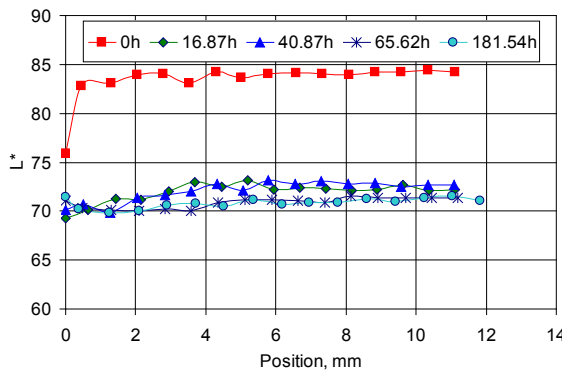
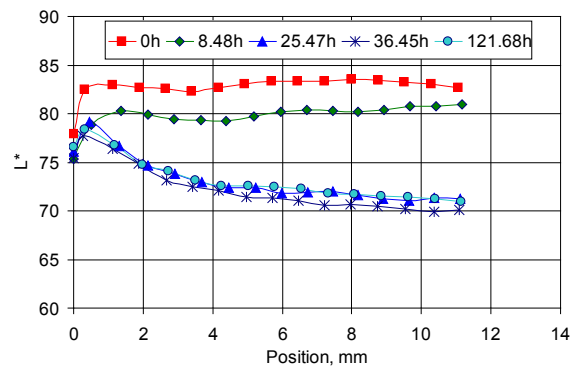
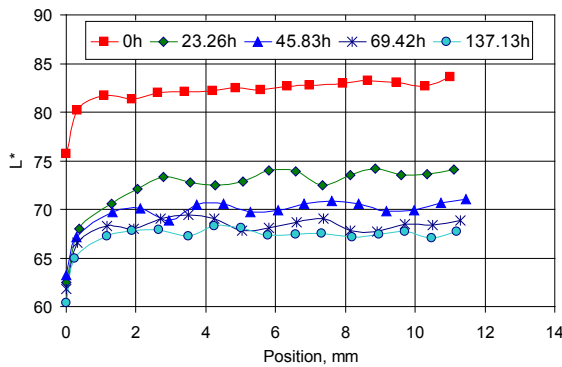
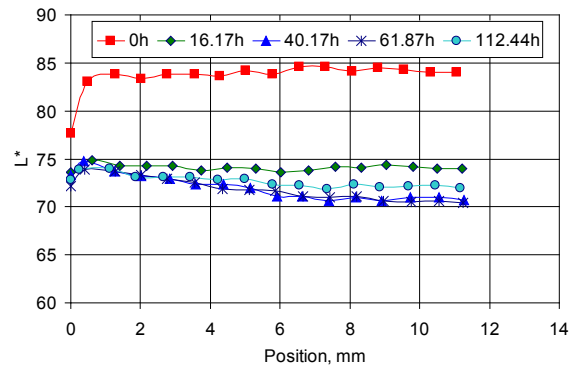
(a) $T = 40^{\circ}\text{C}$ and $\Delta T = 4^{\circ}\text{C}$;(b) $T = 40^{\circ}\text{C}$ and $\Delta T = 15^{\circ}\text{C}$;(c) $T = 60^{\circ}\text{C}$ and $\Delta T = 4^{\circ}\text{C}$;(d) $T = 60^{\circ}\text{C}$ and $\Delta T = 15^{\circ}\text{C}$;(e) $T = 80^{\circ}\text{C}$ and $\Delta T = 4^{\circ}\text{C}$;(f) $T = 80^{\circ}\text{C}$ and $\Delta T = 15^{\circ}\text{C}$;

Figure 3.5 Wood lightness profiles through the board thickness of paper birch at five different times during drying at six different drying conditions.

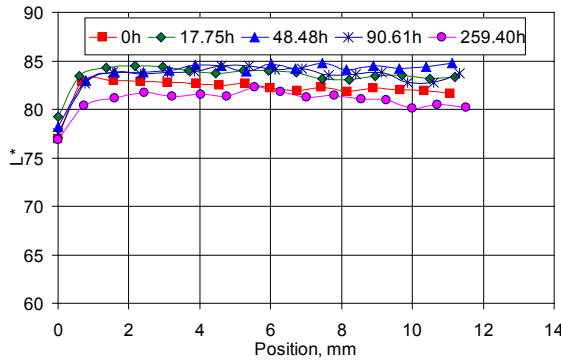
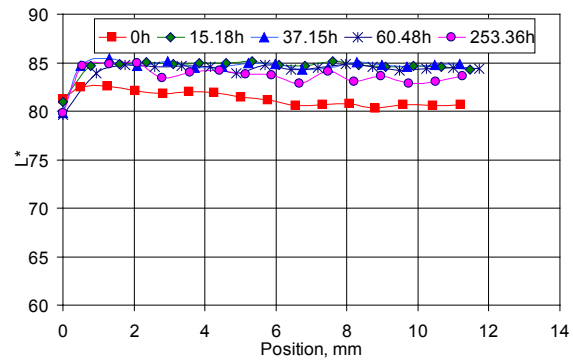
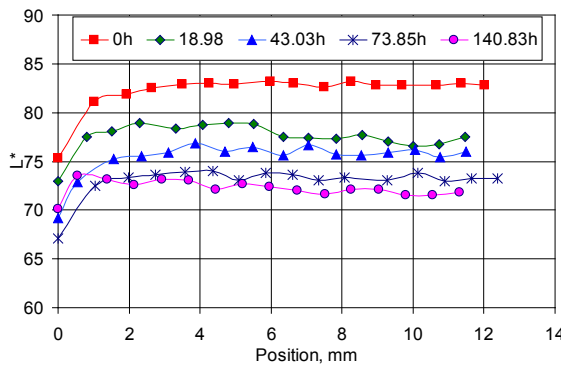
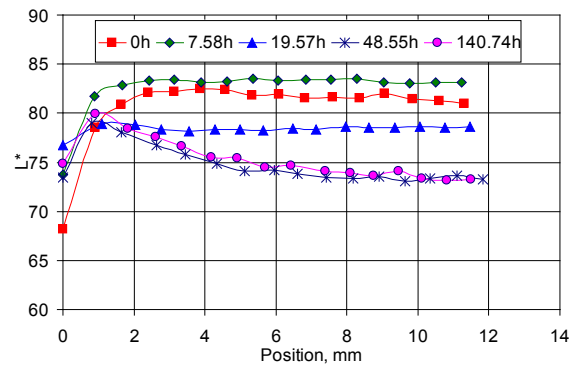
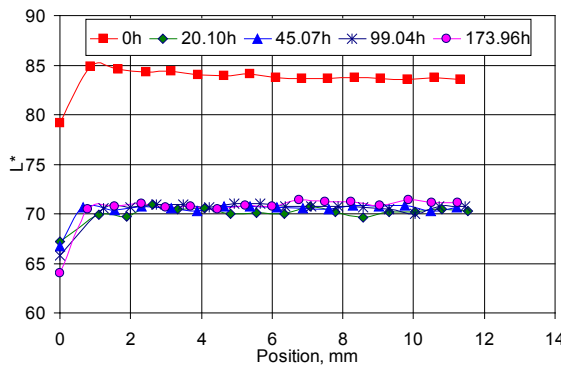
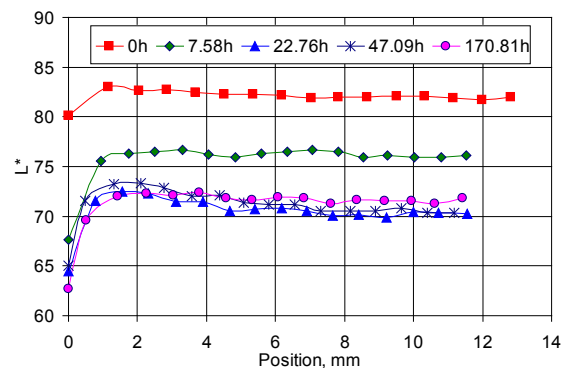
(a) $T = 40^{\circ}\text{C}$ and $\Delta T = 4^{\circ}\text{C}$;(b) $T = 40^{\circ}\text{C}$ and $\Delta T = 15^{\circ}\text{C}$;(c) $T = 60^{\circ}\text{C}$ and $\Delta T = 4^{\circ}\text{C}$;(d) $T = 60^{\circ}\text{C}$ and $\Delta T = 15^{\circ}\text{C}$;(e) $T = 80^{\circ}\text{C}$ and $\Delta T = 4^{\circ}\text{C}$;(f) $T = 80^{\circ}\text{C}$ and $\Delta T = 15^{\circ}\text{C}$;

Figure 3.6 Wood lightness profiles through the board thickness of sugar maple at five different times during drying at six different drying conditions.

The L^* values at the surface decrease as the moisture content decreases for most cases. Relating the L^* profiles to M profiles, it was found that the L^* values below the surface decrease rapidly when the moisture content decreases, but below about 30% M , the L^* values decrease slowly until about 15 ~ 25% M where the L^* values level out or begin to increase. The majority of L^* change occurs above FSP. According to Kreber et al. (1998) and Sundqvist (2002b), compared with the whole drying process, the discoloration of wood induced by drying was considered to be dominant when the capillary water existed in the wood. Yeo and Simith (2004) also found that interior darkening develops in the boards of hard maple if temperatures were above 43°C when the moisture content was at and above the FSP, and that there was minimal color change during the drying below the FSP.

The measured a^* and b^* profiles are shown in Appendix B. The variation of a^* (red to green) follows the same tendency as that of the lightness L^* with respect to the dry bulb temperature and the wet bulb depression. However, contrarily to L^* , a^* increases with a decrease of M , from an initial value below surface of about 4 to a maximum value between 7 and 11, and the a^* values on the surface of the board are generally greater than those below surface. Furthermore, the a^* values below surface show a constant evolution with respect to the depth in the board, which is not the case for L^* .

Concerning the component b^* (yellow to blue), its variation with respect to M and the position in the board follows the same tendency as the component a^* , except that it is much smaller from a relative standpoint. Below surface, b^* varies from an initial value of about 20 to about 27 at the end of the drying run. On the surface, b^* varies very little during the drying process.

3.2 Development of statistical models of wood color change during drying

In the wood industry, the lightness (L^*) is generally the most important and frequently measured coordinate of the CIEL*a*b* color space where the wood color changes are concerned (McMillen 1975, Möttönen and Luostarinen 2001, Ledig and Seyfarth 2001). Therefore, only the wood lightness will be modelled here. The fact that the changes in L^* during drying are in the opposite direction of those in a^* and b^* components would also make difficult the interpretation of the overall color change ΔE .

3.2.1 Determination of separate equations for the six drying conditions

In this work, statistical methods were used to study the relationship between the wood lightness (L^*) and wood moisture content (M), depth below the wood surface through the board thickness (e), dry-bulb temperature (T), as well as wet-bulb depression (ΔT). The data obtained from sugar maple and paper birch were separately studied. Also, the data obtained on the wood surface and below the wood surface through the board thickness were also separately studied in order to get two different lightness models. In fact, looking at Figures 3.5 and 3.6, one can foresee that it would have been very difficult to fit a unique model for the evolution of the lightness throughout the whole thickness, having an apparent linear model close to the surface and another one away from the surface with two very different behaviors. Furthermore, most models reported in the literature refer to the planed surface of the board. For each run, individual characteristics (M , L^*) were collected for different control boards, different positions through the board thickness and different drying times to comprise a data set. After six runs, the six data sets were joined together one by one to form one whole data set for each species. The experimental data was statistically analyzed with the SAS[®] software using random coefficient models.

The random coefficient model is a specific case of mixed models. It was used in this study in order to take into account the dependency among observations coming from the same board, i.e. among the observations taken from five different plugs within a board and among the observations taken at different thickness within a plug. This model is different from the ordinary least square regression model since all observations are considered as

independent from each other in the latter. In our mixed model, the variables T , ΔT , M and e were considered as fixed effects because we were interested to study the relationship between those explanatory variables and the response (L^*). Moreover, the boards were considered as a random effect with a Gaussian distribution because we did not want to make any inferences about a specific board. In this random coefficient model, each board had its own relationship with the response, i.e. its own parameter estimate, but was expressed as a random deviation from the average of overall boards at a specific combination of T and ΔT .

SAS[®] programs used for analyzing the data obtained on and below the wood surface are shown in Appendix D and E for details, respectively. Separate equations showing the evolution of lightness with respect to the moisture content (surface) or moisture content and position (inside wood) were then obtained for the six drying conditions tested with each species (Table F.1 in Appendix F). As mentioned above, an assumption was made that the moisture content on the wood surface was equal to that of the whole slice first cut out of a plug. For each wood species, linear regression equations were separately obtained for the wood lightness on the surface and below the surface of boards at different drying conditions. The equation parameter estimates along with the p value of the “ t ” test are given in Tables 3.3 and 3.4. Table 3.5 shows the values of the coefficient of determination R^2 for each of the whole equations.

For the dry-bulb temperature of 40°C, the p values of slopes estimated for M in the wood surface model of both species, and for e and M in the wood interior model, are all greater than 0.05, except for the test on paper birch at 4°C wet-bulb depression below the wood surface. Therefore, at 40°C, M has no significant influence on the wood surface L^* values. Likewise, M and e have no significant influence on the wood interior L^* values. The p values for the temperatures of 60 and 80°C, however, are all below 0.05, except for two cases with paper birch, meaning that both M and e have an effect on the magnitude of L^* . In further analysis with alternative global models, separate equations will then be obtained for three temperatures (40, 60 and 80°C) and two temperatures (60 and 80°C).

Table 3.3 Regression parameter estimates for the fixed part of the random coefficient model for the wood lightness of paper birch for different drying conditions.

Paper birch		T (°C)	ΔT (°C)	Estimate	Standard error	Degrees of freedom	t Value	Pr > t
On the wood surface	Intercept	40	4	73.6	1.05	12	70.00	<0.0001
		40	15	71.2	0.854	12	83.32	<0.0001
		60	4	68.6	0.963	12	71.26	<0.0001
		60	15	76.1	0.810	12	93.94	<0.0001
		80	4	58.4	0.835	12	69.89	<0.0001
		80	15	71.9	0.815	12	88.26	<0.0001
	Slope for M	40	4	-0.0774	0.0587	65	-1.32	0.1916
		40	15	0.0728	0.0536	65	1.36	0.1789
		60	4	0.132	0.0569	65	2.33	0.0232
		60	15	0.0350	0.0524	65	0.67	0.5065
		80	4	0.306	0.0526	65	5.81	<0.0001
		80	15	0.134	0.0550	65	2.43	0.0180
Below the wood surface	Intercept	40	4	75.0	1.36	12	54.97	<0.0001
		40	15	81.4	1.34	12	60.82	<0.0001
		60	4	67.1	1.34	12	49.92	<0.0001
		60	15	73.7	1.34	12	55.21	<0.0001
		80	4	64.7	1.34	12	48.34	<0.0001
		80	15	71.8	1.33	12	53.78	<0.0001
	Slope for M	40	4	0.268	0.0502	1320	5.34	<0.0001
		40	15	0.0527	0.0489	1320	1.08	0.2811
		60	4	0.241	0.0490	1320	4.91	<0.0001
		60	15	0.203	0.0488	1320	4.15	<0.0001
		80	4	0.279	0.0489	1320	5.70	<0.0001
		80	15	0.239	0.0489	1320	4.89	<0.0001
	Slope for e	40	4	-0.363	0.0850	1320	-4.27	<0.0001
		40	15	-0.135	0.0845	1320	-1.60	0.1104
		60	4	-0.181	0.0839	1320	-2.15	0.0314
		60	15	-0.644	0.0842	1320	-7.65	<0.0001
		80	4	-0.0533	0.0832	1320	-0.64	0.5217
		80	15	-0.370	0.0835	1320	-4.43	<0.0001

Table 3.4 Regression parameter estimates for the fixed part of the random coefficient model for the wood lightness of sugar maple at different drying conditions.

Sugar maple		T, (°C)	ΔT , (°C)	Estimate	Standard Error	Degrees of Freedom	t Value	Pr > t
On the wood surface	Intercept	40	4	78.1	2.02	12	38.67	<0.0001
		40	15	79.4	1.93	12	41.06	<0.0001
		60	4	66.4	2.01	12	33.05	<0.0001
		60	15	77.0	1.95	12	39.45	<0.0001
		80	4	61.1	1.92	12	31.82	<0.0001
		80	15	58.8	1.95	12	30.17	<0.0001
	Slope for M	40	4	-0.0141	0.0768	65	-0.18	0.8549
		40	15	0.0644	0.0768	65	0.84	0.4047
		60	4	0.230	0.0772	65	2.98	0.0041
		60	15	-0.212	0.0788	65	-2.69	0.0090
		80	4	0.490	0.0773	65	6.33	<0.0001
		80	15	0.626	0.0805	65	7.77	<0.0001
Below the wood surface	Intercept	40	4	83.1	0.863	12	96.35	<0.0001
		40	15	85.4	0.843	12	101.34	<0.0001
		60	4	69.5	0.859	12	80.90	<0.0001
		60	15	76.2	0.850	12	89.69	<0.0001
		80	4	66.4	0.851	12	78.12	<0.0001
		80	15	70.2	0.839	12	83.63	<0.0001
	Slope for M	40	4	0.0106	0.0319	1318	0.33	0.7402
		40	15	-0.0601	0.0313	1318	-1.92	0.0552
		60	4	0.305	0.0320	1318	9.53	<0.0001
		60	15	0.210	0.0315	1318	6.67	<0.0001
		80	4	0.405	0.0320	1318	12.64	<0.0001
		80	15	0.287	0.0315	1318	9.10	<0.0001
	Slope for ϵ	40	4	-0.0567	0.0450	1318	-1.26	0.2086
		40	15	-0.00236	0.0446	1318	-0.05	0.9578
		60	4	-0.216	0.0440	1318	-4.90	<0.0001
		60	15	-0.464	0.0454	1318	-10.22	<0.0001
		80	4	-0.218	0.0451	1318	-4.84	<0.0001
		80	15	-0.281	0.0444	1318	-6.33	<0.0001

Table 3.5 Coefficient of determination R^2 (%) values for the separate regression equations of wood lightness for the six drying conditions of paper birch and sugar maple.

Wood species	T, (°C)	ΔT , (°C)	R^2 (%) for equations for L^* on the wood surface	R^2 (%) for equations for L^* below the wood surface ($e \geq 0.24$ mm)
Paper birch	40	4	93.4	34.8
		15	53.1	23.2
	60	4	74.7	63.7
		15	66.9	73.3
	80	4	96.1	90.9
		15	91.6	80.3
Sugar maple	40	4	12.6	1.0
		15	90.9	20.2
	60	4	74.3	90.0
		15	65.3	66.6
	80	4	97.3	73.5
		15	92.6	82.8

Note: e = depth below the wood surface through the board thickness, mm.

With regard to the coefficient of determination R^2 values shown in Table 3.5, which indicate the proportion of the L^* value explained by the independent variables M and e , they agree in general with the “t” test analysis discussed in the previous paragraph. In fact, the R^2 values at 60 and 80°C varied between 63.7 and 97.3%, while the corresponding values at 40°C are very small, except for two cases.

3.2.2 Global models of wood color change during drying

The application of each separate equation, although simple, is limited to a given drying condition. In order to extend the application of the color model to a wider range of drying conditions, and make it more useful in practice, two more global models for the lightness change on the wood surface and below the wood surface are needed for each species.

As a first tentative to develop a suitable model with SAS[®] programs turn out to be very complicated, a graphical technique was then used to identify the general pattern of the model that would fit best the experimental data. Once we had obtained the rough model, the final tuning was completed with stepwise backward SAS[®] procedures by eliminating the

variables or combinations of variables found not significant to the significance level of 0.05. Starting with the general regression model for each drying condition:

$$L^* = \alpha_0 + \alpha_1 M \quad [3.1]$$

for the wood surface,

$$L^* = \beta_0 + \beta_1 M + \beta_2 e \quad [3.2]$$

and below the wood surface, where α_0 and β_0 stand for the intercepts, α_1 and β_1 stand for regression coefficients for the moisture content (M), and β_2 stands for regression coefficient for the depth below the wood surface (e). By plotting the values of the intercepts and the regression coefficients given in Tables 3.3 and 3.4 against the dry-bulb temperature, and then substituting the obtained regression equations into Equations [3.1] and [3.2], two sub-global models were found. Finally, in order to take into account the effect of wet-bulb depression, the intercepts and all the coefficients of the sub-global models were plotted against ΔT . After some mathematical arrangements, two global equations that take into account both the dry-bulb temperature and the wet-bulb depression were obtained. A three-temperature (3T) wood color model was first established by considering the three drying temperatures. Since the data obtained at 40°C were of low significance, a two-temperature (2T) wood color model was also established (60 and 80°C).

3.2.2.1 Wood color 3T global models

One can find in Appendix F all the graphics constructed to obtain the 3T sub-global models (Figures F.1 and F.2, Table F.2). Since a polynomial equation was used, there is of course a perfect fit in all cases, some of the relationships being however doubtful. But as the graphical approach was only used to find a rough idea of the final model, no screening was done at that stage. Equations [3.3] and [3.4] presented below separately show the general patterns of both sub-global models developed for the wood surface and the wood interior:

$$L^* = \alpha_0 + \alpha_1 T^2 M + \alpha_2 T^2 + \alpha_3 T M + \alpha_4 T + \alpha_5 M \quad [3.3]$$

$$L^* = \beta_0 + \beta_1 T^2 e + \beta_2 T^2 M + \beta_3 T^2 + \beta_4 T e + \beta_5 T M + \beta_6 T + \beta_7 e + \beta_8 M \quad [3.4]$$

where, $\alpha_0, \dots, \alpha_5$ represent deductive regression coefficients in the sub-global equations for the wood surface, and β_0, \dots, β_8 represent deductive regression coefficients in the sub-global equations for the wood interior.

Figures F.3 to F.6 show the graphical representation of the sub-global model intercepts and regression coefficients (y-axis) expressed in terms of the wet-bulb depression (x-axis). In this case, linear equations were necessarily used since there were only two data points, i.e. two wet-bulb depression temperatures.

The 3T global graphical model for L^* was then expressed in the following form:

$$\begin{aligned} L^* = & \alpha_0 + \alpha_1 T^2 \Delta T M + \alpha_2 T^2 M + \alpha_3 T^2 \Delta T + \alpha_4 T^2 + \alpha_5 \Delta T T M \\ & + \alpha_6 T M + \alpha_7 \Delta T T + \alpha_8 \Delta T M + \alpha_9 T + \alpha_{10} M + \alpha_{11} \Delta T \end{aligned} \quad [3.5]$$

for the wood surface model, and:

$$\begin{aligned} L^* = & \beta_0 + \beta_1 T^2 \Delta T e + \beta_2 T^2 \Delta T M + \beta_3 T^2 e + \beta_4 T^2 M + \beta_5 T^2 \Delta T + \beta_6 T^2 \\ & + \beta_7 \Delta T T e + \beta_8 \Delta T T M + \beta_9 T e + \beta_{10} T M + \beta_{11} \Delta T T + \beta_{12} \Delta T e \\ & + \beta_{13} \Delta T M + \beta_{14} T + \beta_{15} e + \beta_{16} \Delta T + \beta_{17} M \end{aligned} \quad [3.6]$$

for below the wood surface model, where, $\alpha_0, \dots, \alpha_{11}$ represent deductive regression coefficients in the 3T global equations for the wood surface, and $\beta_0, \dots, \beta_{17}$ represent deductive regression coefficients in the 3T global equations for the wood interior. Looking at the complexity of these equations, it is easy to see why it would have been very difficult to get the correct form of global models by going directly through the conventional statistical approach. But since the graphical approach cannot optimize the model in term of significance of each of the independent factor used, the final tuning of the models had to be done with the statistical approach.

A deductive SAS[®] program was therefore built for each case (on and below the wood surface) and each species (Appendix H). After the programs were run, the significance of

factors and their correlations were evaluated. The insignificant factors and combinations were removed from the corresponding equations before the program was run again. The process was repeated until all factors and their combinations were found significant, as shown in Table 3.6 and 3.7. Then, a global equation for each case (on and below the wood surface) and each species was obtained by combining the products of the items in the “Effect” column multiplied by their respective values in the “Estimate” column. Equations [3.7] to [3.10] give the final statistical model obtained for the wood surface and below the wood surface, for paper birch and sugar maple.

Table 3.6 Regression parameter estimates for the fixed part of the random coefficient model for 3T global equations of paper birch.

Paper birch	Effect	Estimate	Standard Error	Degrees of Freedom	t Value	Pr > t
On the wood surface	Intercept	67.9	7.045	13	9.63	<0.0001
	T^2	-0.00841	0.00184	54	-4.58	<0.0001
	$\Delta T T M$	-0.00072	0.00024	54	-3.00	0.0041
	$T M$	0.0123	0.00267	54	4.61	<0.0001
	$\Delta T T$	0.0359	0.00413	54	8.70	<0.0001
	$\Delta T M$	0.0391	0.0151	54	2.59	0.0122
	T	0.488	0.229	54	2.13	0.0375
	M	-0.601	0.170	14	-3.53	0.0033
	ΔT	-1.60	0.266	54	-6.01	<0.0001
Below the wood surface	Intercept	107	6.36	14	16.78	<0.0001
	$T^2 \Delta T e$	0.000044	0.0000150	1296	2.94	0.0033
	T^2	0.00667	0.00186	1296	3.59	0.0003
	$\Delta T e T$	-0.00607	0.00181	1296	-3.36	0.0008
	$e T$	0.0115	0.00368	1296	3.12	0.0019
	$\Delta T T$	0.00996	0.00157	1296	6.35	<0.0001
	$\Delta T e$	0.180	0.0538	1296	3.35	0.0008
	$\Delta T M$	-0.00866	0.00395	1296	-2.19	0.0287
	T	-1.10	0.225	1296	-4.89	<0.0001
	e	-0.815	0.237	13	-3.44	0.0044
	M	0.293	0.0441	16	6.64	<0.0001

Table 3.7 Regression parameter estimates for the fixed part of the random coefficient model for 3T global equations of sugar maple.

Sugar maple	Effect	Estimate	Standard Error	Degrees of Freedom	t Value	Pr > t
On the wood surface	Intercept	78.6	2.995	14	26.25	<0.0001
	$T^2 \Delta T M$	0.000069	8.51E-6	53	8.06	<0.0001
	$T^2 \Delta T$	-0.00055	0.000120	53	-4.56	<0.0001
	$\Delta T M T$	-0.00749	0.000975	53	-7.69	<0.0001
	$M T$	0.00486	0.00115	53	4.23	<0.0001
	$\Delta T T$	0.0413	0.00870	53	4.75	<0.0001
	$\Delta T M$	0.175	0.0265	53	6.61	<0.0001
	T	-0.202	0.0557	53	-3.62	0.0007
Below the wood surface	Intercept	152	9.16	13	16.61	<0.0001
	$T^2 \Delta T e$	0.000052	9.04E-6	1293	5.71	<0.0001
	$T^2 M$	-0.00025	0.0000630	1293	-3.93	<0.0001
	$T^2 \Delta T$	-0.00084	0.000213	1293	-3.92	<0.0001
	T^2	0.0167	0.00268	1293	6.24	<0.0001
	$\Delta T e T$	-0.00668	0.00109	1293	-6.13	<0.0001
	$M T$	0.0387	0.00762	1293	5.09	<0.0001
	$\Delta T T$	0.102	0.0257	1293	3.98	<0.0001
	$\Delta T e$	0.194	0.0310	1293	6.27	<0.0001
	$\Delta T M$	-0.00837	0.00225	1293	-3.72	0.0002
	T	-2.42	0.324	1293	-7.49	<0.0001
	e	-0.131	0.0386	14	-3.38	0.0044
	M	-1.10	0.217	15	-5.06	0.0001
	ΔT	-2.53	0.729	1293	-3.48	0.0005

For paper birch, the exact 3T global equation for the L^* value on the wood surface is:

$$\begin{aligned}
 L^* = & 67.9 - 0.00841 T^2 - 0.000720 T \Delta T M + 0.0123 T M + 0.0359 T \Delta T \\
 & + 0.0391 \Delta T M + 0.488 T - 0.601 M - 1.60 \Delta T
 \end{aligned}
 \quad [3.7]$$

and the exact 3T global equation for the L^* value below the wood surface is:

$$L^* = 107 + 0.0000440 T^2 \Delta T e + 0.00667 T^2 - 0.00607 \Delta T e T + 0.0115 e T$$

$$\begin{aligned}
&+ 0.00996 T \Delta T + 0.180 \Delta T e - 0.00866 \Delta T M \\
&- 1.10 T - 0.815 e + 0.293 M
\end{aligned} \tag{3.8}$$

For sugar maple, the exact 3T global equation for the L^* value on the wood surface is:

$$\begin{aligned}
L^* = &78.6 + 0.0000690 T^2 \Delta T M - 0.000550 T^2 \Delta T - 0.00749 T \Delta T M \\
&+ 0.00486 T M + 0.0413 T \Delta T + 0.175 \Delta T M - 0.202 T
\end{aligned} \tag{3.9}$$

and the exact 3T global equation for the L^* value below the wood surface is:

$$\begin{aligned}
L^* = &152 + 0.0000520 T^2 \Delta T e - 0.000250 T^2 M - 0.000840 T^2 \Delta T + 0.0167 T^2 \\
&- 0.00668 \Delta T e T + 0.0387 T M + 0.102 T \Delta T + 0.194 \Delta T e \\
&- 0.00837 \Delta T M - 2.42 T - 0.131 e - 1.10 M - 2.53 \Delta T
\end{aligned} \tag{3.10}$$

Notice that the variables M and e , which were found linearly related to the L^* in the separate equations (Tables 3.3 and 3.4), remain of course at the first degree level in the global equation. Concerning ΔT , the fact of having only two wet-bulb depressions led also to a first degree level of this variable in the global equation.

3.2.2.2 Wood color 2T global models

Because the R^2 values were very low for most of the separate equations of two species at 40°C (Table 3.5), the 2T wood color models were established by excluding the data at 40°C (Table G.1 in Appendix G). The same graphical procedure as for the 3T global models was first used, and then the final tuning with the statistical approach. Figures G.1 and G.2 in Appendix G showing the relationships between the regression coefficients in the equations and the dry-bulb temperatures from 60°C to 80°C were first built in order to obtain the 2T sub-global models of Table G.2. The general patterns of the 2T sub-global models were:

$$L^* = \alpha_0 + \alpha_1 T M + \alpha_2 T + \alpha_3 M \tag{3.11}$$

$$L^* = \beta_0 + \beta_1 T e + \beta_2 T M + \beta_3 T + \beta_4 e + \beta_5 M \tag{3.12}$$

where, $\alpha_0, \dots, \alpha_3$ represent deductive regression coefficients in the 2T global equations for the wood surface, and β_0, \dots, β_5 represent deductive regression coefficients in the 2T global equations for the wood surface coefficients.

Figures G.3 to G.6 present the linear equations obtained by taking into account the effect of the wet-bulb depression. The 2T graphical global models for L^* on the wood surface took the form:

$$L^* = \alpha_0 + \alpha_1 T \Delta T M + \alpha_2 T \Delta T + \alpha_3 T M + \alpha_4 \Delta T M + \alpha_5 T + \alpha_6 \Delta T + \alpha_7 M \quad [3.13]$$

and below the wood surface:

$$\begin{aligned} L^* = & \beta_0 + \beta_1 T \Delta T e + \beta_2 T \Delta T M + \beta_3 T \Delta T + \beta_4 T e + \beta_5 T M + \beta_6 \Delta T e + \beta_7 \Delta T M \\ & + \beta_8 T_s + \beta_9 \Delta T + \beta_{10} e + \beta_{11} M \end{aligned} \quad [3.14]$$

where, $\alpha_0, \dots, \alpha_7$ represent deductive regression coefficients in the 2T global equations for the wood surface, and $\beta_0, \dots, \beta_{11}$ represent deductive regression coefficients in the 2T global equations for the wood interior.

As for the 3T models, the statistical approach was then used to get the final global equations with significant independent variables. Tables 3.8 and 3.9 present the final results of the statistical analysis for the model on the surface and below the surface of boards of each species, respectively. Equations [3.15] to [3.18] present the four 2T global models in question.

Table 3.8 Regression parameter estimates for the fixed part of the random coefficient model for 2T global equations of paper birch.

Paper birch	Effect	Estimate	Standard Error	Degrees of Freedom	t Value	Pr > t
On the wood surface	Intercept	91.1	3.56	9	25.57	<0.0001
	$T \Delta T$	0.0142	0.00131	36	10.81	<0.0001
	$T M$	0.00429	0.000584	36	7.35	<0.0001
	$\Delta T M$	-0.0149	0.00372	36	-4.01	0.0003
	T	-0.457	0.0513	36	-8.92	<0.0001
Below the wood surface	Intercept	71.4	3.11	9	22.97	<0.0001
	$T \Delta T$	0.00697	0.00111	864	6.31	<0.0001
	$T e$	0.0116	0.00385	864	3.01	0.0027
	$\Delta T e$	-0.0393	0.00691	864	-5.68	<0.0001
	T	-0.0967	0.0446	864	-2.17	0.0302
	e	-0.733	0.281	9	-2.61	0.0282
	M	0.236	0.0136	11	17.39	<0.0001

Table 3.9 Regression parameter estimates for the fixed part of the random coefficient model for 2T global equations of sugar maple.

Sugar maple	Effect	Estimate	Standard Error	Degrees of Freedom	t Value	Pr > t
On the wood surface	Intercept	62.2	2.02	9	30.79	<0.0001
	$T \Delta T M$	0.00282	0.000407	35	6.94	<0.0001
	$T \Delta T$	-0.0609	0.00917	35	-6.64	<0.0001
	$\Delta T M$	-0.212	0.0295	35	-7.17	<0.0001
	ΔT	4.65	0.666	35	6.98	<0.0001
	M	0.416	0.0867	9	4.80	0.0010
Below the wood surface	Intercept	74.0	3.33	8	22.25	<0.0001
	$T \Delta T$	-0.0123	0.00427	863	-2.89	0.0040
	$T M$	0.00552	0.000480	863	11.51	<0.0001
	$\Delta T e$	-0.0137	0.00530	863	-2.59	0.0099
	$\Delta T M$	-0.00936	0.00308	863	-3.04	0.0024
	T	-0.111	0.0480	863	-2.32	0.0207
	ΔT	1.33	0.310	863	4.28	<0.0001
	e	-0.156	0.0579	10	-2.69	0.0226

For paper birch, the exact 2T global equation for the L^* value on the wood surface is:

$$L^* = 91.1 + 0.0142 T \Delta T + 0.00429 T M - 0.0149 \Delta T M - 0.457 T \quad [3.15]$$

and the exact 2T global equation for the L^* value below the wood surface is:

$$\begin{aligned} L^* = & 71.4 + 0.00697 T \Delta T + 0.0116 T e - 0.0393 \Delta T e \\ & - 0.0967 T - 0.733 e + 0.236 M \end{aligned} \quad [3.16]$$

For sugar maple, the exact 2T global equation for the L^* value on the wood surface is:

$$\begin{aligned} L^* = & 62.2 + 0.00282 T \Delta T M - 0.0609 T \Delta T \\ & - 0.212 \Delta T M + 4.65 \Delta T + 0.416 M \end{aligned} \quad [3.17]$$

and the exact 2T global equation for the L^* value below the wood surface is:

$$\begin{aligned} L^* = & 74.0 - 0.0123 T \Delta T + 0.00552 T M - 0.0137 \Delta T e \\ & - 0.00936 \Delta T M - 0.111 T + 1.33 \Delta T - 0.156 e \end{aligned} \quad [3.18]$$

3.3 Physical material properties of the heat and mass transfer model

3.3.1 Determination of the M- ψ relationship of wood

A summary of experimental results of the M- ψ relationship determinations is given in Table 3.10 and is presented graphically in Figure 3.7 for paper birch. The corresponding results are presented in Table 3.11 and Figure 3.8 for sugar maple. A semi-log scale is used to avoid congestion of data points at high ψ values. Each data point represents the average equilibrium moisture content (EMC) of each group of 4 specimens of each tree (12 specimens under each level of pressure). Near or below the FSP, the water potential values of both wood species were calculated according to the data obtained by Djolani (1970) and Keylwerth and Noack (1964). For sugar maple, the desorption curves for sugar maple (Figure 1.12) obtained by Defo et al. (1999a) at 40 and 60°C were also adapted. The shape of both curves obtained in the different studies at the same temperature is similar, but the

equilibrium moisture contents above FSP obtained by Defo et al. (1999a) are higher at a given water potential value. The possible reason is that the initial average moisture content in this study was about 54%, while it was 60% in the study performed by Defo et al. (1999a). It may be expected that numerous drainage curves could be measured from the green condition due to the seasonal variation of M in standing trees (Linzon 1969). The practical implication is that, depending on the green M in the trees at the time of felling, and depending on whether M before felling is toward an increasing or a decreasing trend, the effectiveness of a given drainage or drying process may be quite different (Fortin 1979).

At a given temperature, the M - ψ curves of sugar maple and paper birch are different at high M values. The initial moisture contents of both wood species are different. In addition, variations in the shape of the M - ψ relationship at high moisture contents within or between wood species can be explained on the basis of anatomical differences, reflected in the pore size distribution, since water potential takes capillary forces into account (Tremblay et al. 1996). According to Panshin and de Zeeuw (1980), the volumetric composition of sugar maple is 21% vessels, 61% fibers (including fiber tracheids and libriform fibers), and 17.9% rays and 0.1% axial parenchyma, whereas paper birch is constituted of 10.6% vessels, 75.7% fibers, 11.7% rays and 2.0% axial parenchyma.

Table 3.10 Summary of the results of the M- ψ determinations for paper birch.

Paper birch						
Temperature	RH	ψ	EMC	IMC	SE for EMC	SE for IMC
°C	%	J kg ⁻¹	%	%	%	%
40	99.981	-28	79.5	86.6	4.1	3.7
	99.962	-55	78.3	91.6	3.9	3.8
	99.933	-97	77.3	89.5	4.8	4.6
	99.782	-315	66.3	88.8	2.9	2.5
	99.506	-715	47.9	91.3	3.0	2.9
	98.626	-2000	39.2	87.9	1.1	4.4
	96.579	-5030	36.8	89.6	2.2	3.8
60	99.987	-21	77.4	92.4	2.8	3.0
	99.955	-69	73.4	87.3	3.2	3.0
	99.799	-310	57.3	92.3	3.0	3.8
	99.555	-685	43.1	87.7	2.2	1.9
	98.708	-2000	33.0	83.4	1.0	2.3
	96.800	-5000	30.7	91.1	2.3	3.9
80	99.983	-28	68.0	85.6	4.5	4.3
	99.945	-90	63.0	91.0	4.0	3.9
	99.920	-131	58.7	88.7	3.2	4.5
	99.388	-1000	31.7	90.5	1.2	2.3
	98.732	-2080	26.0	91.7	0.2	3.1
	97.050	-4880	25.4	89.6	1.2	4.2

Note: EMC = Equilibrium moisture content. IMC = Initial moisture content.

SE = Standard error based on 12 specimens.

Table 3.11 Summary of the results of the M- ψ determinations for sugar maple.

Sugar maple						
Temperature	RH	ψ	EMC	IMC	SE for EMC	SE for IMC
°C	%	J kg ⁻¹	%	%	%	%
40	99.982	-26	55.9	56.1	2.0	1.3
	99.950	-72	47.0	53.0	0.9	0.9
	99.924	-110	45.5	55.5	0.8	1.2
	99.786	-310	42.0	53.2	0.4	0.9
	99.558	-640	40.1	51.7	0.5	1.1
	98.591	-2050	36.6	53.9	0.3	1.1
	96.519	-5120	35.0	51.7	0.3	1.0
60	99.987	-21	51.4	53.4	1.7	1.7
	99.960	-62	45.2	55.7	1.2	1.1
	99.915	-131	40.6	53.3	0.6	0.7
	99.766	-360	37.7	55.4	0.2	1.7
	99.578	-650	35.1	53.2	0.4	1.2
	98.675	-2050	33.0	53.7	0.2	1.5
	96.939	-4780	28.8	52.7	0.2	1.6
80	99.983	-28	42.0	54.5	1.3	1.4
	99.949	-83	37.9	56.0	0.4	1.0
	99.810	-310	31.3	56.5	0.1	1.5
	99.568	-705	26.4	57.1	0.3	1.1
	98.780	-2000	26.0	55.5	0.4	1.2
	96.967	-5020	21.7	54.6	0.4	1.3

Note: EMC = Equilibrium moisture content. IMC = Initial moisture content.

SE = Standard error based on 12 specimens.

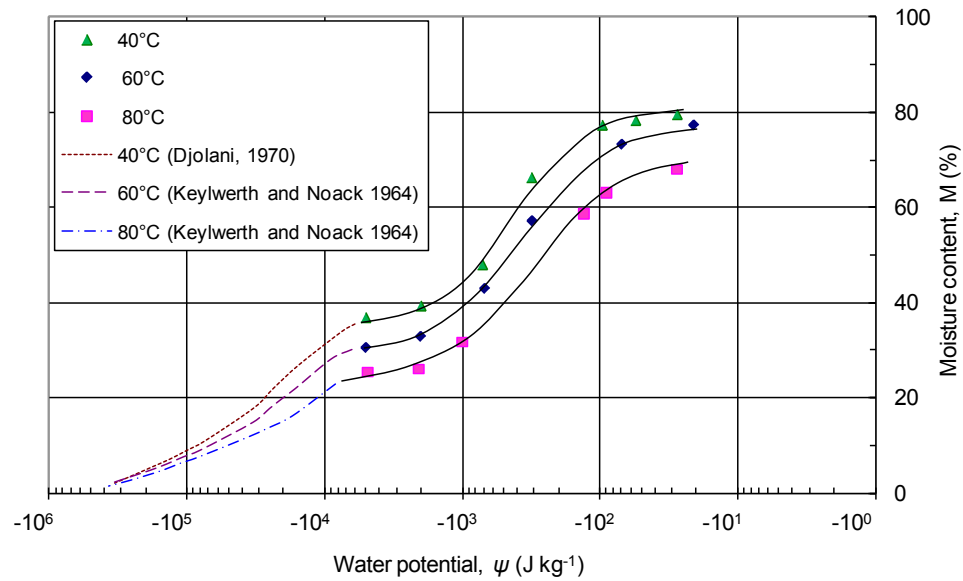


Figure 3.7 M- ψ relationship of paper birch sapwood at 40, 60 and 80°C from green to dry conditions. The water potential values near or below the FSP were calculated according to the data obtained by Djolani (1970) and Keylwerth and Noack (1964).

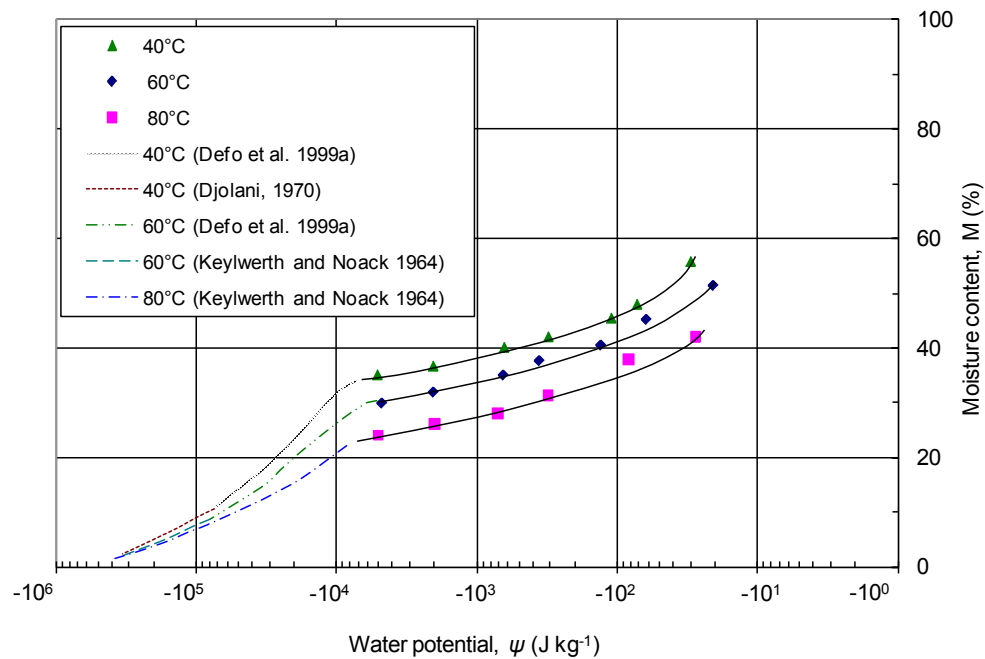


Figure 3.8 M- ψ relationship of sugar maple sapwood at 40, 60 and 80°C from green to dry conditions. The water potential values near or below the FSP were calculated according to the data obtained by Djolani (1970), Keylwerth and Noack (1964) and Defo et al. (1999a).

In Figures 3.7 and 3.8, the moisture content decreases very slowly with a decrease in water potential in the range of -2,000 and -6,000 J kg⁻¹ in the M- ψ curves of both wood species, which agrees with the results of sugar maple obtained by Defo et al. (1999a). In this characteristic plateau, moisture content values fell into the range of 24 and 38% around the fiber saturation point. Following Hart (1984) and Wheeler (1982), Defo et al. (1999a) deduced that water in the fiber lumina has been removed and the remainder is held firmly by high capillary tension into pit openings in the fibers or in ray parenchyma. The parenchyma-parenchyma pit membranes are thicker than both the intervessel pit membranes and the fiber-fiber pit membranes, and consequently are less efficient pathways for liquid flow.

As shown in Figures 3.7 and 3.8, at a given temperature, water potential increases with moisture content for both wood species. At a given M, water potential increases with temperature. According to Defo et al. (1999a), assuming that the specific volume of water and the capillary radius are independent of temperature, the derivative of ψ_m with respect to temperature leads to:

$$\left(\frac{\partial \psi_m}{\partial T} \right)_M = \psi_m \frac{1}{\gamma} \frac{\partial \gamma}{\partial T} \quad [3.19]$$

where, $(\partial \psi_m / \partial T)_M$ = temperature coefficient of ψ_m at a constant moisture content (J kg⁻¹ °C⁻¹); γ = surface tension of water (N m⁻¹) and T = temperature (°C).

The experimental values of the temperature coefficient of ψ_m for sugar maple are presented in Table 3.12 for some arbitrary M values above FSP. The experimental and calculated values of the temperature coefficient of ψ_m for sugar maple obtained at 60°C by Defo et al. (1999a) are also presented for comparison purposes. The experimental values obtained in the present study are lower than those obtained by Defo et al. (1999a). The difference may be mainly ascribed to the lower initial moisture contents in the former case. In general, the experimental values are several times higher than the calculated values, which is in agreement with the findings of Cloutier and Fortin (1991), Tremblay et al. (1996) and Defo

Table 3.12 Experimental and calculated temperature coefficients for the M- ψ relationship of sugar maple obtained in the present study in comparison of those reported by Defo et al. (1999a).

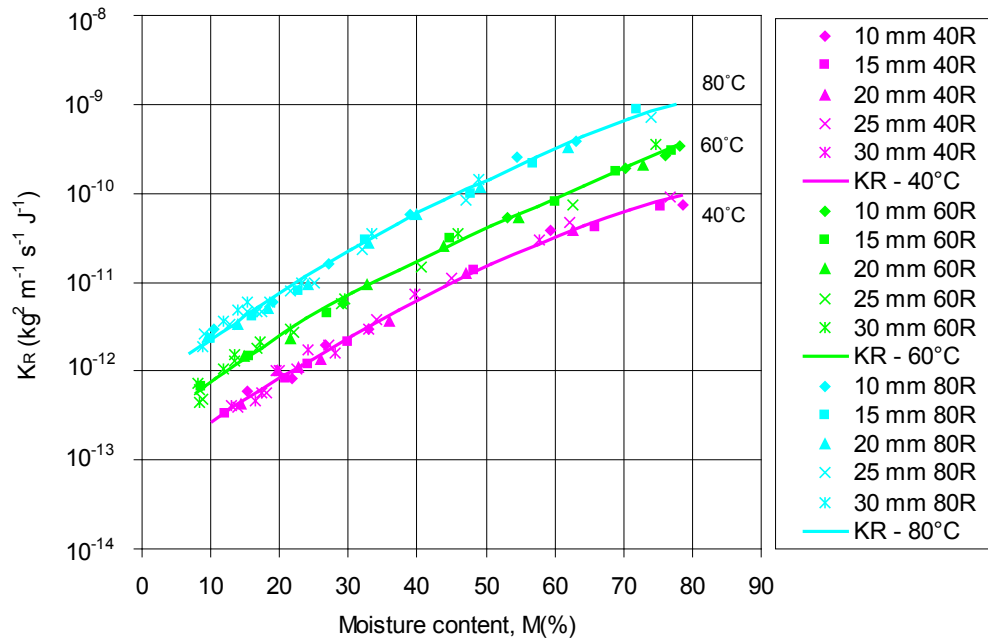
Sugar maple (in this study)				Sugar maple (from Defo et al. 1999a)		
M	ψ (at 60°C)	$\partial\psi/\partial T$ (J kg ⁻¹ °C ⁻¹)		ψ (at 60°C)	$\partial\psi/\partial T$ (J kg ⁻¹ °C ⁻¹)	
%	J kg ⁻¹	Experimental	Calculated	J kg ⁻¹	Experimental	Calculated
60	-20	0.40	0.04	-20	0.95	0.05
50	-26	1.00	0.06	-32	2.12	0.08
40	-150	13.96	0.33	-236	31.2	0.59

et al. (1999a). It was concluded by these authors that the dependence of the surface tension of water on temperature cannot entirely explain the increase in ψ_m with temperature. Entrapped air (Chahal 1965) and surface active contaminants at the air-water interface (Saha and Tripathi 1981) were proposed to explain the behavior.

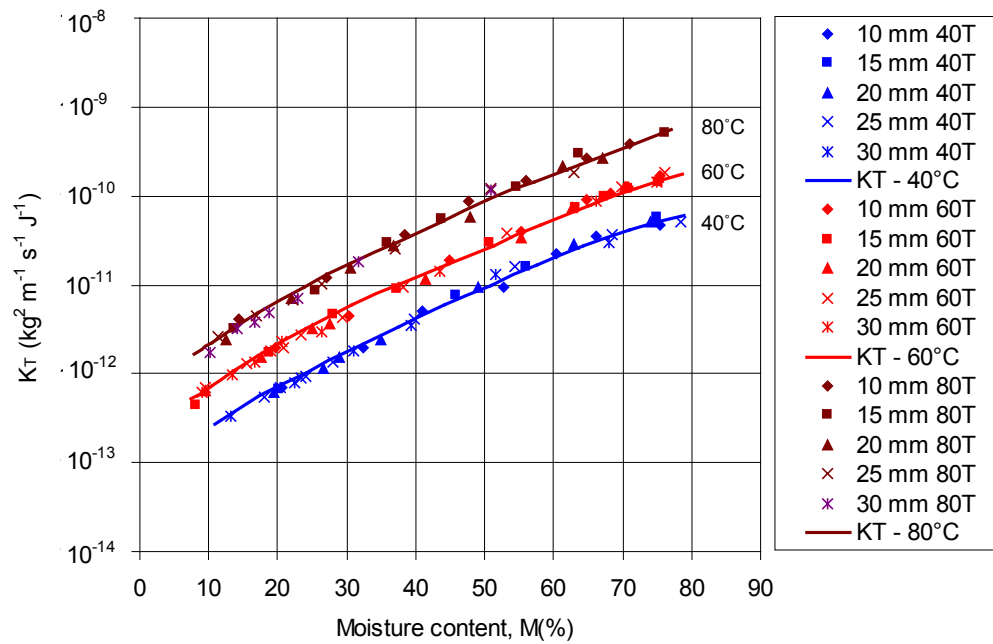
3.3.2 Determination of the effective water conductivity

The results of the effective water conductivity $K_{R,T}(M, T)$ determinations at 40, 60 and 80°C in the radial and tangential directions from green to dry conditions are shown in Figure 3.9 for paper birch sapwood and in Figure 3.10 for sugar maple sapwood. The curves were hand fitted to the data points. For comparison purposes, the curves in the radial and tangential directions are also shown together in Figure 3.11 for paper birch and in Figure 3.12 for sugar maple. A first noticeable observation is that paper birch and sugar maple exhibit different curve shape of the effective water conductivity. The convex curves of paper birch are similar to those of aspen sapwood (Cloutier and Fortin 1993) and red pine sapwood (Tremblay et al. 2000a). The concave curve shapes of effective water conductivity of sugar maple are similar to those obtained under vacuum by Defo et al. (1999b).

At a given M, for both species, the effective water conductivity $K_{R,T}(M, T)$ values increase with the drying temperature. As Cloutier and Fortin (1993) mentioned, this characteristic can be mainly related to the effect of temperature on the M- ψ relationship and ψ gradients ($\partial\psi/\partial x$) (Equation [2.2]).

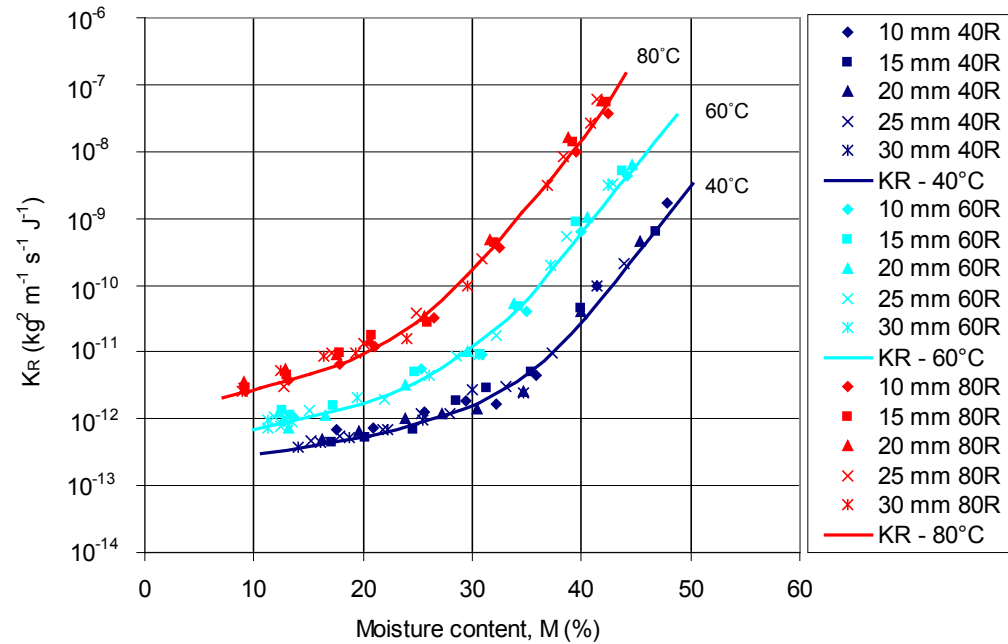


(a)

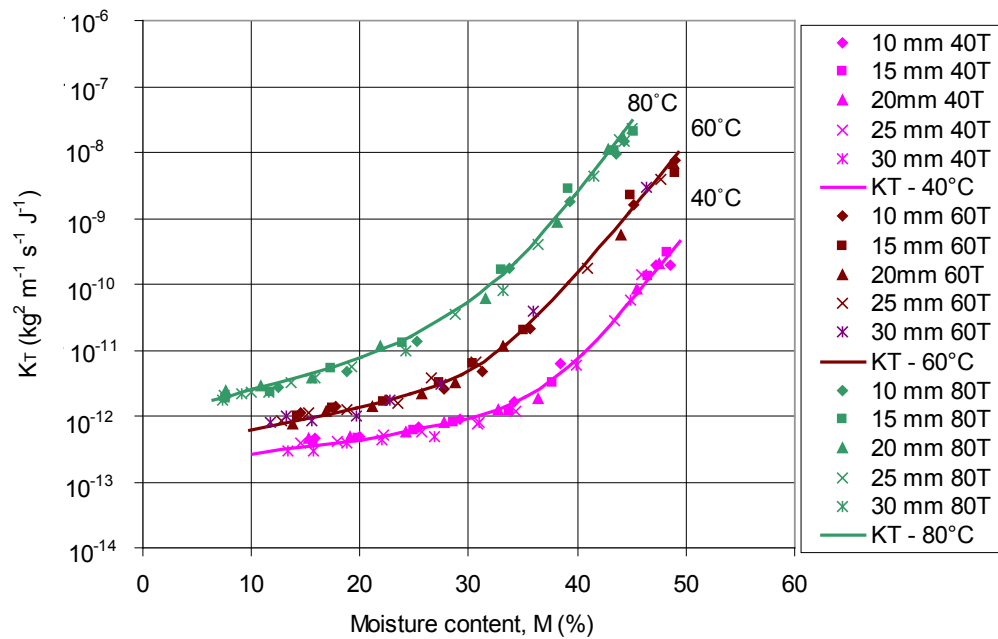


(b)

Figure 3.9 Effective water conductivity of paper birch at 40, 60 and 80°C from green to dry conditions: (a) radial direction (K_R); (b) tangential direction (K_T).



(a)



(b)

Figure 3.10 Effective water conductivity of sugar maple at 40, 60 and 80°C from green to dry conditions: (a) radial direction (K_R); (b) tangential direction (K_T).

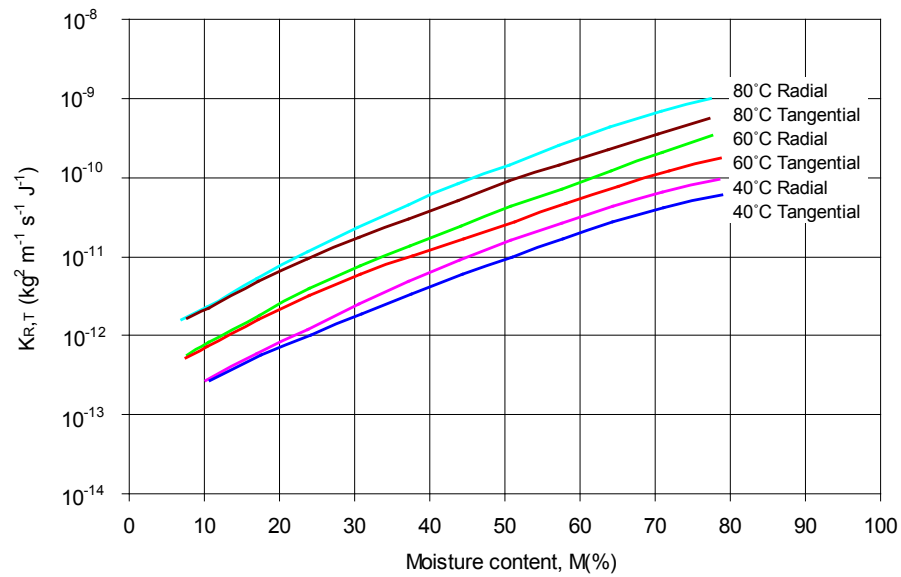


Figure 3.11 Comparison of the effective water conductivity of paper birch sapwood in the radial (K_R) and tangential (K_T) directions from green to dry conditions at 40, 60 and 80 C.

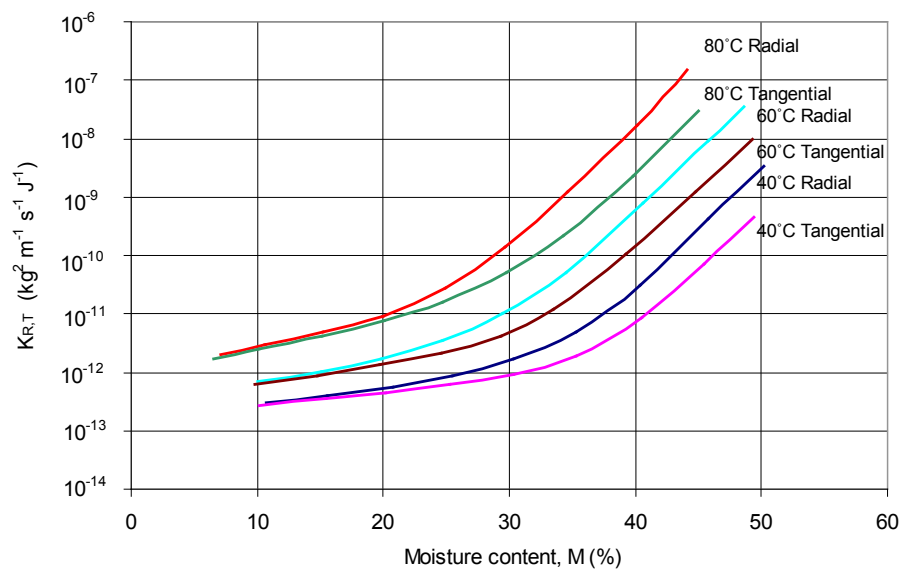


Figure 3.12 Comparison of the effective water conductivity of sugar maple sapwood in the radial (K_R) and tangential (K_T) directions from green to dry conditions at 40, 60 and 80 C.

The effective water conductivity $K_{R,T}(M, T)$ values increase with moisture content and temperature by a ratio of about 10^6 for sugar maple and by a ratio of about 10^4 for paper birch from the dry state to the green state.

As Defo et al. (1999b) mentioned, the effective water conductivity of sugar maple decreases abruptly from the green condition to about 35% M. Below 35% M, the effective water conductivity decreases more gradually with a change in the moisture content. Cloutier and Fortin (1993) mentioned that the M dependence of the cross-sectional area available for flow in the vapor and liquid phases, the variation of the tortuosity of the flow paths and the increasing probability of failure in the liquid continuity can explain the reduction of effective water conductivity as M decreases at high M values (Philip 1969, Hartley 1986). The rapid drainage of very conductive pores can explain the steep decrease in $K_{R,T}(M, T)$ as the moisture content decreases from the green condition to 35% M.

Under the same hygrothermal conditions, above about 35% M, sugar maple has noticeably higher $K_{R,T}(M, T)$ value than paper birch. Below 35% M, the difference becomes small and even negligible in dry condition. This may be explained to some extent by the initial moisture content of the wood and also by the differences in anatomical structure, sugar maple wood having a larger percentage of vessels and rays than paper birch.

At the same drying temperature, for both species, at a given M, $K_R(M, T)$ is higher than $K_T(M, T)$, except at the almost dry condition. The phenomenon was also observed by Cloutier and Fortin (1993), Tremblay et al. (2000a) and Defo et al. (1999b). The phenomenon almost vanishes below FSP. The contribution of ray cells to liquid water flow above FSP would explain this difference while below the FSP, the diffusion type of water transport makes the contribution of ray cells much less effective.

3.3.3 Determination of the convective mass transfer coefficient for wood drying

3.3.3.1 Calculation of the convective mass transfer coefficient in the constant drying rate period

Using Equation [2.3], the convective mass transfer coefficients (h_ψ) of paper birch and sugar maple were calculated from the constant rate period of the drying curve of each of the six color tests. The results are presented in Table 3.13 and Figure I.1 in Appendix I. At the same drying condition, the convective mass transfer coefficients of paper birch and sugar maple are very similar. The h_ψ values increase with dry-bulb temperature at a given wet-bulb depression while they decrease with wet-bulb depression at a given dry-bulb temperature. The increase of wet-bulb depression has two different influences. On one hand, the drying rate increases, which leads to the increase of the moisture flux. On the other hand, the relative humidity of the environmental air surrounding wood decreases, therefore, the water potential of air-water vapour mixture ψ_∞ decreases. The decrease of ψ_∞ has more influence on the value of h_ψ than the increase of the moisture flux. Thus, the h_ψ value decreases.

In order to express the h_ψ values in terms of the dry-bulb temperature, regression analysis was used to obtain the equations shown in Figure I.1 of Appendix I. These equations have the same structure, so they can be expressed into the representative form below:

$$h_\psi = a + b T + c T^2 \quad [3.20]$$

In a second step, the coefficients a , b and c were expressed in terms of the wet-bulb depression for each wood species as shown in Figure I.2 of Appendix I.

The resulting equation obtained by this graphical approach took the following form:

$$h_\psi = \tau_0 + \tau_1 T^2 \Delta T + \tau_2 T^2 + \tau_3 \Delta T T + \tau_4 T + \tau_5 \Delta T \quad [3.21]$$

where τ_0, \dots, τ_5 stand for the regression coefficients.

Table 3.13 Convective mass transfer coefficients of paper birch and sugar maple for wood drying during the constant drying rate period.

Wood species	T, (°C)	ΔT , (°C)	h_{ψ} , ($\times 10^{-10} \text{ kg}^2 \text{ m}^{-2} \text{ s}^{-1} \text{ J}^{-1}$)
Paper birch	40	4	3.98
		15	1.87
	60	4	4.84
		15	2.57
	80	4	6.21
		15	3.16
Sugar maple	40	4	4.20
		15	1.50
	60	4	4.60
		15	2.50
	80	4	5.49
		15	3.76

Multiple regression analysis was then performed with MATLAB to obtain the exact equations. For paper birch, the exact h_{ψ} equation was expressed as follows:

$$h_{\psi} = 5.92 \times 10^{-10} - 6.71 \times 10^{-15} T^2 \Delta T + 1.14 \times 10^{-13} T^2 + 5.90 \times 10^{-13} \Delta T T - 7.42 \times 10^{-12} T - 3.21 \times 10^{-11} \Delta T, R^2 = 98.8\% \quad [3.22]$$

For sugar maple, the exact h_{ψ} equation was:

$$h_{\psi} = 7.41 \times 10^{-10} - 2.00 \times 10^{-15} T^2 \Delta T + 9.58 \times 10^{-14} T^2 + 4.56 \times 10^{-13} \Delta T T - 9.35 \times 10^{-12} T - 3.95 \times 10^{-11} \Delta T, R^2 = 98.2\% \quad [3.23]$$

By drying red pine (*Pinus resinosa* Ait.) sapwood from nearly saturated to dry conditions at 56°C and an air velocity of 1.0 m s⁻¹, Tremblay et al. (2000b) reported a convective mass transfer coefficient h_{ψ} of $8.6 \times 10^{-10} \text{ kg}^2 \text{ m}^{-2} \text{ s}^{-1} \text{ J}^{-1}$ for the constant drying rate period. Nabhani et al. (2003) obtained $8.0 \times 10^{-10} \text{ kg}^2 \text{ m}^{-2} \text{ s}^{-1} \text{ J}^{-1}$ at 60°C and an air velocity of 1.2 m s⁻¹. But in the current study, at T = 60°C, $\Delta T = 4$ and 15°C and an air velocity of 1.5 m s⁻¹,

the measured mean h_{ψ} value is $3.7 \times 10^{-10} \text{ kg}^2 \text{ m}^{-2} \text{ s}^{-1} \text{ J}^{-1}$ for paper birch and $3.6 \times 10^{-10} \text{ kg}^2 \text{ m}^{-2} \text{ s}^{-1} \text{ J}^{-1}$ for sugar maple. The apparent discrepancy between the latter values and those reported in the literature may be due to the differences among the material properties. It had been proposed that the convective mass transfer on the wood surface is dependent on the specimen surface properties, such as specific gravity and moisture content (Choong and Skaar 1972; Siau and Avramidis 1996).

3.3.3.2 Fine tuning of the convective mass transfer coefficient below the constant dring rate period

After substituting the Equations [3.22] and [3.23] in the DRYTEK code, and using a correction factor for the moisture content below the constant rate period derived for softwood species, several simulations at the drying conditions used for the wood color tests mentioned above were run. The h_{ψ} - S_p relationship of both species was then adjusted by modifying the correction factor so as to get a good agreement between the simulated drying curves and the experimental drying curves obtained at the dry bulb temperatures of 40, 60 and 80°C and the wet-bulb depression values of 4 and 15°C.

The simulated and experimental drying curves are shown in Figure J.1 and J.2 of Appendix J for paper birch and for sugar maple, respectively. For both wood species, the simulated results match the respective experimental results very well when the wet-bulb depression is 15°C. At 4°C wet-bulb depression, there are differences between the simulated results and the respective experimental results. But, if the wet-bulb depression in the DRYTEK program was changed to 5°C, the simulated results were approaching the respective experimental ones. The differences may be explained by the experimental errors caused by the thermocouples installed in the drying tunnel and the moisture content measurement.

For paper birch, the h_{ψ} correction factor was defined as a function of the saturation percentage (S_p) as follows,

$$F = 0.22e^{(0.04S_p)} \quad (20 < S_p < 37) \quad [3.24]$$

$$F = 0.28e^{(0.028S_p)} \quad (S_p \leq 20) \quad [3.25]$$

For sugar maple, the h_{ψ} correction factor was defined as a function of the saturation percentage (S_p) as follows,

$$F = 0.065 e^{(0.076 S_p)} \quad (16 < S_p < 37) \quad [3.26]$$

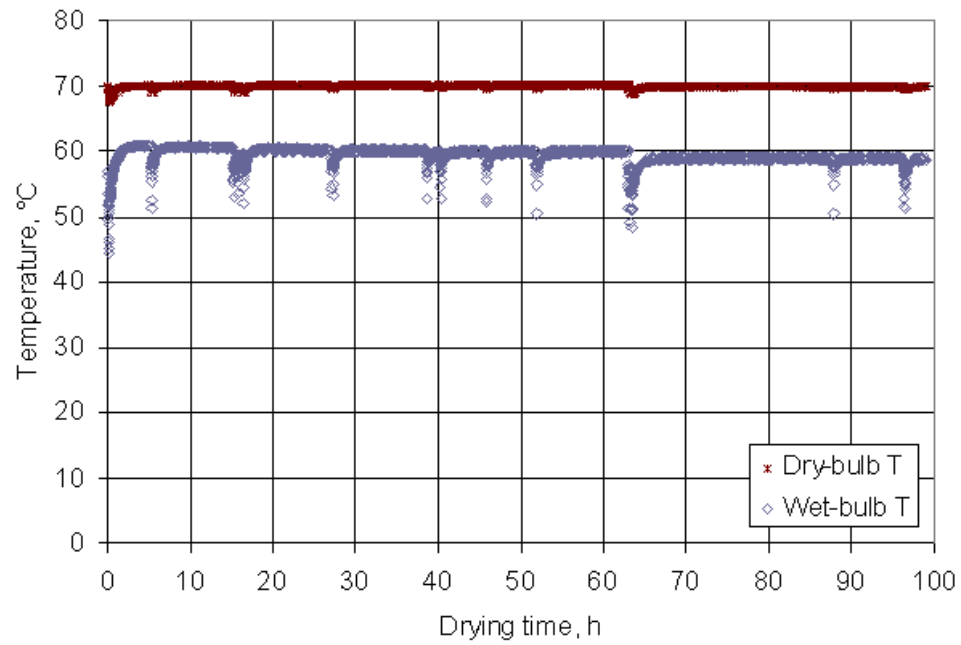
$$F = 0.115 e^{(0.04 S_p)} \quad (S_p \leq 16) \quad [3.27]$$

3.4 Validation tests for the statistical and the integrated color change models

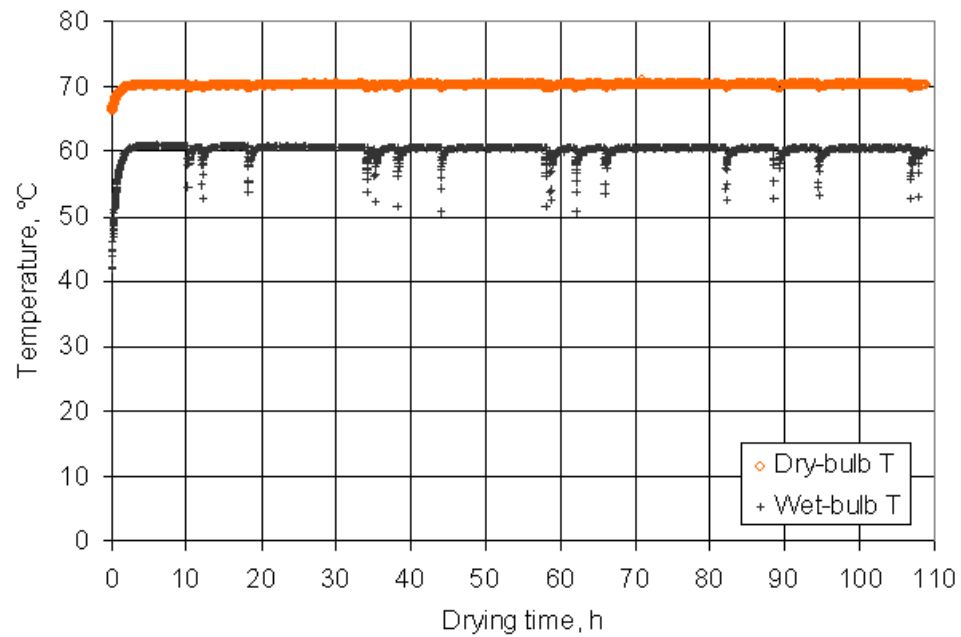
3.4.1 Experimental results

The evolution of dry- and wet-bulb temperatures in the drying chamber during both validation drying runs is shown in Figure 3.13 (a) for paper birch and Figure 3.13 (b) for sugar maple. The average dry-bulb temperature was 69.9°C and the average wet-bulb depression was 10.5°C during the validation test on paper birch. For sugar maple, the corresponding values were 70.1°C and 9.9°C, respectively. These values are therefore fairly close to the setpoint temperatures of 70°C for the dry-bulb temperature and 10°C for the wet-bulb depression.

Figures 3.14 (a) and 3.14 (b) present the moisture content profiles obtained during both validation tests. Each data point represents the average value of the measurements on the three sampling plugs. The moisture content profile at 0 h for birch shows that there was an important moisture gradient through the thickness at the start of the drying test. In the case of sugar maple, the initial moisture content profile was rather flat. A similar observation was made for the drying tests conducted for color change determination (Figures 3.3 and 3.4).

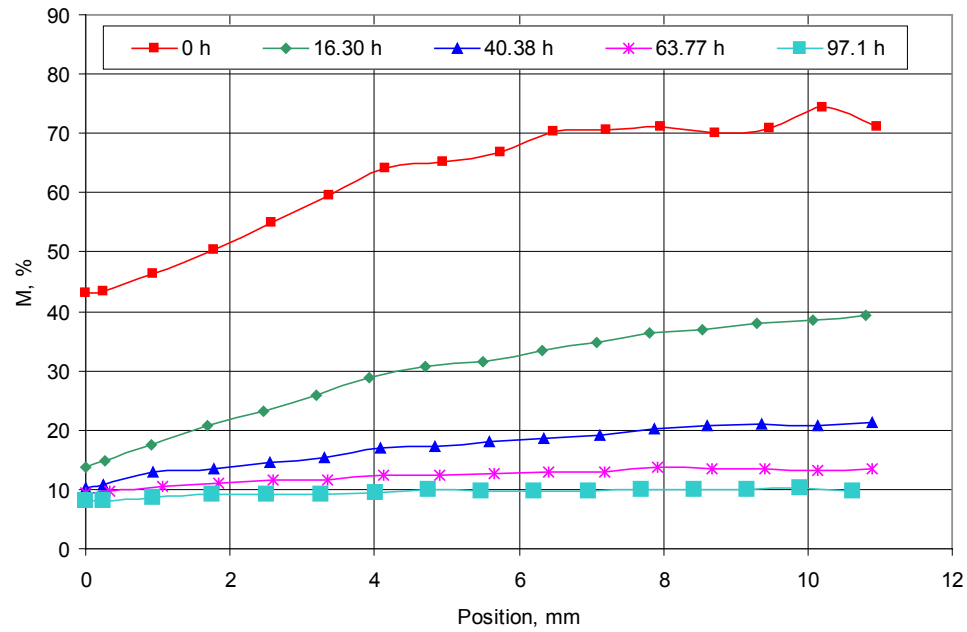


(a) paper birch

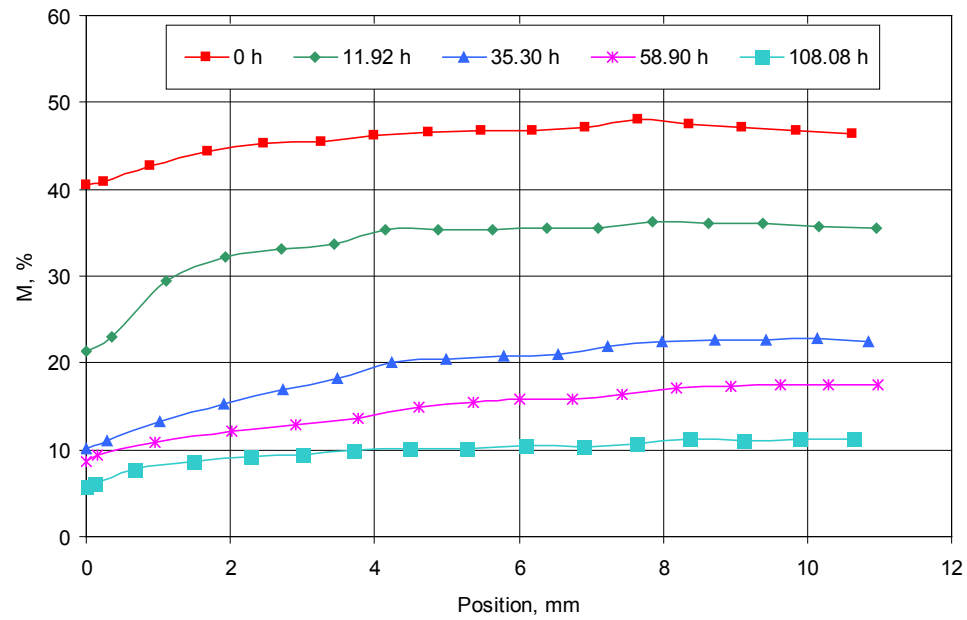


(b) sugar maple

Figure 3.13 Drying schedules obtained from the validation tests at $T_s = 70^\circ\text{C}$ and $\Delta T = 10^\circ\text{C}$.



(a) paper birch



(b) sugar maple

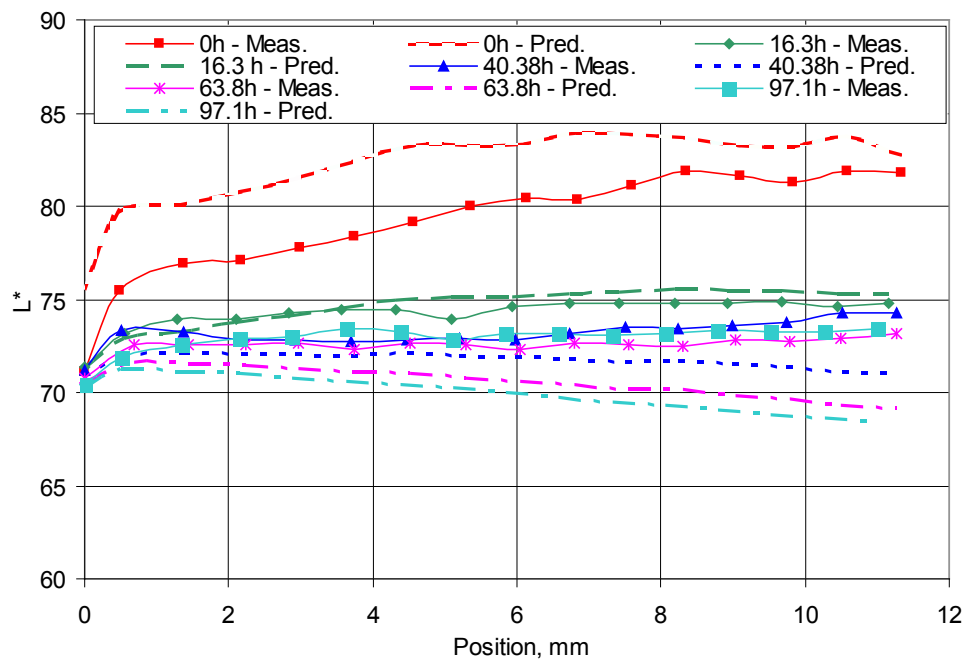
Figure 3.14 The evolution of the M profiles measured during drying at $T = 70^{\circ}\text{C}$ and $\Delta T = 10^{\circ}\text{C}$.

3.4.2 Prediction of wood color change from the global statistical models

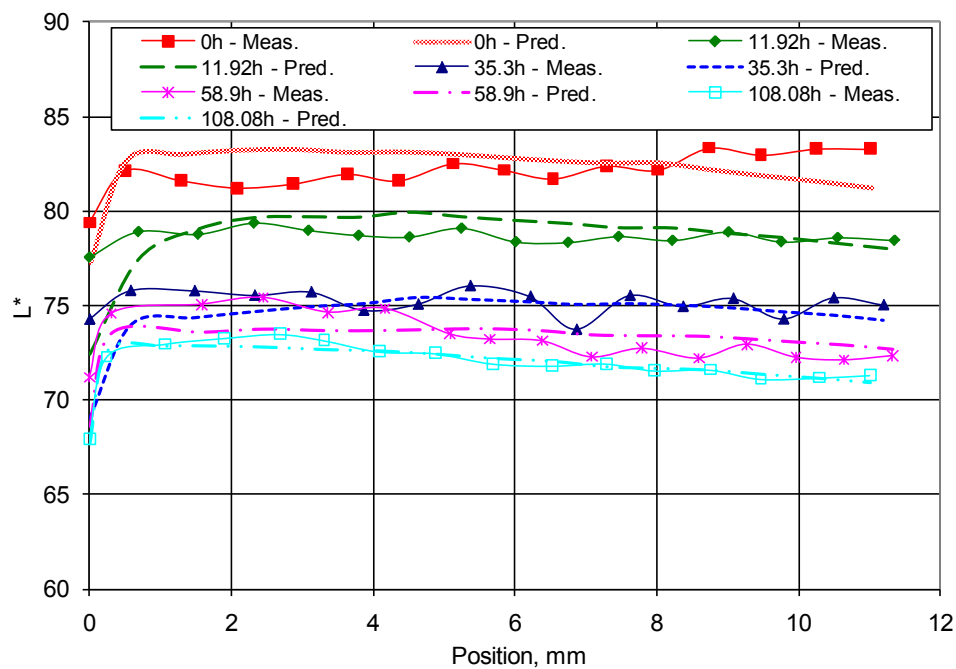
The experimental data obtained from the validations tests were substituted in Equations [3.7] to [3.10] and Equations [3.15] to [3.18] in order to compare the predicted values of L^* to the measured values at $T = 70^\circ\text{C}$ and $\Delta T = 10^\circ\text{C}$. The predicted L^* values for the 3T and 2T models were found in good agreement with the experimental values at some drying times while there was some discrepancy at others. However, both kinds of models predicted the same tendency of L^* profiles. Only the predicted results with 2T global models are presented here because the dry-bulb temperature of the validation test was between 60 and 80°C . Figures 3.15 (a) and 3.15 (b) illustrate the comparison between these two sets of data, where the term “Meas.” stands for “measured” and “Pred.” for “predicted”.

For paper birch, the predicted initial L^* profile is much higher than the measured one. At 16.3 h, the predicted and measured L^* profiles are in good agreement with each other. Both types of profiles are also in good agreement at 40.4 h although the predicted L^* value tends to be too low near the center of the board. This discrepancy between the predicted and measured values from the quarter thickness to mid thickness is growing for the rest of the drying test. Moreover, a similar decrease of the L^* value toward the center of the board was observed during the color test experiments at a wet-bulb depression of 15°C (Figure 3.5). It is therefore normal that the global prediction model reflects this tendency. On the wood surface, one can observe a very good agreement between the predicted and measured L^* values, except for the 0 h profile.

Concerning sugar maple, the predicted L^* profiles below the surface of the board are in a very good agreement with the measured L^* profiles. However, on the wood surface, the predicted L^* values are always lower than their respective measurements except at 108.08 h. Here again, this may be explained by the lower surface L^* values measured during the wood color tests at the dry-bulb temperatures of 60°C and 80°C (Figure 3.6).



(a) paper birch



(b) sugar maple

Figure 3.15 Comparison of the experimentally determined wood lightness profiles with the predicted values of the 2T statistical global wood color models for the validation drying test conducted at $T = 70^{\circ}\text{C}$ and $\Delta T = 10^{\circ}\text{C}$.

3.4.3 Numerical simulations

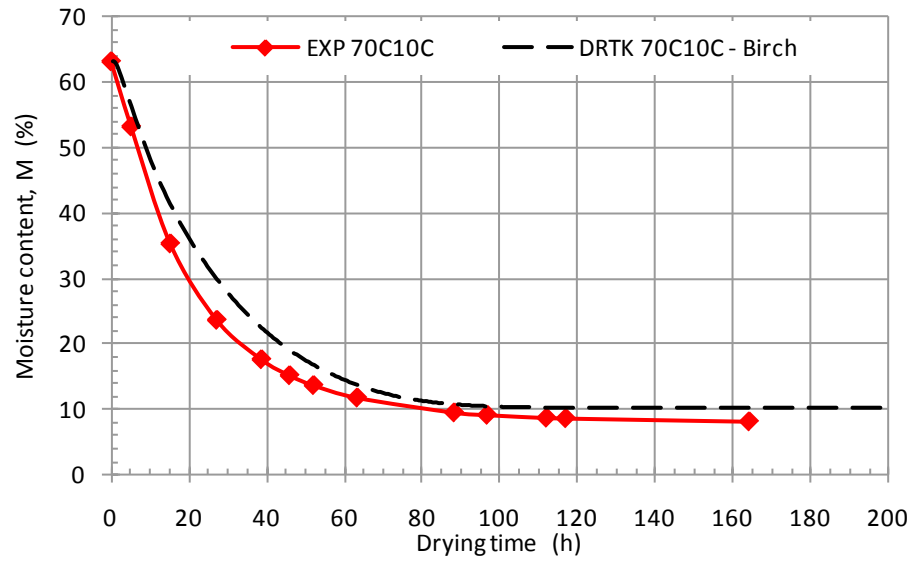
3.4.3.1 Drying curves

Figure 3.16 (a) and 3.16 (b) show a comparison between the average drying curves obtained from the validation tests and the predicted drying curves obtained with the DRYTEK simulation code. In this figure, “EXP” means “experimental results” and “DRTK” stands for “simulation results”.

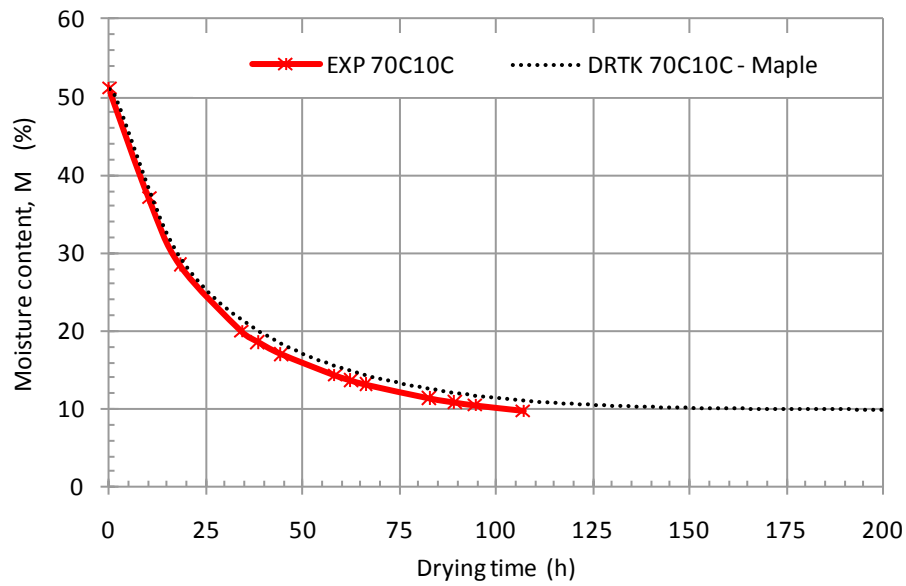
For paper birch, the simulated drying curve almost overlaps with the measured curve from the beginning of drying to about 50% M, and then it becomes significantly higher until about 10% M, where again it is approaching the measured drying curve. An excellent fit can be seen in the case of sugar maple, the simulated drying curve being very slightly above the measured drying curve from 25% M to the end of the test.

3.4.3.2 Moisture content and lightness profiles of wood

Figure 3.17 presents a comparison between the simulated M profiles and the measured M profiles for the validation test on birch and maple. One must point out that the drying times for both sets of profiles do not exactly coincide because of the limitations of the time step interval in the DRYTEK code, which was set as 0.25 h. Also, the shape of the initial M profiles obtained from both methods is very different because of the assumption in the DRYTEK code that the initial M profile of the board is uniform. This is specially the case for paper birch where the experimentally determined initial M profile exhibits a M difference of 31% between surface and core due to air drying during storage (Figure 3.17 a). Although the average M value at 0 h was about the same, at 16.3 h of drying, the simulated M profile of paper birch is found much higher than the measured one with the maximum difference of 21% M at the board center. This discrepancy between both types of profiles is, however, decreasing as the drying goes on and the shape of both profiles becomes very similar. At 64 h of drying, the simulated profile is almost parallel to the measured one with the maximum difference of only 3%. At 97 h of drying, both profiles overlap almost perfectly with only a 2% difference in M at the wood surface.



(a) paper birch



(b) sugar maple

Figure 3.16 Comparison of the drying curves simulated with with the DRYTEK code and those measured during the validation tests.

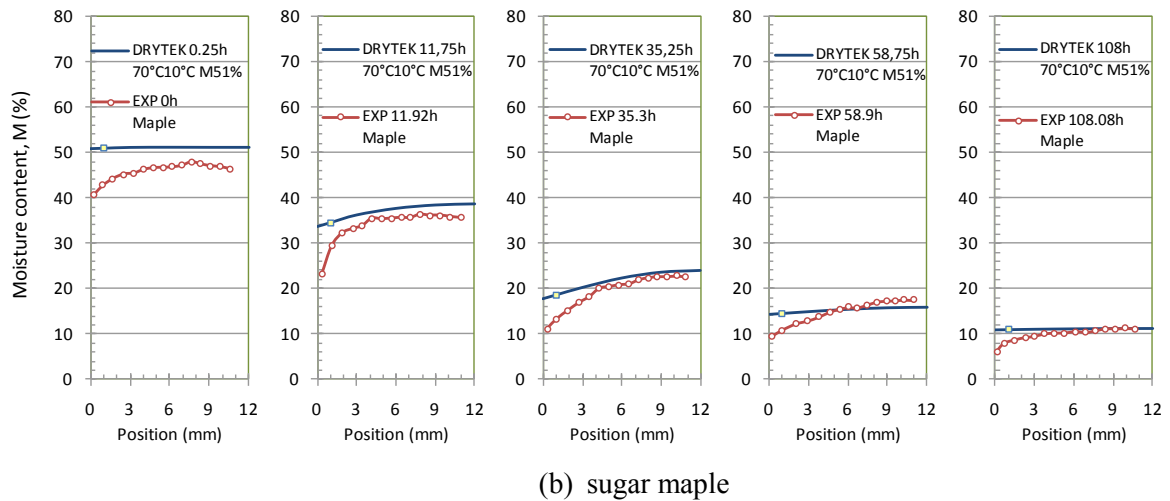
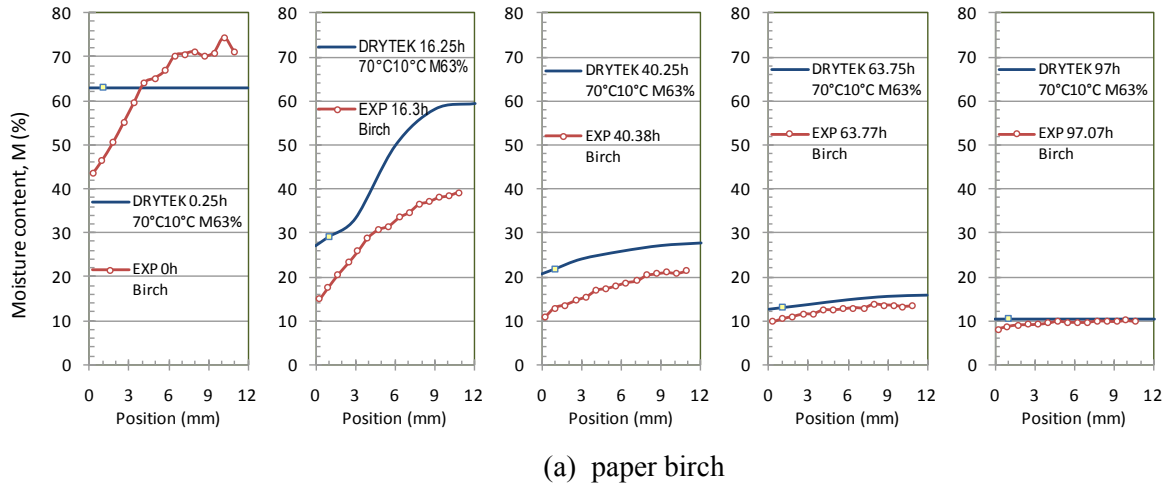


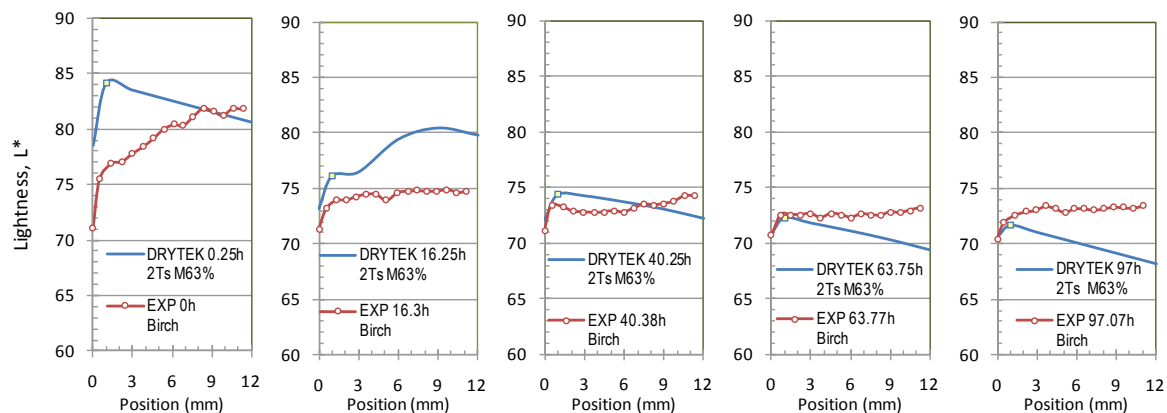
Figure 3.17 Comparison of the M profiles simulated with the DRYTEK code and those measured during drying at $T = 70^{\circ}\text{C}$ and $\Delta T = 10^{\circ}\text{C}$.

The comparison between the simulated and the measured M profiles is, however, much better for sugar maple (Figure 3.17 b). Considering the error associated with the M measurement of the wood slices, which was greater at high moisture contents due to the pressure of slicing knife, the agreement between both types of results is very good, except near the surface of the board. Moreover, this is a common feature of the DRYTEK simulation code which tends in general to underestimate the M gradients near the surface of the board.

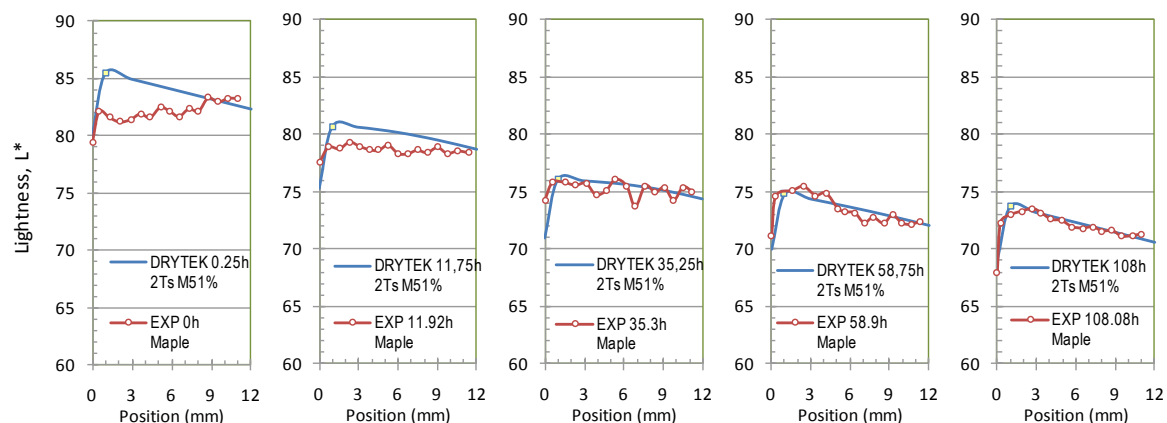
Figure 3.18 shows the simulated L^* profiles using the combination of the DRYTEK code with the 2T global wood color models (mentioned above) in comparison with the experimental values obtained from the validation tests. As it was observed in Figure 3.15 (a) with the predicted L^* profiles from the statistical models, the simulated L^* profiles for paper birch are significantly higher than the measured profiles for the first part of the drying test whereas the reverse is true for the last part of the drying test. Here again, the simulated profiles below the wood surface show a negative slope inwards from 40 h of drying to the end of the drying test. The simulated and measured values of L^* at the surface are, however, very similar, except at 0 h time of drying.

The comparison between the simulated L^* profiles to the measured ones for sugar maple is (Figure 3.18 b) very good, except at the start of drying. From 12 h drying time to the end, it is interesting to note that the shape of both types of profiles below the surface is also very similar. It is therefore clear from these results that the data used for the development of the color models have a great influence on the predicted results. For one reason or the other, the experimental color profiles for paper birch during the validation run did not behave similarly as the ones during the original color measurement tests. Furthermore, the fact that one has to assume a uniform M content profile at the beginning of drying with the DRYTEK code creates another distortion in the simulated results. It is in fact virtually impossible in practice to obtain a uniform M content profile in a piece of wood in the green condition. Finally, because of the natural variability of wood properties, it is normal that a predicting model does not give an exact fit with the experimental values.

Taking into account these facts, in addition of all the measurements errors, one can conclude that the simulated results obtained from the integration of the DRYTEK simulation code with the global statistical models gave very good results for sugar maple. For paper birch, the agreement between both types of results is not so good below the surface but quite acceptable at the surface of the board. Of course, the global statistical predicting wood color models presented in this study were derived from one-step drying schedules and further work would be needed to extend the use of these models to multi-steps drying schedules.



(a) paper birch



(b) sugar maple

Figure 3.18 Comparison of L* profiles simulated using the integrated DRYTEK with the 2T global wood color models and those measured during the validation drying test at $T = 70^{\circ}\text{C}$ and $\Delta T = 10^{\circ}\text{C}$.

Chapter 4. Conclusions et recommandations

L'objectif général de cette étude était de développer un modèle de prédiction des changements de couleur dans le bois d'aubier du bouleau à papier et de l'érable à sucre dans des conditions hygrothermiques représentatives du séchage à moyenne température. Un modèle statistique de la couleur du bois a été d'abord développé et ensuite combiné à un modèle existant de transfert de masse et de chaleur en vue de pouvoir simuler les changements de couleur pour tout programme de séchage à moyenne température utilisé dans l'industrie. Des mesures de changements de couleur dans le bois ont été réalisées au cours d'essais de séchage à une étape à trois températures sèches (40, 60 et 80°C) et deux dépressions au thermomètre humide (4 et 15°C). Des essais ont également été réalisés afin de déterminer les paramètres du modèle de transfert de masse et de chaleur aux trois températures de séchage. Le modèle statistique de prédiction de la couleur ainsi que le modèle combiné (modèle statistique et modèle numérique) furent finalement validés au moyen d'un essai de séchage indépendant réalisé à une température de 70°C et à une dépression au thermomètre humide de 10°C.

Les résultats des mesures de la couleur du bois en cours de séchage montrent qu'aux températures sèches de 60 et 80°C, les valeurs de l'indice de clarté L^* des deux espèces sous la surface du bois diminuent rapidement avec une diminution de la teneur en humidité (M) de l'état vert jusqu'au point de saturation des fibres. Par la suite, les valeurs de L^* diminuent lentement jusqu'à 15 - 25% M, où elles peuvent même commencer à augmenter. La majeure partie du changement de L^* intervient donc au-dessus du point de saturation

des fibres. Un effet marqué de l'épaisseur fut observé pour la dépression au thermomètre humide de 15°C, où les valeurs de L^* diminuent avec la profondeur dans la planche. Les changements de clarté sont négligeables à 40°C, les valeurs de L^* augmentant même à différentes périodes du processus de séchage. Les valeurs de L^* à la surface diminuent avec une diminution de la teneur en humidité et une augmentation de la température. En général, plus élevée est la température de séchage, plus grande est la diminution de la clarté L^* . Inversement, plus élevée est la dépression au thermomètre humide, plus faibles sont les changements de L^* . Les valeurs finales de L^* variaient entre 60 et 77 à la surface du bois et entre 65 et 80 à l'intérieur du bois. Les valeurs initiales correspondantes de L^* variaient entre 68 et 81 et entre 79 et 85.

Les variations de la composante de couleur a^* (rouge au vert) ont suivi une tendance similaire à celle de la clarté L^* par rapport à la température de séchage et à la dépression au thermomètre humide. Contrairement à L^* , les valeurs de a^* ont cependant augmenté avec une diminution de la teneur en humidité, d'une valeur initiale d'environ 4 à une valeur maximale variant entre 7 et 11. De plus, les valeurs de a^* à la surface furent toujours supérieures à celles sous la surface. Ces dernières ont d'ailleurs montré une évolution constante par rapport à l'épaisseur du bois, ce qui ne fut pas le cas pour la clarté L^* .

Concernant la composante de couleur b^* (jaune au bleu), les variations ont suivi la même tendance que la composante a^* , excepté que celles-ci furent beaucoup plus faibles relativement parlant. Ainsi, à l'intérieur de la planche les valeurs initiales de b^* qui étaient d'environ 20 ont augmenté avec une diminution de la teneur en humidité pour atteindre une valeur d'environ 27 à la fin du cycle de séchage. À la surface, les valeurs de b^* ont varié très peu au cours du cycle de séchage.

Une approche graphique combinée à une analyse de régression fut utilisée afin de développer le modèle statistique de changement de couleur, limité dans cette thèse à la clarté L^* , et cela de façon séparée pour la surface de la planche et l'intérieur de la planche. Le modèle statistique global de prédiction pour la clarté L^* fut exprimé en fonction des paramètres température de séchage, dépression au thermomètre humide, teneur en humidité

du bois, et position de la planche sous la surface. La comparaison des valeurs prédites de L^* avec les valeurs mesurées expérimentalement lors des essais de validation montre une très bonne similitude entre les deux types de résultats pour l'érable à sucre. Pour le bouleau à papier, une différence assez appréciable est observée dans la première partie du séchage mais la ressemblance est meilleure en fin de cycle. Les différences de teneur en humidité initiale des échantillons utilisés pour les différents essais expliqueraient une bonne partie des écarts observés pour le bouleau à papier.

Les résultats de la mesure de la relation teneur en humidité-potential hydrique montrent que le potentiel hydrique augmente avec la température à une teneur en humidité donnée. L'allure différente de cette relation chez les deux espèces peut s'expliquer par les écarts dans les teneurs en humidité initiales et vraisemblablement dans les distributions effectives des pores spécifiques aux deux espèces. Un plateau caractéristique existe cependant dans les deux cas dans la gamme de potentiel hydrique entre -2000 et -6000 J kg^{-1} . Tel que prévu, la conductivité hydrique effective augmente avec la teneur en humidité et la température. Dans ce cas également, les relations conductivité hydrique-teneur en humidité sont différentes pour les deux espèces, ce qui s'explique une fois de plus par les différences dans les teneurs en humidité initiales et les distributions effectives des pores. De plus, la conductivité hydrique effective en direction radiale est plus grande qu'en direction tangentielle, exceptée aux très faibles teneurs en humidité. La contribution des rayons en direction radiale expliquerait cette différence.

Le coefficient de transfert de masse (h_ψ) du bouleau à papier et de l'érable à sucre fut exprimé en fonction de la température de séchage et de la dépression au thermomètre humide. Les valeurs de h_ψ augmentent avec la température sèche à une dépression au thermomètre humide donnée, alors qu'elles diminuent avec la dépression au thermomètre humide à une température sèche donnée.

La comparaison des mesures de couleur lors des essais de validation sur le bouleau à papier et l'érable à sucre avec les valeurs de couleur simulées avec le modèle statistique combiné au modèle de transfert de masse et de chaleur montre encore une fois une très bonne

similitude des deux types de résultats dans le cas de l'érable à sucre. Et comme il fut observé pour le modèle statistique, la ressemblance entre les deux types de résultats est beaucoup moins bonne dans le cas du bouleau à papier.

Il est évidemment difficile de spéculer à savoir si les modèles de changement de couleur développés dans le cadre de cette étude pourraient s'appliquer dans le cas de programmes de séchage industriels à étapes multiples. Seuls de futurs travaux sur le sujet pourraient le confirmer ou l'infirmer. Cependant, le fait d'avoir utilisé une gamme représentative de températures sèches pour le séchage à moyenne température et deux dépressions au thermomètre humide que l'on retrouve en début et en fin de cycle, donne certainement une bonne idée des résultats attendus pour des programmes industriels. L'utilisation d'un code de simulation de transfert de masse et de chaleur en cours de séchage augmente l'application pratique de tels modèles de prédiction, n'ayant pas à mesurer en cours de séchage les profils de teneur en humidité, ce qui est difficile à réaliser dans un contexte industriel. Même si l'utilisation d'un programme de séchage doux pour minimiser les changements de couleur dans les bois blancs des espèces feuillues est une pratique bien connue, de tels modèles de prédiction de la couleur peuvent permettre l'utilisation de programmes plus rigoureux et rapides en ajustant mieux les conditions hygrothermiques du séchoir aux propriétés de la matière première et l'évolution de la teneur en humidité du chargement.

Quelques recommandations peuvent découler de cette étude. Premièrement, il serait intéressant de modéliser le comportement des composantes C^* et h dans le système CIE L^*C^*h à partir des mesures des composantes a^* et b^* . De plus, il serait opportun de refaire un essai de validation avec le bouleau à papier en s'assurant de la présence d'un gradient de teneur en humidité minimal en début de séchage. Des essais de validation pour l'érable et le bouleau devraient également être conduits dans un séchoir de laboratoire avec un système d'humidification à la vapeur basse pression. Finalement, il serait intéressant de vérifier l'applicabilité des modèles de prédiction proposés pour le changement de couleur dans un programme de séchage à étapes multiples, et s'il y a lieu, de développer de nouveaux modèles pour de tels programmes.

Bibliography

- Barton, G. M. and J. A. F. Gardner. 1966. Brown stain formation and the phenolic extractives of western hemlock (*Tsuga heterophylla* (Raf.) Sarg.). Canada Dept. of Forestry Pub. No. 1147. 20 pp.
- Bekhta, P. and P. Niemz. 2003. Effect of high temperature on the change in color, dimensional stability and mechanical properties of spruce wood. *Holzforschung*. 57: 539-546.
- Ben Nasrallah, S. and P. Perré. 1988. Detailed study of a model of heat and mass transfer during convective drying of porous media. *Int. J. Heat Mass Transfer*. 31(5): 957-967.
- Billmeyer, Jr. F.W. and M. Saltzman. 1981. *Principles of Color Technology*. 2nd ed. John Wiley and Sons Inc., New York, NY. 240 pp.
- Boone, R. S., C. J. Kozlik, P. J. Bois and E. M. Wengert. 1988. Dry Kiln Schedules for Commercial Woods – temperate and tropical. Gen. Tech. Rep. FPL-GTR-57. U. S. Department of Agriculture, Forest Service, Forest Products Laboratory, Madison, WI. 158 pp.
- Brunner, C. C., G. B. Shaw, D. A. Butler and J. W. Funck. 1990. Using color in machine vision systems for wood processing. *Wood Fiber Sci*. 22(4): 413-428
- Chahal, L. S. 1965. Effect of temperature and trapped air on matric suction. *Soil Sci*. 100: 262-266.
- Charrier, B., J. P. Haluk and G. Janin. 1992. Prevention of brown discoloration in European oak wood occurring during kiln drying by a vacuum process: Calorimetric comparative study with a traditional process. *Holz Roh-Werkstoff*. 50: 433-437.
- Charrier, B., J. P. Haluk and M. Metche. 1995. Characterization of European oakwood constituents acting in the brown discolouration during kiln drying. *Holzforschung*. 49 (2): 168-172.
- Choong, E. T. 1965. Diffusion coefficients of softwoods by steady-state and theoretical methods. *Forest Prod. J*. 15(1): 21-27.
- Choong, E. T. and C. Skaar. 1972. Diffusivity and surface emissivity in wood drying. *Wood Fiber Sci*. 4(2): 80-86.
- Cloutier, A. 2005. Notes de cours “Anatomie Du Bois Avancée”. Université Laval, Québec, Canada.

- Cloutier, A. and Y. Fortin. 1991. Moisture content-water potential relationship of wood from saturated to dry conditions. *Wood Sci. Technol.* 25(4): 263-280.
- Cloutier, A., Y. Fortin and G. Dhett. 1992: Wood drying modelling based on the water potential concept: recent developments. *Drying Technol.* 10(5): 1151-1181.
- Cloutier, A. and Y. Fortin. 1993. A model of moisture movement in wood based on the water potential concept and the determination of the effective water conductivity. *Wood Sci. Technol.* 27(1): 95-114.
- Cloutier, A. and Y. Fortin. 1994. Wood drying modelling based on the water potential concept: Hysteresis effect. *Drying Technol.* 12(8): 1793-1814.
- Cloutier, A., C. Tremblay and Y. Fortin. 1995. Effect of specimen structural orientation on the moisture content-water potential relationship of wood. *Wood Sci. Technol.* 29: 235-242.
- Comstock, G. 1963. Moisture diffusion coefficients in wood as calculated from adsorption, desorption and steady-state data. *Forest Prod. J.* 13(3): 97-103.
- Dawson-Andoh, B. E., M. Wiemann, L. Matuana and J. Baumgras. 2004. Infrared and colorimetric characterization of discolored kiln-dried hard maple lumber. *Forest Prod. J.* 54 (1): 53-57.
- Defo, M. 1999. Modélisation du séchage du bois sous vide par contact: l'approche du potentiel hydrique. Thèse de Doctorat, Université Laval, Québec, Canada. 246 pp.
- Defo, M., Y. Fortin and A. Cloutier. 1999a. Moisture content-water potential relationship of sugar maple and white spruce wood from green to dry conditions, *Wood Fiber Sci.* 31(1): 62-70.
- Defo, M., Y. Fortin and A. Cloutier. 1999b. Determination of the effective water conductivity of sugar maple sapwood and white spruce heartwood under vacuum. *Wood Fiber Sci.* 31(4): 343-359.
- Denig, J., E. M. Wengert and W.T. Simpson. 2000. Drying hardwood lumber, Gen. Tech. Rep. FPL-GTR-118. U.S. Dept. of Agriculture, Forest Service, Forest Products Laboratory, Madison, WI. 138 pp.
- Djolani, B. 1970. Hystérèse et effets de second ordre de la sorption d'humidité dans le bois aux températures de 5, 21, 35 et 50°C. Note de recherches no 8, Département d'exploitation et utilisation des bois, Université Laval, Québec, Canada. 58 pp.
- Doering, E. J. 1965. Soil-water diffusivity by the one-step method. *Soil Sci.* 99(5): 322-326.

- Falkehag, S. I., J. Marton and E. Adler. 1966. Chromophores in Kraft lignin. *In: Lignin structure and reactions. Ed., Marton, J. Am. Chem. Soc., Washington D. C. 75-89.*
- Fengel, D. and G. Wegener. 1984. Wood: Chemistry, Ultrastructure, Reactions. Walter de Gruyter, Inc. Berlin, Germany. 613 pp.
- Fortin, Y. 1979. Moisture content – matric potential relationship and water flow properties of wood at high moisture contents. PhD dissertation, The University of British Columbia, Vancouver, Canada. 187 pp.
- Fortin, Y. 1981. Relationships between water potential and equilibrium moisture content of sugar maple wood. Unpublished data.
- Fortin, Y., M. Defo, M. Nabhani, C. Tremblay and G. Gendron. 2004. A simulation tool for the optimization of lumber drying schedules. *Drying Technol.* 22 (5): 963-983.
- Forsyth, P. G. and T. L. Amburgey. 1991. Microscopic characterization of nonmicrobial gray sapstain in southern hardwood lumber. *Wood Fiber Sci.* 23(3):376-383.
- Fuentealba, D., P. N. Diouf, Y. Fortin and T. Stevanovic. 2008. Characterisation of Birch (*Betula papyrifera* Marsh.) wood discoloration during drying. *In: Proc. of the 51st International Convention of Society of Wood Science and Technology, Concepción, Chile. WS. 01: 1-7.*
- Gardner, W. R. 1962. Note on the separation and solution of diffusion type equations. *Soil Sci. Soc. Amer. Proc.* 26(4): 404.
- Gui, Y. Q., E. W. Jones, F. W. Taylor and C. A. Issa. 1994. An application of finite element analysis to wood drying. *Wood Fiber Sci.* 26(2): 281-293.
- Hart, C. A. 1984. Relative humidity, EMC, and collapse shrinkage in wood. *Forest Prod. J.* 34(11/12): 45-54.
- Hartley, J. G. 1986. Coupled heat and moisture transfer in soils: a review. *In: Advances in Drying, Ed., Mujumdar A. S. Hemisphere Publ. Corp. New York. Vol. 4: 199-248.*
- Hernández, R. E. and M. Bizoň. 1994. Changes in shrinkage and tangential compression strength of sugar maple below and above fiber saturation points. *Wood Fiber Sci.* 26(3): 360-369.
- Hiltunen, E., T. T. Pakkanen and L. Alvila. 2004. Phenolic extractives from wood of birch (*Betula pendula*). *Holzforschung.* 58(3): 326-329.
- Hon, D. N. S. and N. Minemura. 1991. Color and Discoloration. *In: Wood and Cellulosic Chemistry. Eds. Hon, D. N. S. and Shiraishi, N., Marcel Dekker Inc., New York, NY. 395-454.*

- Hon, D. N. S. and N. Shiraishi. 2001. Wood and Cellulosic Chemistry. 2nd ed. Revised and Expanded. Marcel Dekker Inc. New York, NY. 914 pp.
- Hrutfjord, B. F., R. Luthi and K. F. Hanover. 1985. Color formation in Western hemlock. J. of Wood Chem. and Tech. 5(4): 451-460.
- Hunt, R. W. G. 1991. Measuring Colour. 2nd ed. Ellis Horwood, New York, NY. 313 pp.
- Hunt, R. W. G. 1998. Measuring Colour. 3rd ed. Ellis Horwood Series in Applied Science and Industrial Technology. Ellis Horwood Limited, Chichester, UK. 344 pp.
- Irudayaraj, J., K. Haghighi and R. L. Stroshine. 1990. Nonlinear finite element analysis of coupled heat and mass transfer problems with an application to timber drying. Drying Technol. 8(4):731-749.
- Kawai, S., K. Nakato and T. Sadoh. 1978. Moisture movement in wood below the fiber saturation point. Mokuzai Gakkaishi. 24(5): 273-280.
- Keylwerth, R. and D. Noack. 1964. Works pamphlet 1. Kiln-drying of sawn timber (German). Holz als Roh- und Werkstoff. 22(1): 29-36.
- King, B., T. A. Oxley and K. D. Long. 1976. Some biological effects of redistribution of soluble nutrients during drying of wood. Material und Organismen. 3: 263-276.
- Kreber, B. and A. Byrne. 1994. Discolorations of hem-fir wood: A review of the mechanisms. Forest Prod. J. 44(5): 35-43.
- Kreber, B. and A. N. Haslett. 1997. A study of some factors promoting kiln brown stain formation in radiata pine. Holz Roh-Werkstoff. 55: 215-220.
- Kreber, B., M. Fernandez and A. G. McDonald. 1998. Migration of kiln brown stain precursors during the drying of radiata pine sapwood. Holzforschung. 52(4):441-446.
- Ledig, S. F. and R. Seyfarth. 2001. Characterization of surface color during wood processing. In: Proc. of the 7th International IUFRO Wood Drying Conference, Tsukuba, Japan. 288-293.
- Linzon, S. N. 1969. Seasonal water content and distribution in eastern white pine. Forestry Chron. 45(1): 38-43.
- Liu, J. Y. and S. Cheng. 1989. Heat and moisture transfer in wood during drying. In: Proc. of the 3rd Joint ASCE/ASME Mechanics Conference, Ed., San Diego, CA, USA. 79-85.

- Liu, J. Y. and S. Cheng. 1991. Solutions of Luikov equations of heat and mass transfer in capillary porous bodies. *Int. J. Heat Mass Transfer* 34(7): 1747-1754.
- Luikov, A. V. 1966. Heat and mass transfer in capillary-porous bodies. Pergamon Press, New York, NY. 523 pp.
- Luostarinen, K., V. Möttönen, A. Asikainen, T. Lahtinen and Y. Tolonen. 2000. Birch (*Betula pendula*) wood discoloration during drying. *In: Proc. of the 2nd COST E15 Advances in Drying of Wood (1999-2003) Workshop on "Quality Drying of Hardwood"*. Sopron, Hungary.
- Luostarinen, K. and J. Luostarinen. 2001. Discolouration and deformations of birch parquet boards during conventional drying. *Wood Sci. Technol.* 35: 517-528.
- Luostarinen, K., V. Möttönen, A. Asikainen and J. Luostarinen. 2002. Birch (*Betula pendula*) wood discoloration during drying. Effect of environmental factors and wood location in the trunk. *Holzforschung*. 56(4): 348-354.
- Luostarinen, K. and V. Möttönen. 2004. Effects of log storage and drying on birch (*Betula pendula*) wood proanthocyanidin concentration and discoloration. *J. Wood Sci.* 50:151-156.
- McCurdy, M., S. Pang and R. Keey. 2003. Measurement of color development in *Pinus radiata* sapwood boards during drying at various schedules. *In: Proc. of the 8th International IUFRO Wood Drying Conference*. Brasov, Romania. 445-448.
- McGinnes, Jr. A. E. and H. N. Rosen. 1984. Macroscopic and microscopic analyses of color changes of wood pressure steam-dried above atmospheric pressure. *Wood Fiber Sci.* 16(1): 48-56.
- McMillen, J. M. 1968. Prevention of pinkish-brown discoloration in drying maple sapwood. Res. Note FPL-0193. USDA Forest Serv., Forest Prod. Lab., Madison, WI. 9 pp.
- McMillen, J. M. 1975. Physical characteristics of seasoning discolorations in sugar maple sapwood. Res. Paper FPL248. USDA Forest Serv., Forest Prod. Lab., Madison, WI. 31 pp.
- Miller, D., R. Sutcliffe and J. Thauvette. 1990. Sticker stain formation in hardwoods: isolation of scopoletin from sugar maple (*Acer saccharum* Marsh.). *Wood Sci. Technol.* 24(4): 339-344.
- Millett, M. A. 1952. Chemical brown stain in sugar pine. *Forest Prod. J.* 2: 232-236.

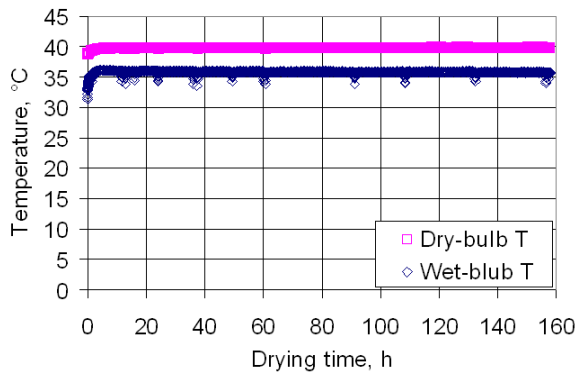
- Mononen, K., L. Alvila and T. T. Pakkanen. 2002. CIEL*a*b* measurements to determine the role of felling season, log storage and kiln drying on coloration of silver birch wood. *Scandinavian Journal of Forest Research*. 17 (2): 179-191
- Möttönen, V. 2005. Variation of color and selected physical and mechanical properties related to artificial drying of sawn silver birch (*Betula pendula* Roth) timber from plantations. Doctoral thesis. Faculty of Forestry, University of Joensuu. Joensuu, Finland. 43 pp.
- Möttönen, V. and K. Luostarinen. 2001. Discoloration of silver birch wood from plantation forests during drying. *In: Proc. of the 7th International IUFRO Wood Drying Conference*, Vienna, Austria. 426-429.
- Nabhani, M. 2002. Détermination expérimentale des coefficients de transfert convectif de masse et de chaleur lors du séchage du bois. Mémoire de maîtrise, Université Laval, Québec, Canada. 4-69.
- Nabhani, M., C. Tremblay and Y. Fortin. 2003. Experimental determination of the convective heat and mass transfer coefficients during wood drying. *In: Proc. of the 8th International IUFRO Wood Drying Conference*, Brasov, Romania. 225-230.
- Panshin, A. J. and C. de Zeeuw. 1980. Textbook of wood technology. Fourth edition. McGraw-Hill Book Co. New York, NY. 722 pp.
- Perré, P. 1987. Le séchage convectif des bois résineux, choix, validation et utilisation d'un modèle. Thèse de Doctorat. Université de Paris VII. Paris, France. 251 pp.
- Perré, P. and D. Maillet. 1989. Drying of softwoods. The interest of a two-dimensional model to simulate anisotropy or to predict degrade. *In: Proc. of the 2nd IUFRO International Wood Drying Symposium*. Ed., Kayihan F., Johnson J. A., Smith W. R. Seattle, WA, USA. 226-237.
- Philip, J. R. 1969. Theory of infiltration. *Adv. Hydrosci.* 5: 215-296.
- Plumb, O. A., G. A. Spolek and B. A. Olmstead. 1985. Heat and mass transfer in wood during drying. *Int. J. Heat Mass Transfer*. 28(9): 1669-1678.
- Rappold, P. M. and W. B. Smith. 2004. An investigation of the relationships between harvest season, log age, and drying schedule on the coloration of hard maple lumber. *Forest Prod. J.* 54(12): 178-184.
- Saha, R. S., and R. I. Tripathi 1981. Effect of temperature on the soil-water content-suction relationship. *Indian Soc. Soil Sci.* 29(2):143-147.
- Siau, J. F. 1983. Chemical potential as a driving force for nonisothermal moisture movement in wood. *Wood Sci. Technol.* 17(2): 101-105.

- Siau, J. F. 1984. Transport processes in wood. Springer-Verlag. New York. 245 pp.
- Siau, J. F. 1992. Nonisothermal diffusion model based on irreversible thermodynamics. *Wood Sci. Technol.* 26(5): 325-328.
- Siau, J. F. 1995. Wood: influence of moisture on physical properties, Dept. of Wood Sci. and Forest Prod. Virginia Polytechnic Institute and State University, Blacksburg, VA, USA. 227 pp.
- Siau, J. F. and S. Avramidis. 1996. The surface emission coefficient of wood. *Wood Fiber Sci.* 28: 178-185.
- Simpson, W. T. (ed.). 1991. Dry Kiln Operator's Manual. USDA Agricultural Handbook No. 188. Forest Serv., Forest Products Lab., Madison, WI. 275 pp.
- Skaar, C. 1988. Wood-water relations. Springer-Verlag, New York, NY. 283 pp.
- Skaar, C. and N. Kuroda. 1985. Application of irreversible thermodynamics to moisture transport phenomena in wood. *In: Proc. of the North American Drying Symposium*, Mississippi Forest Products Utilization Laboratory, Mississippi State Univ., MS. 152-158 pp.
- Smith, W. B. and D. J. Herdman. 1998. Effects of kiln schedules and sticker variables on board color and sticker stain in hard maple. *In: Proc. of the 26th Annual Hardwood Symposium: Technology and Market Information for the Next Millenium*, National Hardwood Lumber Association, Memphis, TN. 121-133.
- Smith, W. B. and D. E. Montoney. 2000. Wood color change and control during drying. *In: Quality Lumber Drying in the Pacific Northwest - Vertical Integration = Improved Profit*. September 30 - October 2, 1999. Forest Products Society, Madison. WI. 111-118 pp.
- Stamm, A. J. and E. E. Harris. 1953. Chemical processing of wood. Chem. Publ. Co. Inc., New York, NY. 113-138 pp.
- Stanish, M. A., G. S. Schajer and F. Kayihan. 1986. A mathematical model of drying for hygroscopic porous media. *AIChE J.* 32(8): 1301-1311.
- Stenudd, S. 2001. Color changes in birch and beech during kiln-drying. *In: Proc. of the 7th International IUFRO Wood Drying Conference*, Vienna, Austria. 300-305.
- Stenudd, S. 2004. Color response in silver birch during kiln-drying. *Forest Prod. J.* 54(6): 31-36.
- Stokke, D. D., A. D. Pugel and J. E. Phelps. 1995. Variation in lightness of white oak dimension stock. *Forest Prod. J.* 45(10): 51-56.

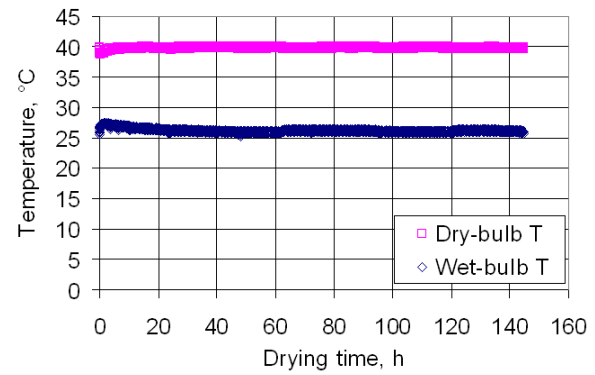
- Straze, A., P. Oven, M. Zupancic and Z. Gorisek. 2003. Color changes of ash-wood (*Fraxinus excelsior* L.) during conventional drying, *In: Proc. of the 8th International IUFRO Wood Drying Conference*. Brasov, Romania. 465-469.
- Sundqvist, B. 2002a. Wood color control during kiln-drying. *Forest Prod. J.* 52(2): 30-37.
- Sundqvist, B. 2002b. Color response of Scots pine (*Pinus sylvestris*), Norway spruce (*Picea abies*) and birch (*Betula pubescens*) subjected to heat treatment in capillary phase. *Holz-als-Roh-und-Werkstoff*. 60(2): 106-114.
- Sundqvist, B. 2004. Color changes and acid formation in wood during heating. Doctoral thesis. Luleå Univ. of Tech. Sweden. 154 pp.
- Sutherland, J. W., I. W. Turner and R. L. Northway. 1992. A theoretical and experimental investigation of the convective drying of Australian *Pinus radiata* timber. *In: Proc. of the 3rd International IUFRO Wood Drying Conference*. Vienna, Austria. 145-155.
- Taylor, F. W. 1997. Prevention of stain associated with kiln drying. *In: Prevention of discolorations in hardwood and softwood logs and lumber*. Forest Products Society, Madison, WI. 90 pp.
- Tarvainen, V., P. Saranpää and J. Repola. 2001. Discoloration of Norway spruce and Scots pine timber during drying. *In: Proc. of the 7th International IUFRO Wood Drying Conference*, Vienna, Austria. 294-299.
- Terziev, N. 1995. Migration of low-molecular sugars and nitrogen in *Pinus sylvestris* L. during kiln and air drying. *Holzforschung*. 49: 565-574.
- Terziev, N. and J. Boutelje. 1998. Effect of felling time and kiln drying on color and susceptibility of wood to mold and fungal stain during an above ground field test. *Wood Fiber Sci.* 30: 360-367.
- Theander, O., J. Bjurman and J. B. Boutelje. 1993. Increase in the content of low molecular carbohydrates at lumber surfaces during drying and correlations with nitrogen content, yellowing and mould growth. *Wood Sci. Technol.* 27: 381-389.
- Thomas, H. R., R. W. Lewis and K. Morgan. 1980. An application of finite element method to the drying of timber. *Wood Fiber*. 11(4): 237-243.
- Thomassen, T. 1986. Brown discoloration of sawn beech wood during kiln-drying. Teknologisk Institut, Tåstrup, Denmark. 17 pp.
- Tjeerdsma, B. F., M. Boonstra, A. Pizzi, P. Tekely and H. Militz. 1998. Characterisation of thermally modified wood: molecular reasons for wood performance improvement. *Holz Roh- Werkstoff*. 56: 149-153.

- Tremblay, C., A. Cloutier and Y. Fortin. 1996. Moisture content-water potential relationship of red pine sapwood above the fiber saturation point and the determination of the effective pore size distribution. *Wood Sci. Technol.* 30: 361-371.
- Tremblay, C. 1999. Détermination expérimentale des paramètres caractérisant les transferts de chaleur et de masse dans le bois lors du séchage. Thèse de Doctorat, Université Laval, Québec, Canada. 243 pp.
- Tremblay, C., A. Cloutier and B. Grandjean. 1999. Experimental determination of the ratio of vapour diffusion to the total water movement in wood during drying. *Wood Fiber Sci.* 31 (3): 235-248.
- Tremblay, C., A. Cloutier and Y. Fortin. 2000a. Determination of the effective water conductivity of red pine sapwood. *Wood Sci. Technol.* 34(2): 109-124.
- Tremblay, C., A. Cloutier and Y. Fortin. 2000b. Experimental determination of the convective heat and mass transfer coefficients for wood drying. *Wood Sci. Technol.* 34(3): 253-276.
- Voss, D. H. and W. N. Hale. 1998. A comparison of the three editions of the Royal Horticultural Society Color Chart. *HortScience* 33: 13-17.
- Viktorin, Z. 1991. Vypocet nestacionarnich poli teplot a vikhkosti ve dreve I. Cast – Teoreticke reseni. *Drevarsky Vyslcum, Zvazok* 129: 23-42.
- Wengert, E. M. 1992. Causes and cures for stains in dried lumber: Sticker stain, chemical stain, iron stain, and blue stain. *Uni. of Wisconsin Forestry Facts No. 64*. Madison, WI.
- Wheeler, E. A. 1982. Ultrastructural characteristics of red maple (*Acer rubrum* L.) wood. *Wood Fiber.* 14(1): 43-53.
- Whitaker, S. 1977. Simultaneous heat, mass and momentum transfer in porous media: a theory of drying. *In: Advances in heat transfer. Ed., Harnett, J. P., Irvine, T. F. Jr.* Academic Press. New York, NY. Vol.13: 119-203.
- Wiberg, P. 1996. Color changes of Scots pine and Norway spruce. A comparison between three different drying treatments. *Holz-als-Roh-und-Werkstoff.* 54(5): 349-354.
- Yeo, H., W. B. Smith. 2004. Control of interior darkening in hard maple. *Wood Fiber Sci.* 36(3): 417-422.
- Zink, P. and D. Fengel. 1988. Studies on the coloring matter of blue-stain fungi. Part 1. General characterization and the associated compounds. *Holzforschung* 42(4): 217-220.

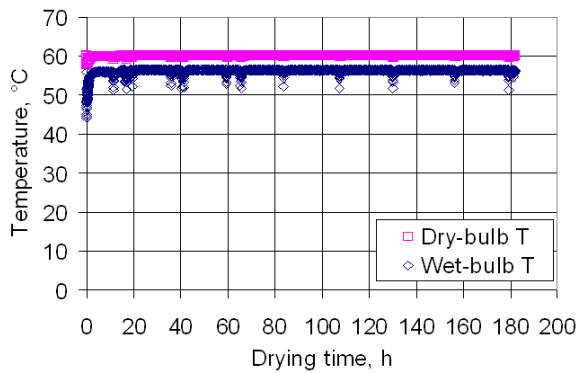
Appendix A: Drying schedules used for the color measurement tests and the measured wood temperature profiles



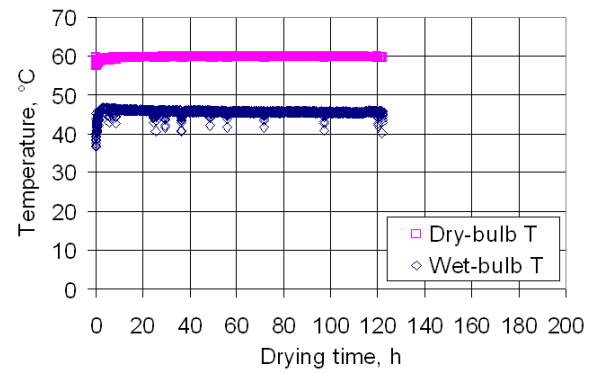
(a) $T = 40^{\circ}\text{C}$ and $\Delta T = 4^{\circ}\text{C}$;



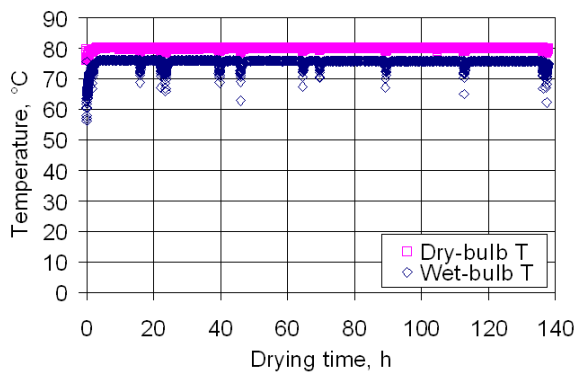
(b) $T = 40^{\circ}\text{C}$ and $\Delta T = 15^{\circ}\text{C}$;



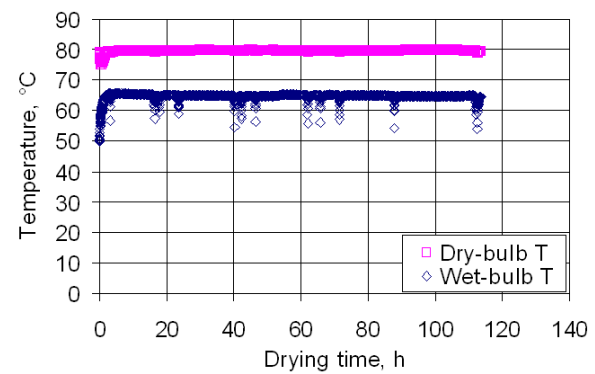
(c) $T = 60^{\circ}\text{C}$ and $\Delta T = 4^{\circ}\text{C}$;



(d) $T = 60^{\circ}\text{C}$ and $\Delta T = 15^{\circ}\text{C}$;

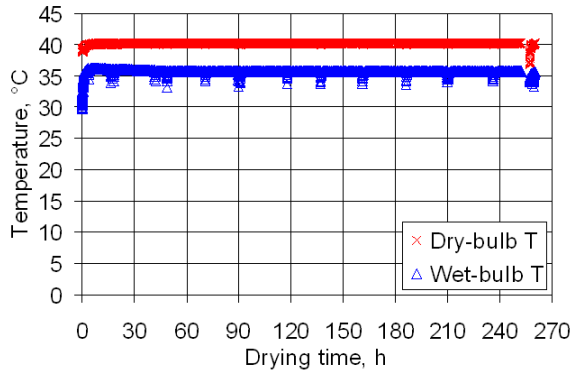


(e) $T = 80^{\circ}\text{C}$ and $\Delta T = 4^{\circ}\text{C}$;

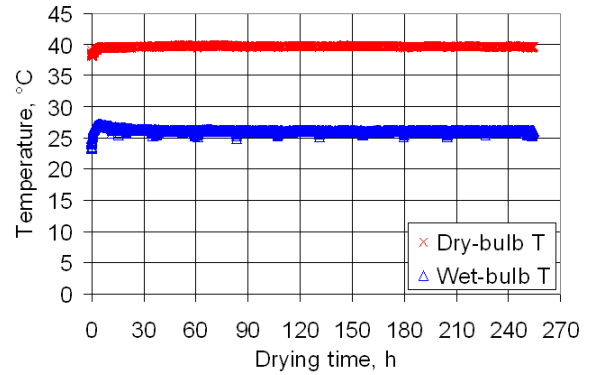


(f) $T = 80^{\circ}\text{C}$ and $\Delta T = 15^{\circ}\text{C}$;

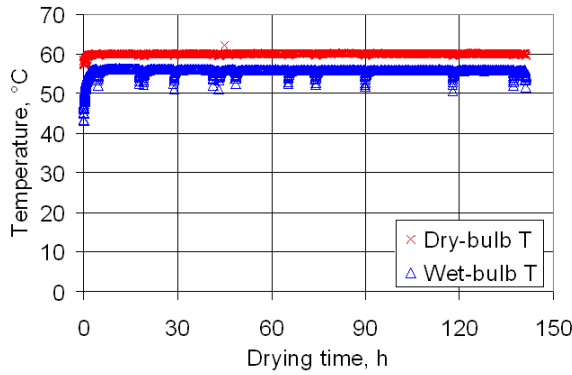
Figure A.1 Drying schedules measured from the six wood color tests on paper birch.



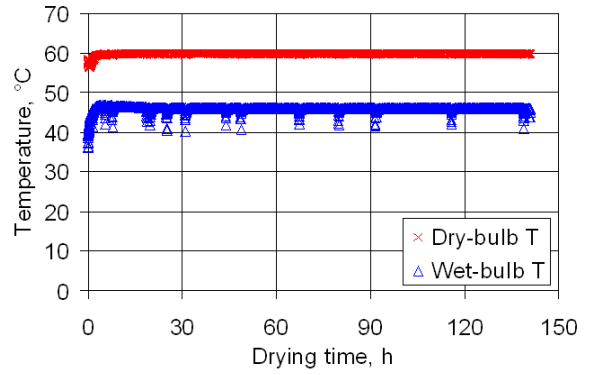
(a) $T = 40^{\circ}\text{C}$ and $\Delta T = 4^{\circ}\text{C}$;



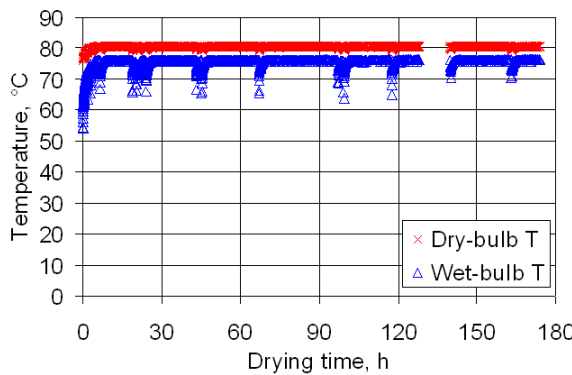
(b) $T = 40^{\circ}\text{C}$ and $\Delta T = 15^{\circ}\text{C}$;



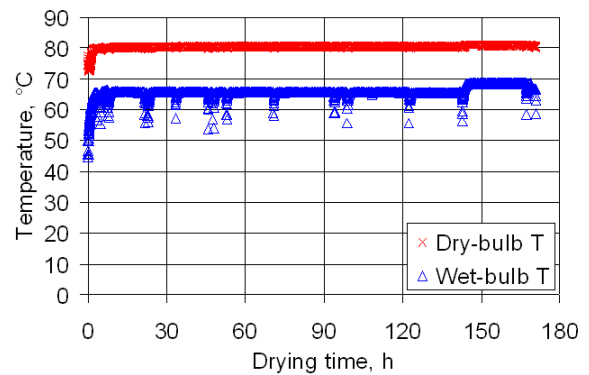
(c) $T = 60^{\circ}\text{C}$ and $\Delta T = 4^{\circ}\text{C}$;



(d) $T = 60^{\circ}\text{C}$ and $\Delta T = 15^{\circ}\text{C}$;

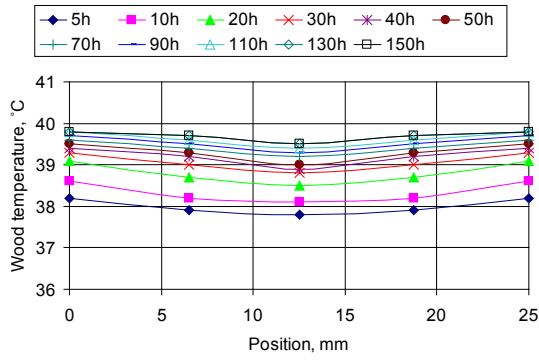


(e) $T = 80^{\circ}\text{C}$ and $\Delta T = 4^{\circ}\text{C}$;

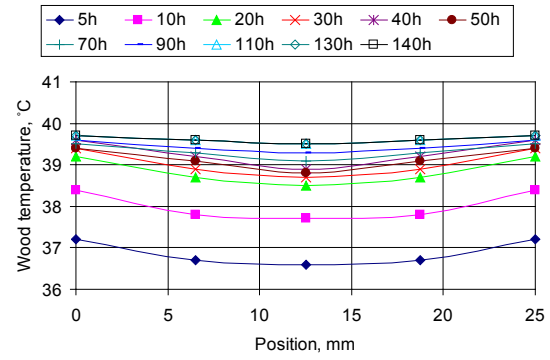


(f) $T = 80^{\circ}\text{C}$ and $\Delta T = 15^{\circ}\text{C}$;

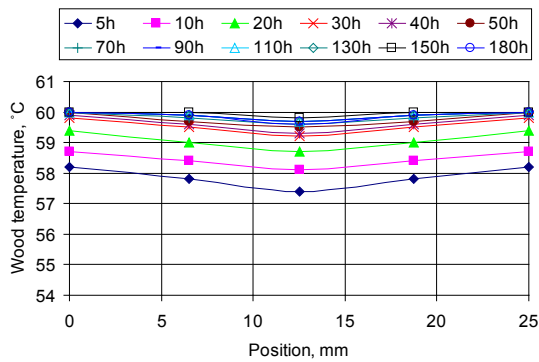
Figure A.2 Drying schedules measured from the six wood color tests on sugar maple.



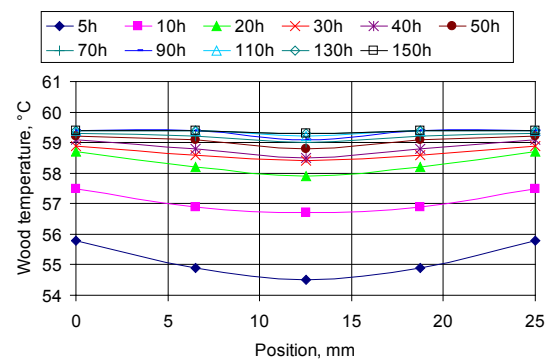
(a) $T = 40^{\circ}\text{C}$ and $\Delta T = 4^{\circ}\text{C}$;



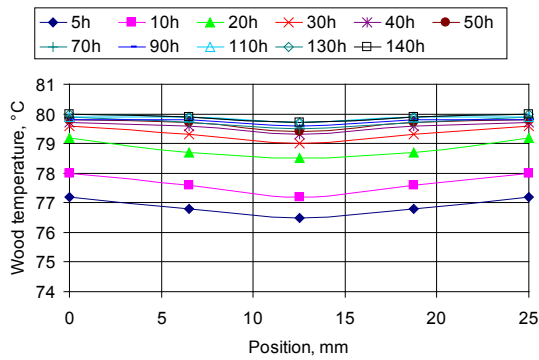
(b) $T = 40^{\circ}\text{C}$ and $\Delta T = 15^{\circ}\text{C}$;



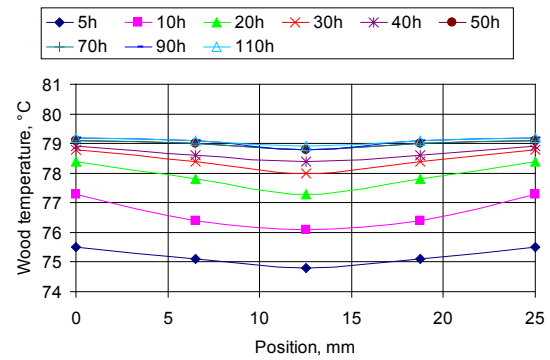
(c) $T = 60^{\circ}\text{C}$ and $\Delta T = 4^{\circ}\text{C}$;



(d) $T = 60^{\circ}\text{C}$ and $\Delta T = 15^{\circ}\text{C}$;

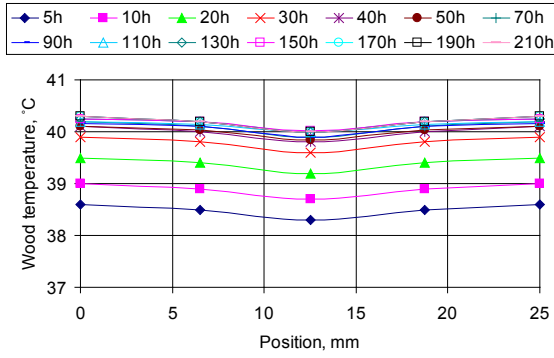


(e) $T = 80^{\circ}\text{C}$ and $\Delta T = 4^{\circ}\text{C}$;

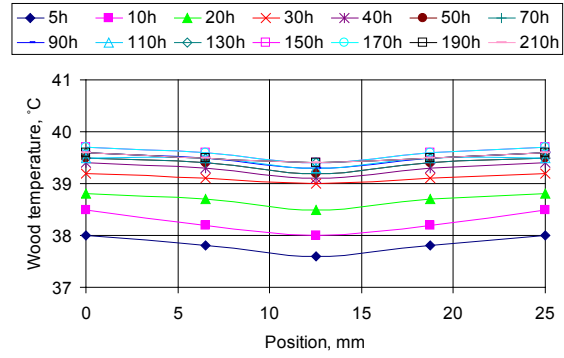


(f) $T = 80^{\circ}\text{C}$ and $\Delta T = 15^{\circ}\text{C}$;

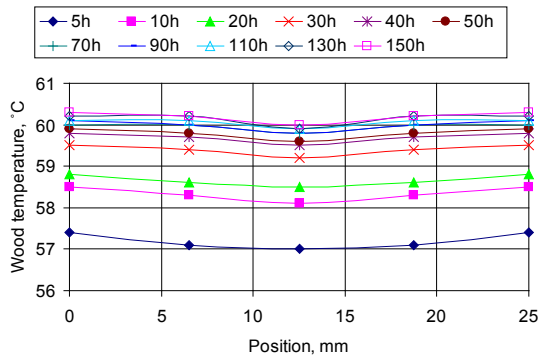
Figure A.3 Wood temperature profiles measured from wood color tests on paper birch.



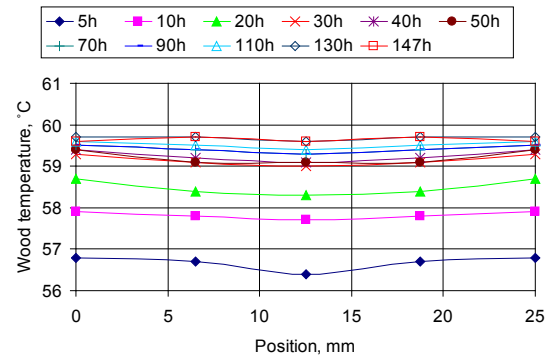
(a) $T = 40^{\circ}\text{C}$ and $\Delta T = 4^{\circ}\text{C}$;



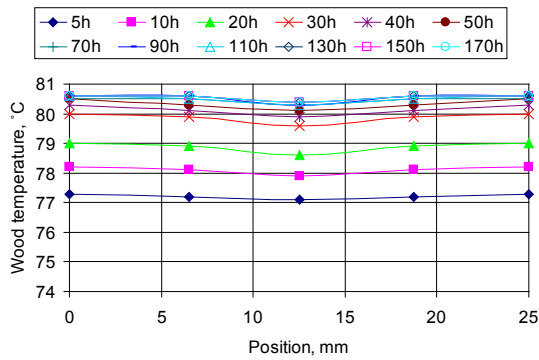
(b) $T = 40^{\circ}\text{C}$ and $\Delta T = 15^{\circ}\text{C}$;



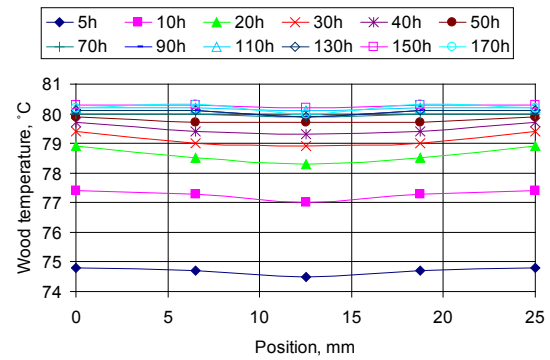
(c) $T = 60^{\circ}\text{C}$ and $\Delta T = 4^{\circ}\text{C}$;



(d) $T = 60^{\circ}\text{C}$ and $\Delta T = 15^{\circ}\text{C}$;



(e) $T = 80^{\circ}\text{C}$ and $\Delta T = 4^{\circ}\text{C}$;



(f) $T = 80^{\circ}\text{C}$ and $\Delta T = 15^{\circ}\text{C}$;

Figure A.4 Wood temperature profiles measured from wood color tests on sugar maple.

Appendix B: Color component a^* and b^* profiles obtained during color measurement tests

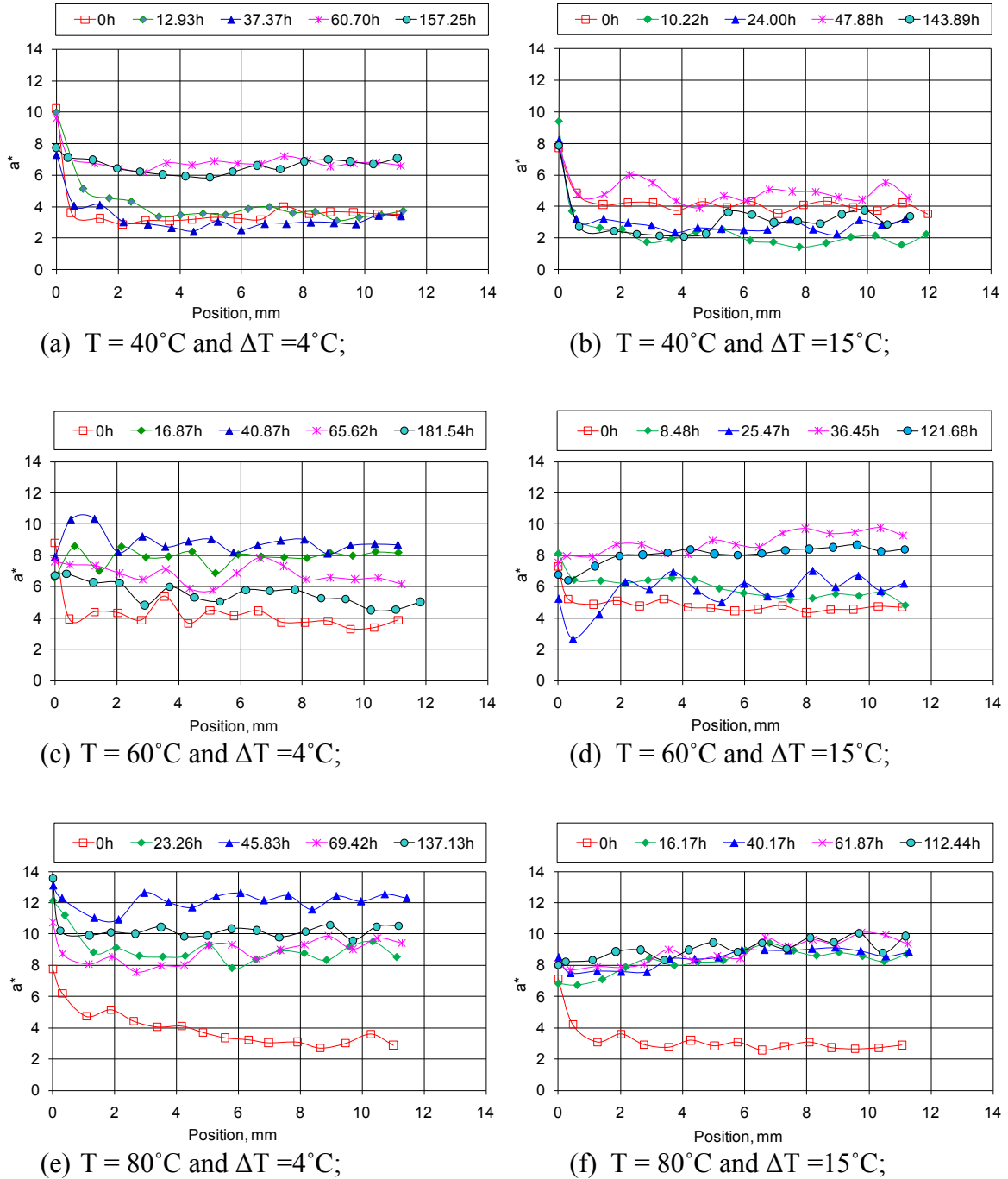


Figure B.1 Wood a^* profiles through the board thickness of paper birch at five different times during drying at six different drying conditions.

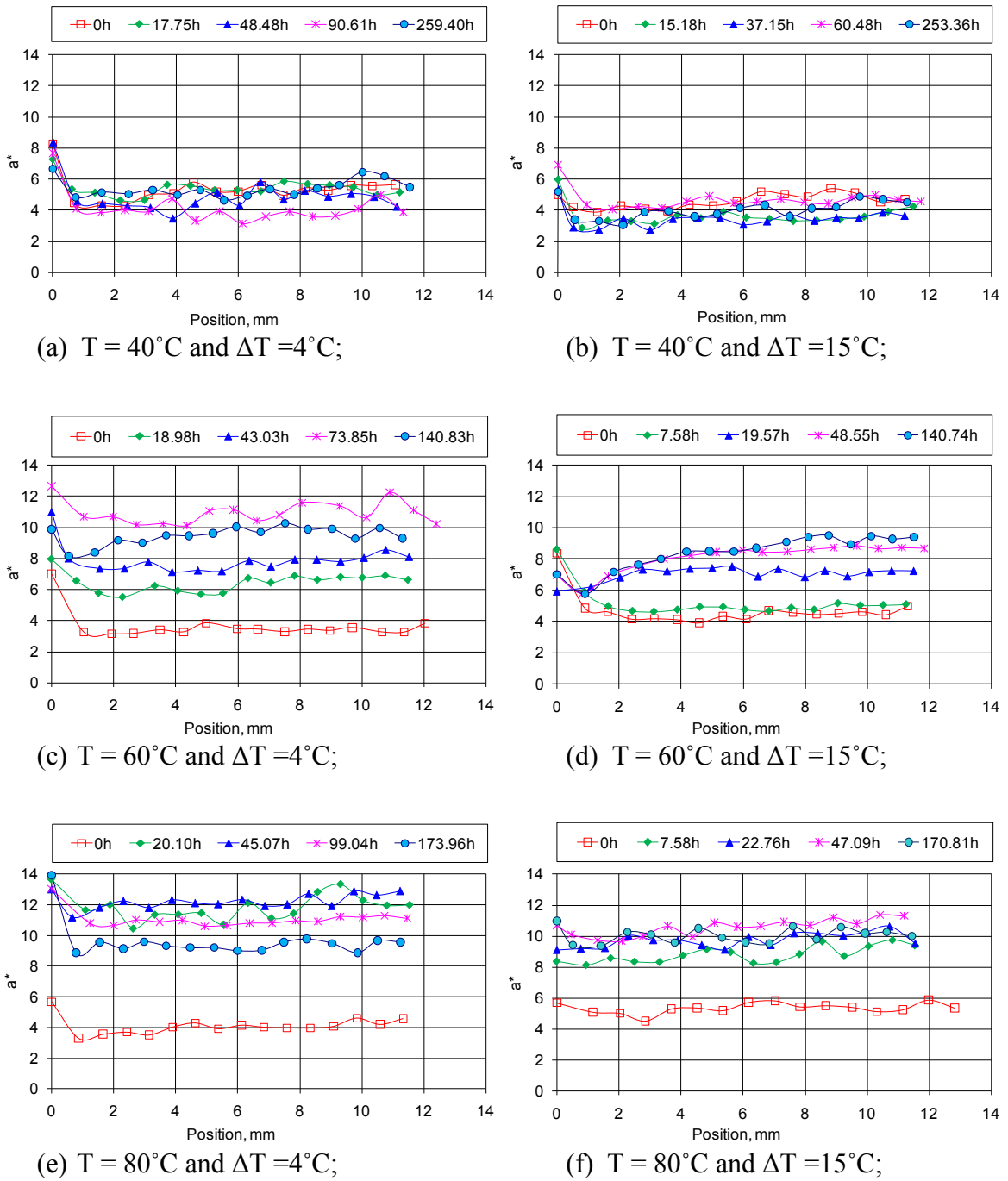
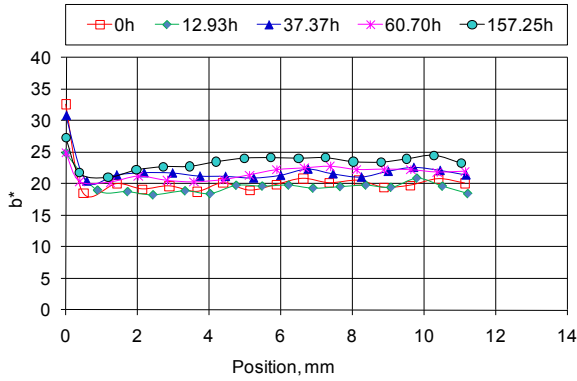
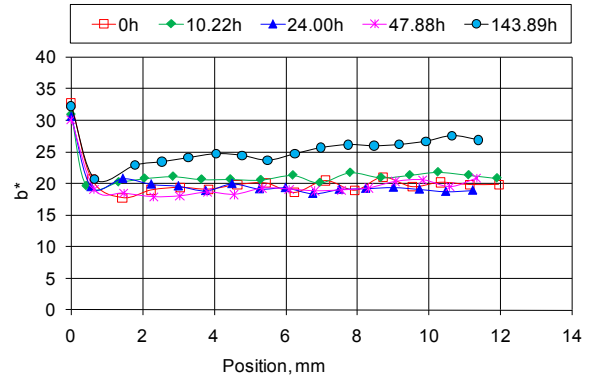


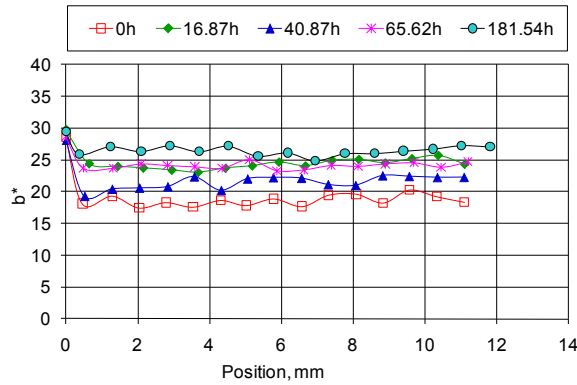
Figure B.2 Wood a^* profiles through the board thickness of sugar maple at five different times during drying at six different drying conditions.



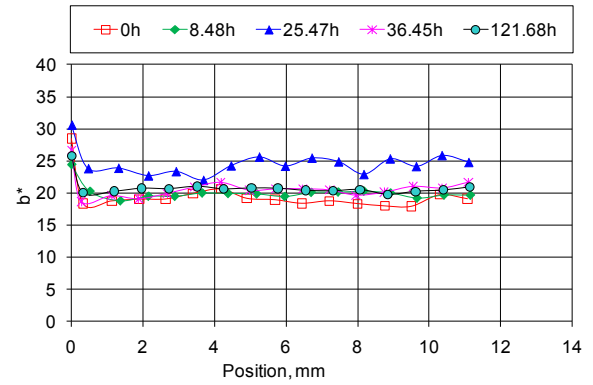
(a) $T = 40^{\circ}\text{C}$ and $\Delta T = 4^{\circ}\text{C}$;



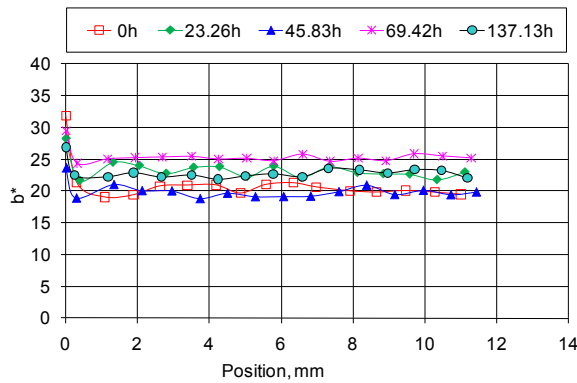
(b) $T = 40^{\circ}\text{C}$ and $\Delta T = 15^{\circ}\text{C}$;



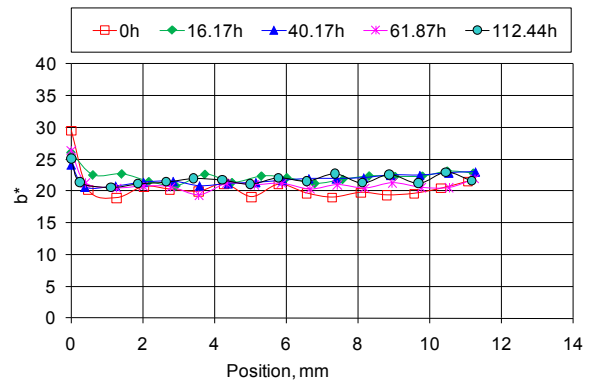
(c) $T = 60^{\circ}\text{C}$ and $\Delta T = 4^{\circ}\text{C}$;



(d) $T = 60^{\circ}\text{C}$ and $\Delta T = 15^{\circ}\text{C}$;

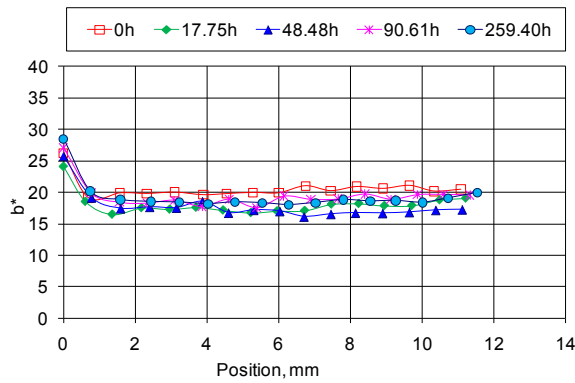


(e) $T = 80^{\circ}\text{C}$ and $\Delta T = 4^{\circ}\text{C}$;

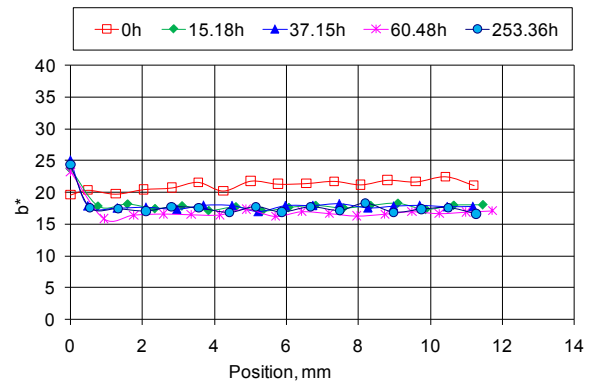


(f) $T = 80^{\circ}\text{C}$ and $\Delta T = 15^{\circ}\text{C}$;

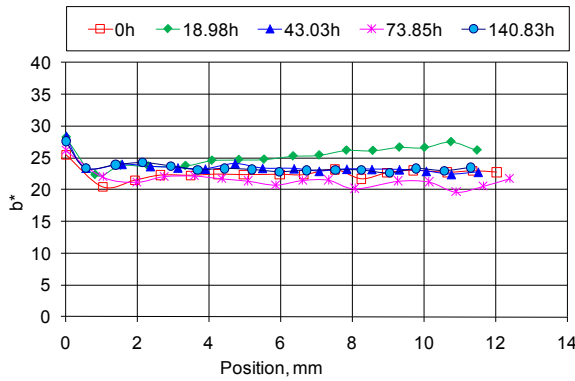
Figure B.3 Wood b^* profiles through the board thickness of paper birch at five different times during drying at six different drying conditions.



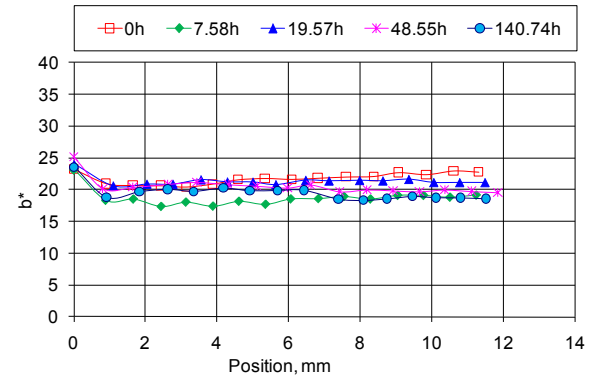
(a) $T = 40^{\circ}\text{C}$ and $\Delta T = 4^{\circ}\text{C}$;



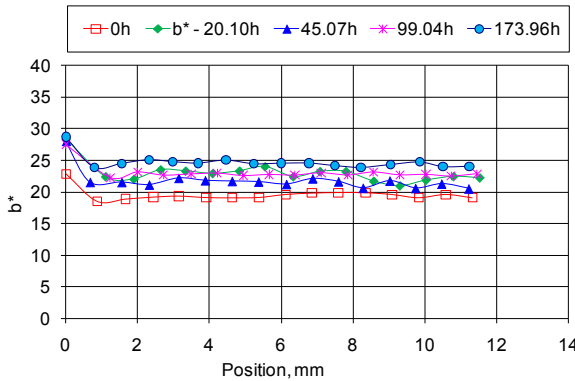
(b) $T = 40^{\circ}\text{C}$ and $\Delta T = 15^{\circ}\text{C}$;



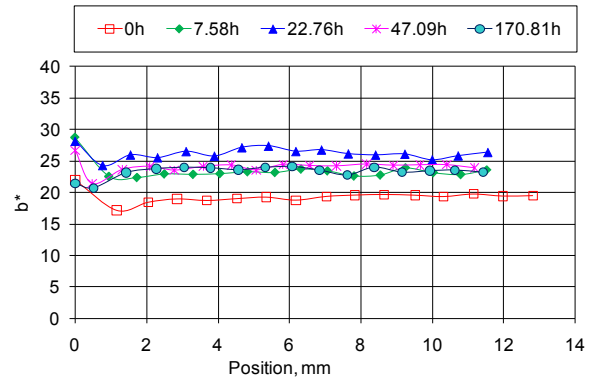
(c) $T = 60^{\circ}\text{C}$ and $\Delta T = 4^{\circ}\text{C}$;



(d) $T = 60^{\circ}\text{C}$ and $\Delta T = 15^{\circ}\text{C}$;



(e) $T = 80^{\circ}\text{C}$ and $\Delta T = 4^{\circ}\text{C}$;



(f) $T = 80^{\circ}\text{C}$ and $\Delta T = 15^{\circ}\text{C}$;

Figure B.4 Wood b^* profiles through the board thickness of sugar maple at five different times during drying at six different drying conditions.

Appendix C: M-L* relationship measured from the color measurement tests

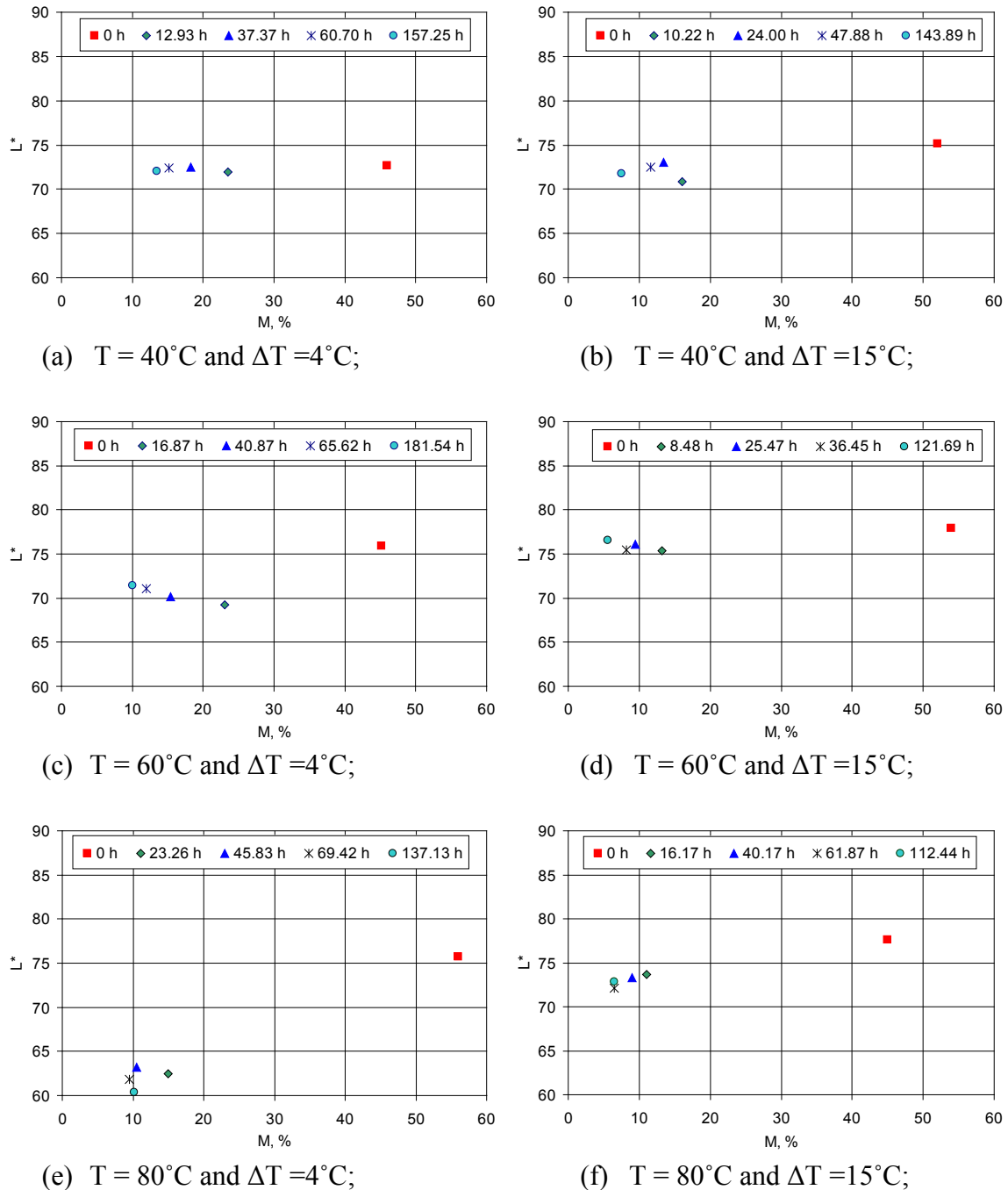
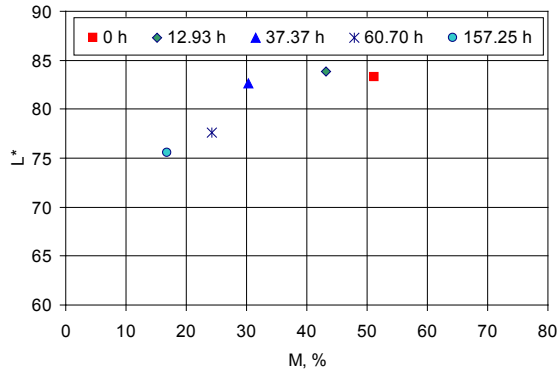
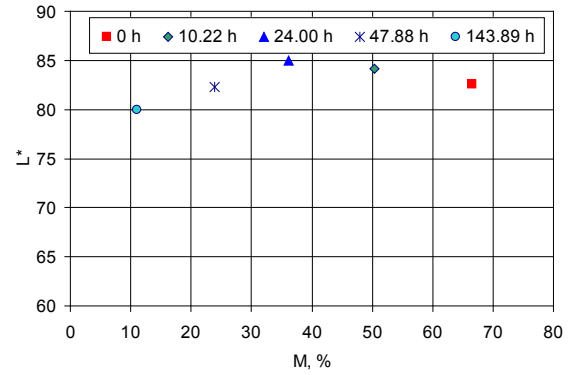


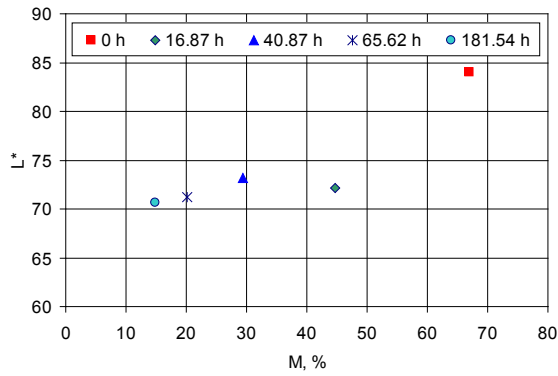
Figure C.1 M-L* relationship on the wood surface of paper birch boards at five different drying times and at six different drying conditions.



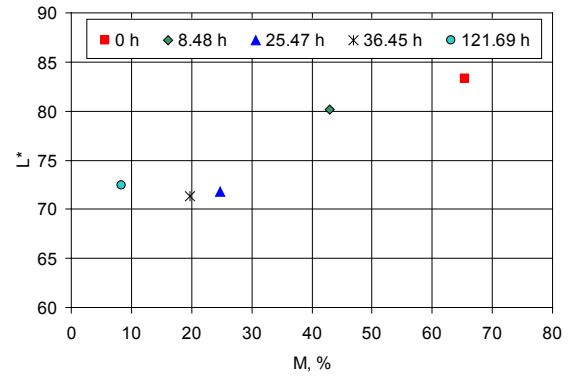
(a) $T = 40^{\circ}\text{C}$ and $\Delta T = 4^{\circ}\text{C}$;



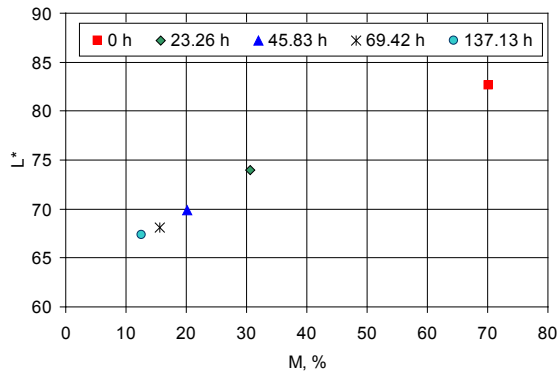
(b) $T = 40^{\circ}\text{C}$ and $\Delta T = 15^{\circ}\text{C}$;



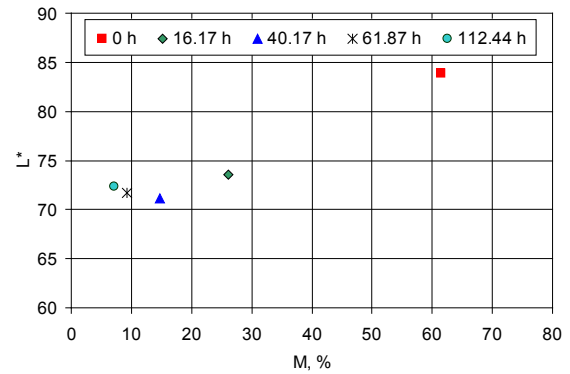
(c) $T = 60^{\circ}\text{C}$ and $\Delta T = 4^{\circ}\text{C}$;



(d) $T = 60^{\circ}\text{C}$ and $\Delta T = 15^{\circ}\text{C}$;

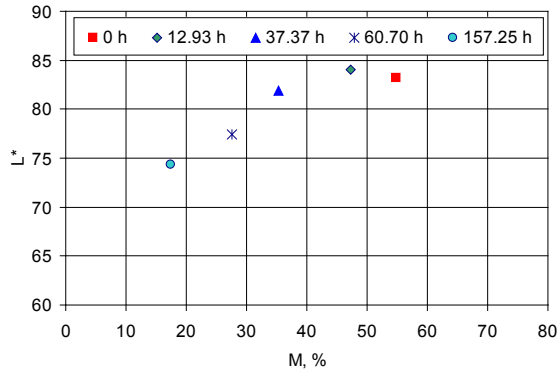


(e) $T = 80^{\circ}\text{C}$ and $\Delta T = 4^{\circ}\text{C}$;

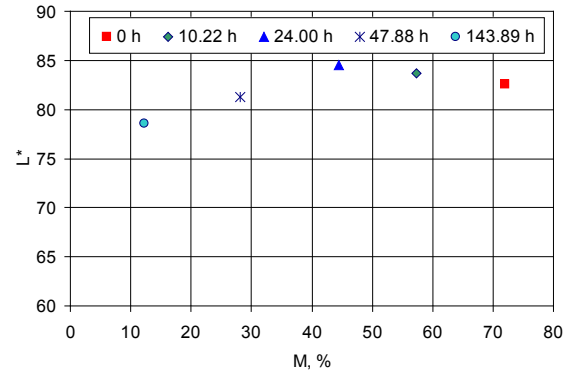


(f) $T = 80^{\circ}\text{C}$ and $\Delta T = 15^{\circ}\text{C}$;

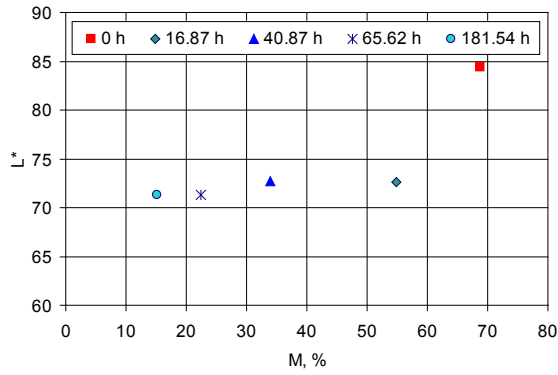
Figure C.2 M-L* relationship at 6 mm below the wood surface of paper birch boards at five different drying times and at six different drying conditions.



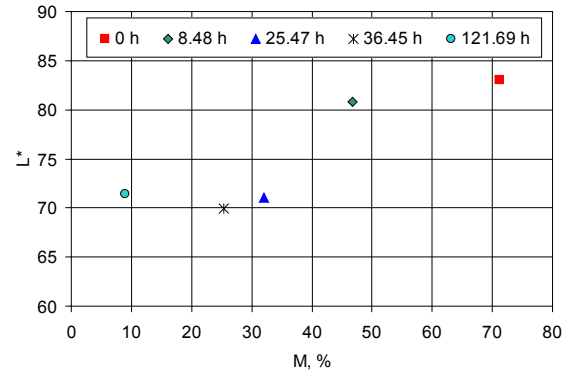
(a) $T = 40^{\circ}\text{C}$ and $\Delta T = 4^{\circ}\text{C}$;



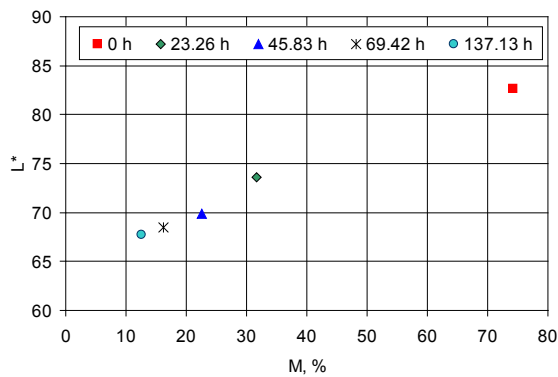
(b) $T = 40^{\circ}\text{C}$ and $\Delta T = 15^{\circ}\text{C}$;



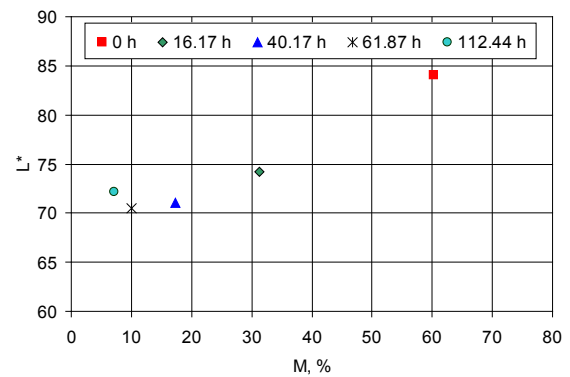
(c) $T = 60^{\circ}\text{C}$ and $\Delta T = 4^{\circ}\text{C}$;



(d) $T = 60^{\circ}\text{C}$ and $\Delta T = 15^{\circ}\text{C}$;

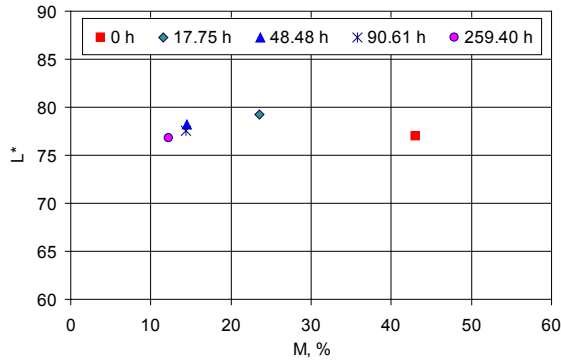


(e) $T = 80^{\circ}\text{C}$ and $\Delta T = 4^{\circ}\text{C}$;

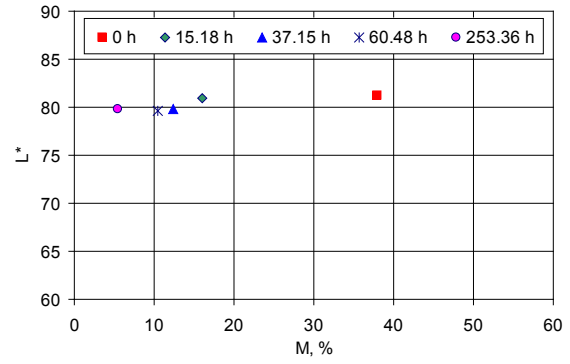


(f) $T = 80^{\circ}\text{C}$ and $\Delta T = 15^{\circ}\text{C}$;

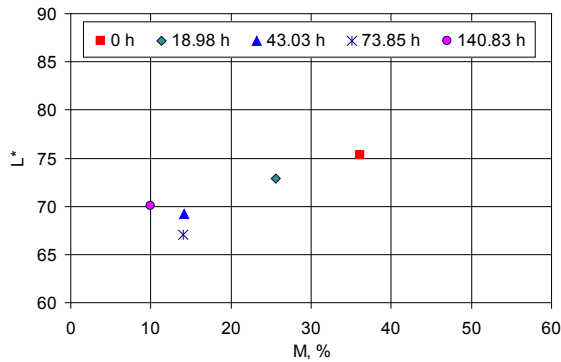
Figure C.3 M-L* relationship at 10 mm below the wood surface of paper birch boards at five different drying times and at six different drying conditions.



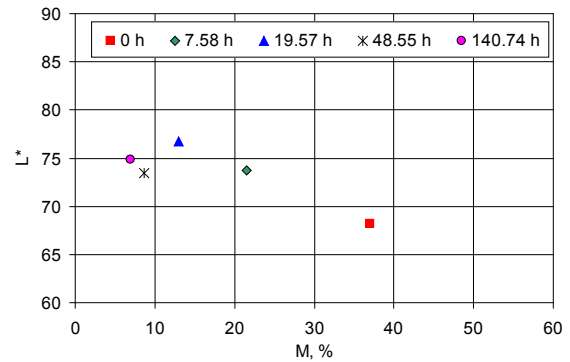
(a) $T = 40^{\circ}\text{C}$ and $\Delta T = 4^{\circ}\text{C}$;



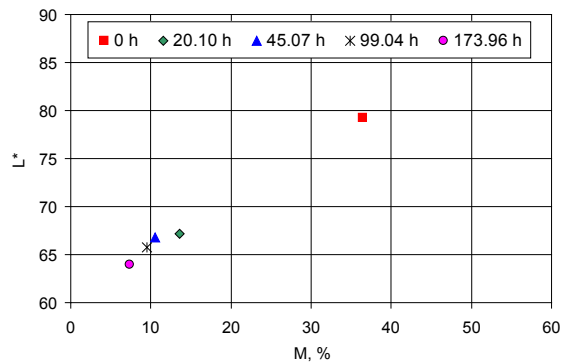
(b) $T = 40^{\circ}\text{C}$ and $\Delta T = 15^{\circ}\text{C}$;



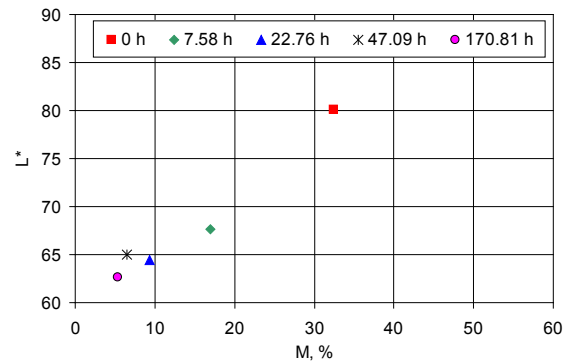
(c) $T = 60^{\circ}\text{C}$ and $\Delta T = 4^{\circ}\text{C}$;



(d) $T = 60^{\circ}\text{C}$ and $\Delta T = 15^{\circ}\text{C}$;

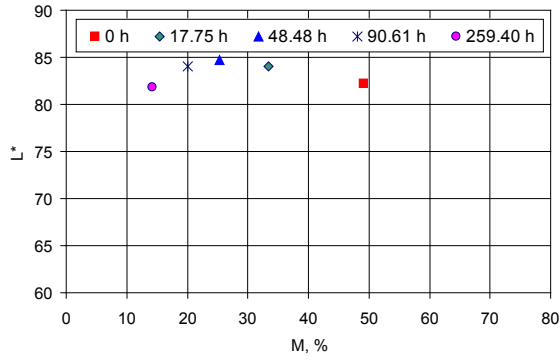


(e) $T = 80^{\circ}\text{C}$ and $\Delta T = 4^{\circ}\text{C}$;

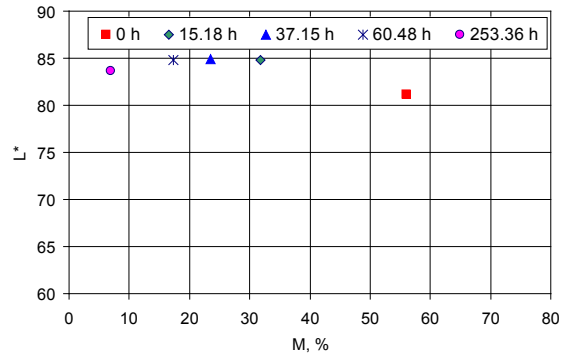


(f) $T = 80^{\circ}\text{C}$ and $\Delta T = 15^{\circ}\text{C}$;

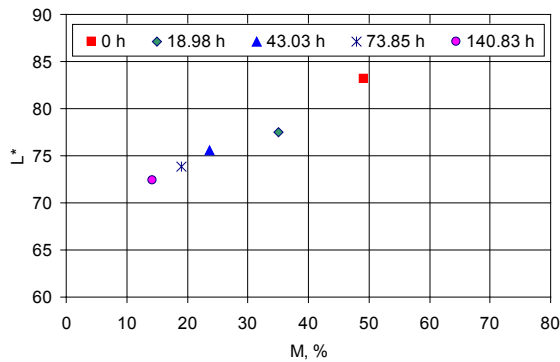
Figure C.4 M-L* relationship on the wood surface of sugar maple boards at five different drying times and at six different drying conditions



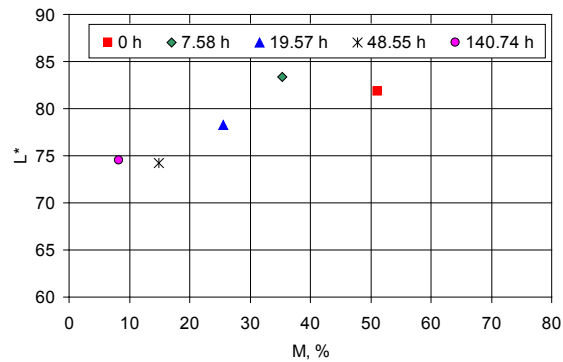
(a) $T = 40^{\circ}\text{C}$ and $\Delta T = 4^{\circ}\text{C}$;



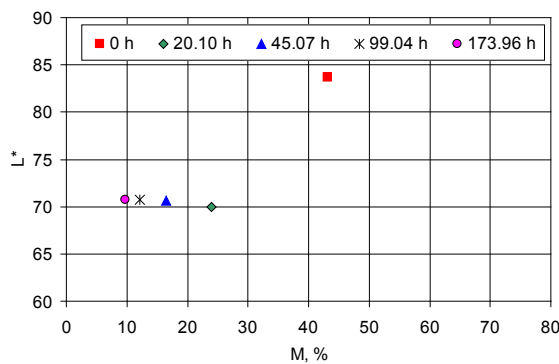
(b) $T = 40^{\circ}\text{C}$ and $\Delta T = 15^{\circ}\text{C}$;



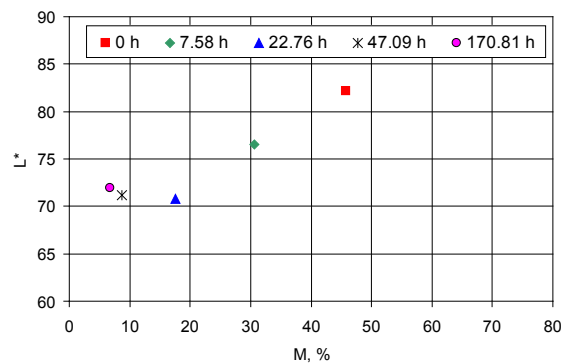
(c) $T = 60^{\circ}\text{C}$ and $\Delta T = 4^{\circ}\text{C}$;



(d) $T = 60^{\circ}\text{C}$ and $\Delta T = 15^{\circ}\text{C}$;

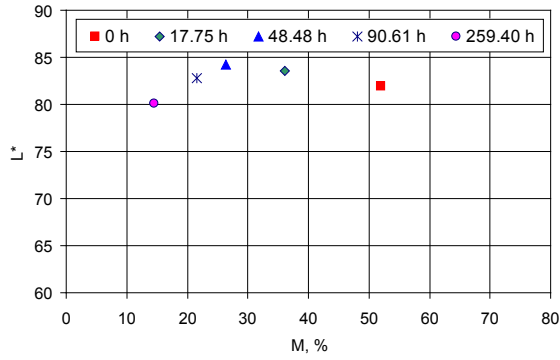


(e) $T = 80^{\circ}\text{C}$ and $\Delta T = 4^{\circ}\text{C}$;

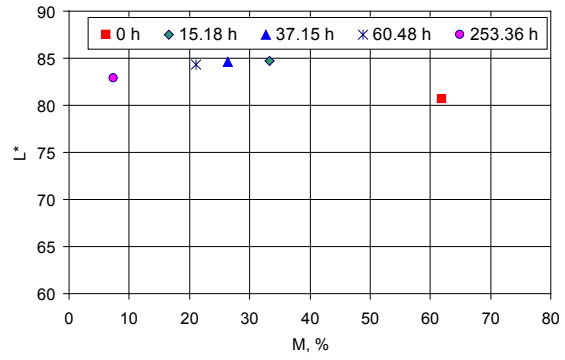


(f) $T = 80^{\circ}\text{C}$ and $\Delta T = 15^{\circ}\text{C}$;

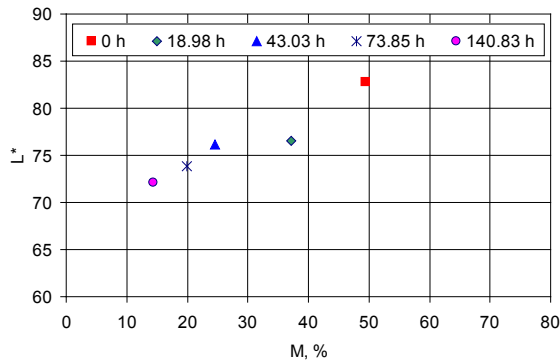
Figure C.5 M-L* relationship at 6 mm below the wood surface of sugar maple board at five different drying times and at six different drying conditions.



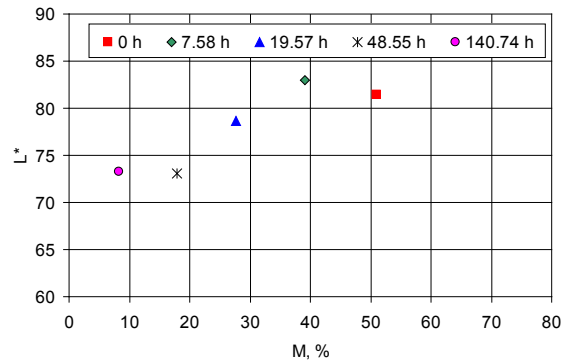
(a) $T = 40^{\circ}\text{C}$ and $\Delta T = 4^{\circ}\text{C}$;



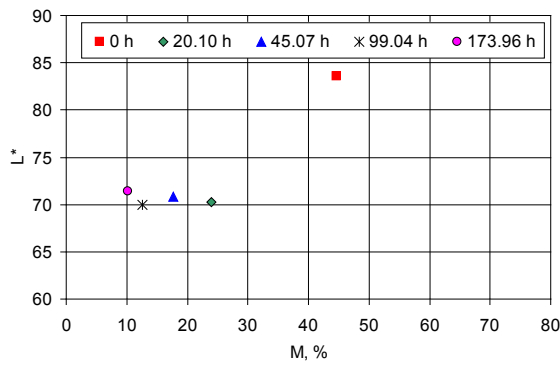
(b) $T = 40^{\circ}\text{C}$ and $\Delta T = 15^{\circ}\text{C}$;



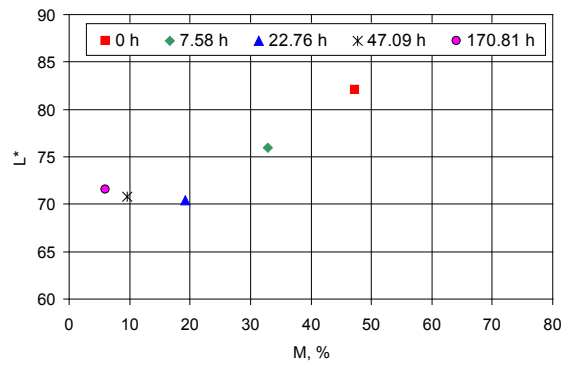
(c) $T = 60^{\circ}\text{C}$ and $\Delta T = 4^{\circ}\text{C}$;



(d) $T = 60^{\circ}\text{C}$ and $\Delta T = 15^{\circ}\text{C}$;



(e) $T = 80^{\circ}\text{C}$ and $\Delta T = 4^{\circ}\text{C}$;



(f) $T = 80^{\circ}\text{C}$ and $\Delta T = 15^{\circ}\text{C}$;

Figure C.6 M-L* relationship at 10 mm below the wood surface of sugar maple boards at five different drying times and at six different drying conditions.

Appendix D: SAS[®] program for the separate wood color model on the wood surface

The SAS[®] program below was written by Gaétan DAIGLE (M.Sc., P.Stat.) of Département de mathématiques et de statistique of Université Laval for analyzing the data obtained on the wood surface. Separate equations were obtained for different drying conditions by running this program.

```
*****
*** Lecture des données ***
*****;

data bouleau;
infile "Liu.Wenhua\Bouleau.txt" dlm="09"x firstobs=3 dsd missover;
input t delta_t no_planche temps epaisseur L a b humidite;
trt = compress(t||"-"||delta_t," ");
essence = "BP";
run;

data erable;
infile "Liu.Wenhua\Erable.txt" dlm="09"x firstobs=3 dsd missover;
input t delta_t no_planche temps epaisseur L a b humidite;
trt = compress(t||"-"||delta_t," ");
essence = "ER";
run;

*****
*** Comparaison à la surface ***
*****;

proc sort data=bouleau; by t delta_t temps no_planche descending
epaisseur;
data bouleau2;
set bouleau;
humidity = lag(humidite);
run;
data bouleau3;
set bouleau2;
if epaisseur=0;
obs = _n_;
run;

proc mixed data=bouleau3;
class t delta_t no_planche ;
model L = t delta_t t*delta_t humidity humidity*t humidity*delta_t
humidity*t*delta_t/outp=stat ddfm=bw;
random intercept humidity / subject=no_planche(t*delta_t) type=un;
lsmeans t delta_t t*delta_t / at humidity=0 pdiff;
```

```

estimate "humidity t=40" humidity 1 humidity*t 1 0 0;
estimate "humidity t=60" humidity 1 humidity*t 0 1 0;
estimate "humidity t=80" humidity 1 humidity*t 0 0 1;
estimate "humidity delta_t=4" humidity 1 humidity*delta_t 1 0;
estimate "humidity delta_t=15" humidity 1 humidity*delta_t 0 1;
estimate "humidity t=40,delta_t=4" humidity 1 humidity*t 1 0 0
humidity*delta_t 1 0 humidity*t*delta_t 1 0 0 0 0 0;
estimate "humidity t=40,delta_t=15" humidity 1 humidity*t 1 0 0
humidity*delta_t 0 1 humidity*t*delta_t 0 1 0 0 0 0;
estimate "humidity t=60,delta_t=4" humidity 1 humidity*t 0 1 0
humidity*delta_t 1 0 humidity*t*delta_t 0 0 1 0 0 0;
estimate "humidity t=60,delta_t=15" humidity 1 humidity*t 0 1 0
humidity*delta_t 0 1 humidity*t*delta_t 0 0 0 1 0 0;
estimate "humidity t=80,delta_t=4" humidity 1 humidity*t 0 0 1
humidity*delta_t 1 0 humidity*t*delta_t 0 0 0 0 1 0;
estimate "humidity t=80,delta_t=15" humidity 1 humidity*t 0 0 1
humidity*delta_t 0 1 humidity*t*delta_t 0 0 0 0 0 1;

contrast "humidity (t=40) vs (t=60)" humidity*t 1 -1 0;
contrast "humidity (t=40) vs (t=80)" humidity*t 1 0 -1;
contrast "humidity (t=60) vs (t=80)" humidity*t 0 1 -1;
contrast "humidity (delta_t=4) vs (delta_t=15)" humidity*delta_t 1
-1;
contrast "humidity (t=40, delta_t=4) vs (t=60, delta_t=4)"
humidity*t 1 -1 0 humidity*t*delta_t 1 0 -1 0 0 0;
contrast "humidity (t=40, delta_t=4) vs (t=80, delta_t=4)"
humidity*t 1 0 -1 humidity*t*delta_t 1 0 0 0 -1 0;
contrast "humidity (t=60, delta_t=4) vs (t=80, delta_t=4)"
humidity*t 0 1 -1 humidity*t*delta_t 0 0 1 0 -1 0;
contrast "humidity (t=40, delta_t=15) vs (t=60, delta_t=15)"
humidity*t 1 -1 0 humidity*t*delta_t 0 1 0 -1 0 0;
contrast "humidity (t=40, delta_t=15) vs (t=80, delta_t=15)"
humidity*t 1 0 -1 humidity*t*delta_t 0 1 0 0 0 -1;
contrast "humidity (t=60, delta_t=15) vs (t=80, delta_t=15)"
humidity*t 0 1 -1 humidity*t*delta_t 0 0 0 1 0 -1;
contrast "humidity (t=40, delta_t=4) vs (t=40, delta_t=15)"
humidity*delta_t 1 -1 humidity*t*delta_t 1 -1 0 0 0 0;
contrast "humidity (t=60, delta_t=4) vs (t=60, delta_t=15)"
humidity*delta_t 1 -1 humidity*t*delta_t 0 0 1 -1 0 0;
contrast "humidity (t=80, delta_t=4) vs (t=80, delta_t=15)"
humidity*delta_t 1 -1 humidity*t*delta_t 0 0 0 0 1 -1;
run;

title; footnote;
proc gplot data=stat;
symbol1 v=dot i=none c=black line=1;
symbol2 v=triangle i=none c=black line=2;
symbol3 v=dot i=none c=red line=1;
symbol4 v=triangle i=none c=red line=2;
symbol5 v=dot i=none c=blue line=1;
symbol6 v=triangle i=none c=blue line=2;
symbol7 v=none i=rl c=black line=1 width=4;
symbol8 v=none i=rl c=black line=2 width=4;
symbol9 v=none i=rl c=red line=1 width=4;
symbol10 v=none i=rl c=red line=2 width=4;
symbol11 v=none i=rl c=blue line=1 width=4;
symbol12 v=none i=rl c=blue line=2 width=4;

```

```

plot L*humidity = trt/vaxis=50 to 90 by 10;
plot2 pred*humidity=trt/vaxis=50 to 90 by 10;
run; quit;

proc sort data=stat; by t delta_t;
proc corr data=stat outp=pearson noprint;
var L; with pred;
by t delta_t;
run;
data pearson;
set pearson;
R2 = L**2;
run;
proc print data=pearson noobs;
where _type_="CORR";
run;

ods select moments TestsForNormality;
proc univariate data=stat plot normal;
id obs;
var resid;
histogram resid / normal;
run;

*****
*** Comparaison à la surface ***
*****;
proc sort data=erable; by t delta_t temps no_planche descending
epaisseur;
data erable2;
set erable;
humidity = lag(humidite);
run;
data erable3;
set erable2;
if epaisseur=0;
obs = _n_;
run;

proc mixed data=erable3;
class t delta_t no_planche ;
model L = t delta_t t*delta_t humidity humidity*t humidity*delta_t
humidity*t*delta_t/outp=stat ddfm=bw;
random intercept humidity / subject=no_planche(t*delta_t) type=un;
lsmeans t delta_t t*delta_t / at humidity=0 pdiff;
estimate "humidity t=40" humidity 1 humidity*t 1 0 0;
estimate "humidity t=60" humidity 1 humidity*t 0 1 0;
estimate "humidity t=80" humidity 1 humidity*t 0 0 1;
estimate "humidity delta_t=4" humidity 1 humidity*delta_t 1 0;
estimate "humidity delta_t=15" humidity 1 humidity*delta_t 0 1;
estimate "humidity t=40,delta_t=4" humidity 1 humidity*t 1 0 0
humidity*delta_t 1 0 humidity*t*delta_t 1 0 0 0 0 0;
estimate "humidity t=40,delta_t=15" humidity 1 humidity*t 1 0 0
humidity*delta_t 0 1 humidity*t*delta_t 0 1 0 0 0 0;

```



```

estimate "humidity t=60,delta_t=4" humidity 1 humidity*t 0 1 0
humidity*delta_t 1 0 humidity*t*delta_t 0 0 1 0 0 0;
estimate "humidity t=60,delta_t=15" humidity 1 humidity*t 0 1 0
humidity*delta_t 0 1 humidity*t*delta_t 0 0 0 1 0 0;
estimate "humidity t=80,delta_t=4" humidity 1 humidity*t 0 0 1
humidity*delta_t 1 0 humidity*t*delta_t 0 0 0 0 1 0;
estimate "humidity t=80,delta_t=15" humidity 1 humidity*t 0 0 1
humidity*delta_t 0 1 humidity*t*delta_t 0 0 0 0 0 1;

contrast "humidity (t=40) vs (t=60)" humidity*t 1 -1 0;
contrast "humidity (t=40) vs (t=80)" humidity*t 1 0 -1;
contrast "humidity (t=60) vs (t=80)" humidity*t 0 1 -1;
contrast "humidity (delta_t=4) vs (delta_t=15)" humidity*delta_t 1
-1;
contrast "humidity (t=40, delta_t=4) vs (t=60, delta_t=4)"
humidity*t 1 -1 0 humidity*t*delta_t 1 0 -1 0 0 0;
contrast "humidity (t=40, delta_t=4) vs (t=80, delta_t=4)"
humidity*t 1 0 -1 humidity*t*delta_t 1 0 0 0 -1 0;
contrast "humidity (t=60, delta_t=4) vs (t=80, delta_t=4)"
humidity*t 0 1 -1 humidity*t*delta_t 0 0 1 0 -1 0;
contrast "humidity (t=40, delta_t=15) vs (t=60, delta_t=15)"
humidity*t 1 -1 0 humidity*t*delta_t 0 1 0 -1 0 0;
contrast "humidity (t=40, delta_t=15) vs (t=80, delta_t=15)"
humidity*t 1 0 -1 humidity*t*delta_t 0 1 0 0 0 -1;
contrast "humidity (t=60, delta_t=15) vs (t=80, delta_t=15)"
humidity*t 0 1 -1 humidity*t*delta_t 0 0 0 1 0 -1;
contrast "humidity (t=40, delta_t=4) vs (t=40, delta_t=15)"
humidity*delta_t 1 -1 humidity*t*delta_t 1 -1 0 0 0 0;
contrast "humidity (t=60, delta_t=4) vs (t=60, delta_t=15)"
humidity*delta_t 1 -1 humidity*t*delta_t 0 0 1 -1 0 0;
contrast "humidity (t=80, delta_t=4) vs (t=80, delta_t=15)"
humidity*delta_t 1 -1 humidity*t*delta_t 0 0 0 0 1 -1;
run;

title; footnote;
proc gplot data=stat;
symbol1 v=dot i=none c=black line=1;
symbol2 v=triangle i=none c=black line=2;
symbol3 v=dot i=none c=red line=1;
symbol4 v=triangle i=none c=red line=2;
symbol5 v=dot i=none c=blue line=1;
symbol6 v=triangle i=none c=blue line=2;
symbol7 v=none i=rl c=black line=1 width=4;
symbol8 v=none i=rl c=black line=2 width=4;
symbol9 v=none i=rl c=red line=1 width=4;
symbol10 v=none i=rl c=red line=2 width=4;
symbol11 v=none i=rl c=blue line=1 width=4;
symbol12 v=none i=rl c=blue line=2 width=4;
plot L*humidity = trt/vaxis=50 to 90 by 10;
plot2 pred*humidity=trt/vaxis=50 to 90 by 10;
run; quit;

proc sort data=stat; by t delta_t;
proc corr data=stat outp=pearson noprint;
var L; with pred;
by t delta_t;
run;

```

```
data pearson;
set pearson;
R2 = L**2;
run;
proc print data=pearson noobs;
where _type_="CORR";
run;

ods select moments TestsForNormality;
proc univariate data=stat plot normal;
id obs;
var resid;
histogram resid / normal;
run;
```

Appendix E: SAS[®] program for the separate wood color model below the wood surface

The SAS[®] program below was written by Gaétan DAIGLE (M.Sc., P.Stat.) of Département de mathématiques et de statistique of Université Laval for analyzing the data obtained below the wood surface. Separate equations were obtained for different drying conditions by running this program.

```
*****
*** Lecture des données ***
*****;

data bouleau;
infile "Liu.Wenhua\Bouleau.txt" dlm="09"x firstobs=3 dsd missover;
input t delta_t no_planche temps epaisseur L a b humidite;
trt = compress(t||"-"||delta_t," ");
essence = "BP";
t_L = (L**1.5);
run;

data erable;
infile "Liu.Wenhua\Erable.txt" dlm="09"x firstobs=3 dsd missover;
input t delta_t no_planche temps epaisseur L a b humidite;
trt = compress(t||"-"||delta_t," ");
essence = "ER";
t_L = (L**1.5);
obs = _n_;
run;

data donnees;
set bouleau erable;
run;

*****
*** Description des données ***
*****;

proc sort data=donnees; by essence;
proc freq data=donnees; by essence;
tables t delta_t no_planche;
run;

proc means data=donnees; by essence;
class t delta_t;
var L humidite;
run;

proc sort data=lecture; by trt;
proc boxplot data=lecture;
plot (L humidite)*trt;
run; quit;
```

```

*****
*** MODÉLISATION pour le bouleau ***
*****;

    *A) Transformation de Box-Cox;
    ods output boxcox=b details=d;
    proc transreg data=bouleau detail;
    model BoxCox(L / lambda=-2 to 3 by 0.1) = class(t delta_t)
identity(epaisseur humidite);
run;
data _null_;
set d;
if description = 'CI Limit'
then call symput('vref', formattedvalue);
if description = 'Lambda Used'
then call symput('lambda', formattedvalue);
run;
data _null_;
set b end=eof;
where ci ne ' ';
if _n_ = 1
then call symput('href1', compress(put(lambda, best12.)));
if ci = '<'
then call symput('href2', compress(put(lambda, best12.)));
if eof
then call symput('href3', compress(put(lambda, best12.)));
run;

* Plot log likelihood, confidence interval;
axis1 label=(angle=90 rotate=0) minor=none;
axis2 minor=none;
proc gplot data=b;
title2 'Log Likelihood';
plot loglike * lambda / vref=&vref href=&href1 &href2 &href3
lvref=2 lhref=2
vaxis=axis1 haxis=axis2 frame cframe=ligr;
footnote "Confidence Interval: &href1 - &href2 - &href3, "
"Lambda = &lambda";
symbol v=none i=spline c=blue width=4;
run; quit;

proc mixed data=bouleau;
class t delta_t no_planche;
model L = t delta_t t*delta_t epaisseur epaisseur*t
epaisseur*delta_t epaisseur*t*delta_t
humidite humidite*t humidite*delta_t humidite*t*delta_t /
ddfm=bw outpm=stat;
random intercept epaisseur humidite/ subject=no_planche(t*delta_t)
type=un;
lsmeans t delta_t t*delta_t/pdiff at (epaisseur humidite)=(0 0);
estimate "Epaisseur t=40" epaisseur 1 epaisseur*t 1 0 0;
estimate "Epaisseur t=60" epaisseur 1 epaisseur*t 0 1 0;
estimate "Epaisseur t=80" epaisseur 1 epaisseur*t 0 0 1;
estimate "Epaisseur delta_t=4" epaisseur 1 epaisseur*delta_t 1 0;
estimate "Epaisseur delta_t=15" epaisseur 1 epaisseur*delta_t 0 1;
estimate "Epaisseur t=40,delta_t=4" epaisseur 1 epaisseur*t 1 0 0
epaisseur*delta_t 1 0 epaisseur*t*delta_t 1 0 0 0 0 0;

```

```

estimate "Epaisseur t=40,delta_t=15" epaisseur 1 epaisseur*t 1 0 0
epaisseur*delta_t 0 1 epaisseur*t*delta_t 0 1 0 0 0 0;
estimate "Epaisseur t=60,delta_t=4" epaisseur 1 epaisseur*t 0 1 0
epaisseur*delta_t 1 0 epaisseur*t*delta_t 0 0 1 0 0 0;
estimate "Epaisseur t=60,delta_t=15" epaisseur 1 epaisseur*t 0 1 0
epaisseur*delta_t 0 1 epaisseur*t*delta_t 0 0 0 1 0 0;
estimate "Epaisseur t=80,delta_t=4" epaisseur 1 epaisseur*t 0 0 1
epaisseur*delta_t 1 0 epaisseur*t*delta_t 0 0 0 0 1 0;
estimate "Epaisseur t=80,delta_t=15" epaisseur 1 epaisseur*t 0 0 1
epaisseur*delta_t 0 1 epaisseur*t*delta_t 0 0 0 0 0 1;

estimate "humidite t=40" humidite 1 humidite*t 1 0 0;
estimate "humidite t=60" humidite 1 humidite*t 0 1 0;
estimate "humidite t=80" humidite 1 humidite*t 0 0 1;
estimate "humidite delta_t=4" humidite 1 humidite*delta_t 1 0;
estimate "humidite delta_t=15" humidite 1 humidite*delta_t 0 1;
estimate "humidite t=40,delta_t=4" humidite 1 humidite*t 1 0 0
humidite*delta_t 1 0 humidite*t*delta_t 1 0 0 0 0 0;
estimate "humidite t=40,delta_t=15" humidite 1 humidite*t 1 0 0
humidite*delta_t 0 1 humidite*t*delta_t 0 1 0 0 0 0;
estimate "humidite t=60,delta_t=4" humidite 1 humidite*t 0 1 0
humidite*delta_t 1 0 humidite*t*delta_t 0 0 1 0 0 0;
estimate "humidite t=60,delta_t=15" humidite 1 humidite*t 0 1 0
humidite*delta_t 0 1 humidite*t*delta_t 0 0 0 1 0 0;
estimate "humidite t=80,delta_t=4" humidite 1 humidite*t 0 0 1
humidite*delta_t 1 0 humidite*t*delta_t 0 0 0 0 1 0;
estimate "humidite t=80,delta_t=15" humidite 1 humidite*t 0 0 1
humidite*delta_t 0 1 humidite*t*delta_t 0 0 0 0 0 1;

contrast "Epaisseur (t=40) vs (t=60)" Epaisseur*t 1 -1 0;
contrast "Epaisseur (t=40) vs (t=80)" Epaisseur*t 1 0 -1;
contrast "Epaisseur (t=60) vs (t=80)" Epaisseur*t 0 1 -1;
contrast "Epaisseur (delta_t=4) vs (delta_t=15)" Epaisseur*delta_t
1 -1;
contrast "Epaisseur (t=40, delta_t=4) vs (t=60, delta_t=4)"
epaisseur*t 1 -1 0 epaisseur*t*delta_t 1 0 -1 0 0 0;
contrast "Epaisseur (t=40, delta_t=4) vs (t=80, delta_t=4)"
epaisseur*t 1 0 -1 epaisseur*t*delta_t 1 0 0 0 -1 0;
contrast "Epaisseur (t=60, delta_t=4) vs (t=80, delta_t=4)"
epaisseur*t 0 1 -1 epaisseur*t*delta_t 0 0 1 0 -1 0;
contrast "Epaisseur (t=40, delta_t=15) vs (t=60, delta_t=15)"
epaisseur*t 1 -1 0 epaisseur*t*delta_t 0 1 0 -1 0 0;
contrast "Epaisseur (t=40, delta_t=15) vs (t=80, delta_t=15)"
epaisseur*t 1 0 -1 epaisseur*t*delta_t 0 1 0 0 0 -1;
contrast "Epaisseur (t=60, delta_t=15) vs (t=80, delta_t=15)"
epaisseur*t 0 1 -1 epaisseur*t*delta_t 0 0 0 1 0 -1;
contrast "Epaisseur (t=40, delta_t=4) vs (t=40, delta_t=15)"
epaisseur*delta_t 1 -1 epaisseur*t*delta_t 1 -1 0 0 0 0;
contrast "Epaisseur (t=60, delta_t=4) vs (t=60, delta_t=15)"
epaisseur*delta_t 1 -1 epaisseur*t*delta_t 0 0 1 -1 0 0;
contrast "Epaisseur (t=80, delta_t=4) vs (t=80, delta_t=15)"
epaisseur*delta_t 1 -1 epaisseur*t*delta_t 0 0 0 0 1 -1;

contrast "humidite (t=40) vs (t=60)" humidite*t 1 -1 0;
contrast "humidite (t=40) vs (t=80)" humidite*t 1 0 -1;
contrast "humidite (t=60) vs (t=80)" humidite*t 0 1 -1;

```

```

contrast "humidite (delta_t=4) vs (delta_t=15)" humidite*delta_t 1
-1;
contrast "humidite (t=40, delta_t=4) vs (t=60, delta_t=4)"
humidite*t 1 -1 0 humidite*t*delta_t 1 0 -1 0 0 0;
contrast "humidite (t=40, delta_t=4) vs (t=80, delta_t=4)"
humidite*t 1 0 -1 humidite*t*delta_t 1 0 0 0 -1 0;
contrast "humidite (t=60, delta_t=4) vs (t=80, delta_t=4)"
humidite*t 0 1 -1 humidite*t*delta_t 0 0 1 0 -1 0;
contrast "humidite (t=40, delta_t=15) vs (t=60, delta_t=15)"
humidite*t 1 -1 0 humidite*t*delta_t 0 1 0 -1 0 0;
contrast "humidite (t=40, delta_t=15) vs (t=80, delta_t=15)"
humidite*t 1 0 -1 humidite*t*delta_t 0 1 0 0 0 -1;
contrast "humidite (t=60, delta_t=15) vs (t=80, delta_t=15)"
humidite*t 0 1 -1 humidite*t*delta_t 0 0 0 1 0 -1;
contrast "humidite (t=40, delta_t=4) vs (t=40, delta_t=15)"
humidite*delta_t 1 -1 humidite*t*delta_t 1 -1 0 0 0 0;
contrast "humidite (t=60, delta_t=4) vs (t=60, delta_t=15)"
humidite*delta_t 1 -1 humidite*t*delta_t 0 0 1 -1 0 0;
contrast "humidite (t=80, delta_t=4) vs (t=80, delta_t=15)"
humidite*delta_t 1 -1 humidite*t*delta_t 0 0 0 0 1 -1;
run;

```

```

title; footnote;
proc gplot data=stat;
symbol1 v=dot i=None c=black line=1;
symbol2 v=triangle i=None c=black line=2;
symbol3 v=dot i=None c=red line=1;
symbol4 v=triangle i=None c=red line=2;
symbol5 v=dot i=None c=blue line=1;
symbol6 v=triangle i=None c=blue line=2;
symbol7 v=None i=rl c=black line=1 width=4;
symbol8 v=None i=rl c=black line=2 width=4;
symbol9 v=None i=rl c=red line=1 width=4;
symbol10 v=None i=rl c=red line=2 width=4;
symbol11 v=None i=rl c=blue line=1 width=4;
symbol12 v=None i=rl c=blue line=2 width=4;
plot L*humidite = trt/vaxis=50 to 90 by 10;
plot2 pred*humidite=trt/vaxis=50 to 90 by 10;
run; quit;

```

```

title; footnote;
proc gplot data=stat;
symbol1 v=dot i=None c=black line=1;
symbol2 v=triangle i=None c=black line=2;
symbol3 v=dot i=None c=red line=1;
symbol4 v=triangle i=None c=red line=2;
symbol5 v=dot i=None c=blue line=1;
symbol6 v=triangle i=None c=blue line=2;
symbol7 v=None i=rl c=black line=1 width=4;
symbol8 v=None i=rl c=black line=2 width=4;
symbol9 v=None i=rl c=red line=1 width=4;
symbol10 v=None i=rl c=red line=2 width=4;
symbol11 v=None i=rl c=blue line=1 width=4;
symbol12 v=None i=rl c=blue line=2 width=4;
plot L*epaisseur = trt/vaxis=50 to 90 by 10;
plot2 pred*epaisseur=trt/vaxis=50 to 90 by 10;
run; quit;

```

```
proc sort data=stat; by t delta_t;
proc corr data=stat outp=pearson noprint;
var L; with pred;
by t delta_t;
run;
data pearson;
set pearson;
R2 = L**2;
run;
proc print data=pearson noobs;
where _type_="CORR";
run;

goptions reset=all reset=global;
ods select Moments TestsForNormality;
proc univariate data=stat plot normal;
symbol1 width=4 c=black ;
symbol2 c=red line=2 width=4;
var resid;
histogram resid/normal;
run;

proc gplot data=stat;
symbol1 v=dot;
plot resid*pred/vref=0 lvref=2;
run; quit;

*****
*** MODÉLISATION pour l'ERABLE ***
*****;

    *A) Transformation de Box-Cox;
    ods output boxcox=b details=d;
    proc transreg data=erable detail;
    model BoxCox(L / lambda=-2 to 3 by 0.1) = class(t delta_t)
identity(epaisseur humidite);
    run;
data _null_;
    set d;
    if description = 'CI Limit'
        then call symput('vref', formattedvalue);
    if description = 'Lambda Used'
        then call symput('lambda', formattedvalue);
    run;
data _null_;
    set b end=eof;
    where ci ne ' ';
    if _n_ = 1
        then call symput('href1', compress(put(lambda, best12.)));
    if ci = '<'
        then call symput('href2', compress(put(lambda, best12.)));
    if eof
        then call symput('href3', compress(put(lambda, best12.)));
    run;

* Plot log likelihood, confidence interval;
```

```

axis1 label=(angle=90 rotate=0) minor=none;
axis2 minor=none;
proc gplot data=b;
  title2 'Log Likelihood';
  plot loglike * lambda / vref=&vref href=&href1 &href2 &href3
  lvref=2 lhref=2
                                vaxis=axis1 haxis=axis2 frame cframe=ligr;
  footnote "Confidence Interval: &href1 - &href2 - &href3, "
    "Lambda = &lambda";
  symbol v=none i=spline c=blue width=4;
run; quit;

title; footnote;
proc mixed data=erable;
  class t delta_t no_planche;
  model L = t delta_t t*delta_t epaisseur epaisseur*t
epaisseur*delta_t epaisseur*t*delta_t
    humidite humidite*t humidite*delta_t humidite*t*delta_t /
  ddfm=bw outpm=stat;
  random intercept epaisseur humidite/ subject=no_planche(t*delta_t)
  type=un;
  lsmeans t delta_t t*delta_t/pdiff at (epaisseur humidite)=(0 0);
  estimate "Epaisseur t=40" epaisseur 1 epaisseur*t 1 0 0;
  estimate "Epaisseur t=60" epaisseur 1 epaisseur*t 0 1 0;
  estimate "Epaisseur t=80" epaisseur 1 epaisseur*t 0 0 1;
  estimate "Epaisseur delta_t=4" epaisseur 1 epaisseur*delta_t 1 0;
  estimate "Epaisseur delta_t=15" epaisseur 1 epaisseur*delta_t 0 1;
  estimate "Epaisseur t=40,delta_t=4" epaisseur 1 epaisseur*t 1 0 0
epaisseur*delta_t 1 0 epaisseur*t*delta_t 1 0 0 0 0 0;
  estimate "Epaisseur t=40,delta_t=15" epaisseur 1 epaisseur*t 1 0 0
epaisseur*delta_t 0 1 epaisseur*t*delta_t 0 1 0 0 0 0;
  estimate "Epaisseur t=60,delta_t=4" epaisseur 1 epaisseur*t 0 1 0
epaisseur*delta_t 1 0 epaisseur*t*delta_t 0 0 1 0 0 0;
  estimate "Epaisseur t=60,delta_t=15" epaisseur 1 epaisseur*t 0 1 0
epaisseur*delta_t 0 1 epaisseur*t*delta_t 0 0 0 1 0 0;
  estimate "Epaisseur t=80,delta_t=4" epaisseur 1 epaisseur*t 0 0 1
epaisseur*delta_t 1 0 epaisseur*t*delta_t 0 0 0 0 1 0;
  estimate "Epaisseur t=80,delta_t=15" epaisseur 1 epaisseur*t 0 0 1
epaisseur*delta_t 0 1 epaisseur*t*delta_t 0 0 0 0 0 1;

  estimate "humidite t=40" humidite 1 humidite*t 1 0 0;
  estimate "humidite t=60" humidite 1 humidite*t 0 1 0;
  estimate "humidite t=80" humidite 1 humidite*t 0 0 1;
  estimate "humidite delta_t=4" humidite 1 humidite*delta_t 1 0;
  estimate "humidite delta_t=15" humidite 1 humidite*delta_t 0 1;
  estimate "humidite t=40,delta_t=4" humidite 1 humidite*t 1 0 0
humidite*delta_t 1 0 humidite*t*delta_t 1 0 0 0 0 0;
  estimate "humidite t=40,delta_t=15" humidite 1 humidite*t 1 0 0
humidite*delta_t 0 1 humidite*t*delta_t 0 1 0 0 0 0;
  estimate "humidite t=60,delta_t=4" humidite 1 humidite*t 0 1 0
humidite*delta_t 1 0 humidite*t*delta_t 0 0 1 0 0 0;
  estimate "humidite t=60,delta_t=15" humidite 1 humidite*t 0 1 0
humidite*delta_t 0 1 humidite*t*delta_t 0 0 0 1 0 0;
  estimate "humidite t=80,delta_t=4" humidite 1 humidite*t 0 0 1
humidite*delta_t 1 0 humidite*t*delta_t 0 0 0 0 1 0;
  estimate "humidite t=80,delta_t=15" humidite 1 humidite*t 0 0 1
humidite*delta_t 0 1 humidite*t*delta_t 0 0 0 0 0 1;

```



```

contrast "Epaisseur (t=40) vs (t=60)" Epaisseur*t 1 -1 0;
contrast "Epaisseur (t=40) vs (t=80)" Epaisseur*t 1 0 -1;
contrast "Epaisseur (t=60) vs (t=80)" Epaisseur*t 0 1 -1;
contrast "Epaisseur (delta_t=4) vs (delta_t=15)" Epaisseur*delta_t
1 -1;
contrast "Epaisseur (t=40, delta_t=4) vs (t=60, delta_t=4)"
epaisseur*t 1 -1 0 epaisseur*t*delta_t 1 0 -1 0 0 0;
contrast "Epaisseur (t=40, delta_t=4) vs (t=80, delta_t=4)"
epaisseur*t 1 0 -1 epaisseur*t*delta_t 1 0 0 0 -1 0;
contrast "Epaisseur (t=60, delta_t=4) vs (t=80, delta_t=4)"
epaisseur*t 0 1 -1 epaisseur*t*delta_t 0 0 1 0 -1 0;
contrast "Epaisseur (t=40, delta_t=15) vs (t=60, delta_t=15)"
epaisseur*t 1 -1 0 epaisseur*t*delta_t 0 1 0 -1 0 0;
contrast "Epaisseur (t=40, delta_t=15) vs (t=80, delta_t=15)"
epaisseur*t 1 0 -1 epaisseur*t*delta_t 0 1 0 0 0 -1;
contrast "Epaisseur (t=60, delta_t=15) vs (t=80, delta_t=15)"
epaisseur*t 0 1 -1 epaisseur*t*delta_t 0 0 0 1 0 -1;
contrast "Epaisseur (t=40, delta_t=4) vs (t=40, delta_t=15)"
epaisseur*delta_t 1 -1 epaisseur*t*delta_t 1 -1 0 0 0 0;
contrast "Epaisseur (t=60, delta_t=4) vs (t=60, delta_t=15)"
epaisseur*delta_t 1 -1 epaisseur*t*delta_t 0 0 1 -1 0 0;
contrast "Epaisseur (t=80, delta_t=4) vs (t=80, delta_t=15)"
epaisseur*delta_t 1 -1 epaisseur*t*delta_t 0 0 0 0 1 -1;

contrast "humidite (t=40) vs (t=60)" humidite*t 1 -1 0;
contrast "humidite (t=40) vs (t=80)" humidite*t 1 0 -1;
contrast "humidite (t=60) vs (t=80)" humidite*t 0 1 -1;
contrast "humidite (delta_t=4) vs (delta_t=15)" humidite*delta_t 1
-1;
contrast "humidite (t=40, delta_t=4) vs (t=60, delta_t=4)"
humidite*t 1 -1 0 humidite*t*delta_t 1 0 -1 0 0 0;
contrast "humidite (t=40, delta_t=4) vs (t=80, delta_t=4)"
humidite*t 1 0 -1 humidite*t*delta_t 1 0 0 0 -1 0;
contrast "humidite (t=60, delta_t=4) vs (t=80, delta_t=4)"
humidite*t 0 1 -1 humidite*t*delta_t 0 0 1 0 -1 0;
contrast "humidite (t=40, delta_t=15) vs (t=60, delta_t=15)"
humidite*t 1 -1 0 humidite*t*delta_t 0 1 0 -1 0 0;
contrast "humidite (t=40, delta_t=15) vs (t=80, delta_t=15)"
humidite*t 1 0 -1 humidite*t*delta_t 0 1 0 0 0 -1;
contrast "humidite (t=60, delta_t=15) vs (t=80, delta_t=15)"
humidite*t 0 1 -1 humidite*t*delta_t 0 0 0 1 0 -1;
contrast "humidite (t=40, delta_t=4) vs (t=40, delta_t=15)"
humidite*delta_t 1 -1 humidite*t*delta_t 1 -1 0 0 0 0;
contrast "humidite (t=60, delta_t=4) vs (t=60, delta_t=15)"
humidite*delta_t 1 -1 humidite*t*delta_t 0 0 1 -1 0 0;
contrast "humidite (t=80, delta_t=4) vs (t=80, delta_t=15)"
humidite*delta_t 1 -1 humidite*t*delta_t 0 0 0 0 1 -1;
run;

title; footnote;
proc gplot data=stat;
symbol1 v=dot i=none c=black line=1;
symbol2 v=triangle i=none c=black line=2;
symbol3 v=dot i=none c=red line=1;
symbol4 v=triangle i=none c=red line=2;
symbol5 v=dot i=none c=blue line=1;

```

```
symbol6 v=triangle i=none c=blue line=2;
symbol7 v=none i=r1 c=black line=1 width=4;
symbol8 v=none i=r1 c=black line=2 width=4;
symbol9 v=none i=r1 c=red line=1 width=4;
symbol10 v=none i=r1 c=red line=2 width=4;
symbol11 v=none i=r1 c=blue line=1 width=4;
symbol12 v=none i=r1 c=blue line=2 width=4;
plot L*humidite = trt/vaxis=40 to 90 by 10;
plot2 pred*humidite=trt/vaxis=40 to 90 by 10;
run; quit;

title; footnote;
proc gplot data=stat;
symbol1 v=dot i=none c=black line=1;
symbol2 v=triangle i=none c=black line=2;
symbol3 v=dot i=none c=red line=1;
symbol4 v=triangle i=none c=red line=2;
symbol5 v=dot i=none c=blue line=1;
symbol6 v=triangle i=none c=blue line=2;
symbol7 v=none i=r1 c=black line=1 width=4;
symbol8 v=none i=r1 c=black line=2 width=4;
symbol9 v=none i=r1 c=red line=1 width=4;
symbol10 v=none i=r1 c=red line=2 width=4;
symbol11 v=none i=r1 c=blue line=1 width=4;
symbol12 v=none i=r1 c=blue line=2 width=4;
plot L*epaisseur = trt/vaxis=50 to 90 by 10;
plot2 pred*epaisseur=trt/vaxis=50 to 90 by 10;
run; quit;

proc sort data=stat; by t delta_t;
proc corr data=stat outp=pearson noprint;
var L; with pred;
by t delta_t;
run;
data pearson;
set pearson;
R2 = L**2;
run;
proc print data=pearson noobs;
where _type_="CORR";
run;

goptions reset=all reset=global;
ods select Moments TestsForNormality;
proc univariate data=stat plot normal;
id obs;
symbol1 width=4 c=black ;
symbol2 c=red line=2 width=4;
var resid;
histogram resid/normal;
run;

proc gplot data=stat;
symbol1 v=dot;
plot resid*pred/vref=0 lvref=2;
run; quit;
```

Appendix F: Graphical technique for the 3T global wood color models

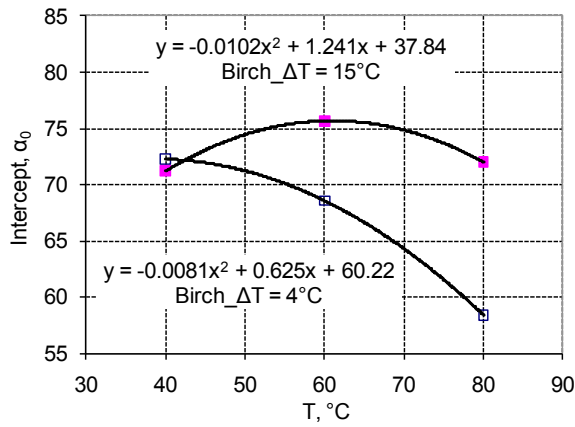
Table F.1 Separate regression models of wood lightness for the six drying conditions of paper birch and sugar maple.

Wood species	T, (°C)	ΔT, (°C)	L^* on the wood surface	L^* below the wood surface ($e \geq 0.24\text{mm}$)
Paper birch	40	4	$L^* = 73.6 - 0.0774M$, $R^2 = 93.4\%$	$L^* = 75.0 + 0.268M - 0.363e$, $R^2 = 34.8\%$
		15	$L^* = 71.2 + 0.0728M$, $R^2 = 53.1\%$	$L^* = 81.4 + 0.0527M - 0.135e$, $R^2 = 23.2\%$
	60	4	$L^* = 68.6 + 0.132M$, $R^2 = 74.7\%$	$L^* = 67.1 + 0.241M - 0.181e$, $R^2 = 63.7\%$
		15	$L^* = 76.1 + 0.0350M$, $R^2 = 66.9\%$	$L^* = 73.7 + 0.203M - 0.644e$, $R^2 = 73.3\%$
	80	4	$L^* = 58.4 + 0.306M$, $R^2 = 96.1\%$	$L^* = 64.7 + 0.279M - 0.0533e$, $R^2 = 90.9\%$
		15	$L^* = 71.9 + 0.134M$, $R^2 = 91.6\%$	$L^* = 71.8 + 0.239M - 0.370e$, $R^2 = 80.3\%$
Sugar maple	40	4	$L^* = 78.1 - 0.0141M$, $R^2 = 12.6\%$	$L^* = 83.1 + 0.0106M - 0.0567e$, $R^2 = 1.0\%$
		15	$L^* = 79.4 + 0.0644M$, $R^2 = 90.9\%$	$L^* = 85.4 - 0.0601M - 0.00236e$, $R^2 = 20.2\%$
	60	4	$L^* = 66.4 + 0.230M$, $R^2 = 74.3\%$	$L^* = 69.5 + 0.305M - 0.216e$, $R^2 = 90.0\%$
		15	$L^* = 77.0 - 0.212M$, $R^2 = 65.3\%$	$L^* = 76.2 + 0.210M - 0.464e$, $R^2 = 66.6\%$
	80	4	$L^* = 61.1 + 0.490M$, $R^2 = 97.3\%$	$L^* = 66.4 + 0.405M - 0.218e$, $R^2 = 73.5\%$
		15	$L^* = 58.8 + 0.626M$, $R^2 = 92.6\%$	$L^* = 70.2 + 0.287M - 0.281e$, $R^2 = 82.8\%$

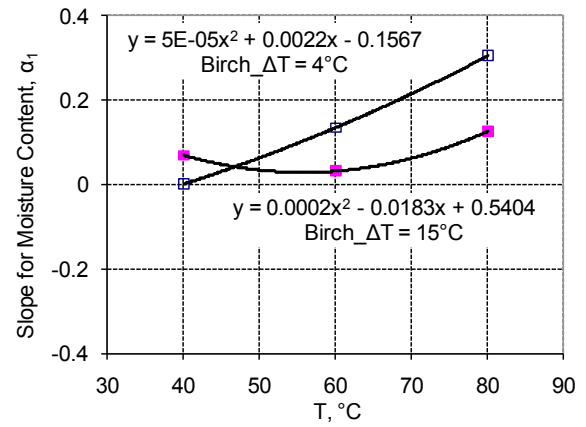
Note: M = wood moisture content, %; e = depth below the wood surface through the board thickness, mm. The general patterns of the separate regression models are expressed below for the wood surface and the wood interior, respectively:

$$L^* = \alpha_0 + \alpha_1 M$$

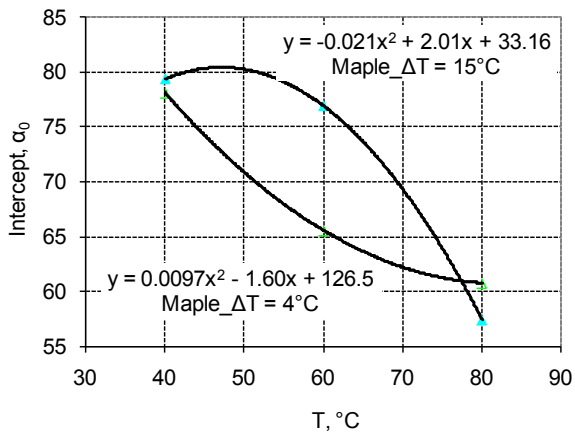
$$L^* = \beta_0 + \beta_1 M + \beta_2 e$$



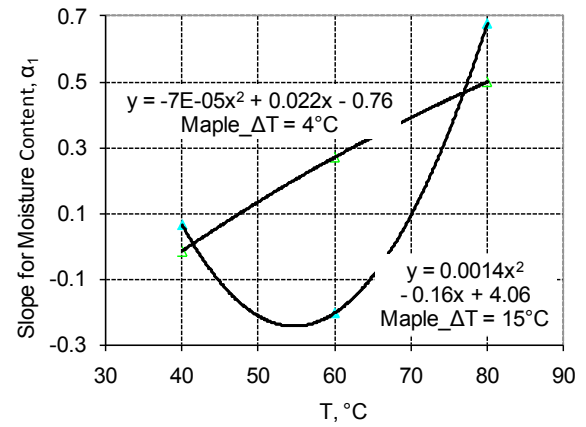
(a) α_0 vs. T , paper birch sapwood



(b) α_1 vs. T , paper birch sapwood

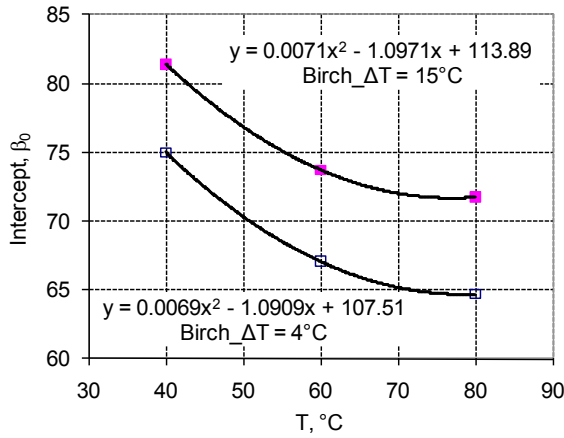


(c) α_0 vs. T , sugar maple sapwood

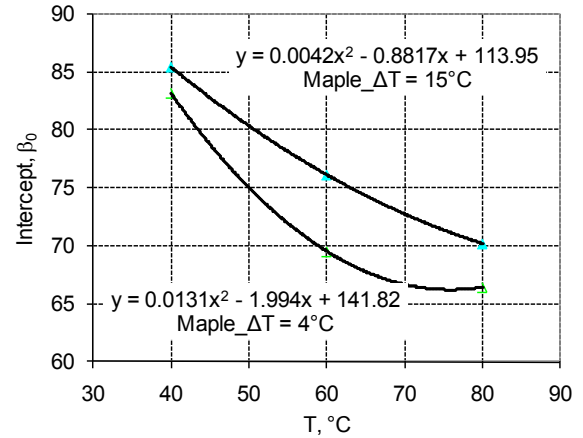


(d) α_1 vs. T , sugar maple sapwood

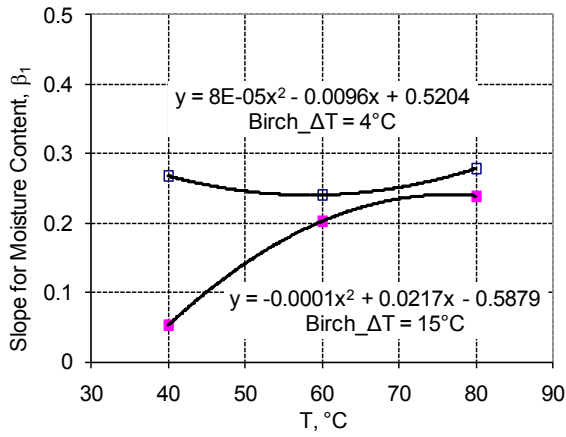
Figure F.1 Relationships between the regression coefficients in all separate equations for L^* values on the wood surface and the dry-bulb temperatures



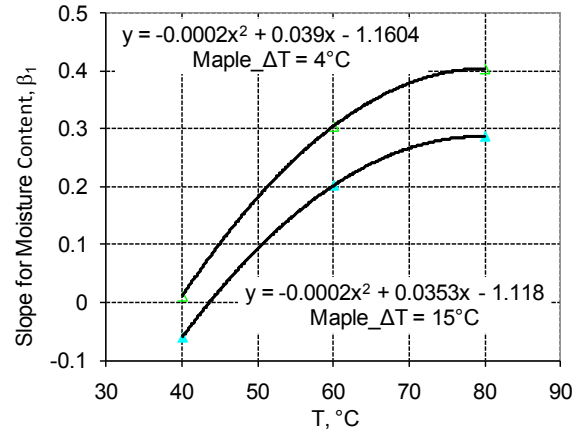
(a) β_0 vs. T , paper birch sapwood



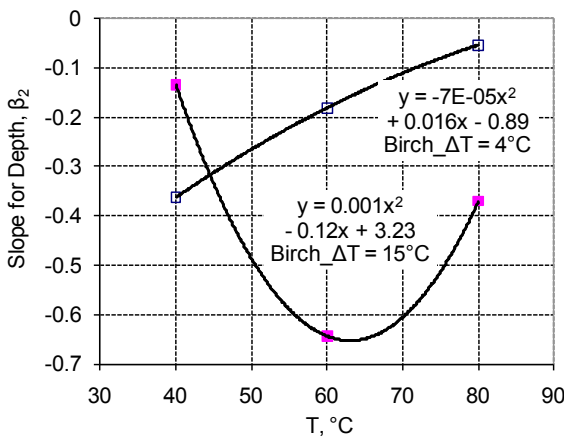
(b) β_0 vs. T , sugar maple sapwood



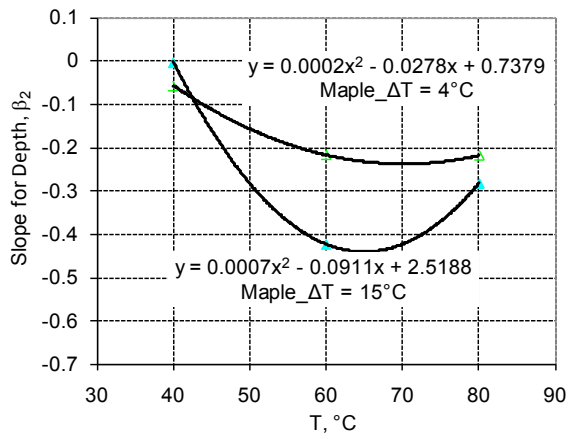
(c) β_1 vs. T , paper birch sapwood



(d) β_1 vs. T , sugar maple sapwood



(e) β_2 vs. T , paper birch sapwood



(f) β_2 vs. T , sugar maple sapwood

Figure F.2 Relationships between the regression coefficients in all separate equations for L^* values below the wood surface and the dry-bulb temperatures.

Table F.2 Wood color 3T sub-global equations for the lightness on and below the wood surface of paper birch and sugar maple at two wet-bulb depressions.

Wood species	Position	ΔT , (°C)	3T sub-global equations obtained from tests at 40, 60 and 80 °C
Paper birch	On the wood surface	4	$L^* = 68.0 - 5.00 \times 10^{-5} T^2 M - 6.50 \times 10^{-3} T^2$ $+ 0.0151 T M + 0.403 T - 0.607 M$
		15	$L^* = 33.7 + 2.00 \times 10^{-4} T^2 M - 0.0115 T^2$ $- 0.0189 T M + 1.40 T + 0.557 M$
	Below the wood surface	4	$L^* = 108 - 7.00 \times 10^{-5} T^2 e + 7.00 \times 10^{-5} T^2 M + 0.00720 T^2$ $+ 0.0158 T e - 0.00810 T M - 1.124 T - 0.884 e + 0.478 M$
		15	$L^* = 116 + 9.00 \times 10^{-4} T^2 e - 1.00 \times 10^{-4} T^2 M + 7.60 \times 10^{-3} T^2$ $- 0.110 T e + 0.0204 T M - 1.16 T + 2.88 e - 0.557 M$
Sugar maple	On the wood surface	4	$L^* = 121 + 2.00 \times 10^{-5} T^2 M + 8.00 \times 10^{-3} T^2$ $+ 0.0103 T M - 1.39 T - 0.456 M$
		15	$L^* = 36.5 + 1.40 \times 10^{-3} T^2 M - 0.0198 T^2$ $- 0.153 T M + 1.87 T + 3.96 M$
	Below the wood surface	4	$L^* = 143 + 2.00 \times 10^{-4} T^2 e - 3.00 \times 10^{-4} T^2 M + 0.0137 T^2$ $- 0.0254 T e + 0.0402 T M - 2.05 T + 0.667 e - 1.19 M$
		15	$L^* = 113 + 8.00 \times 10^{-4} T^2 e - 2.00 \times 10^{-4} T^2 M + 3.80 \times 10^{-3} T^2$ $- 0.104 T e + 0.0377 T M - 0.831 T + 2.87 e - 1.18 M$

Note: The general patterns of the 3T sub-global models are expressed below for the wood surface and the wood interior, respectively:

$$L^* = \alpha_0 + \alpha_1 T^2 M + \alpha_2 T^2 + \alpha_3 T M + \alpha_4 T + \alpha_5 M$$

$$L^* = \beta_0 + \beta_1 T^2 e + \beta_2 T^2 M + \beta_3 T^2 + \beta_4 T e + \beta_5 T M + \beta_6 T + \beta_7 e + \beta_8 M$$

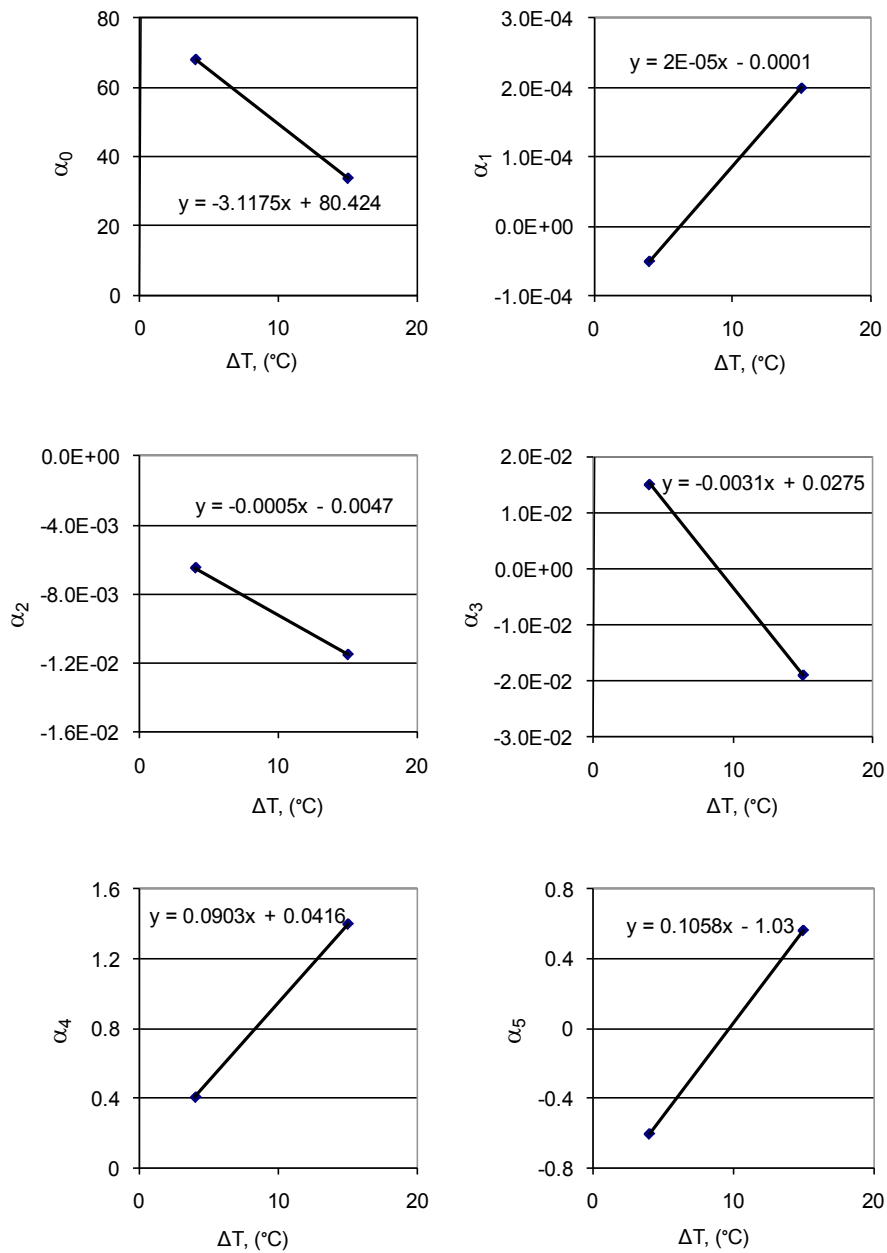


Figure F.3 Relationships between the regression coefficients in the 3T sub-global equations for L^* values on the surface of paper birch sapwood boards and the wet-bulb depression.

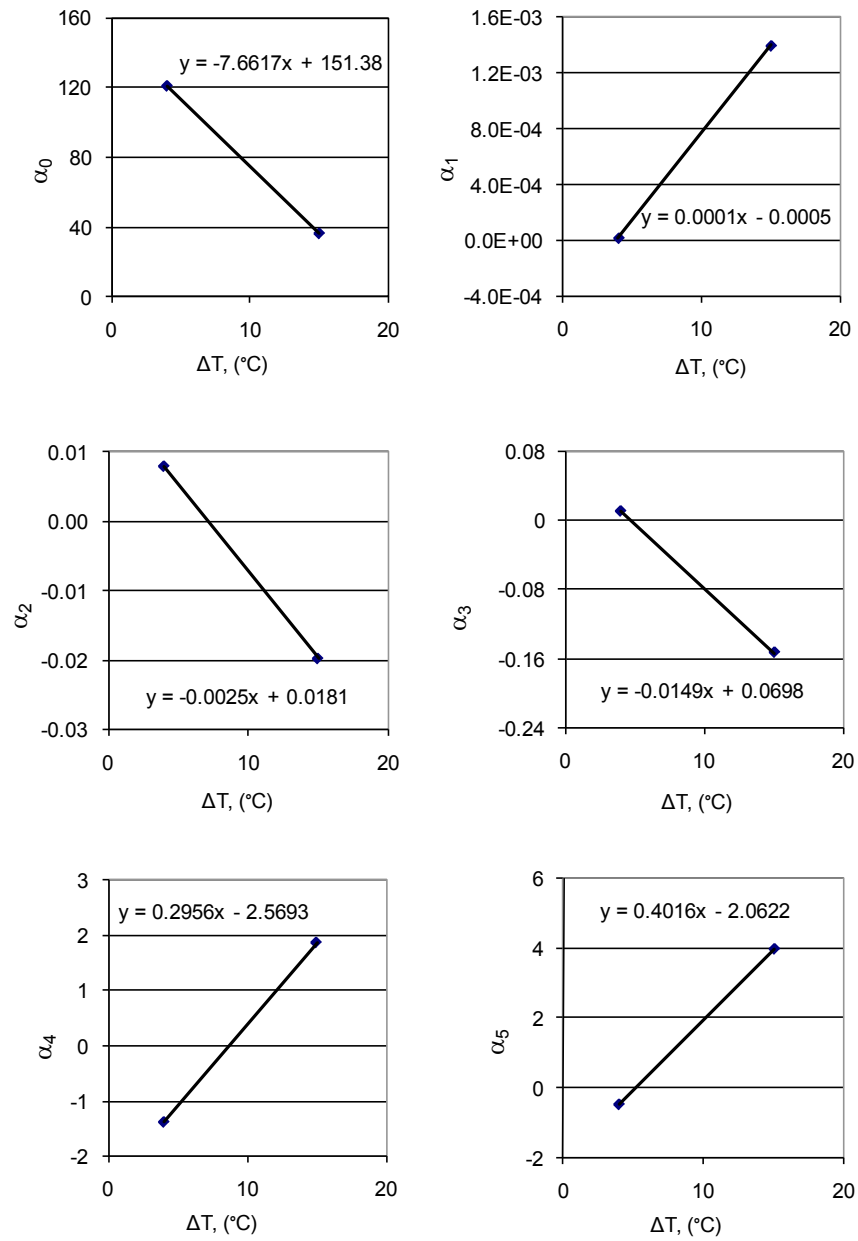


Figure F.4 Relationships between the regression coefficients in the 3T sub-global equations for L^* values on the surface of sugar maple sapwood boards and the wet-bulb depression.

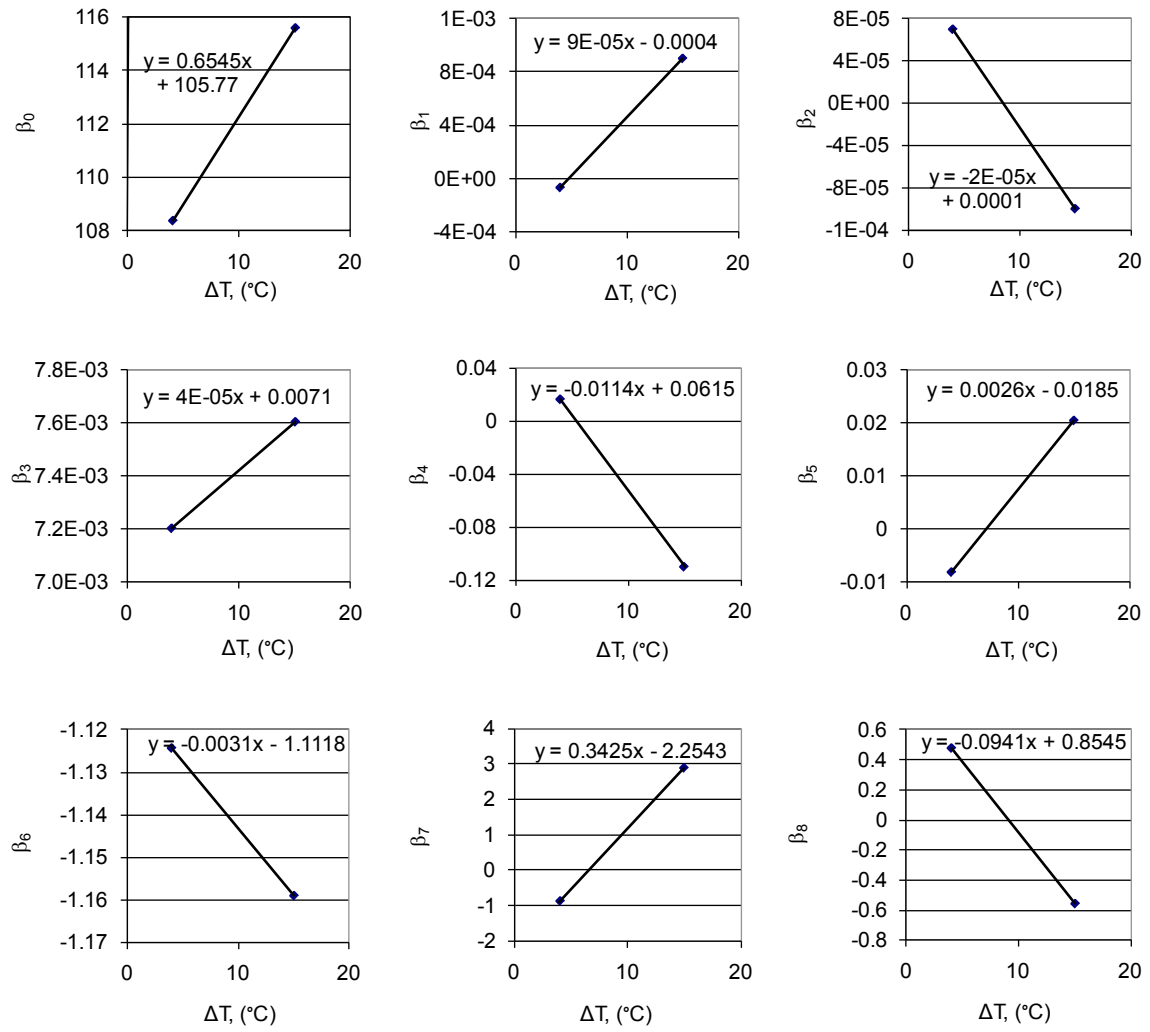


Figure F.5 Relationships between the regression coefficients in the 3T sub-global equations for L^* values below the surface of paper birch sapwood boards and the wet-bulb depression.

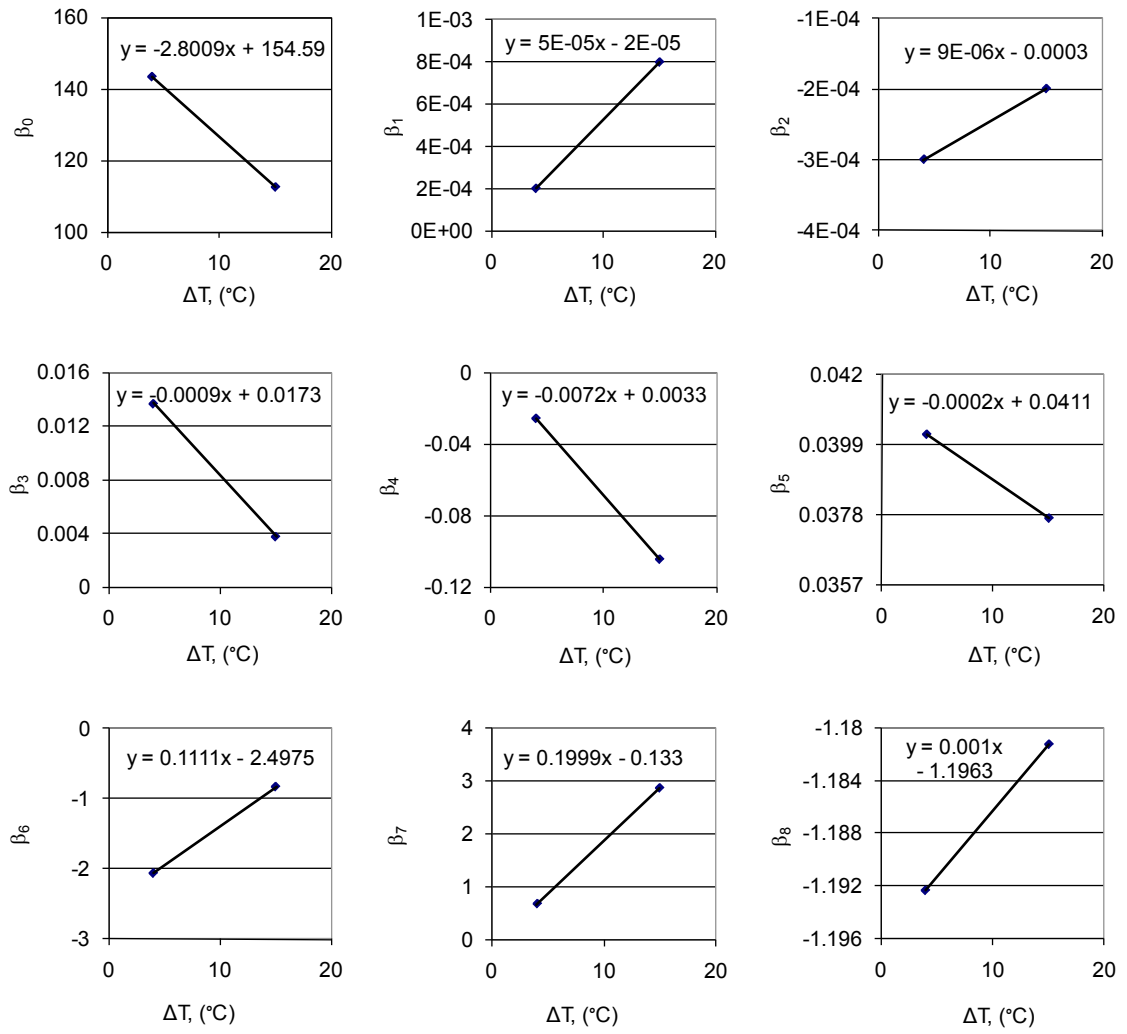


Figure F.6 Relationships between the regression coefficients in the 3T sub-global equations for L^* values below the surface of sugar maple sapwood boards and the wet-bulb depression.

Appendix G: Graphical technique used for the 2T global wood color models

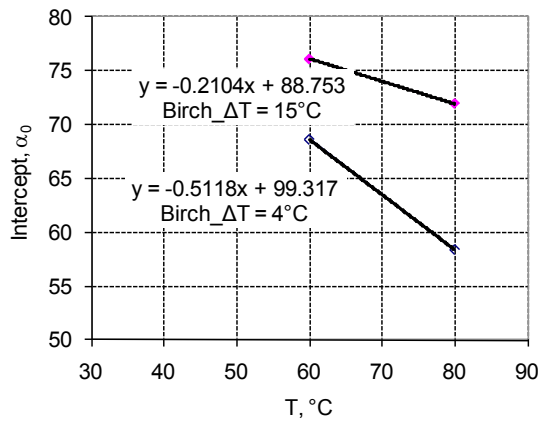
Table G.1 Separate regression models of wood lightness for the four drying conditions of paper birch and sugar maple at 60 and 80°C (This table is a part of Table F.1)

Wood species	T, (°C)	ΔT, (°C)	L^* on the wood surface	L^* below the wood surface ($e \geq 0.24\text{mm}$)
Paper birch	60	4	$L^* = 68.6 + 0.132M$, $R^2 = 74.7\%$	$L^* = 67.1 + 0.241M - 0.181e$, $R^2 = 63.7\%$
		15	$L^* = 76.1 + 0.0350M$, $R^2 = 66.9\%$	$L^* = 73.7 + 0.203M - 0.644e$, $R^2 = 73.3\%$
	80	4	$L^* = 58.4 + 0.306M$, $R^2 = 96.1\%$	$L^* = 64.7 + 0.279M - 0.0533e$, $R^2 = 90.9\%$
		15	$L^* = 71.9 + 0.134M$, $R^2 = 91.6\%$	$L^* = 71.8 + 0.239M - 0.370e$, $R^2 = 80.3\%$
Sugar maple	60	4	$L^* = 66.4 + 0.230M$, $R^2 = 74.3\%$	$L^* = 69.5 + 0.305M - 0.216e$, $R^2 = 90.0\%$
		15	$L^* = 77.0 - 0.212M$, $R^2 = 65.3\%$	$L^* = 76.2 + 0.210M - 0.464e$, $R^2 = 66.6\%$
	80	4	$L^* = 61.1 + 0.490M$, $R^2 = 97.3\%$	$L^* = 66.4 + 0.405M - 0.218e$, $R^2 = 73.5\%$
		15	$L^* = 58.8 + 0.626M$, $R^2 = 92.6\%$	$L^* = 70.2 + 0.287M - 0.281e$, $R^2 = 82.8\%$

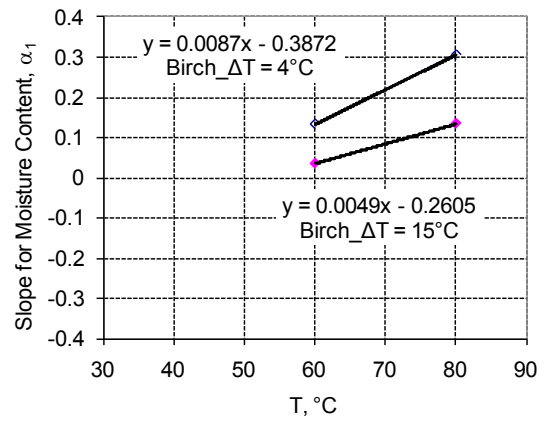
Note: M = wood moisture content, %; e = depth below the wood surface through the board thickness, mm. The general patterns of the separate regression models are expressed below for the wood surface and the wood interior, respectively:

$$L^* = \alpha_0 + \alpha_1 M$$

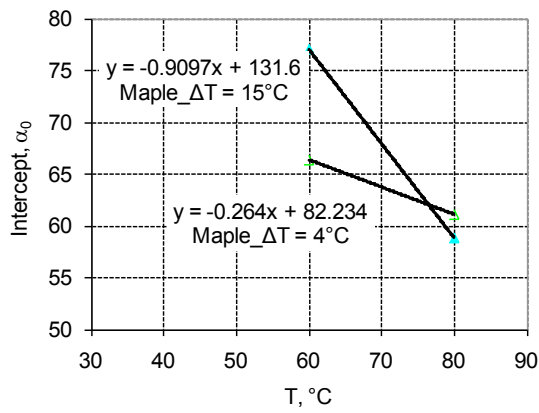
$$L^* = \beta_0 + \beta_1 M + \beta_2 e$$



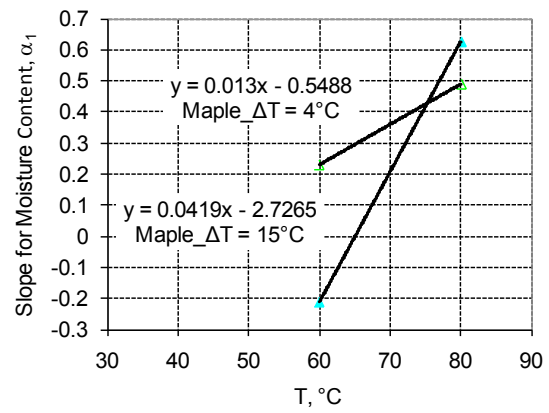
(a) α_0 vs. T , paper birch sapwood



(b) α_1 vs. T , paper birch sapwood

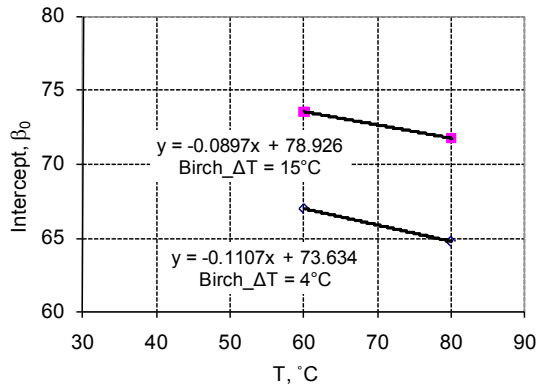


(c) α_0 vs. T , sugar maple sapwood

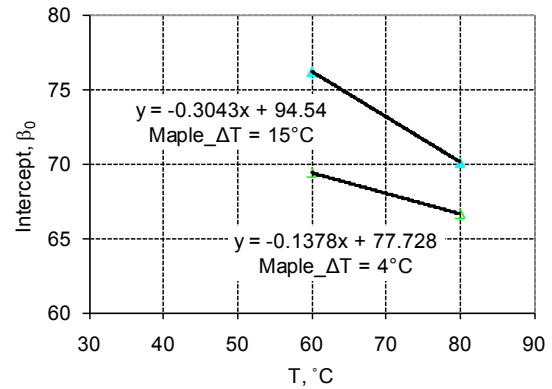


(d) α_1 vs. T , sugar maple sapwood

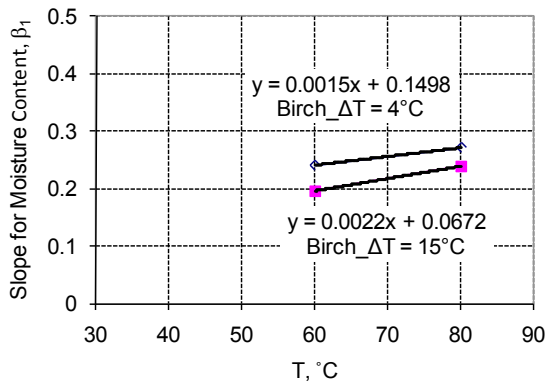
Figure G.1 Relationships between the regression coefficients in the separate equations for L^* values on the wood surface and the dry-bulb temperature from 60°C to 80°C .



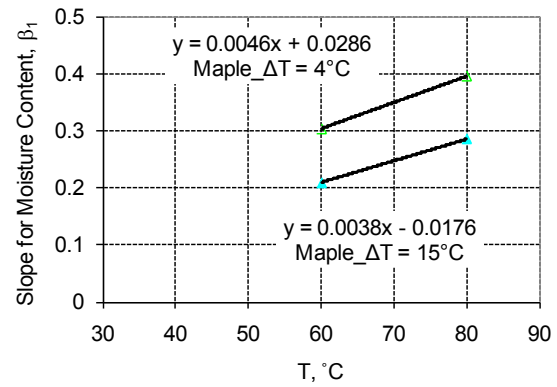
(a) β_0 vs. T , paper birch sapwood



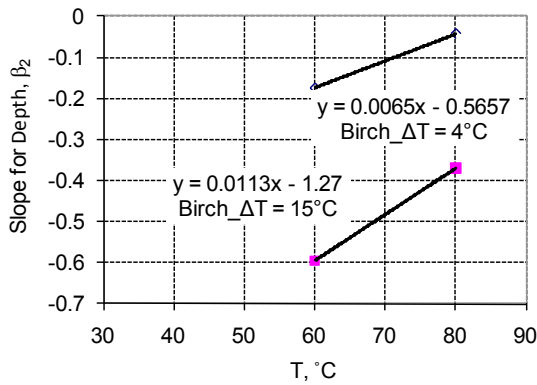
(b) β_0 vs. T , sugar maple sapwood



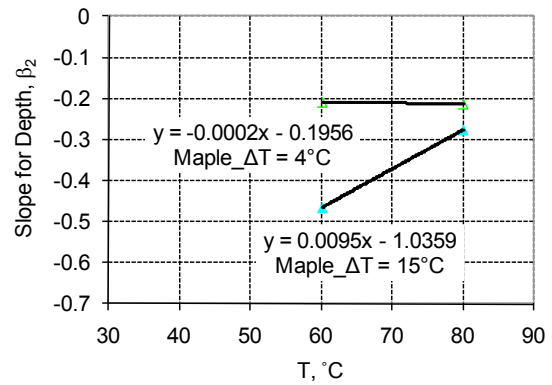
(c) β_1 vs. T , paper birch sapwood



(d) β_1 vs. T , sugar maple sapwood



(e) β_2 vs. T , paper birch sapwood



(f) β_2 vs. T , sugar maple sapwood

Figure G.2 Relationships between the regression coefficients in the separate equations for L^* values below the wood surface and the dry-bulb temperature from 60°C to 80°C .

Table G.2 Wood color 2T sub-global equations for the lightness on and below the wood surface of paper birch and sugar maple at two wet-bulb depressions.

Wood species	Position	ΔT , (°C)	2T sub-global equations for 60 and 80 °C
Paper birch	on wood surface	4	$L^* = 99.32 + 0.00870 T M - 0.512 T - 0.387 M$
		15	$L^* = 88.8 + 0.00490 T M - 0.210 T - 0.261 M$
	below wood surface	4	$L^* = 73.6 + 0.00650 T e + 0.00150 T M - 0.111 T - 0.566 e + 0.150 M$
		15	$L^* = 78.9 + 0.0113 T e + 0.00220 T M - 0.0897 T - 1.27 e + 0.0672 M$
Sugar maple	on wood surface	4	$L^* = 82.2 + 0.0130 T M - 0.264 T - 0.549 M$
		15	$L^* = 132 + 0.0419 T M - 0.910 T - 2.73 M$
	below wood surface	4	$L^* = 77.7 - 0.000200 T e + 0.00460 T M - 0.138 T - 0.196 e + 0.0286 M$
		15	$L^* = 94.5 + 0.00950 T e + 0.00380 T M - 0.304 T - 1.04 e - 0.0176 M$

Note: The general patterns of the 2T sub-global models are expressed below for the wood surface and the wood interior, respectively:

$$L^* = \alpha_0 + \alpha_1 T M + \alpha_2 T + \alpha_3 M$$

$$L^* = \beta_0 + \beta_1 T e + \beta_2 T M + \beta_3 T + \beta_4 e + \beta_5 M$$

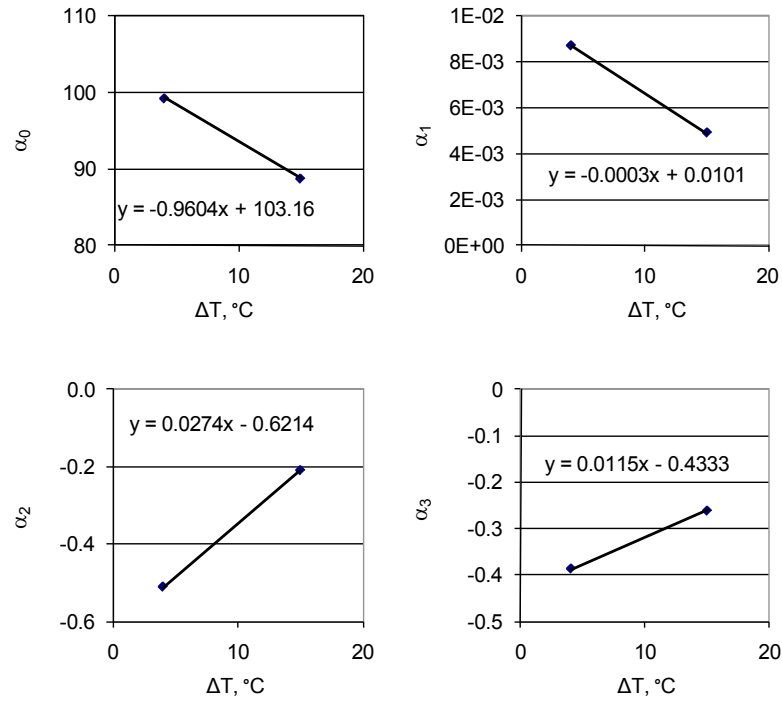


Figure G.3 Relationships between the regression coefficients in the 2T sub-global equations and the wet-bulb depression for L^* values on the surface of paper birch sapwood boards.

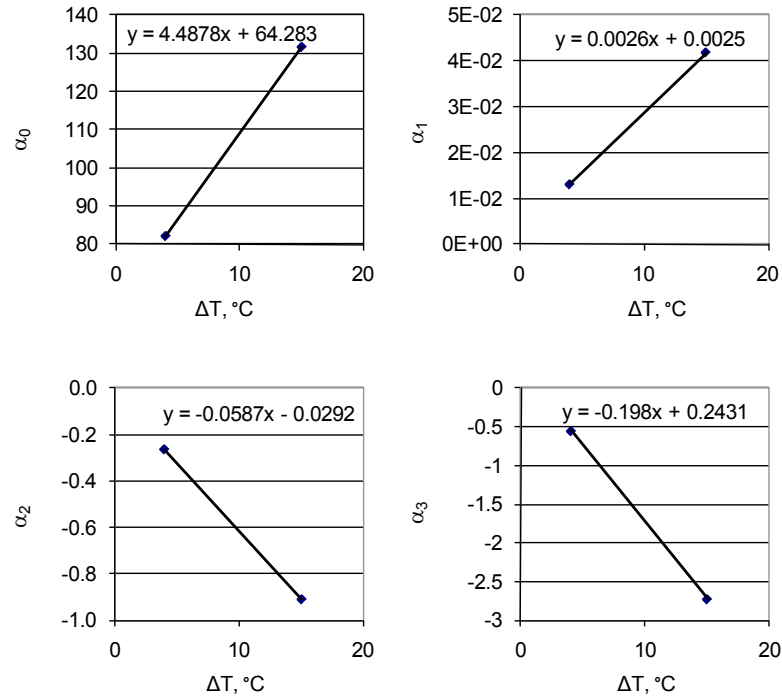


Figure G.4 Relationships between the regression coefficients in the 2T sub-global equations and the wet-bulb depression for L^* values on the surface of sugar maple sapwood boards.

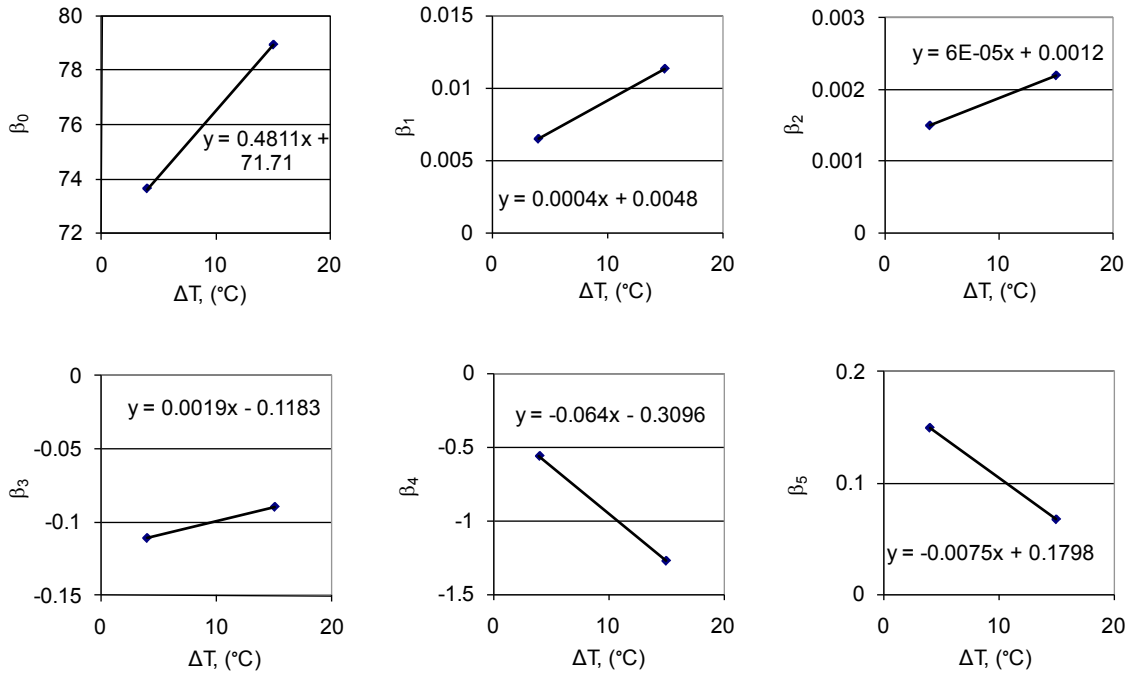


Figure G.5 Relationships between the regression coefficients in the 2T sub-global equations and the wet-bulb depression for L^* values below the surface of paper birch sapwood boards.

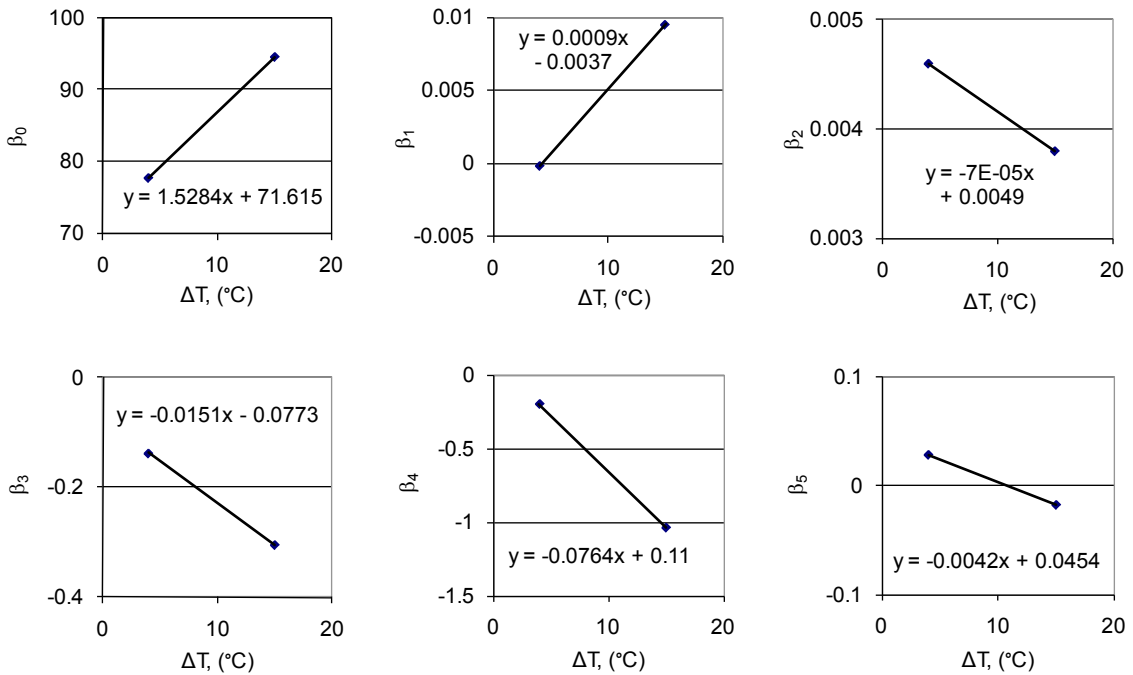


Figure G.6 Relationships between the regression coefficients in the 2T sub-global equations and the wet-bulb depression for L^* values below the surface of sugar maple sapwood boards.

Appendix H: SAS[®] programs for the global predictive models

According to the global equations which were inferred from the separate equations for L* values at and below the wood surface of paper birch sapwood boards at different drying conditions, the further SAS[®] program below was written by Gaétan Daigle (M.Sc., P.Stat.) of Département de mathématiques et de statistique of Université Laval to get more accurate and more statistically significant global equations.

H.1 For paper birch

```
*****
      Reading the DATA Bouleau (Paper Birch)
*****;
      PROC IMPORT OUT= LECTURE DATAFILE= "data27fev09.xls" DBMS=xls
REPLACE;
      SHEET="Bouleau";
      GETNAMES=YES;
      RUN;

*****
      Analyses des données de l'onglet Bouleau
*****;

      proc sort data=lecture; by Ts Dt planche Time descending e;
run;
      data analyse;
      set lecture; by Ts Dt planche Time descending e;
      lagM = lag(M);
      if M=. then M=lagM;
      Ts2 = Ts*Ts;
      observation = _n_;
      copie_Ts = Ts;
      copie_Dt = Dt;
run;

      proc freq data=analyse; tables Ts; run;

      data below surface;
      set analyse;
      if E=0 then output surface;
      if E>0 then output below;
run;

      *** Model On the surface;
      proc Mixed data=Surface;
```

```
class copie_Ts copie_Dt planche;
model L = Ts2 Dt*Ts*M Ts*M Dt*Ts Dt*M Ts M Dt/solution outp=stat;
random intercept M/subject=planche(copie_Ts*copie_Dt) type=un;
run;
ods select TestsforNormality;
proc univariate data=stat plot normal;
id observation;
var resid;
histogram Resid/normal;
run;
options reset=all reset=global;
proc gplot data=stat;
symbol1 v=dot; * pointlabel=("#observation");
plot Resid*Pred/vref=0 lvref=2;
run; quit;
proc corr data=stat;
var L pred;
run;

options reset=all reset=global;
proc gplot data=stat;
symbol1 v=dot c=black;
symbol2 v=none i=join ci=red width=2;
plot L*(pred L)/overlay;
run; quit;

*** Model BELOW the surface;
proc Mixed data=Below;
class copie_Ts copie_Dt planche;
model L = Ts2*Dt*e Ts2 Dt*e*Ts e*Ts Dt*Ts Dt*e Dt*M Ts e M
/solution outp=stat;
random intercept M e/subject=planche(copie_Ts*copie_Dt) type=un;
run;
ods select TestsforNormality;
proc univariate data=stat plot normal;
id observation;
var resid;
histogram Resid/normal;
run;
options reset=all reset=global;
proc gplot data=stat;
symbol1 v=dot; *pointlabel=("#observation");
plot Resid*(Pred Ts e M Dt)/vref=0 lvref=2;
run; quit;
proc corr data=stat;
var L pred;
run;

options reset=all reset=global;
proc gplot data=stat;
symbol1 v=dot c=black; * pointlabel=("#observation");
symbol2 v=none i=join ci=red width=2;
plot L*(pred L)/overlay;
run; quit;
```

```

***** EXCLUDING Ts=40*****

*** Model On the surface;
proc Mixed data=Surface;
where Ts ne 40;
class copie_Ts copie_Dt planche;
model L = Ts*Dt Ts*M Dt*M Ts /solution outp=stat;
random intercept M/subject=planche(copie_Ts*copie_Dt) type=un;
run;
ods select TestsforNormality;
proc univariate data=stat plot normal;
id observation;
var resid;
histogram Resid/normal;
run;
options reset=all reset=global;
proc gplot data=stat;
symbol1 v=dot; * pointlabel=("#observation");
plot Resid*Pred/vref=0 lvref=2;
run; quit;
proc corr data=stat;
var L pred;
run;
options reset=all reset=global;
proc gplot data=stat;
symbol1 v=dot c=black;
symbol2 v=none i=join ci=red width=2;
plot L*(pred L)/overlay;
run; quit;

*** Model BELOW the surface;
proc Mixed data=Below;
where Ts ne 40;
class copie_Ts copie_Dt planche;
model L = Ts*Dt Ts*e Dt*e Ts e M/solution outp=stat;
random intercept M e/subject=planche(copie_Ts*copie_Dt) type=un;
run;
ods select TestsforNormality;
proc univariate data=stat plot normal;
id observation;
var resid;
histogram Resid/normal;
run;
options reset=all reset=global;
proc gplot data=stat;
symbol1 v=dot; *pointlabel=("#observation");
plot Resid*(Pred Ts e M Dt)/vref=0 lvref=2;
run; quit;
proc corr data=stat;
var L pred;
run;

options reset=all reset=global;
proc gplot data=stat;
symbol1 v=dot c=black; * pointlabel=("#observation");
symbol2 v=none i=join ci=red width=2;

```

```
plot L*(pred L)/overlay;
run; quit;
```

H.2 For sugar maple

```
*****
      Reading the DATA MAPLE
*****;
      PROC IMPORT OUT= LECTURE DATAFILE= "data27fev09.xls" DBMS=xls
REPLACE;
      SHEET="Erable";
      GETNAMES=YES;
      RUN;

*****
      Analyses des données de l'onglet Erable
*****;

      proc sort data=lecture; by Ts Dt planche Time descending e;
run;
      data analyse;
      set lecture; by Ts Dt planche Time descending e;
      lagM = lag(M);
      if M=. then M=lagM;
      Ts2 = Ts*Td;
      observation = _n_;
      copie_Ts = Ts;
      copie_Dt = Dt;
run;

      proc freq data=analyse; tables Ts; run;

      data below surface;
      set analyse;
      if E=0 then output surface;
      if E>0 then output below;
run;

      *** Model On the surface;
      options ls=90 ps=63;
      proc Mixed data=Surface;
      class copie_Ts copie_Dt planche;
      where observation not in(1360);
      model L = Ts2*Dt*M Ts2*Dt
              Dt*Td*M Ts*M Ts*Dt
              Dt*M Ts/solution outp=stat;
      random intercept M/subject=planche(copie_Ts*copie_Dt) type=un;
run;
      ods select TestsforNormality;
      proc univariate data=stat plot normal;
      id observation;
      var resid;
```

```
histogram Resid/normal;
run;
options reset=all reset=global;
proc gplot data=stat;
symbol1 v=dot; * pointlabel=("#observation");
plot Resid*Pred/vref=0 lvref=2;
run; quit;
proc corr data=stat;
var L pred;
run;

options reset=all reset=global;
proc gplot data=stat;
symbol1 v=dot c=black;
symbol2 v=none i=join ci=red width=2;
plot L*(pred L)/overlay;
run; quit;

*** Model BELOW the surface;
proc Mixed data=Below;
class copie_Ts copie_Dt planche;
where observation not in(895);
model L = Ts2*Dt*e Ts2*M Ts2*Dt Ts2
          DT*Ts*e Ts*M Ts*Dt
          Dt*e Dt*M Ts e M Dt/solution outp=stat;
random intercept M e/subject=planche(copie_Ts*copie_Dt) type=un;
run;
ods select TestsforNormality;
proc univariate data=stat plot normal;
id observation;
var resid;
histogram Resid/normal;
run;
options reset=all reset=global;
proc gplot data=stat;
symbol1 v=dot; *pointlabel=("#observation");
plot Resid*(Pred Ts e M Dt)/vref=0 lvref=2;
run; quit;
proc corr data=stat;
var L pred;
run;

options reset=all reset=global;
proc gplot data=stat;
symbol1 v=dot c=black; * pointlabel=("#observation");
symbol2 v=none i=join ci=red width=2;
plot L*(pred L)/overlay;
run; quit;

***** EXCLUDING Ts=40*****

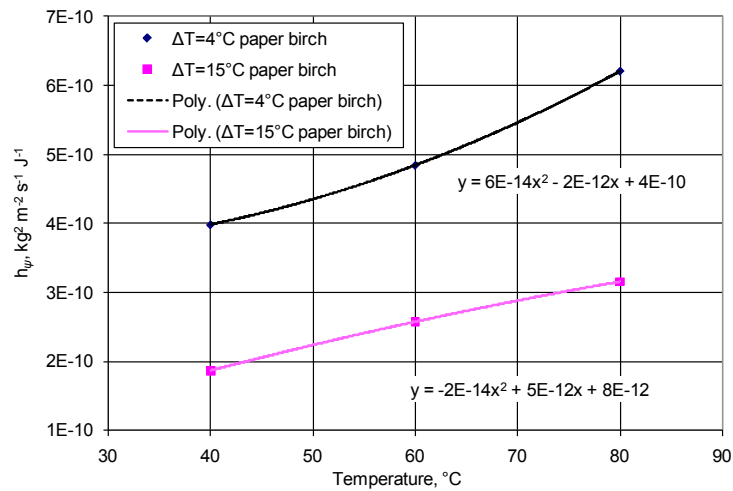
*** Model On the surface;
proc Mixed data=Surface;
where observation not in(1360) and Ts ne 40;
class copie_Ts copie_Dt planche;
```

```
model L = Ts*Dt*M Ts*Dt Dt*M Dt M/solution outp=stat;
random intercept M/subject=planche(copie_Ts*copie_Dt) type=un;
run;
ods select TestsforNormality;
proc univariate data=stat plot normal;
id observation;
var resid;
histogram Resid/normal;
run;
options reset=all reset=global;
proc gplot data=stat;
symbol1 v=dot; * pointlabel=("#observation");
plot Resid*Pred/vref=0 lvref=2;
run; quit;
proc corr data=stat;
var L pred;
run;
options reset=all reset=global;
proc gplot data=stat;
symbol1 v=dot c=black;
symbol2 v=none i=join ci=red width=2;
plot L*(pred L)/overlay;
run; quit;

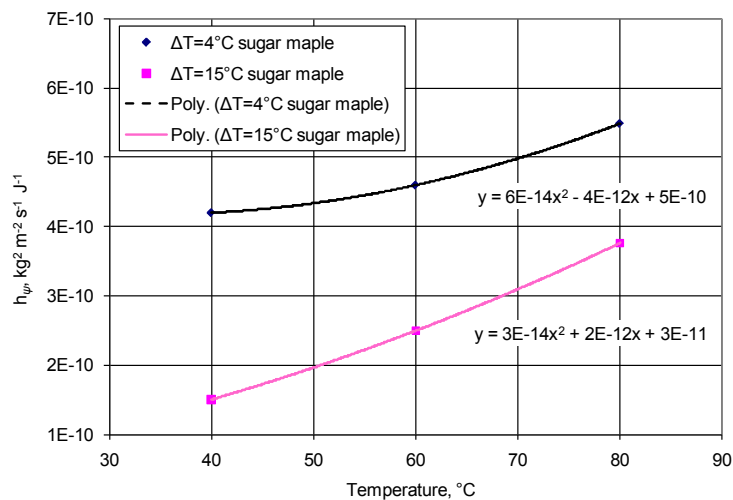
*** Model BELOW the surface;
proc Mixed data=Below;
where observation not in(895) and Ts ne 40;
class copie_Ts copie_Dt planche;
model L = Ts*Dt Ts*M Dt*e Dt*M Ts Dt e/solution outp=stat;
random intercept M e/subject=planche(copie_Ts*copie_Dt) type=un;
run;
ods select TestsforNormality;
proc univariate data=stat plot normal;
id observation;
var resid;
histogram Resid/normal;
run;
options reset=all reset=global;
proc gplot data=stat;
symbol1 v=dot; *pointlabel=("#observation");
plot Resid*(Pred Ts e M Dt)/vref=0 lvref=2;
run; quit;
proc corr data=stat;
var L pred;
run;

options reset=all reset=global;
proc gplot data=stat;
symbol1 v=dot c=black; * pointlabel=("#observation");
symbol2 v=none i=join ci=red width=2;
plot L*(pred L)/overlay;
run; quit;
```

Appendix I: Calculation of the convective mass transfer coefficient in the constant drying rate period

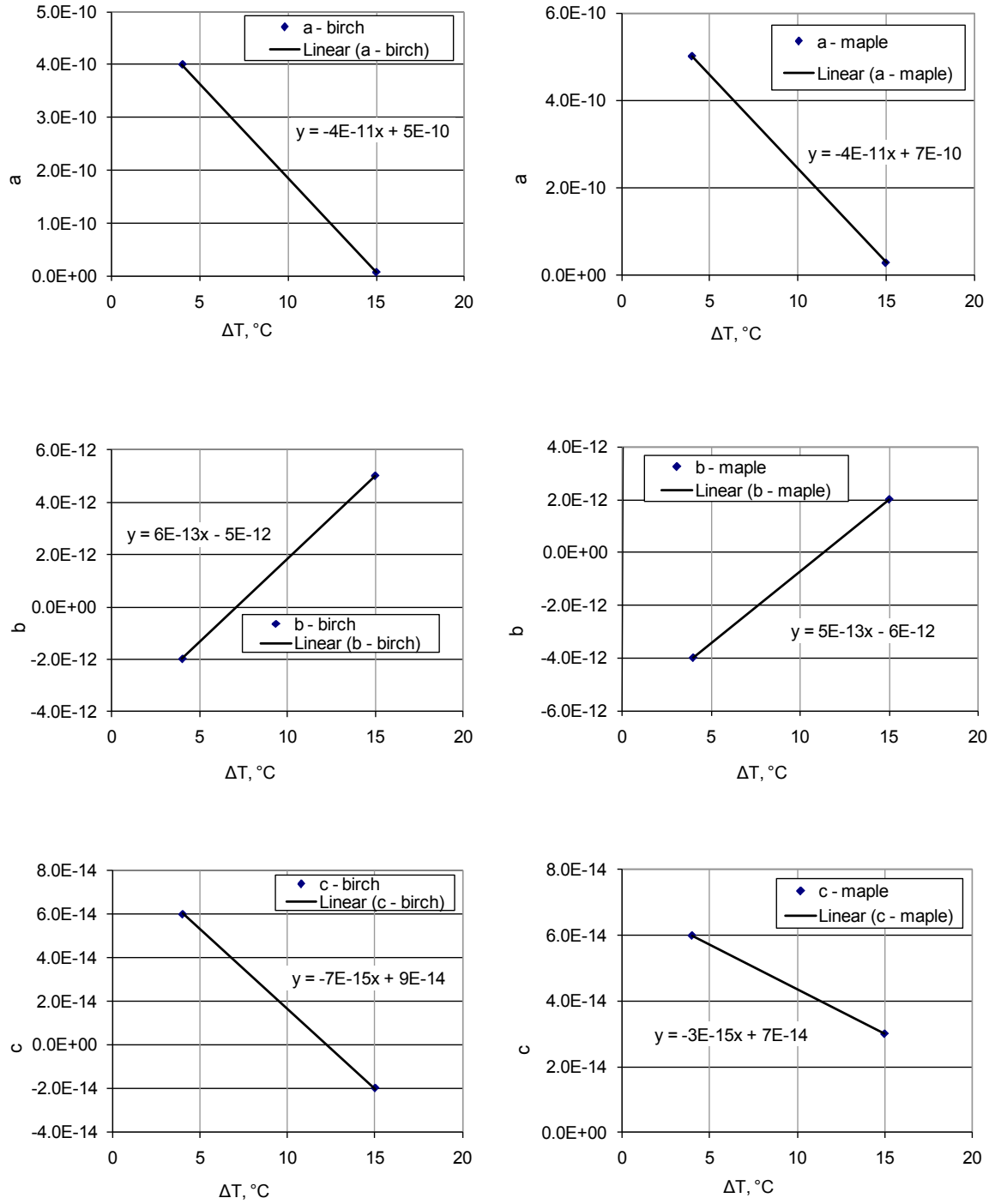


(a) paper birch



(b) sugar maple

Figure I.1 Relationships between dry-bulb temperature and convective mass transfer coefficient for drying paper birch and sugar maple sapwood during the constant drying rate period.

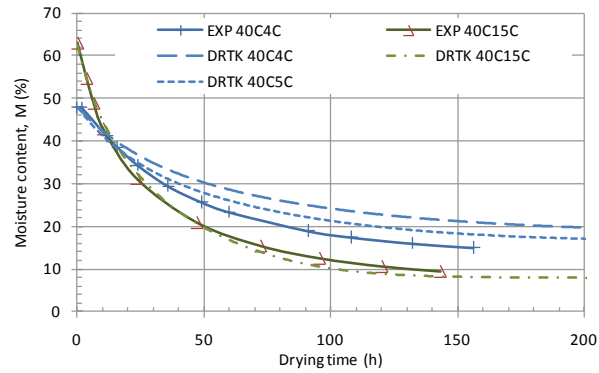


(a) paper birch,

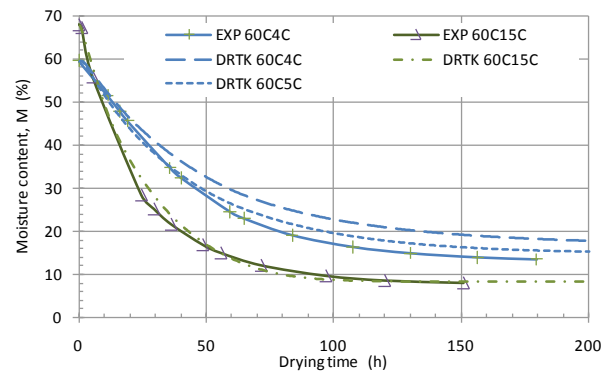
(b) sugar maple

Figure I.2 Relationships between wet-bulb depression and coefficients in the equations of convective mass transfer coefficients for drying paper birch and sugar maple sapwood during the constant drying rate period.

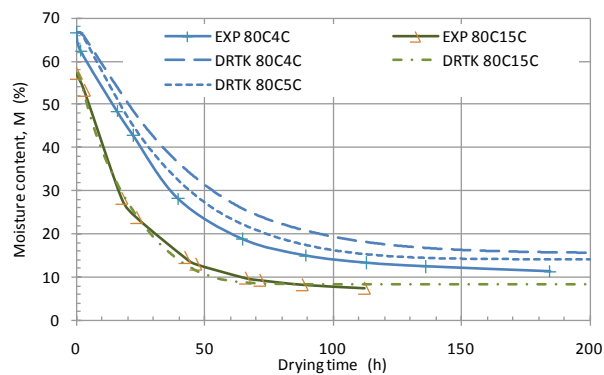
Appendix J: Curve fitting of simulated and experimental results from the color measurement tests



(a) paper birch, at $T = 40^\circ\text{C}$ and $\Delta T = 4, 15^\circ\text{C}$

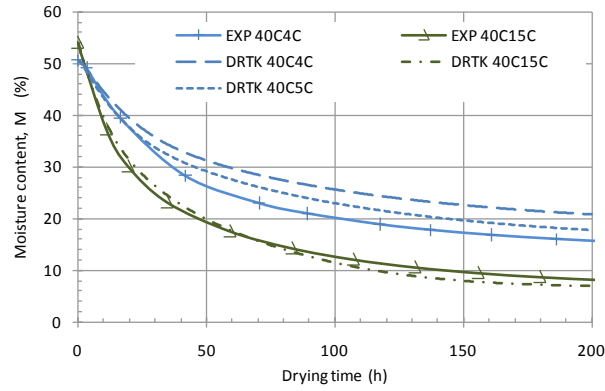


(b) paper birch, at $T = 60^\circ\text{C}$ and $\Delta T = 4, 15^\circ\text{C}$

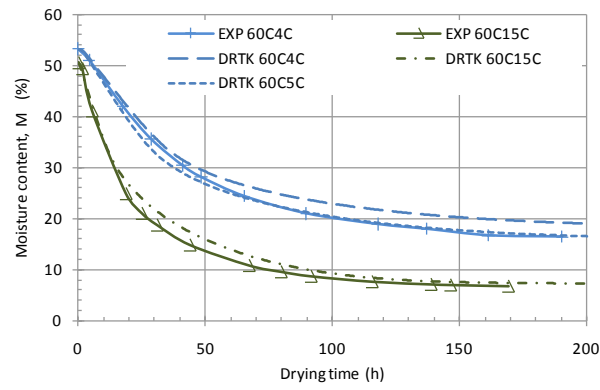


(c) paper birch, at $T = 80^\circ\text{C}$ and $\Delta T = 4, 15^\circ\text{C}$

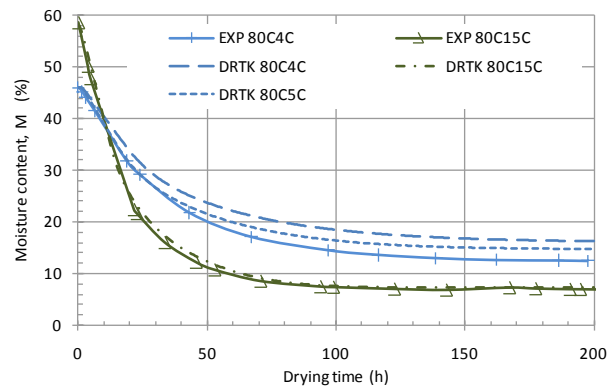
Figure J.1 Comparison of simulated and measured drying curves of paper birch.



(a) sugar maple, at $T = 40^{\circ}\text{C}$ and $\Delta T = 4, 15^{\circ}\text{C}$



(b) sugar maple, at $T = 60^{\circ}\text{C}$ and $\Delta T = 4, 15^{\circ}\text{C}$



(c) sugar maple, at $T = 80^{\circ}\text{C}$ and $\Delta T = 4, 15^{\circ}\text{C}$

Figure J.2 Comparison of simulated and measured drying curves of sugar maple.